Electrosynthesis II

Edited by Siegfried R. Waldvogel

Imprint

Synthesis of naturally-derived macromolecules through simplified electrochemically mediated ATRP

Paweł Chmielarz[*], Tomasz Pacześniak, Katarzyna Rydel-Ciszek, Izabela Zaborniak, Paulina Biedka and Andrzej Sobkowiak

Abstract

The flavonoid-based macroinitiator was received for the first time by the transesterification reaction of quercetin with 2-bromoisobutyryl bromide. In accordance with the "grafting from" strategy, a naturally-occurring star-like polymer with a polar 3,3',4',5,6-pentahydroxyflavone core and hydrophobic poly(*tert*-butyl acrylate) (P*t*BA) side arms was synthesized via a simplified electrochemically mediated ATRP (*se*ATRP), utilizing only 78 ppm by weight (wt) of a catalytic Cu^{II} complex. To demonstrate the possibility of temporal control, *se*ATRP was carried out utilizing a multiple-step potential electrolysis. The rate of the polymerizations was well-controlled by applying optimal potential values during preparative electrolysis to prevent the possibility of intermolecular coupling of the growing polymer arms. This appears to be the first report using on-demand *se*ATRP for the synthesis of QC-(P*t*BA-Br)$_5$ *pseudo*-star polymers. The naturally-derived macromolecules showed narrow MWDs ($Đ$ = 1.08–1.11). ^{1}H NMR spectral results confirm the formation of quercetin-based polymers. These new flavonoid-based polymer materials may find applications as antifouling coatings and drug delivery systems.

Introduction

In the last decade, there have been increasing research activities in the use of atom transfer radical polymerization (ATRP) to prepare naturally-derived star-like polymers [1-4]. Considering this method, naturally-occurring polymers can be synthesized via three main strategies: "grafting onto" [5-10], "grafting through" [11,12], or "grafting from" [10,13-21]. The "grafting from" approach in particular, allows the tailoring of the side chain composition and the introduction of functional groups via polymerization [21]. This technique consists in the application of a multifunctional macromolecule. The number of initiating groups on this macromolecule codes the number of arms in the synthesized star polymer. Moreover, by extension of ω-chain ends on the periphery of the star we can easily introduce a next segment to the polymer [22,23].

This article aims at the synthesis of quercetin-based star-like polymers with a polar quercetin (QC) core and hydrophobic poly(*tert*-butyl acrylate) (P*t*BA) arms which has not yet been reported. Quercetin with five terminal hydroxy groups was chosen as an efficacious solution to receive functionalised polymers. It is a naturally occurring flavonoid, which is abundantly found in citrus fruits, herbs, vegetables, seeds, tea, nuts, and red wine [24-26]. It is considered to be a strong antioxidant due to its ability to scavenge free radicals and bind transition metal ions [27]. Quercetin inhibits xanthine oxidase [27-29], inhibits lipid peroxidation in vitro [27,28,30], and scavenges oxygen radicals [27,28,31-33]. There is a tremendous importance of this antioxidant in the prevention of a range of cardiovascular diseases [27,34,35], cancer [26,27,36], and neurodegenerative diseases [27]. P*t*BA was selected as functional arm of polymer stars because it can be readily transformed to poly(acrylic acid) via deprotection, yielding polyelectrolytes. Such polymers are one of the most extensively studied, industrially important, water-soluble macromolecules [37-39], widely used as dental adhesives, controlled release devices, coatings, and in pharmaceutical industry [40,41]. Therefore, it is expected that these synthesized naturally-derived macromolecules can become key elements of antifouling coatings and drug delivery systems.

ATRP is one of the most versatile techniques that allow obtaining a wide range of polymers with controlled composition, molecular weight (MW), molecular weight distribution (M_w/M_n, MWD, $Đ$), and degrees of polymerization (DP) [42-53]. Significant efforts have been dedicated to the development of the "green chemistry" variety of this method. The catalyst complex concentration has been substantially reduced to parts per million (ppm) level in the reaction system, due to the development of the simplified electrochemically mediated ATRP (*se*ATRP) approach [54], which offers elimination of chemical reducing agents, catalyst recycle possibility, and an option to receive polymers with narrow MWD [55,56]. Additionally, application of external stimuli offered a possibility of temporal control, such as the stopping and restarting of the polymerization by switching the "off" and "on" stages, respectively [53,55], while maintaining the well-controlled characteristic of the process [55-57]. A similar effect was received by turning the light source "on" and "off" in the photoATRP approach [58]. However, in this case, substantial light scattering could interfere or even prevent efficient polymerization [56]. Therefore, *se*ATRP offers a new opportunity to synthesize well-defined star-like polymers with predefined molecular structure.

The main objective of this study is to present the first example of a synthesis of a macromolecule initiator from the group of flavonoids and with well-defined star-like polymers, consisting of a quercetin core and hydrophobic P*t*BA arms with narrow MWDs by ATRP under multiple-step potential electrolysis conditions.

Results and Discussion

A flavonoid-based macromolecule initiator with 5 Br atoms (QC-Br$_5$) was synthesized by the transesterification reaction (Figure S1, Supporting Information File 1; $M_n = 1,050$, $M_w/M_n = 1.02$). The chemical structure of QC-Br$_5$ was confirmed by ^{1}H NMR (Figure 1): δ (ppm) = 1.88–2.24 (30H, CH$_3$–, a$_1$), 6.93–7.10 (1H, =CH–, c$_1$), 7.35–7.54 (2H, =CH–, c$_2$ and c$_3$), 7.81–7.90 (1H, =CH–, c$_4$), and 7.91–7.98 ppm (1H, =CH–, c$_5$). The degree of substitution of the hydroxy groups of 3,3',4',5,6-pentahydroxyflavone was determined by the area ratio of the methyl protons at the regions of δ = 1.88–2.24 ppm (30H) to the 1-benzene protons at the region of δ = 6.93–7.10 ppm (1H). According to this analysis, the quercetin-based product has 5 Br functionalities.

Cyclic voltammetry was used for the electrochemical characterization of the QC (Figure S2, Supporting Information File 1), QC-Br$_5$ (Figure S3), and Cu^{II}Br$_2$/tris(2-pyridylmethyl)amine (TPMA) in the absence (Figures S5 and S6) and in the presence of QC-Br$_5$ (Figures S7 and S8), all the reaction solutions contained *N*,*N*-dimethylformamide (DMF) and *tert*-butyl acrylate (*t*BA). One can observe, that quercetin is not reduced in the applied potential window (Figure S2, Supporting Information File 1), meanwhile it shows two small anodic peaks at 0.2 V and 0.5 V. According to the commonly accepted mechanism, both for water-containing [28,59] and for aprotic media [28,60,61] the first oxidation peak corresponds to the oxidation of the catechol moiety, the 3',4'-dihydroxy group of quercetin, while the second peak relates to the oxidation of the –OH substituent next to the carbonyl group of quercetin. Brominated quercetin is electrochemically inactive between –0.75 V and 0.75 V (Figure S3, Supporting Information File 1). As expected, the Cu^{II}Br$_2$/TPMA catalyst complex is quasi-reversibly reduced to Cu^{I}Br/TPMA at −0.3 V (Figure S5, Supporting Information File 1). The peak current for the cathodic peak (−0.3 V) and reverse anodic peak (−0.2 V) increases linearly with correlation coefficients 0.999 and 0.996 for the corresponding regression lines (Figure S6, Supporting Information File 1). The high linearity indicates that the processes are controlled by the rate of diffusion of the electroactive substance into the electrode surface. However, the separation of the peaks is characteristic for a quasi-reversible process at each scan rate applied. After introduction of QC-Br$_5$ to the system containing Cu^{II}Br$_2$/TPMA complex a higher wave-shaped cathodic response was observed (Figure S7, Supporting Information File 1). Due to the fact that QC-Br$_5$ is not reduced electrochemically at least to −0.75 (Figure S3, Supporting Information File 1), solely Cu^{II}Br$_2$/TPMA can be reduced at −0.3 V in electrochemical systems,
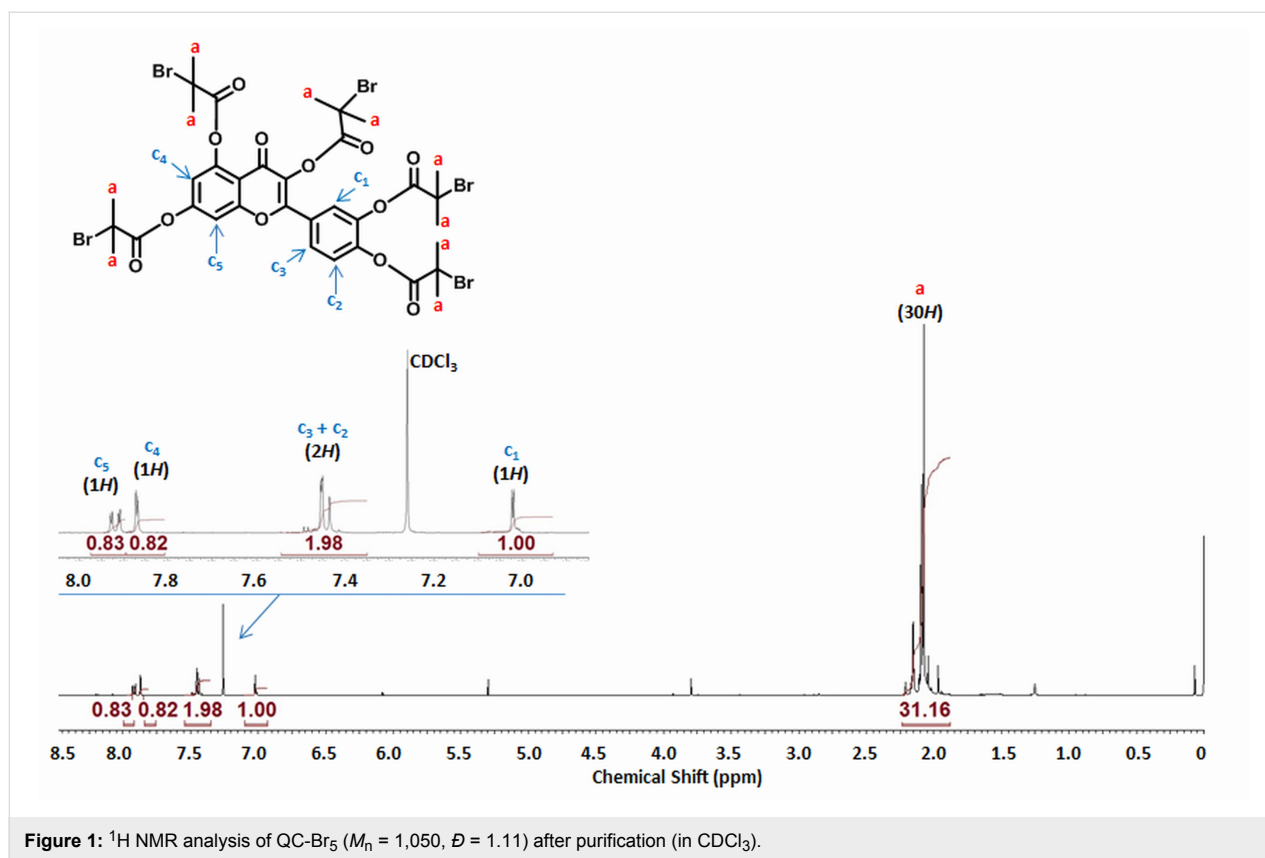
Figure 1: ^{1}H NMR analysis of QC-Br$_5$ (M_n = 1,050, Đ = 1.11) after purification (in CDCl$_3$).

effectuating subsequent, fast chemical reduction of QC-Br$_5$ and regeneration of Cu^{II}Br/TPMA. As expected, addition of an alkyl halide initiator to a solution of Cu^{II}Br$_2$/TPMA during the voltammetric measurements causes a loss of reversibility and an increase of the cathodic current because of reduction of the regenerated Cu^{II}Br$_2$/TPMA via the catalytic electrochemical catalytic process (EC') (Figure S7, Supporting Information File 1) [55]. The disturbance from linearity for the dependence of the peak current on the square root of the scan rate (Figure S8, Supporting Information File 1) indicates the distinct non-diffusional component of the process, related to consecutive chemical regeneration of the Cu^{II}Br$_2$/TPMA complex.

To investigate the kinetics of the electrochemical catalytic process, the dependence of the ratio (catalytic current)/(reduction peak current in the absence of QC-Br$_5$) – for the peak at −0.3 V, on the square root of different QC-Br$_5$ concentration was analyzed (Figures S9 and S10, Supporting Information File 1). The dependence was linear (R = 0.997). The rate constant of the chemical reaction between the Cu^I complex and QC-Br$_5$, i.e., the C' reaction of the catalytic process (EC'), using the equations from the classic works of Savéant, Vianello [62] and Nicolson, Shine [63] was calculated. Dividing the equation for the peak of the catalytic current by the Randles-Sevčik equation for the quasi-reversible peak (for 298 K),

we obtain

$$\frac{I_c}{I_p} = \frac{k_f^{1/2} c_{QCBr5}^{1/2}}{2.740 v^{1/2}},$$

where v is a scan rate. Because

$$\frac{k_f^{1/2}}{2.740 \cdot 0.1^{1/2}}$$

is the slope of the regression line for $I_c/I_p = f(c_{QC\text{-}Br5})^{1/2}$ dependence (equal 58.1), the calculated k_f is $2.5 \cdot 10^3$ M/s.

Flavonoid-based *pseudo*-star polymers with a quercetin core and PtBA side chains have been synthesized for the first time using only 78 ppm by weight (wt) of Cu^{II} complex, following the *se*ATRP procedure (Table 1).

The synthesis of quercetin-based macromolecule initiator with 5 side arms of PtBA under constant potential preparative electrolysis conditions was realized (Table 1, entry 1, Figure 2a,b and Figures S11a, and S11b, Supporting Information File 1). At the beginning of the constant potential polymerization approach (Figure S11a, Supporting Information File 1), merely deacti-

Table 1: Summary of quercetin-based *pseudo*-star polymers synthesis by *se*ATRP.

entry	[M]/[MI]/ [Cu^{II}Br$_2$]/[TPMA]	E_{app}[a]	k_p^{app} (h^{-1})[b]	conv (%)[b]	DP$_{n,theo}$ (arm)[b]	$M_{n,theo}$ (×10^{-3})[c]	$M_{n,app}$ (×10^{-3})[d]	M_w/M_n[d]
1	110/1/0.011/0.022	−240 mV	0.471	73	80	52.6	36.6	1.08
2	110/1/0.011/0.022	*Multi-constant E_{app} Electrolysis*[e]	0.452[f]	75	82	53.6	37.3	1.11

General reaction conditions: T = 65 °C; V_{tot} = 16 ml; t = 3 h [except entry 2: t = 6 h ("on" stages = 3 h; "off" stages = 3 h)]; [M]: [tBA] = 3.4 M; [MI]: [QC-Br$_5$] = 6.2 mM calculated per 5 Br initiation sites; [Cu^{II}Br$_2$/TPMA] = 0.34 mM; [tetrabutylammonium perchlorate (TBAP)] = 0.2 M. Constant potential *se*ATRP: entry 1; Controlled multi-constant potential *se*ATRP: entry 2. [a]Applied potentials (E_{app}) were selected based on cyclic voltammetry (CV) analysis of catalytic complex (Figures S5 and S7, Supporting Information File 1); [b]Monomer conversion, apparent propagation constants (k_p^{app}), and apparent theoretical degree of polymerization of monomer unit per arm (DP$_{n,theo}$) were determined by NMR [64]; [c]$M_{n,theo}$ = ([M]$_0$/[MI]$_0$) × conversion × $M_{monomer}$ + $M_{macroinitiator}$; [d]apparent M_n and MWD were determined by GPC; [e]controlled potential program (E_{app} = −240 mV for the "on" stage and E_{app} = 600 mV for the "off" stage vs SCE); [f]only for the "on" stages.

vator is prevalent, thus the cathodic current decays as deactivator is transformed to an activator, after which it achieves constant value corresponding to the deactivator/activator ratio, adjusted by E_{app} [55]. The rate of the electrolysis was well-controlled by applying optimum E_{app} values in order to preclude coupling of side chains [64,65]. The first-order kinetic relationship (Figure S11b, Supporting Information File 1) was observed. Figure 2a,b shows that MW increased linearly with conversion and that narrow MWD course toward higher MW was achieved.

To verify the living character of the electrochemically mediated process, the sufficient applied potential was imposed to repetitively switch the system between active and dormant states according to previous research [55,57]. This was achieved by cycling E_{app} between −0.29 V and 0.55 V vs SCE (Table 1, entry 2, Figure 3a,b, and Figures S12a and S12b, Supporting Information File 1). The first of these potentials favors formation of Cu^I at the electrode and hence polymerization was activated, whereas the second potential, being more positive than $E_{1/2}$, promotes Cu^{II} regeneration and leads to a dormant species of propagating radicals (Figure S12a, Supporting Information File 1) [57]. This potential cycle was repeated three times, efficiently increasing the monomer conversion to 25, 51, and then to 75% during active periods (Figure 3a). MW steadily increased during the "on" periods, while no low-MW polymers were detected (Figure 3b and Figure S12b, Supporting Information File 1). These observations illustrate the living characteristics of the polymerization with regard to efficient reinitiation of chain ends, owing to the applicable preservation of chain-end functionality [57]. Such "pausing" of the reaction could be beneficial in preparation of wide range of naturally-derived
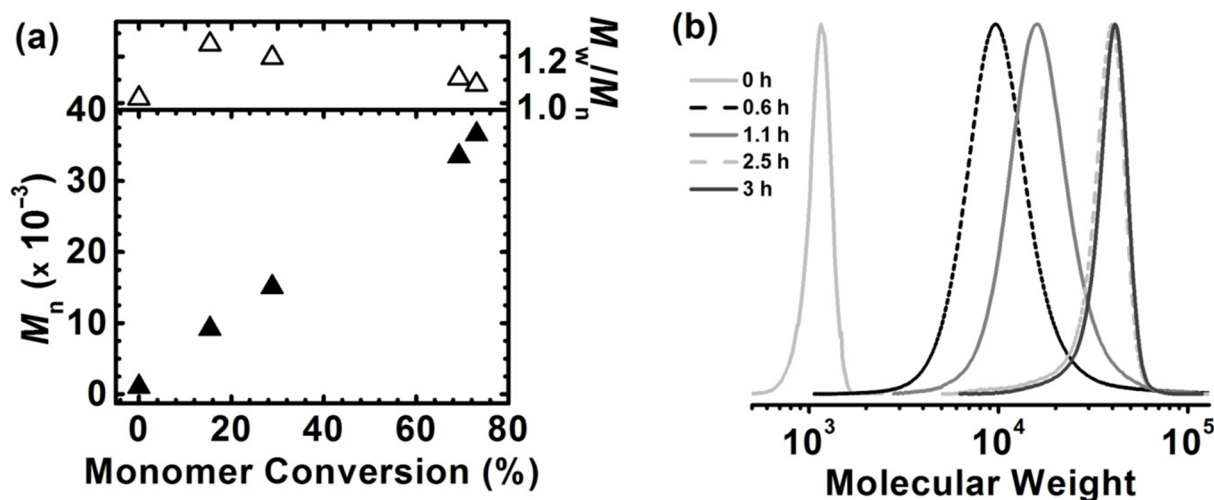

Figure 2: Synthesis of PtBA homopolymers grafted from quercetin-based macroinitiator via *se*ATRP under constant potential conditions; (a) M_n and M_w/M_n vs monomer conversion, and (b) GPC traces of tBA polymerization and their evolution over time. Reaction conditions: [tBA]/[QC-Br$_5$ (per 5 initiation sites)]/[Cu^{II}Br$_2$]/[TPMA] = 110/1/0.011/0.022, [tBA] = 3.4 M, [Cu^{II}Br$_2$/TPMA] = 0.34 mM, [TBAP] = 0.2 M, T = 65 °C. Table 1, entry 1.
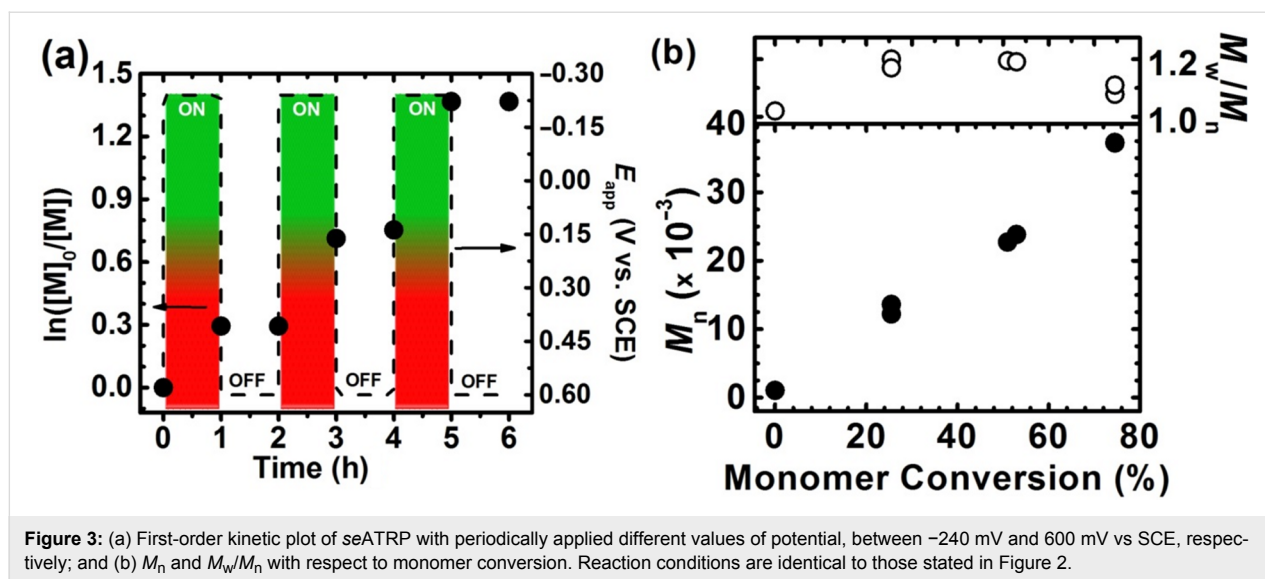
Figure 3: (a) First-order kinetic plot of *se*ATRP with periodically applied different values of potential, between −240 mV and 600 mV vs SCE, respectively; and (b) M_n and M_w/M_n with respect to monomer conversion. Reaction conditions are identical to those stated in Figure 2.

macromolecular stars and brushes with predictable molecular weights of the polymer grafts.

The chemical structure of the received QC-(P*t*BA$_{82}$-Br)$_5$ *pseudo*-star-shaped polymer (Table 1, entry 2) was confirmed by ^{1}H NMR spectroscopy (Figure S13, Supporting Information File 1). The chemical shifts, 1.10–2.00 ppm and 2.10–2.40 ppm, are ascribed to the –C*H$_2$*– (β), –C*H$_3$* (b), and –C*H*– (α) groups of the P*t*BA units, denoting the inherence of P*t*BA arms [48,66-68].

Conclusion

Naturally-derived macromolecules were synthesized based on a new strategy including the synthesis of a 3,3',4',5,6-pentahydroxyflavone-based core with 2-bromoisobutyryl bromide as initiation molecule, and grafting of the P*t*BA arms of the flavonoid-based moiety by facile *se*ATRP technique. To demonstrate the possibility of temporal control, on-demand *se*ATRP was carried out utilizing multiple-step potential electrolysis. The feasibility of the electrochemical switch exploitation for the control of cooper oxidation states and therefore activation or deactivation of the polymerization was demonstrated by the sequence of repeated stepping E_{app} from −0.24 V to 0.60 V vs SCE. Such "pausing" of the reaction could be beneficial in preparation of more complex architectures with predictable molecular weights of the polymer grafts. This is the first report announcing using simplified constant potential and multi-step constant potential mediated ATRP for the synthesis of flavonoid-based star-like polymers. The results of GPC, and ^{1}H NMR prove the successful preparation of the star-shaped polymers. These new polymer materials create potential possibilities of using them as key elements of biologically active thin films in tissue engineering and as drug delivery systems.

Supporting Information

Supporting Information File 1

Experimental section including NMR spectra, first-order kinetic plot, GPC traces, preparative electrolysis and CV results.

[http://www.beilstein-journals.org/bjoc/content/supplementary/1860-5397-13-243-S1.pdf]

ORCID® iDs

Paweł Chmielarz - https://orcid.org/0000-0002-9101-6264

References

1. Spain, S. G.; Gibson, M. I.; Cameron, N. R.
   J. Polym. Sci., Part A: Polym. Chem. **2007,** *45,* 2059–2072.
   doi:10.1002/pola.22106
2. Khanna, K.; Varshney, S.; Kakkar, A. *Polym. Chem.* **2010,** *1,*
   1171–1185. doi:10.1039/c0py00082e
3. Kassi, E.; Patrickios, C. S. *Macromolecules* **2010,** *43,* 1411–1415.
   doi:10.1021/ma9023312
4. Cameron, D. J. A.; Shaver, M. P. *Chem. Soc. Rev.* **2011,** *40,*
   1761–1776. doi:10.1039/C0CS00091D
5. Pfaff, A.; Müller, A. H. E. *Macromolecules* **2011,** *44,* 1266–1272.
   doi:10.1021/ma102794z
6. Sudre, G.; Siband, E.; Hourdet, D.; Creton, C.; Cousin, F.; Tran, Y.
   Macromol. Chem. Phys. **2012,** *213,* 293–300.
   doi:10.1002/macp.201100394

7. Ozlem, S.; Iskin, B.; Yilmaz, G.; Kukut, M.; Hacaloglu, J.; Yagci, Y.
Eur. Polym. J. **2012,** *48,* 1755–1767.
doi:10.1016/j.eurpolymj.2012.07.014

8. Yan, Y.; Shi, Y.; Zhu, W.; Chen, Y. *Polymer* **2013,** *54,* 5634–5642.
doi:10.1016/j.polymer.2013.08.036

9. Sudre, G.; Hourdet, D.; Creton, C.; Cousin, F.; Tran, Y.
Macromol. Chem. Phys. **2013,** *214,* 2882–2890.
doi:10.1002/macp.201300477

10. Gosecka, M.; Basinska, T. *Polym. Adv. Technol.* **2015,** *26,* 696–706.
doi:10.1002/pat.3554

11. Hadjichristidis, N.; Pitsikalis, M.; Iatrou, H.; Pispas, S.
Macromol. Rapid Commun. **2003,** *24,* 979–1013.
doi:10.1002/marc.200300050

12. Neugebauer, D.; Zhang, Y.; Pakula, T.; Sheiko, S. S.;
Matyjaszewski, K. *Macromolecules* **2003,** *36,* 6746–6755.
doi:10.1021/ma0345347

13. Cheng, G.; Böker, A.; Zhang, M.; Krausch, G.; Müller, A. H. E.
Macromolecules **2001,** *34,* 6883–6888. doi:10.1021/ma0013962

14. Ballauff, M. *Prog. Polym. Sci.* **2007,** *32,* 1135–1151.
doi:10.1016/j.progpolymsci.2007.05.002

15. Wu, Y.; Ni, P.; Zhang, M.; Zhu, X. *Soft Matter* **2010,** *6,* 3751–3758.
doi:10.1039/c000979b

16. Pan, K.; Zhang, X.; Zhu, J.; Cao, B. *Polym. Adv. Technol.* **2011,** *22,*
1948–1952. doi:10.1002/pat.1699

17. Däbritz, F.; Lederer, A.; Komber, H.; Voit, B.
J. Polym. Sci., Part A: Polym. Chem. **2012,** *50,* 1979–1990.
doi:10.1002/pola.25972

18. Zhang, M.; Shen, W.; Xiong, Q.; Wang, H.; Zhou, Z.; Chen, W.;
Zhang, Q. *RSC Adv.* **2015,** *5,* 28133–28140.
doi:10.1039/C5RA02115D

19. Altay, E.; Rzayev, J. *Polymer* **2016,** *98,* 487–494.
doi:10.1016/j.polymer.2016.02.022

20. Chmielarz, P.; Krys, P.; Wang, Z.; Wang, Y.; Matyjaszewski, K.
Macromol. Chem. Phys. **2017,** *218,* 1700106.
doi:10.1002/macp.201700106

21. Pelras, T.; Duong, H. T. T.; Kim, B. J.; Hawkett, B. S.; Müllner, M.
Polymer **2017,** *112,* 244–251. doi:10.1016/j.polymer.2017.02.001

22. Cao, P.-F.; Wojnarowska, J.; Hong, T.; Carroll, B.; Li, B.; Feng, H.;
Parsons, L.; Wang, W.; Lokitz, B. S.; Cheng, S.; Bocharova, V.;
Sokolov, A. P.; Saito, T. *Polymer* **2017,** *124,* 117–127.
doi:10.1016/j.polymer.2017.07.052

23. Shi, X.; Ma, X.; Hou, M.; Gao, Y.-E.; Bai, S.; Xiao, B.; Xue, P.;
Kang, Y.; Xu, Z.; Li, C. M. *J. Mater. Chem. B* **2017,** *33,* 6847–6859.
doi:10.1039/C7TB01477E

24. Theodoridis, G.; Lasáková, M.; Škeříková, V.; Tegou, A.; Giantsiou, N.;
Jandera, P. *J. Sep. Sci.* **2006,** *29,* 2310–2321.
doi:10.1002/jssc.200500492

25. Gam-Derouich, S.; Ngoc Nguyen, M.; Madani, A.; Maouche, N.;
Lang, P.; Perruchot, C.; Chehimi, M. M. *Surf. Interface Anal.* **2010,** *42,*
1050–1056. doi:10.1002/sia.3210

26. Hemmati, K.; Ghaemy, M. *Int. J. Biol. Macromol.* **2016,** *87,* 415–425.
doi:10.1016/j.ijbiomac.2016.03.005

27. D'Andrea, G. *Fitoterapia* **2015,** *106,* 256–271.
doi:10.1016/j.fitote.2015.09.018

28. Brett, A. M. O.; Ghica, M.-E. *Electroanalysis* **2003,** *15,* 1745–1750.
doi:10.1002/elan.200302800

29. Chen, Y.; Xiao, P.; Ou-Yang, D.-S.; Fan, L.; Guo, D.; Wang, Y.-N.;
Han, Y.; Tu, J.-H.; Zhou, G.; Huang, Y.-F.; Zhou, H.-H.
Clin. Exp. Pharmacol. Physiol. **2009,** *36,* 828–833.
doi:10.1111/j.1440-1681.2009.05158.x

30. Sakanashi, Y.; Oyama, K.; Matsui, H.; Oyama, T. B.; Oyama, T. M.;
Nishimura, Y.; Sakai, H.; Oyama, Y. *Life Sci.* **2008,** *83,* 164–169.
doi:10.1016/j.lfs.2008.05.009

31. de Souza, R. F. V.; De Giovani, W. F. *Redox Rep.* **2004,** *9,* 97–104.
doi:10.1179/135100004225003897

32. Taslidere, E.; Dogan, Z.; Elbe, H.; Vardi, N.; Cetin, A.; Turkoz, Y.
Biotech. Histochem. **2016,** *91,* 116–121.
doi:10.3109/10520295.2015.1085093

33. Lespade, L. *Chem. Phys.* **2016,** *475,* 32–38.
doi:10.1016/j.chemphys.2016.06.006

34. Salmi, Z.; Benmehdi, H.; Lamouri, A.; Decorse, P.; Jouini, M.;
Yagci, Y.; Chehimi, M. M. *Microchim. Acta* **2013,** *180,* 1411–1419.
doi:10.1007/s00604-013-0993-8

35. Osonga, F. J.; Kariuki, V. M.; Yazgan, I.; Jimenez, A.; Luther, D.;
Schulte, J.; Sadik, O. A. *Sci. Total Environ.* **2016,** *563–564,* 977–986.
doi:10.1016/j.scitotenv.2015.12.064

36. Sedghi, R.; Oskooie, H. A.; Heravi, M. M.; Nabid, M. R.; Zarnani, A. H.
J. Mater. Chem. B **2013,** *1,* 773–786. doi:10.1039/C2TB00359G

37. Kurkuri, M. D.; Aminabhavi, T. M. *J. Controlled Release* **2004,** *96,*
9–20. doi:10.1016/j.jconrel.2003.12.025

38. Ma, Z.-y.; Jia, X.; Zhang, G.-x.; Hu, J.-m.; Zhang, X.-l.; Liu, Z.-y.;
Wang, H.-y.; Zhou, F. *J. Agric. Food Chem.* **2013,** *61,* 5474–5482.
doi:10.1021/jf401102a

39. Gao, X.; He, C.; Xiao, C.; Zhuang, X.; Chen, X. *Polymer* **2013,** *54,*
1786–1793. doi:10.1016/j.polymer.2013.01.050

40. Quadrat, O.; Horský, J.; Bradna, P.; Šňupárek, J.; Baghaffar, G. A.
Prog. Org. Coat. **2001,** *42,* 188–193.
doi:10.1016/S0300-9440(01)00166-7

41. Fernandes, A. L. P.; Martins, R. R.; da Trindade Neto, C. G.;
Pereira, M. R.; Fonseca, J. L. C. *J. Appl. Polym. Sci.* **2003,** *89,*
191–196. doi:10.1002/app.12175

42. Matyjaszewski, K.; Jo, S. M.; Paik, H.-j.; Shipp, D. A. *Macromolecules*
1999, *32,* 6431–6438. doi:10.1021/ma9905526

43. Jonsson, M.; Nyström, D.; Nordin, O.; Malmström, E. *Eur. Polym. J.*
2009, *45,* 2374–2382. doi:10.1016/j.eurpolymj.2009.05.002

44. Matyjaszewski, K.; Tsarevsky, N. V. *Nat. Chem.* **2009,** *1,* 276–288.
doi:10.1038/nchem.257

45. Zong, G.; Chen, H.; Tan, Z.; Wang, C.; Qu, R. *Polym. Adv. Technol.*
2011, *22,* 2626–2632. doi:10.1002/pat.1815

46. Król, P.; Chmielarz, P. *eXPRESS Polym. Lett.* **2013,** *7,* 249–260.
doi:10.3144/expresspolymlett.2013.23

47. Król, P.; Chmielarz, P. *Polimery (Warsaw, Pol.)* **2014,** *59,* 279–292.
doi:10.14314/polimery.2014.279

48. Williams, V. A.; Ribelli, T. G.; Chmielarz, P.; Park, S.;
Matyjaszewski, K. *J. Am. Chem. Soc.* **2015,** *137,* 1428–1431.
doi:10.1021/ja512519j

49. Chmielarz, P.; Krys, P.; Park, S.; Matyjaszewski, K. *Polymer* **2015,** *71,*
143–147. doi:10.1016/j.polymer.2015.06.042

50. Boyer, C.; Corrigan, N. A.; Jung, K.; Nguyen, D.; Nguyen, T.-K.;
Adnan, N. N. M.; Oliver, S.; Shanmugam, S.; Yeow, J. *Chem. Rev.*
2016, *116,* 1803–1949. doi:10.1021/acs.chemrev.5b00396

51. Lim, C.-H.; Ryan, M. D.; McCarthy, B. G.; Theriot, J. C.; Sartor, S. M.;
Damrauer, N. H.; Musgrave, C. B.; Miyake, G. M. *J. Am. Chem. Soc.*
2017, *139,* 348–355. doi:10.1021/jacs.6b11022

52. Arteta, S. M.; Vera, R.; Pérez, L. D. *J. Appl. Polym. Sci.* **2017,** *134,*
44482. doi:10.1002/app.44482

53. Krys, P.; Matyjaszewski, K. *Eur. Polym. J.* **2017,** *89,* 482–523.
doi:10.1016/j.eurpolymj.2017.02.034

54. Park, S.; Chmielarz, P.; Gennaro, A.; Matyjaszewski, K. *Angew. Chem., Int. Ed.* **2015,** *54,* 2388–2392. doi:10.1002/anie.201410598

55. Chmielarz, P.; Fantin, M.; Park, S.; Isse, A. A.; Gennaro, A.; Magenau, A. J. D.; Sobkowiak, A.; Matyjaszewski, K. *Prog. Polym. Sci.* **2017,** *69,* 47–78. doi:10.1016/j.progpolymsci.2017.02.005

56. Chmielarz, P.; Yan, J.; Krys, P.; Wang, Y.; Wang, Z.; Bockstaller, M. R.; Matyjaszewski, K. *Macromolecules* **2017,** *50,* 4151–4159. doi:10.1021/acs.macromol.7b00280

57. Magenau, A. J. D.; Strandwitz, N. C.; Gennaro, A.; Matyjaszewski, K. *Science* **2011,** *332,* 81–84. doi:10.1126/science.1202357

58. Konkolewicz, D.; Schröder, K.; Buback, J.; Bernhard, S.; Matyjaszewski, K. *ACS Macro Lett.* **2012,** *1,* 1219–1223. doi:10.1021/mz300457e

59. Nematollahi, D.; Malakzadeh, M. *J. Electroanal. Chem.* **2003,** *547,* 191–195. doi:10.1016/S0022-0728(03)00188-8

60. Bodini, M. E.; Copia, G.; Tapia, R.; Leighton, F.; Herrera, L. *Polyhedron* **1999,** *18,* 2233–2239. doi:10.1016/S0277-5387(99)00124-2

61. Masek, A.; Zaborski, M.; Chrzescijanska, E. *Food Chem.* **2011,** *127,* 699–704. doi:10.1016/j.foodchem.2010.12.127

62. Longmuir, I. S. Advances in polarography; proceedings of the second international congress held at Cambridge, 1959. Oxford, New York,: Symposium Publications Division, Pergamon Press, 1960.

63. Nicholson, R. S.; Shain, I. *Anal. Chem.* **1964,** *36,* 706–723. doi:10.1021/ac60210a007

64. Chmielarz, P. *Polymer* **2016,** *102,* 192–198. doi:10.1016/j.polymer.2016.09.007

65. Chmielarz, P.; Park, S.; Sobkowiak, A.; Matyjaszewski, K. *Polymer* **2016,** *88,* 36–42. doi:10.1016/j.polymer.2016.02.021

66. Yi, L.; Huang, C.; Zhou, W. *J. Polym. Sci., Part A: Polym. Chem.* **2012,** *50,* 1728–1739. doi:10.1002/pola.25939

67. Xu, G.; Wang, D.; Buchmeiser, M. R. *Macromol. Rapid Commun.* **2012,** *33,* 75–79. doi:10.1002/marc.201100521

68. Chmielarz, P. *eXPRESS Polym. Lett.* **2017,** *11,* 140–151. doi:10.3144/expresspolymlett.2017.15

The selective electrochemical fluorination of *S*-alkyl benzothioate and its derivatives

Shunsuke Kuribayashi[1], Tomoyuki Kurioka[2], Shinsuke Inagi[2], Ho-Jung Lu[3],
Biing-Jiun Uang[3] and Toshio Fuchigami[*1]

Letter

Address:
[1]Department of Electronic Chemistry, Tokyo Institute of Technology,
4259 Nagatsuta-cho, Midori-ku, Yokohama 226-8502, Japan,
[2]Department of Chemical Science and Engineering, School of
Materials and Chemical Technology, Tokyo Institute of Technology,
4259 Nagatsuta-cho, Midori-ku, Yokohama 226-8502, Japan and
[3]Department of Chemistry, National Tsing Hua University, 101, Sec 2,
Kuang Fu Rd., Hsinchu 300, Taiwan, R.O.C

Email:
Toshio Fuchigami[*] - fuchi@echem.titech.ac.jp

* Corresponding author

Abstract

We herein report that the regioselective anodic fluorination of *S*-alkyl benzothioate and its derivatives in various aprotic solvents using $Et_3N·nHF$ ($n = 3–5$) and $Et_4NF·nHF$ ($n = 3–5$) as supporting electrolyte and a fluorine source successfully provided the corresponding α-fluorinated products in moderate yields. Dichloromethane containing $Et_4NF·4HF$ was found to be the most suitable combination as electrolytic solvent and supporting salt as well as fluorine source for the anodic fluorination. The electrochemical fluorination of cyclic benzothioates such as benzothiophenone was also achieved.

Introduction

Due to the interesting properties of fluorine atoms and carbon–fluorine bonds, organofluorine compounds are widely used in various fields like pharmaceutical chemistry, agrochemistry, and materials sciences [1,2]. Therefore, the selective fluorination of organic compounds is highly useful for the development of novel organofluorine compounds. Although a number of fluorination reagents have been developed so far, they have still some problems, i.e., they are costly, difficult to

handle, and explosive [3,4]. On the other hand, Rozhkov and Laurent reported an electrochemical partial fluorination of naphthalene and olefins about 30 years ago [5,6]. However, at that time, there has been no report on the anodic fluorination of heteroatom-containing compounds. At almost the same time, we found that the anodic α-methoxylation of organosulfur and amino compounds was generally enhanced by the presence of an α-electron-withdrawing group (EWG) such as a CF_3 group.

Here, the deprotonation of an anodically generated radical cation intermediate is accelerated by an EWG [7,8]. Based on these facts, we successfully achieved the first anodic fluorination of sulfides having various EWGs at their α-position using Et₃N·3HF [9,10]. Since then, we have systematically studied the electrochemical fluorination of numerous organic compounds, heterocycles, and macromolecules by using various fluoride salts such as Et₃N·*n*HF (*n* = 3–5) and Et₄NF·*n*HF (*n* = 3–5) [11-19].

On the other hand, Simonet and co-workers reported the anodic fluorination of alkyl phenyl sulfides having an EWG on the phenyl group in Et₃N·3HF/MeCN to provide α-monofluorinated products in moderate yields [20]. We also achieved the anodic fluorination of benzyl and ethyl thiocyanates as well as *O*-methyl *S*-aralkyl thiocarbonates by using the anodically stable Et₃N·5HF and Et₄NF·4HF [21,22]. In both cases, an EWG attached to the phenyl group and the electron-withdrawing SCN group both contribute to the generation of the cation resulting in a regioselective α-fluorination. Based on these findings, we anticipated that the α-cationic intermediate could also be generated anodically from *S*-alkyl benzothioates. Moreover, we previously successfully carried out an anodic fluorodesulfurization of *S*-aryl thiobenzoates, and found that the indirect electrolysis using a triarylamine mediator gave much better yields of benzoyl fluorides compared to the direct electrolysis [23]. Therefore, we became interested in the anodic behavior of *S*-alkyl benzothioates in the presence of fluoride ions. With this in mind and in order to provide an additional application of our electrochemical fluorination, we have studied the anodic fluorination of *S*-alkyl benzothioate and its derivatives as well as its cyclic analogues such as benzothiophenone.

Results and Discussion
Oxidation potentials of *S*-butyl benzothioates

At first, the anodic oxidation potentials of *S*-butyl benzothioate (**1a**), *S*-butyl *p*-chlorobenzothioate (**1b**), and *S*-butyl *p*-fluorobenzothioate (**1c**) were determined by cyclic voltammetry (CV). The compounds did not exhibit clear oxidation peaks, however, discharge started at around +2.3 V to +2.4 V vs SCE as exemplified in Figure 1 (CV curves of **1a**). Thus, it was found that these compounds have rather high oxidation potentials. DFT calculation of **1a** indicated that the highest occupied molecular orbital (HOMO) is located at the sulfur atom (Figure 2). Although sulfur atoms are easily oxidized, the oxidation potential of **1a** was found to be extremely high, that is due to the strongly electron-withdrawing benzoyl group attached to the sulfur atom. Benzyl thiocyanate is also known to be oxidized at a high potential which is similar to that of **1a** [21].
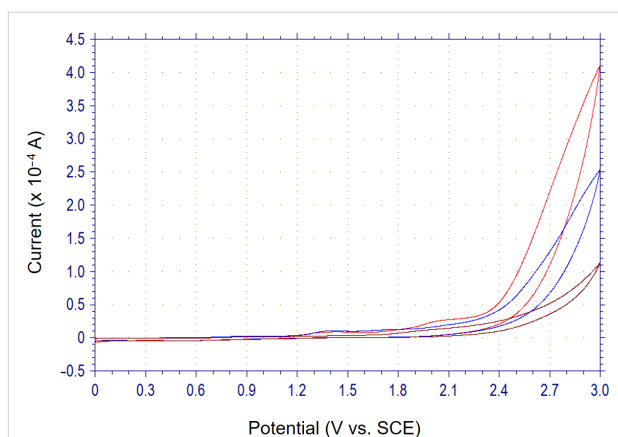

Figure 1: Cyclic voltammograms of 0.1 M Bu₄NBF₄/MeCN with a Pt disk working electrode in the absence (brown line) and presence of 5.0 mM (blue line) and 10.0 mM **1a** (red line). Scan rate of 100 mV/s.
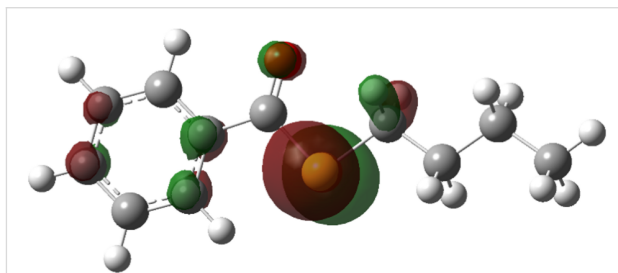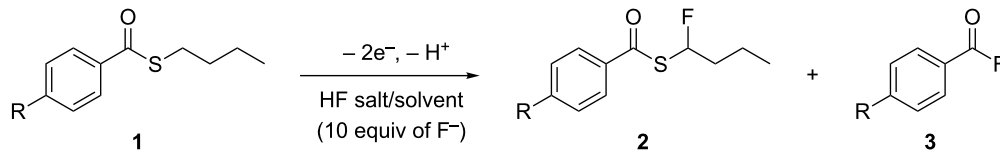

Figure 2: Calculated HOMO diagram of **1a**.

Anodic fluorination of *S*-butyl benzothioates

Next, we carried out the anodic fluorination of **1a** as a model compound under various electrolytic conditions. Electrolysis was performed at a constant current (40 mA) with platinum electrodes (2 cm × 2 cm) in several solvents containing various fluoride salts in an undivided cell at room temperature and current was passed basically until **1a** was consumed. The results are summarized in Table 1.

Regardless of the electrolytic conditions, the anodic fluorination proceeded to provide the desired fluorinated product **2a** except for the electrolysis performed in dimethoxyethane (DME) as the solvent (Table 1, entry 3). The oxidation potential of **1a** is rather high, while that of DME is relatively low [24]. Therefore, DME seems to be oxidized prior to **1a** resulting in no formation of **2a**, and **1a** was mostly recovered even when passing the theoretical amount of electricity (2 F/mol). Among the solvents tested, CH₂Cl₂ was found to be the best and the desired fluorinated product **2a** was obtained in 55% yield (Table 1, entry 1). In this case, the starting **1a** was consumed completely at 4.5 F/mol. It is well known that the fluoride salt, Et₃N·3HF is easily oxidized (2.0 V vs Ag/Ag⁺) because it contains a considerable amount of free Et₃N [25].

Table 1: Electrochemical fluorination of *S*-butyl benzothioate derivatives.

entry	compound	R	supporting electrolyte	solvent	electricity (F/mol)	yield (%)[a] 2	3
1	**1a**	H	$Et_3N·3HF$	CH_2Cl_2	4.5	55	–
2	**1a**	H	$Et_3N·3HF$	CH_3CN	7.0	26	–
3	**1a**	H	$Et_3N·3HF$	DME	2.0	0[b]	–
4	**1a**	H	$Et_3N·3HF$	CH_3NO_2	7.0	29	–
5	**1a**	H	$Et_3N·4HF$	CH_2Cl_2	4.5	56	–
6	**1a**	H	$Et_3N·5HF$	CH_2Cl_2	4.0	43	–
7	**1a**	H	$Et_4NF·3HF$	CH_2Cl_2	5.4	57	–
8	**1a**	H	$Et_4NF·4HF$	CH_2Cl_2	4.0	55	–
9	**1a**	H	$Et_4NF·5HF$	CH_2Cl_2	4.0	38	–
10[c]	**1a**	H	$Et_4NF·4HF$	CH_2Cl_2	4.0	67 (61)	12
11[c]	**1b**	Cl	$Et_4NF·4HF$	CH_2Cl_2	6.0	51 (45)	20
12[c]	**1c**	F	$Et_4NF·4HF$	CH_2Cl_2	4.0	60 (50)	9

[a]Determined by ^{19}F NMR. Isolated yield is shown in parentheses. [b]Substrate **1a** was mostly recovered. [c]Twenty equiv of the fluoride source were used.

However, the fluorination proceeded well particularly in a CH_2Cl_2 solution containing $Et_3N·3HF$. In contrast, when MeCN and $MeNO_2$ were used as an electrolytic solvent, the yield was decreased considerably (Table 1, entries 2 and 4). This is because of a low conversion of **1a** in these solvents and indeed a large amount of **1a** was recovered.
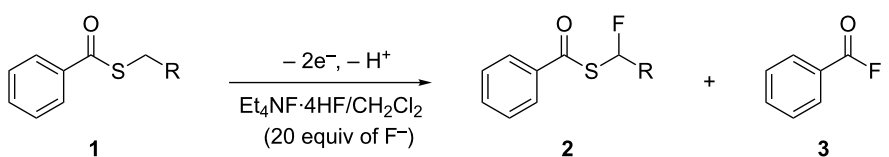
Subsequently the effect of different fluoride salts on the fluorination was investigated similarly (Table 1, entries 5–9). Regardless of the fluoride salts, product **2a** was obtained in moderate yield, however, using $Et_4NF·4HF$ gave the best current efficiency for the formation of **2a** (Table 1, entry 8). Increasing the amount of $Et_4NF·4HF$ from 10 to 20 equiv, the product yield was also increased from 55% to 67% (Table 1, entry 10). However, in this case, C–S bond cleavage also took place to form benzoyl fluoride (**3a**) as a byproduct in considerable amounts. In all cases, no fluorination at the phenyl group took place.

Then, this anodic fluorination was extended to *p*-chloro- and *p*-fluorobenzothioates, (**1b**) and (**1c**), using 20 equiv of $Et_4NF·4HF$ as the supporting electrolyte (Table 1, entries 11 and 12). In both cases, a fluorine atom was introduced selectively to the α-position to provide **2b** and **2c** in moderate yields. However, the corresponding benzoyl fluorides **3b** and **3c** were also formed similarly to the case of **1a**.

Anodic fluorination of *S*-(ω-substituted alkyl) benzylthioates

Initially, the oxidation potentials of various *S*-(substituted alkyl) benzylthioates **1d**–**j** were determined by CVs in 0.1 M Bu_4NBF_4/MeCN similarly to the case of **1a** and the results are collected in Table 2. Unexpectedly, no relationship between the substituents and the oxidation potentials could be observed. Next, the anodic fluorination of **1d**–**j** was carried out at a constant current in $Et_4NF·4HF$/CH_2Cl_2 and the results are summarized also in Table 2.

Regardless of the substituents, the anodic fluorination took place to afford the corresponding α-fluorinated products **2** in moderate to reasonable yields along with benzoyl fluoride as byproduct (Table 2). Generally, no fluorination of the phenyl ring was observed. In the case of **1h**, electron transfer seems to take place from both the sulfur atom and the α-phenyl group, which was suggested by DFT calculation (Figure 3). However, regardless of the discharging sites, the same cationic intermediate is generated through two-electron oxidation and deprotonation (in α position to both the sulfur atom and phenyl group), which forms the α-fluorinated product **2h** selectively. In contrast, the electron transfer of **1i** seems to take place mainly from the β-phenyl group as indicated by DFT calculation (Figure 3). As shown in Scheme 1, an electron transfer from the

**Table 2:** Oxidation potentials and electrochemical fluorination of *S*-substituted alkyl benzothioates.

entry	compound	R	oxidation potential (V vs SCE)	electricity (F/mol)	yield (%)[a]	
					2	**3**
1	**1a**	*n*-Pr-	2.3	4.0	67 (61)	12
2	**1d**	NCCH₂CH₂-	2.1	6.0	43 (35)	12
3	**1e**	MeOCH₂CH₂-	2.0	6.0	33 (29)	19
4	**1f**	EtOOC-	2.2	6.0	36 (29)	12
5	**1g**	HC≡C-	2.3	8.0	40 (37)	10
6	**1h**	Ph-	2.1	4.0	56 (46)	5
7	**1i**	PhCH₂-	2.2	6.0	10 (7)	5
8	**1j**	*p*-CF₃C₆H₄CH₂-	2.1	6.0	48 (40)	12

[a]Determined by ¹⁹F NMR. Isolated yields are shown in parentheses.
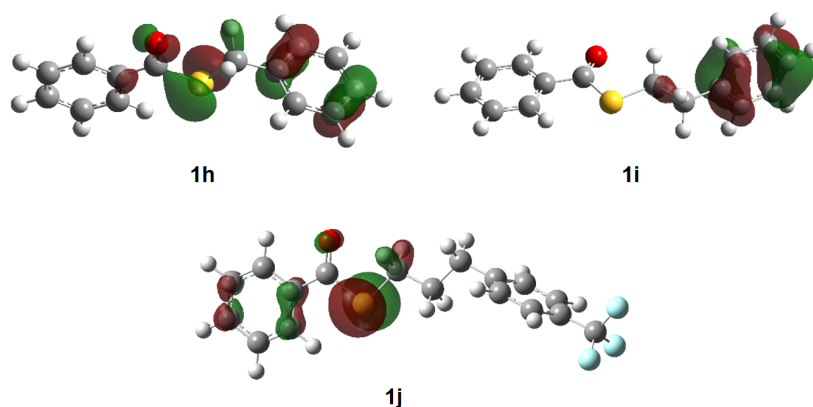
Figure 3: Calculated HOMO diagrams of **1h**, **1i** and **1j**.
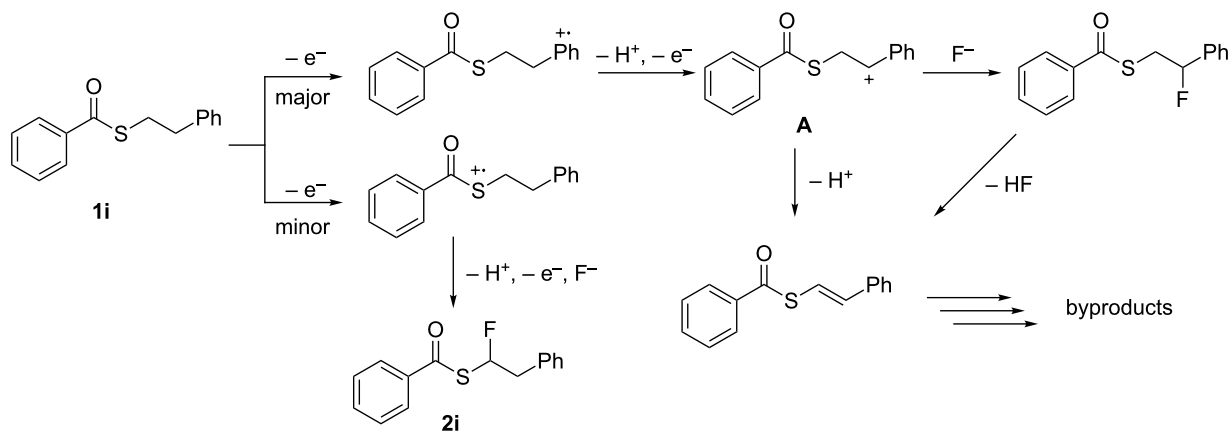
Scheme 1: Plausible reaction paths of the anodic oxidation of **1i** in Et₄NF·4HF/CH₂Cl₂.

β-phenyl group in **1i** followed by deprotonation and an additional electron transfer generates the benzylic cationic intermediate **A**, which affords the benzylic fluorinated product. It is known that benzylic fluorinated compounds are known to be generally prone to lose a fluoride anion [26]. On the other hand, intermediate **A** may undergo also elimination of a β-proton due to the electron-withdrawing benzothioate group prior to the reaction with fluoride as reported before [27]. As a consequence the expected α-fluorinated product **2i** was formed in an only low yield of 10%.

In order to suppress the discharge from the β-phenyl group of **1i**, a strongly electron-withdrawing CF₃ group was introduced in the *para*-position of the phenyl group. The HOMO of **1j** was found to be located mainly at the sulfur atom as determined by DFT calculation (Figure 3). As expected, the anodic fluorination proceeded to provide the α-fluorinated product **2j** in a moderate yield of 48%.

Next, the anodic fluorination was performed with the benzothioate derivative **1k** having a camphor group as a chiral auxiliary. The anodic fluorination proceeded to afford the corresponding α-fluoro products as a diastereoisomeric mixture (43% de) in a reasonable yield 42% along with benzoyl fluoride as byproduct (Scheme 2).

Scheme 2: Anodic fluorination of **1k**.
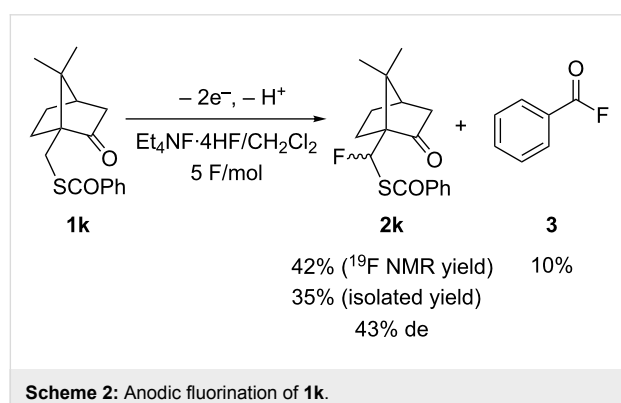
We next also carried out the anodic fluorination of a cyclic benzothioate namely benzothiophenone **1l**. In this case, the fluorination took place predominantly at the benzylic position to

afford the fluorinated product **2l** in 60% isolated yield (Scheme 3). With this substrate, neither C–S bond cleavage nor benzene ring fluorination took place at all.
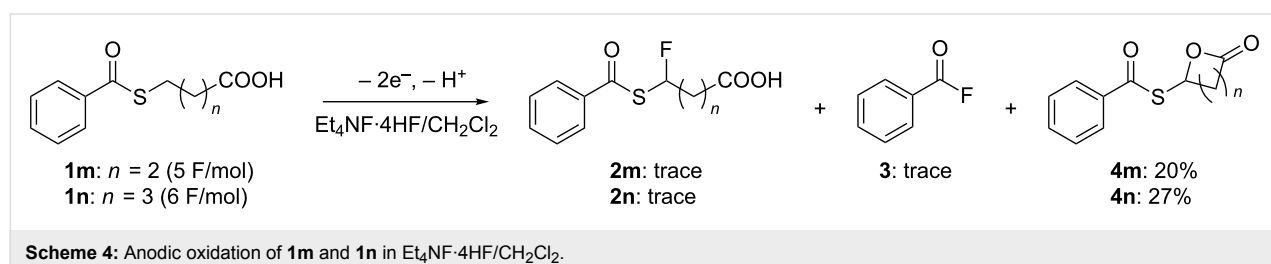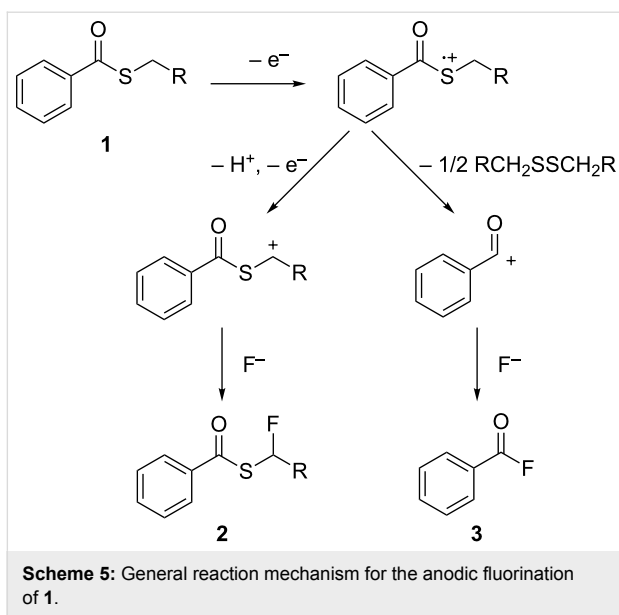

Scheme 3: Anodic fluorination of cyclic derivative **1l**.
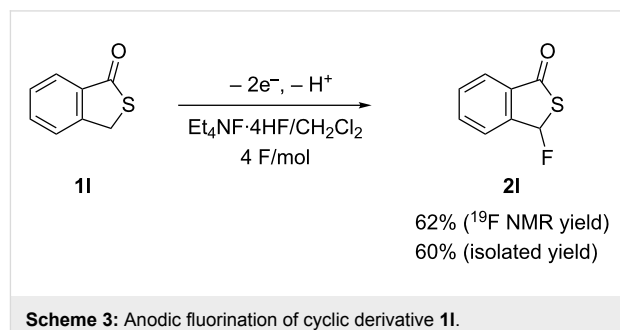
Finally, the anodic fluorination of benzothioates having a γ and δ-carboxyl group, **1m** and **1n**, was examined. The anodic oxidation of **1m** and **1n** proceeded; however, α-fluorination did not occur. In both cases, an anodic intramolecular cyclization took place to give the corresponding lactone derivatives in reasonable yields as shown in Scheme 4.

Reaction mechanism

In the cases of open-chain benzothioate derivatives, the anodic fluorination is initiated by an electron transfer occurring mainly from the sulfur atom of the benzothioates following two pathways (Scheme 5). The main pathway comprises the elimination of an α-proton, which is facilitated by the presence of an electron-withdrawing benzoyl group followed by another one-electron oxidation to generate a cationic intermediate which upon reaction with fluoride forms the α-fluorinated products. On the other hand, a minor pathway involves a C–S bond cleavage to form benzoyl fluoride as is observed in the case of the anodic oxidation of *S*-aryl benzothioates [23].

In the case of *S*-alkyl benzothioates bearing a carboxyl group at the γ and δ-position with respect to the sulfur atom, after generation of an α-cationic intermediate, the intramolecular cyclization seems to take place faster than combination with a fluoride ion as shown in Scheme 6. In support of this, we have reported a fluoride ion-promoted anodic cyclization of α-(phenylthio)-*N*-phenyl- and α-(phenylthio)-*N*-benzylacetamides [28] as well as

Scheme 4: Anodic oxidation of **1m** and **1n** in Et₄NF·4HF/CH₂Cl₂.

Scheme 5: General reaction mechanism for the anodic fluorination of **1**.

2-(*tert*-butoxycarbonyl)oxy-3,3,3-trifluoropropyl phenyl sulfide [29].

Conclusion

In summary, we have achieved the regioselective anodic fluorination of various *S*-alkyl and *S*-substituted alkyl benzothioate derivatives in Et₄NF·4HF/CH₂Cl₂ and a fluorine atom was selectively introduced in the α-position to the sulfur atom. Under the conditions, a camphor-substituted analogue was anodically fluorinated with moderate diastereoselectivity. Moreover, the anodic fluorination of a cyclic benzothioate such as benzothiophenone was also successfully demonstrated. In contrast, the anodic fluorination of *S*-(ω-carboxy)alkyl benzothioates afforded intramolecular cyclization products like lactones instead of the corresponding α-fluorinated products.

Experimental
General information

^{1}H, ^{13}C and ^{19}F NMR spectra were recorded on a JEOL JNM EX-270 (^{1}H: 270 MHz, ^{13}C: 67.8 MHz, ^{19}F: 254.05 MHz) spectrometer in CDCl₃. The chemical shifts for ^{1}H, ^{13}C and ^{19}F NMR spectra are given in δ (ppm) from internal TMS,

CDCl₃ and monofluorobenzene, respectively. Cyclic voltammetry was performed using an ALS Instrument model 600A. Preparative electrolysis experiments were carried out with Metronnix Corp. (Tokyo) constant current power supply model 5944 by monitoring electricity with a Hokutodenko Coulomb/Ampere-hour meter HF-201.
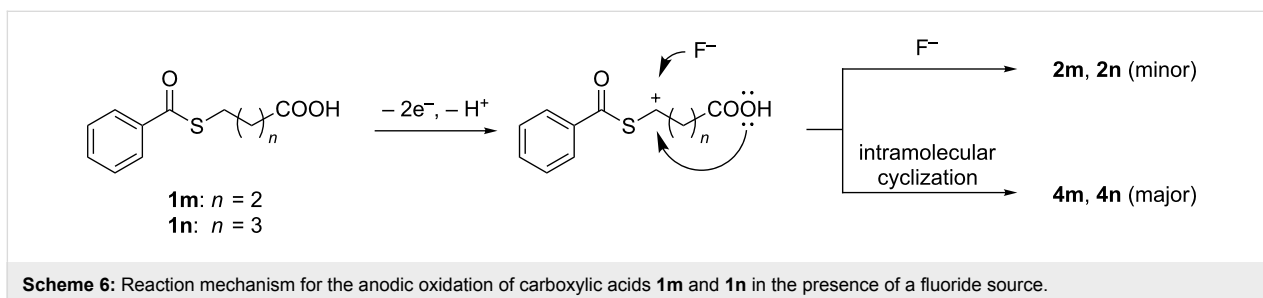
Cyclic voltammetry measurements

Cyclic voltammetry was carried out in 0.1 M Bu₄NBF₄/MeCN using a glass cell. A platinum disk electrode ($\varnothing$ = 0.8 mm) was used as a working electrode. A platinum plate (1 cm × 1 cm) was used as a counter electrode and a saturated calomel electrode was used as a reference electrode. Electrolyte solutions for cyclic voltammetry were deoxygenated with bubbling N₂ gas before use.

Materials

The starting materials were prepared according to the literature procedures [21,23,30,31]. The known compounds, **1a**,**1b** [32], **1c** [33], **1f**–**1h** [34], **1i** [35], **1k** [36], **1l** [31], **1m** [37] and **1n** [38] were characterized by comparison of the spectral data with those reported in the literature.

General procedure for the anodic fluorination

Analogous as described in [17], the anodic oxidation of a substrate (1 mmol) was carried out in a plastic undivided cell equipped with platinum anode and cathode (2 cm × 2 cm) containing 10 mL of HF salt (20 equiv of F⁻ to substrate/solvent) at room temperature. A constant current (40 mA) was passed until the starting material was mostly consumed (monitored by TLC). After electrolysis, the electrolytic solution was passed through a short column filled with silica gel using EtOAc as an eluent to remove the HF salt. The fluorinated product was further purified by silica gel column or preparative thin layer chromatography using a solution of hexane/EtOAc (20:1 to 1:1) as an eluent. The yield of the fluorinated products were estimated by ^{19}F NMR using monofluorobenzene as an internal standard. The known fluorinated products, benzoyl fluoride [39], *p*-chlorobenzoyl fluoride [40] and *p*-fluorobenzoyl fluoride [41] were identified by comparison with ^{19}F NMR and MS spectral data of the authentic samples.

Scheme 6: Reaction mechanism for the anodic oxidation of carboxylic acids **1m** and **1n** in the presence of a fluoride source.

Supporting Information

Supporting Information File 1

Characterization data.

[https://www.beilstein-journals.org/bjoc/content/
supplementary/1860-5397-14-27-S1.pdf]

Acknowledgements

ORCID® iDs

Shinsuke Inagi - https://orcid.org/0000-0002-9867-1210

References

1. Purser, S.; Moore, P. R.; Swallow, S.; Gouvermeur, V. *Chem. Soc. Rev.* **2008,** *37,* 320–330. doi:10.1039/b610213c
2. Boschet, F.; Ameduri, B. *Chem. Rev.* **2014,** *114,* 927–980. doi:10.1021/cr2002933
3. Umemoto, T.; Singh, R. P.; Xu, Y.; Saito, N. *J. Am. Chem. Soc.* **2010,** *132,* 18199–18205. doi:10.1021/ja106343h
4. Tang, P.; Wang, W.; Ritter, T. *J. Am. Chem. Soc.* **2011,** *133,* 11482–11484. doi:10.1021/ja2048072
5. Rozhkov, I. N. In *Organic Electrochemistry,* 2nd ed.; Baizer, M. M.; Lund, H., Eds.; chapter 24; Marcel Decker: New York, 1983.
6. Laurent, E.; Marquet, B.; Tardivel, R.; Thiebault, H. *Bull. Soc. Chim. Fr.* **1986,** 955–964.
7. Fuchigami, T.; Nakagawa, Y.; Nonaka, T. *Tetrahedron Lett.* **1986,** *27,* 3869–3872. doi:10.1016/S0040-4039(00)83902-7
8. Fuchigami, T.; Nakagawa, Y.; Nonaka, T. *J. Org. Chem.* **1987,** *52,* 5489–5491. doi:10.1021/jo00233a043
9. Fuchigami, T.; Shimojo, M.; Konno, A.; Nakagawa, K. *J. Org. Chem.* **1990,** *55,* 6074–6075. doi:10.1021/jo00312a006
10. Konno, A.; Nakagawa, K.; Fuchigami, T. *J. Chem. Soc., Chem. Commun.* **1991,** 1027–1029. doi:10.1039/C39910001027
11. Fuchigami, T. In *Organic Electrochemistry,* 4th ed.; Lund, H.; Hammerich, O., Eds.; chapter 25; Marcel Dekker: New York, 2001.
12. Noel, M.; Suryanarayanan, V. *J. Appl. Electrochem.* **2004,** *34,* 357–369. doi:10.1023/B:JACH.0000016670.97434.c7
13. Dawood, K. M. *Tetrahedron* **2004,** *60,* 1435–1451. doi:10.1016/j.tet.2003.11.017
14. Fuchigami, T.; Inagi, S. *Chem. Commun.* **2011,** *47,* 10211–10223. doi:10.1039/C1CC12414E
15. Fuchigami, T.; Inagi, S. In *Organic Electrochemistry,,* 5th ed.; Hammerich, O.; Speiser, B., Eds.; chapter 20; CRC Press: Boca Raton, FL, 2015.
16. Fuchigami, T.; Inagi, S. Organic Electrosynthesis. In *Fundamentals and Applications of Organic Electrochemistry;* Fuchigami,, T.; Atobe, M.; Inagi, S., Eds.; chapter 5; Wiley: West Sussex, 2015. doi:10.1002/9781118670750.ch05
17. Kuribayashi, S.; Shida, N.; Inagi, S.; Fuchigami, T. *Tetrahedron* **2016,** *72,* 5343–5349. doi:10.1016/j.tet.2016.07.016
18. Tanigawa, M.; Kuriyama, Y.; Inagi, S.; Fuchigami, T. *Electrochim. Acta* **2016,** *199,* 314–318. doi:10.1016/j.electacta.2016.02.051
19. Suzuki, J.; Shida, N.; Inagi, S.; Fuchigami, T. *Electroanalysis* **2016,** *28,* 2797–2801. doi:10.1002/elan.201600130
20. Boroux, P.; Tardivel, R.; Simonet, J. *J. Electrochem. Soc.* **1997,** *144,* 841–847. doi:10.1149/1.1837498
21. Hou, Y.; Higashiya, S.; Fuchigami, T. *Electrochim. Acta* **2000,** *45,* 3005–3010. doi:10.1016/S0013-4686(00)00379-0
22. Cao, Y.; Fuchigami, T. *J. Electroanal. Chem.* **2006,** *587,* 25–30. doi:10.1016/j.jelechem.2005.10.010
23. Shen, Y.; Suzuki, K.; Atobe, M.; Fuchigami, T. *J. Electroanal. Chem.* **2003,** *540,* 189–194. doi:10.1016/S0022-0728(02)01297-4
24. Hou, Y.; Fuchigami, T. *J. Electrochem. Soc.* **2000,** *147,* 4567–4572. doi:10.1149/1.1394102
25. Chen, S.-Q.; Hatakeyama, T.; Fukuhara, T.; Hara, S.; Yoneda, N. *Electrochim. Acta* **1997,** *42,* 1951–1960. doi:10.1016/S0013-4686(97)85466-7
26. Fuchigami, T.; Shimojo, M.; Konno, A. *J. Org. Chem.* **1995,** *60,* 3459–3464. doi:10.1021/jo00116a037
27. Erian, A. W.; Konno, A.; Fuchigami, T. *J. Org. Chem.* **1995,** *60,* 7654–7659. doi:10.1021/jo00128a044
28. Shen, Y.; Atobe, M.; Fuchigami, T. *Org. Lett.* **2004,** *6,* 2441–2444. doi:10.1021/ol049152f
29. Isokawa, M.; Sano, M.; Kubota, K.; Suzuki, K.; Inagi, S.; Fuchigami, T. *J. Electrochem. Soc.* **2017,** *164,* G121–G127. doi:10.1149/2.1601713jes
30. Riyadh, S. M.; Ishii, H.; Fuchigami, T. *Tetrahedron* **2002,** *58,* 5877–5883. doi:10.1016/S0040-4020(02)00559-8
31. Lee, E.-S.; Choi, B.-W.; Jung, D.-I.; Hwang, H.-J.; Han, J.-T.; Lee, B.-H. *Bull. Korean Chem. Soc.* **2003,** *24,* 243–245. doi:10.5012/bkcs.2003.24.2.243
32. Qiao, Z.; Jiang, X. *Org. Lett.* **2016,** *18,* 1550–1553. doi:10.1021/acs.orglett.6b00324
33. Ogawa, K. A.; Boydston, A. J. *Org. Lett.* **2014,** *16,* 1928–1931. doi:10.1021/ol500459x
34. Lu, G.-p.; Cai, C. *Adv. Synth. Catal.* **2013,** *355,* 1271–1276. doi:10.1002/adsc.201201059
35. Moon, H. K.; Sung, G. H.; Kim, B. R.; Park, J. K.; Yoon, Y.-J.; Yoon, H. J. *Adv. Synth. Catal.* **2016,** *358,* 1725–1730. doi:10.1002/adsc.201501177
36. Montenegro, E.; Echarri, R.; Claver, C.; Castillón, S.; Moyano, A.; Pericàs, M. A.; Riera, A. *Tetrahedron: Asymmetry* **1996,** *7,* 3553–3558. doi:10.1016/S0957-4166(96)00463-6
37. Oya, M.; Baba, T.; Kato, E.; Kawashima, Y.; Watanabe, T. *Chem. Pharm. Bull.* **1982,** *30,* 440–461. doi:10.1248/cpb.30.440
38. Beckwith, A. L. J.; Duggan, S. A. M. *J. Chem. Soc., Perkin Trans. 2* **1994,** 1509–1518. doi:10.1039/P29940001509
39. Beaulieu, F.; Beauregard, L.-P.; Courchesne, G.; Couturier, M.; LaFlamme, F.; L'Heureux, A. *Org. Lett.* **2009,** *11,* 5050–5053. doi:10.1021/ol902039q
40. Bildsoe, H.; Schaumburg, K. *J. Magn. Reson.* **1974,** *14,* 223–234. doi:10.1016/0022-2364(74)90275-3
41. Birrell, J. A.; Desrosiers, J.-N.; Jacobsen, E. N. *J. Am. Chem. Soc.* **2011,** *133,* 13872–13875. doi:10.1021/ja205602j

Functionalization of *N*-arylglycine esters: electrocatalytic access to C–C bonds mediated by *n*-Bu₄NI

Mi-Hai Luo[1], Yang-Ye Jiang[1], Kun Xu[1], Yong-Guo Liu[2], Bao-Guo Sun[2] and Cheng-Chu Zeng[*1]

Abstract

An efficient electrocatalytic functionalization of *N*-arylglycine esters is reported. The protocol proceeds in an undivided cell under constant current conditions employing the simple, cheap and readily available *n*-Bu₄NI as the mediator. In addition, it is demonstrated that the mediated process is superior to the direct electrochemical functionalization.

Introduction

The oxidative cross dehydrogenative coupling (CDC) of two C–H bonds has emerged as an versatile and powerful strategy for forming new C–C bonds in organic chemistry due to its step and atom economic characteristic as well as avoiding the prefunctionalization of substrates [1-5]. Most of the CDC reactions occur between the benzylic C–H bonds and α-C–H bonds adjacent to a heteroatom (N or O) [6-10]. However, the oxidative C–C formation of secondary amines, especially amino acids has been more important for studying properties and functions of natural and non-natural amino acids [11]. Consequently, efficient and selective construction of C–C bonds of

amino acids has always been paid much attention in industrial and academic setting and many advances have been made [12-17]. Li et al. first reported the functionalization of glycine derivatives with malonates using a stoichiometric quantity of Cu(OAc)₂ as catalyst and oxidant [12]. Later on, arylation, vinylation and alkynylation of glycine derivatives were also accomplished by the same group (Scheme 1) [13]. Using the Cu(OAc)₂/pyrrolidine dual catalysts system, Huang developed the oxidative cross coupling of glycine derivatives with acetone in the presence of TBHP or DDQ as terminal oxidants [14]. The protocol was also extended to reactions with 2-alkylquinoline
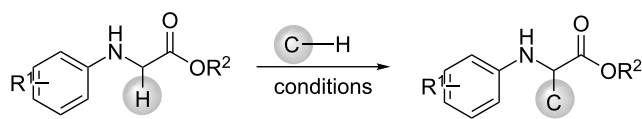
Li: Cu(OAc)$_2$ (2 equiv), (2-py)$_2$CO (0.2 equiv), Cs$_2$CO$_3$ (0.2 equiv), 150 °C

Huang: Cu(OAc)$_2$/O$_2$, 25% PivOH; Cu(OAc)$_2$/TBHP, DDQ or DTBP

Huo: CuCl/O$_2$, THF/H$_2$O

Wu: Ru(bpy)$_3$Cl$_2$, Cu(OTf)$_2$, air, visible light

this work: *n*-Bu$_4$NI (0.3 equiv), AcOH (0.5 equiv), electrolysis at 3 mA/cm^2, rt

Scheme 1: Cross dehydrogenative coupling of *N*-arylglycine esters with C–H nucleophiles.

[15] and phenols [16] using O$_2$ and di-*tert*-butyl peroxide (DTBP) as oxidant, respectively (Scheme 1). A CuCl-catalyzed oxidative cross coupling of glycine derivatives with indoles has been developed by Hou et al., wherein simple copper salts were used as catalysts and oxygen as the co-oxidant (Scheme 1) [17].

Alternatively, photocatalytic versions of CDC reactions of glycine derivatives with C-nucleophiles were also developed [18,19]. For example, combining the visible light catalyst Ru(bpy)$_3$Cl$_2$, and the transition metal catalyst Cu(OTf)$_2$, Wu and co-workers achieved aerobic oxidative coupling of secondary amines with β-keto esters to form C(sp^3)–C(sp^3) bonds (Scheme 1) [18].

Although much advance has been made for the functionalization of glycine derivatives, most of these strategies mentioned above require stoichiometric or excess amounts of chemical oxidants and transition metal (photo)catalysts. The utilization of stoichiometric or excess amounts of chemical oxidants results in producing waste, which is not atomic economically and environmentally benign. In addition, over-oxidation of products likely occurs in the presence of excess amounts of oxidant. On the other hand, the toxicity of residual traces of transition metal (photo)catalyst in products is also highly concerned. Consequently, metal-free and environmentally friendly oxidative C–C bond formation is highly desired.

Electrochemistry has proved to be an environmentally benign method to achieve the formation of a new chemical bond and a functional group conversion by using electrons as redox reagent rather than terminal chemicals [20-27]. In this context, we have applied simple halide ions as redox catalysts to achieve electrochemical C–H bond functionalization, leading to the formation of new C–C, C–N, C–O and C–S bonds [28-31]. Herein, we report the electrochemical α-C–H functionalization of *N*-arylglycine esters with C–H nucleophiles using *n*-Bu$_4$NI as redox catalyst (Scheme 1). The chemistry was performed in an undi-

vided cell under constant current electrolysis. It was observed that *n*-Bu$_4$NI promotes the reaction dramatically and higher yields of α-functionalized products were afforded compared with the direct electrolysis.

Results and Discussion

Initially, *N*-arylglycine ester **1a** and C–H nucleophile 1,3,5-trimethoxybenzene (**2a**) were chosen as model compounds to optimize the electrolytic conditions. As shown in Table 1, when constant current electrolysis (CCE) of **1a** and **2a** was performed in an undivided cell equipped with 0.1 M LiClO$_4$ in CH$_3$CN in the presence of AcOH using two graphite plates as anode and cathode, the desired product **3aa** was isolated in 27% yield (Table 1, entry 1). Replacing CH$_3$CN by other solvents, such as methanol, ethanol or CH$_2$Cl$_2$ failed to improve the reaction efficiency and only trace amounts of **3aa** were detected (Table 1, entries 2–4). Further solvent screening disclosed that a 1:2 ratio of CH$_3$CN and CH$_2$Cl$_2$ was better, giving **3aa** in 66% yield (Table 1, entries 5 and 6). Exploring the influence of current density on the CDC reaction indicated that 3 mA/cm^2 was suitable; lower or higher current density led to a slightly lower yields of **3aa** (entry 5, vs entries 7 and 8). It was observed that the additive plays an important role. Among several additives examined, AcOH was proved to be the best, although TFA also gave comparable yields of **3aa** (Table 1, entries 5 and 11–13), whereas, it gave only 38% yield of **3aa** when the reaction was carried out in the absence of AcOH (Table 1, entry 9). Investigation of the anode proved that graphite was superior to Pt and DSA (Dimensionally Stable Anode, Table 1, entries 14 and 15). Finally, to further improve the reaction efficiency, several halide-containing mediators as redox catalyst were evaluated. To our delight, when *n*-Bu$_4$NI was utilized as a redox catalyst, the yield of **3aa** increased to 81% (Table 1, entries 16–19).

On the basis of the screening of reaction conditions, we could conclude that the electrocatalytic oxidative coupling should be performed in a mixed solution of CH$_3$CN and CH$_2$Cl$_2$

Table 1: Optimization of reaction conditions[a].

entry	solvent	mediator (equiv)	J (mA/cm^2)	additive (equiv)	cathode/anode	yield (%)[b]
1	CH$_3$CN	–[c]	3	AcOH (0.5)	C/C	27
2	MeOH	–[c]	3	AcOH (0.5)	C/C	trace
3	EtOH	–[c]	3	AcOH (0.5)	C/C	trace
4[d]	CH$_2$Cl$_2$	–[c]	3	AcOH(0.5)	C/C	trace
5	CH$_3$CN/CH$_2$Cl$_2$ (1:2)	–[c]	3	AcOH (0.5)	C/C	66
6	CH$_3$CN/CH$_2$Cl$_2$ (2:1)	–[c]	3	AcOH (0.5)	C/C	56
7	CH$_3$CN/CH$_2$Cl$_2$ (1:2)	–[c]	1	AcOH (0.5)	C/C	47
8	CH$_3$CN/CH$_2$Cl$_2$(1:2)	–[c]	5	AcOH (0.5)	C/C	50
9	CH$_3$CN/CH$_2$Cl$_2$ (1:2)	–[c]	3	AcOH (0.0)	C/C	38
10	CH$_3$CN/CH$_2$Cl$_2$ (1:2)	–[c]	3	AcOH (1.0)	C/C	56
11	CH$_3$CN/CH$_2$Cl$_2$ (1:2)	–[c]	3	TFA (0.5)	C/C	60
12	CH$_3$CN/CH$_2$Cl$_2$ (1:2)	–[c]	3	H$_2$SO$_4$ (0.5)	C/C	13
13	CH$_3$CN/CH$_2$Cl$_2$ (1:2)	–[c]	3	Na$_2$CO$_3$ (0.5)	C/C	40
14	CH$_3$CN/CH$_2$Cl$_2$ (1:2)	–[c]	3	AcOH (0.5)	C/Pt	48
15	CH$_3$CN/CH$_2$Cl$_2$ (1:2)	–[c]	3	AcOH (0.5)	C/DSA	41
16	CH$_3$CN/CH$_2$Cl$_2$ (1:2)	*n*-Bu$_4$NI (0.3)	3	AcOH (0.5)	C/C	81
17	CH$_3$CN/CH$_2$Cl$_2$ (1:2)	*n*-Bu$_4$NBr (0.3)	3	AcOH (0.5)	C/C	48
18	CH$_3$CN/CH$_2$Cl$_2$ (1:2)	NH$_4$I (0.3)	3	AcOH (0.5)	C/C	54
19	CH$_3$CN/CH$_2$Cl$_2$ (1:2)	NH$_4$Br (0.3)	3	AcOH (0.5)	C/C	20

[a]Conditions: **1a** (1.0 mmol), **2a** (1.2 mmol) in 15 mL solution, LiClO$_4$ (0.1 M), room temperature, electrode C represents graphite plate. [b]Isolated yield. [c]Without mediator. [d]*n*-Bu$_4$NBF$_4$ was used as supporting electrolyte.

(v/v = 1:2), in the presence of *n*-Bu$_4$NI (30 mol %) as the mediator, AcOH (50 mol %) as the additive and using graphite plate as electrodes under constant current at 3 mA/cm^2. With the optimized conditions in hand, we then investigated the scope of *N*-arylglycine esters in the reaction with **2a**. As a comparison, direct electrochemical coupling of *N*-arylglycine esters with **2a** was also performed. As shown in Scheme 2, substituents including either electron-donating groups (such as methyl and methoxy) or electron-withdrawing groups (Cl, Br and CF$_3$) in the 4-position of the aryl group were tolerated and gave moderate to good yields of **3ba**–**3ea** (61–69% yields), whereas, only 47–58% yields of the desired **3ba**–**3ea** were isolated under the direct electrolytic conditions. However, **3fa** was afforded in 39% and 12% yields, respectively, when the electrochemical reaction was performed in the presence or absence of *n*-Bu$_4$NI as the redox catalyst. The reason for the low yield of **3fa** is not clear yet. Steric factors seem to play an important role in the electrochemical CDC reaction of *N*-arylglycine esters with **2a**. When the methyl group was situated at 2- or 3-position of the aniline, instead of in the 4-position, the corresponding products

3ga and **3ha** were afforded in 36% and 27% yields, respectively. However, **3ga** and **3ha** were isolated in 14% and 11% yields, respectively, under the direct electrolytic conditions. In the cases of *N*-arylglycine methyl ester **1i** and *N*-arylglycine benzyl ester **1j**, the electrocatalytic functionalization afforded excellent yields of **3ia** (76%) and **3ja** (84%), whereas, less efficiency (40–43% yields) was observed without the assistance of *n*-Bu$_4$NI.

Next, the reactivity of different C–H nucleophiles was also investigated. As shown in Scheme 3, β-keto ester and malonates worked well to afford the desired products **3ab**–**3ad** in moderate yields. In addition, naphthanols were also compatible in this transformation, giving the corresponding products **3ae**–**3ag** in good yields. Notably, when styrene and 1-ethynylbenzene were subjected to reaction with **1a** under the standard indirect electrolytic conditions, quinoline-2-carboxylate **3ah** was isolated in 64% and 58% yield, respectively. Substituted styrenes and 1-ethynylbenzene were also tolerated well, giving corresponding products **3ai**–**3aj** in 45–50% yields. The formations of
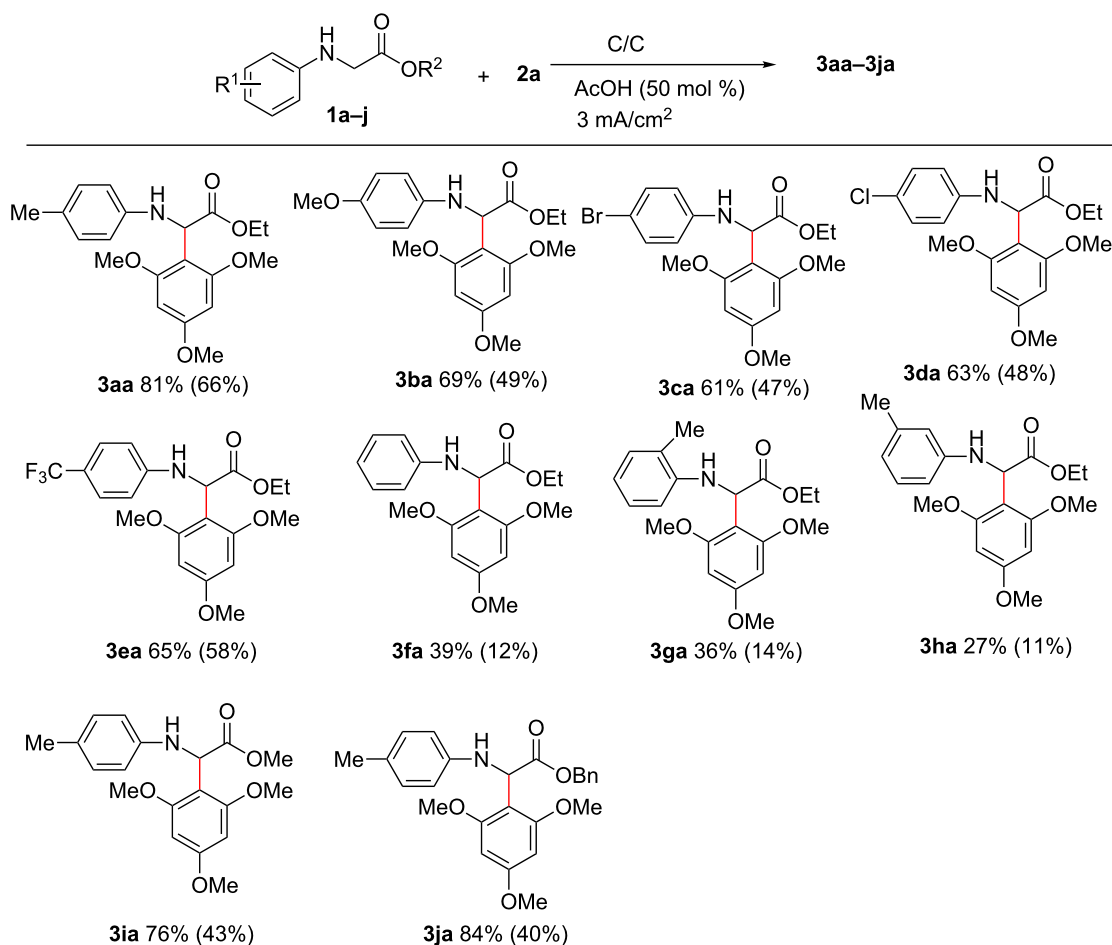
Scheme 2: Electrochemical CDC reaction of **2a** and various *N*-arylglycine esters. Reaction conditions for the indirect electrolysis: **1** (0.5 mmol), **2a** (0.6 mmol), *n*-Bu₄NI (30 mol %), 0.1 M LiClO₄/CH₃CN (5 mL) and CH₂Cl₂ (10 mL), AcOH (50 mol %), current density (3 mA/cm²), graphite anode and cathode, at room temperature; reaction conditions for direct electrolysis: **1** (0.5 mmol), **2a** (0.6 mmol), 0.1 M LiClO₄/CH₃CN (5 mL) and CH₂Cl₂ (10 mL), AcOH (50 mol %), current density (3 mA/cm²), graphite anode and cathode, at room temperature; yields in parenthesis obtained from direct electrolysis.

3ah–3aj likely derives from an azo-Diels–Alder reaction of styrene or ethynylbenzene with an imine intermediate, in situ generated from anodic oxidation of **1a**, followed by additional oxidation [32-36].

To prove the practicability of the protocol, a scaled-up reaction was also carried out. As illustrated in Scheme 4, when 6 mmol of ethyl *p*-tolylglycinate (**1a**) was allowed to react with 1,3,5-trimethoxybenzene (**2a**) under the standard conditions, adduct **3aa** was isolated in a 75% yield, without obvious losing of yield.

To better understand the reaction mechanism, control experiments were performed. As shown in Scheme 5, the anodic oxidation of **1a** in the absence of a C–H nucleophile under the standard conditions gives imine intermediate product **5**,

which was detected by TLC and GC–MS. Moreover, when separated synthesized **5** was subjected to react with **2a**, the corresponding product **3aa** was isolated in 89% yield. These control experiments indicate that **5** is a possible reaction intermediate.

Based on these control experiments described above, as well as related references [4], a plausible mechanism for the electrocatalytic cross dehydrogenative coupling of *N*-arylglycine esters **1** with C–H nucleophiles **2** is outlined in Scheme 6. The anodic oxidation of iodide generates the active species I₂ or I⁺. Followed by a homogeneous reaction with *N*-arylglycine esters, *N*-iodo intermediate **4** was generated. Eliminating a molecule of HI affords imine intermediate **5**. In the presence of acetic acid, the protonated **5**-H⁺ undergoes nucleophilic addition with C–H nucleophiles **2** to give the desired products **3**.
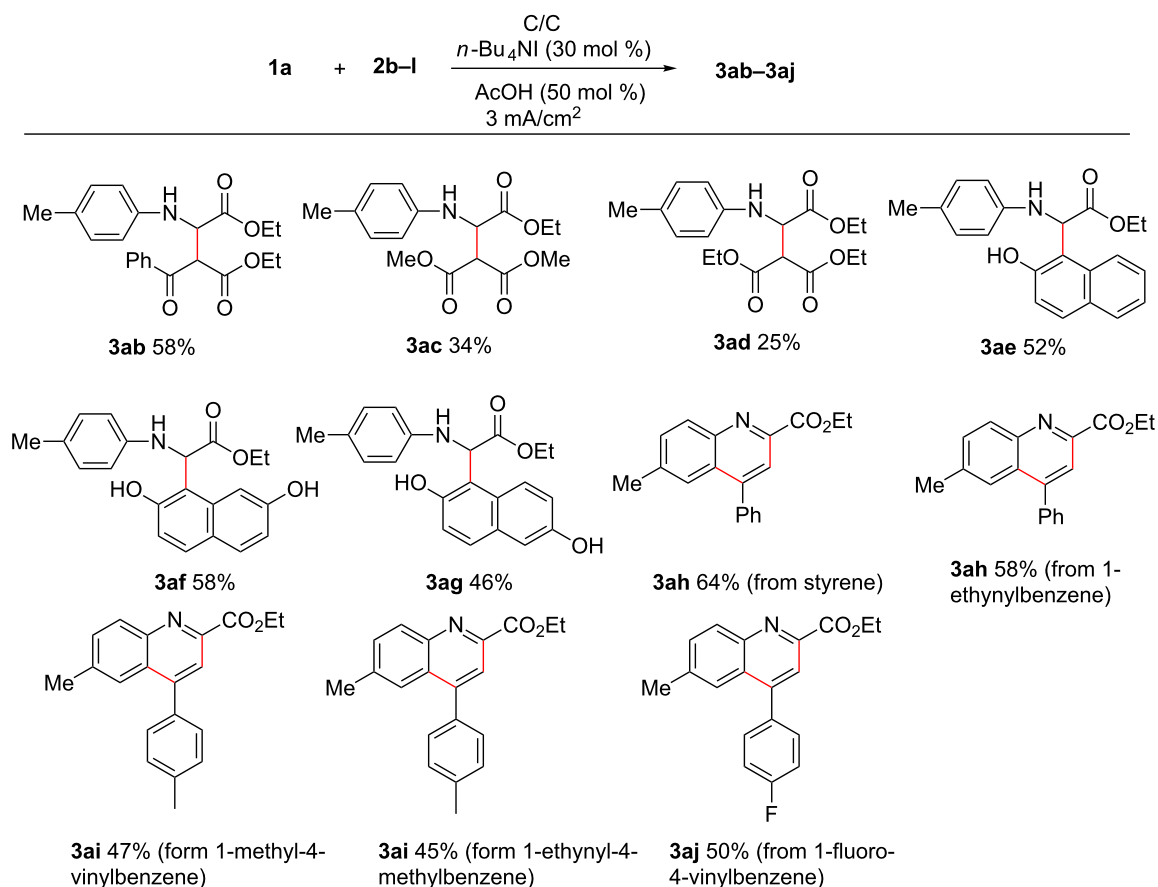
Scheme 3: Scope of **2** using *n*-Bu₄NI as mediator. Reaction conditions: **1a** (0.5 mmol), **2** (0.6 mmol), *n*-Bu₄NI (30 mol %), 0.1 M LiClO₄/CH₃CN (5 mL) and CH₂Cl₂ (10 mL), AcOH (50 mol %), current density (3 mA/cm²), graphite anode and cathode. Isolated yields are given.
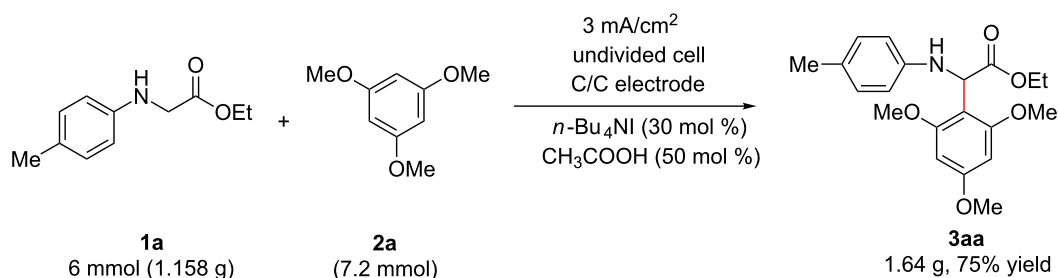

Scheme 4: Scaling up.

Conclusion

In summary, an efficient electrocatalytic cross dehydrogenative coupling of arylglycine esters with C–H nucleophiles has been developed. This protocol employs simple *n*-Bu₄NI as the redox catalyst, avoiding utilization of transition metals and excess amounts of external oxidant, thereby providing an environmentally benign method to the CDC reaction. In addition, it was observed that the electrocatalytic process is superior to the direct electrolysis. Further application of this electrochemical protocol for the formation of new C–C bonds is still on the way in our group.
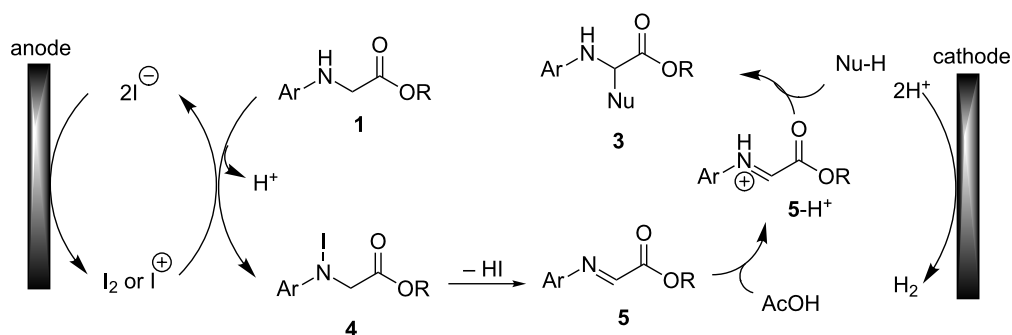
Experimental
Instruments and reagents

All melting points were measured with an electrothermal melting point apparatus and are uncorrected. NMR spectra were recorded using a 400 MHz or 300 MHz spectrometer (400 MHz ^{1}H frequency, 100 MHz ^{13}C frequency; 300 MHz ^{1}H frequen-
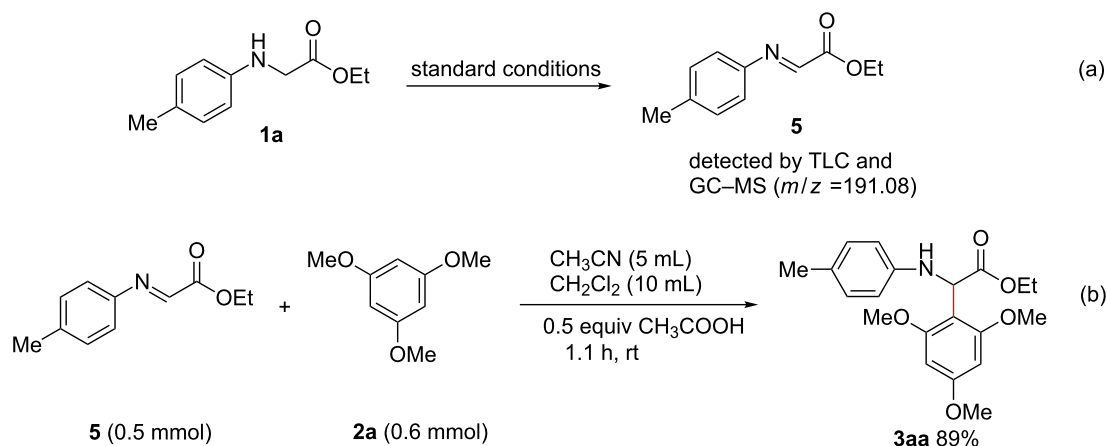
Scheme 5: Control experiments.

Scheme 6: A plausible mechanism for the electrocatalytic cross dehydrogenative coupling of *N*-arylglycine esters with C-nucleophiles.

cy, 75 MHz ^{13}C frequency). Chemical shifts are given as δ values (internal standard: TMS). Coupling constants are reported in Hz. All starting materials and solvents were obtained from commercial sources and used without further purification. Products were purified by chromatography on silica gel (petroleum ether/EtOAc).

Typical procedure for the electrocatalytic cross dehydrogenative coupling of *N*-arylglycine ester and C–H nucleophiles

An undivided cell was equipped with a carbon anode (2 × 2 cm^2) and a carbon cathode (2 × 2 cm^2) and connected to a DC regulated power supply. To the cell was added *N*-arylglycine ester (0.5 mmol), C–H nucleophiles (0.6 mmol), *n*-Bu$_4$NI (0.15 mmol) and 5 mL of 0.1 M LiClO$_4$/CH$_3$CN and 10 mL CH$_2$Cl$_2$. The mixture was electrolyzed using constant current conditions (≈3 mA/cm^2) at room temperature under magnetic stirring. When TLC analysis indicated that the electrolysis was complete (witnessed by the disappearance of the *N*-arylglycine ester), the solvent was removed under reduced

pressure. The residue was poured into a saturated aqueous solution of Na$_2$S$_2$O$_3$ and the product was then extracted with DCM (3 × 20 mL), dried over Na$_2$SO$_4$, and concentrated in vacuo. The residue was purified by column chromatography on silica gel using a mixture of petroleum ether/EtOAc (v/v = 3:1) as eluent to afford the desired pure product.

Typical procedure for the direct electrochemical cross dehydrogenative coupling of *N*-arylglycine ester and C–H nucleophiles

The procedure was identical to that of electrocatalytic synthesis, but without the addition of *n*-Bu$_4$NI as the mediator.

Supporting Information

Supporting Information File 1

General procedure and analytical data.
[https://www.beilstein-journals.org/bjoc/content/supplementary/1860-5397-14-35-S1.pdf]

Acknowledgements

ORCID® iDs

Kun Xu - https://orcid.org/0000-0002-0419-8822

References

1. Girard, S. A.; Knauber, T.; Li, C.-J. *Angew. Chem., Int. Ed.* **2014,** *53,* 74. doi:10.1002/anie.201304268
2. Scheuermann, C. J. *Chem. – Asian J.* **2010,** *5,* 436. doi:10.1002/asia.200900487
3. Ritleng, V.; Sirlin, C.; Pfeffer, M. *Chem. Rev.* **2002,** *102,* 1731. doi:10.1021/cr0104330
4. Xu, H.-J.; Lu, Y.; Farmer, M. E.; Wang, H.-W.; Zhao, D.; Kang, Y.-S.; Sun, W.-Y.; Yu, J.-Q. *J. Am. Chem. Soc.* **2017,** *139,* 2200. doi:10.1021/jacs.6b13269
5. Jiang, H.; He, J.; Liu, T.; Yu, J.-Q. *J. Am. Chem. Soc.* **2016,** *138,* 2055. doi:10.1021/jacs.5b13462
6. Chatani, N.; Asaumi, T.; Yorimitsu, S.; Ikeda, T.; Kakiuchi, F.; Murai, S. *J. Am. Chem. Soc.* **2001,** *123,* 10935. doi:10.1021/ja011540e
7. Li, Z.; Li, C.-J. *J. Am. Chem. Soc.* **2005,** *127,* 6968. doi:10.1021/ja0516054
8. Condie, A. G.; González-Gómez, J. C.; Stephenson, C. R. J. *J. Am. Chem. Soc.* **2010,** *132,* 1464. doi:10.1021/ja909145y
9. Freeman, D. B.; Furst, L.; Condie, A. G.; Stephenson, C. R. J. *Org. Lett.* **2012,** *14,* 94. doi:10.1021/ol202883v
10. Hari, D. P.; König, B. *Org. Lett.* **2011,** *13,* 3852. doi:10.1021/ol201376v
11. Twyman, R. M. *Principles of proteomics;* BIOS Scientific Publishers: New York, 2004.
12. Zhao, L.; Li, C.-J. *Angew. Chem., Int. Ed.* **2008,** *47,* 7075. doi:10.1002/anie.200801367
13. Li, C.-J. *Acc. Chem. Res.* **2009,** *42,* 335. doi:10.1021/ar800164n
14. Xie, J.; Huang, Z.-Z. *Angew. Chem., Int. Ed.* **2010,** *49,* 10181. doi:10.1002/anie.201004940
15. Zhu, Z.-Q.; Bai, P.; Huang, Z.-Z. *Org. Lett.* **2014,** *16,* 4881. doi:10.1021/ol502402s
16. Salman, M.; Zhu, Z.-Q.; Huang, Z.-Z. *Org. Lett.* **2016,** *18,* 1526. doi:10.1021/acs.orglett.6b00162
17. Huo, C.; Wang, C.; Wu, M.; Jia, X.; Xie, H.; Yuan, Y. *Adv. Synth. Catal.* **2014,** *356,* 411. doi:10.1002/adsc.201300535
18. Gao, X.-W.; Meng, Q.-Y.; Xiang, M.; Chen, B.; Feng, K.; Tung, C.-H.; Wu, L.-Z. *Adv. Synth. Catal.* **2013,** *355,* 2158. doi:10.1002/adsc.201300311
19. Yang, X.; Li, L.; Li, Y.; Zhang, Y. *J. Org. Chem.* **2016,** *81,* 12433. doi:10.1021/acs.joc.6b02683
20. Sperry, J. B.; Wright, D. L. *Chem. Soc. Rev.* **2006,** *35,* 605. doi:10.1039/b512308a
21. Francke, R.; Little, R. D. *Chem. Soc. Rev.* **2014,** *43,* 2492. doi:10.1039/c3cs60464k
22. Horn, E. J.; Rosen, B. R.; Baran, P. S. *ACS Cent. Sci.* **2016,** *2,* 302. doi:10.1021/acscentsci.6b00091
23. Yang, Q.-L.; Li, Y.-Q.; Ma, C.; Fang, P.; Zhang, X.-J.; Mei, T.-S. *J. Am. Chem. Soc.* **2017,** *139,* 3293. doi:10.1021/jacs.7b01232
24. Schäfer, H. J. *Angew. Chem., Int. Ed.* **2017,** *56,* 15502. doi:10.1002/anie.201707804
25. Zhao, H.-B.; Hou, Z.-W.; Liu, Z.-J.; Zhou, Z.-F.; Song, J.; Xu, H.-C. *Angew. Chem., Int. Ed.* **2017,** *56,* 587. doi:10.1002/anie.201610715
26. Wang, P.; Tang, S.; Huang, P.; Lei, A. *Angew. Chem., Int. Ed.* **2017,** *56,* 3009. doi:10.1002/anie.201700012
27. Jiang, Y.; Xu, K.; Zeng, C. *Chem. Rev.* **2017,** in press. doi:10.1021/acs.chemrev.7b00271
28. Li, W.-C.; Zeng, C.-C.; Hu, L.-M.; Tian, H.-Y.; Little, R. D. *Adv. Synth. Catal.* **2013,** *355,* 2884. doi:10.1002/adsc.201300502
29. Chen, J.; Yan, W.-Q.; Lam, C. M.; Zeng, C.-C.; Hu, L.-M.; Little, R. D. *Org. Lett.* **2015,** *17,* 986. doi:10.1021/acs.orglett.5b00083
30. Liang, S.; Zeng, C.-C.; Luo, X.-G.; Ren, F.-z.; Tian, H.-Y.; Sun, B.-G.; Little, R. D. *Green Chem.* **2016,** *18,* 2222. doi:10.1039/C5GC02626A
31. Kang, L.-S.; Luo, M.-H.; Lam, C. M.; Hu, L.-M.; Little, R. D.; Zeng, C.-C. *Green Chem.* **2016,** *18,* 3767. doi:10.1039/C6GC00666C
32. Ni, M.; Zhang, Y.; Gong, T.; Feng, B. *Adv. Synth. Catal.* **2017,** *359,* 824. doi:10.1002/adsc.201601066
33. Gandeepan, P.; Rajamalli, P.; Cheng, C.-H. *Asian J. Org. Chem.* **2014,** *3,* 303. doi:10.1002/ajoc.201300262
34. Xie, Z.; Jia, J.; Liu, X.; Liu, L. *Adv. Synth. Catal.* **2016,** *358,* 919. doi:10.1002/adsc.201501015
35. Liu, J.; Wang, Y.; Yu, L.; Huo, C.; Wang, X.; Jia, X. *Adv. Synth. Catal.* **2014,** *356,* 3214. doi:10.1002/adsc.201400005
36. Rohlmann, R.; Stopka, T.; Richter, H.; García Mancheño, O. *J. Org. Chem.* **2013,** *78,* 6050. doi:10.1021/jo4007199

License and Terms

An alternative to hydrogenation processes. Electrocatalytic hydrogenation of benzophenone

Cristina Mozo Mulero, Alfonso Sáez[*], Jesús Iniesta and Vicente Montiel

Abstract

The electrocatalytic hydrogenation of benzophenone was performed at room temperature and atmospheric pressure using a polymer electrolyte membrane electrochemical reactor (PEMER). Palladium (Pd) nanoparticles were synthesised and supported on a carbonaceous matrix (Pd/C) with a 28 wt % of Pd with respect to carbon material. Pd/C was characterised by transmission electron microscopy (TEM), and thermogravimetric analysis (TGA). Cathodes were prepared using Pd electrocatalytic loadings (L_{Pd}) of 0.2 and 0.02 mg cm^{-2}. The anode consisted of hydrogen gas diffusion for the electrooxidation of hydrogen gas, and a 117 Nafion exchange membrane acted as a cationic polymer electrolyte membrane. Benzophenone solution was electrochemically hydrogenated in EtOH/water (90/10 v/v) plus 0.1 M H_2SO_4. Current densities of 10, 15 and 20 mA cm^{-2} were analysed for the preparative electrochemical hydrogenation of benzophenone and such results led to the highest fractional conversion (X_R) of around 30% and a selectivity over 90% for the synthesis of diphenylmethanol upon the lowest current density. With regards to an increase by ten times the Pd electrocatalytic loading the electrocatalytic hydrogenation led neither to an increase in fractional conversion nor to a change in selectivity.

Introduction

Hydrogenation is a common procedure applied in organic chemistry industry based on the use of an external hydrogen source, generally carried out under moderate experimental conditions of high temperature (until 673 K) and high-pressure (even 350 atm). Even though the hydrogenation is performed using either homogeneous or heterogeneous catalysts to enhance chemical kinetics, a number of side reactions reduces the selectivity of the chemical reaction providing also complex and cost-ineffective work-up procedures [1-3]. Alternatively, electrocatalytic hydrogenation has emerged as a technique driven by its operational mild conditions, i.e., in situ "active hydrogen" generation, room temperature and atmospheric pressure, and

higher selectivity [4-10]. This electrochemical "active hydrogen" generation is performed under a cathodic polarization and such mechanism of an unsaturated organic compound (e.g., Y=X) still remains undertrained. Nonetheless, the steps likely involved in this electrochemical process by the literature [11-15] are as follows: (i) formation of adsorbed hydrogen MH_{ads} (defining "M" as a metal adsorption site and H_{ads} as atomic adsorbed hydrogen), (ii) adsorption of the organic molecule on a support site (two distinct adsorption sites are considered) and, (iii) electrocatalytic hydrogenation of the organic molecule through the adsorbed atomic hydrogen. It is important to note that, formation of "active hydrogen" is the main step in this process and hydrogen-active powder electrocatalysts such as Pd/C, Pt/C or Raney-nickel have been demonstrated as the optimal choice [16,17]. Moreover, the organic molecule adsorption rate must be faster than that one associated with the recombination of MH_{ads} to form diatomic hydrogen gas; otherwise electrocatalytic hydrogenation does not occur or displays a low Faraday efficiency because of the fact that diatomic hydrogen formation is not the main reaction, but a competitive one. Clearly, from the above mechanistic steps, the lower the "atomic active hydrogen" generation rate, the more efficient the electrocatalytic hydrogenation process; thus, the higher the used current density, the lower the obtained efficiency. Moreover, selectivity of electrocatalytic hydrogenation of ketones to alcohols is performed in acidic medium as an optimal reaction medium [5].

Currently, developments in nanostructured materials and polymeric solid exchange membranes have led the field of polymer electrolyte membrane fuel cells (PEMFC) to become a mature technology [18-20]. In this regard, a polymer electrolyte membrane electrochemical reactor (PEMER) has already been defined and manufactured to implementing all PEMFC technology advantages for both inorganic and organic electrosynthetic processes [21]. It is worth noting that the use of a polymer electrolyte membrane electrochemical reactor (PEMER) allows obtaining several advantages compared to the use of conventional electrochemical reactors, as follows: i) nanostructurated electrocatalysts can be utilized for both cathodic and anodic reactions, ii) a solid polymer electrolyte is used instead of a conventional electrolyte and iii) a decrease of the anode–cathode gap reduces ohmic drop at the whole process. In the case of organic electrosynthesis, electrocatalytic hydrogenation of aromatic ketones, specifically acetophenone, has been recently carried out [22,23] achieving a high selectivity using the above-mentioned technology. In this work, we have chosen benzophenone, as a more complex aromatic ketone dictated by the presence of two phenyl rings, in order to analyse fractional conversion and selectivity of formed products. Here, the main obtained product is diphenylmethanol (ketone conversion to alcohol) as a high

added value product in chemical industry. Even though several research groups have reported in the literature fundamental aspects about the electrocatalytic hydrogenation of benzophenone as well as its electrolytic performance at laboratory scale using Pd, Ni/Pd or Ni/Pt based either on massive or nanoparticulate cathodes [5,24-26]. The electrocatalytic hydrogenation of benzophenone has not been accomplished using a PEMER yet.

This work aims at exploring the electrocatalytic hydrogenation of benzophenone over palladium nanoparticles supported on carbon black based electrode using a PEMER. A nanoparticulate platinum gas diffusion electrode is used for the hydrogen oxidation reaction and a cationic exchange membrane is used as solid polymeric electrolyte. Fractional conversion, product yield and selectivity are presented upon the Pd electrocatalytic loading and current density. Moreover, the effect of the absence and presence of the supporting electrolyte upon the conversion and product yield of the electrochemical hydrogenation of benzophenone is explored.

Results and Discussion

Pd nanoparticles supported on Vulcan XC72R as electrocatalyst in cathodic reaction (electrocatalytic hydrogenation) were synthesised by reducing K_2PdCl_4 using $NaBH_4$ in a water-in-oil (w/o) microemulsion (water/Brij@30/*n*-heptane). This methodology has been previously used in our laboratory [27,28]. We first explored the morphology, size and dispersion of Pd nanoparticles supported on Vulcan XC72R carbonaceous material (Pd/C electrocatalysts) using TEM micrographs. As shown in Figure 1a, a good dispersion of spherical Pd nanoparticles of about 4–5 nm size is obtained. As expected, EDX analysis of Pd nanoparticles displays palladium as the sole metal, as shown in Figure 1b. With respect to the Pd loading in the Pd/C electrocatalyst, TGA results shown in Figure 1c lead to ca. 30 wt % content. A high drop of weight is observed between 600 K and 700 K since carbonaceous support is volatilized until reaching a residual PdO content (Pd in a N_2/O_2 atmosphere becomes a PdO species as stable residual weight when temperature is increased from 700 K to 1073 K). From the stable residual weight in Figure 1c at higher temperature it can be estimated that there is a content of 32 wt % of PdO in the whole Pd/C electrocatalyst, thereby confirming that the electrocatalyst can be considered as Pd/C with 28 wt %, by correcting the PdO value by subtracting the oxygen atomic percentage content. Thus, the above experimental wt % value of Pd is in agreement with the theoretical one of 30 wt % as described in the experimental section.

Once the Pd/C electrocatalyst characterisation was performed, Pd/C based cathodes either with 0.2 or 0.02 mg Pd per cm^2
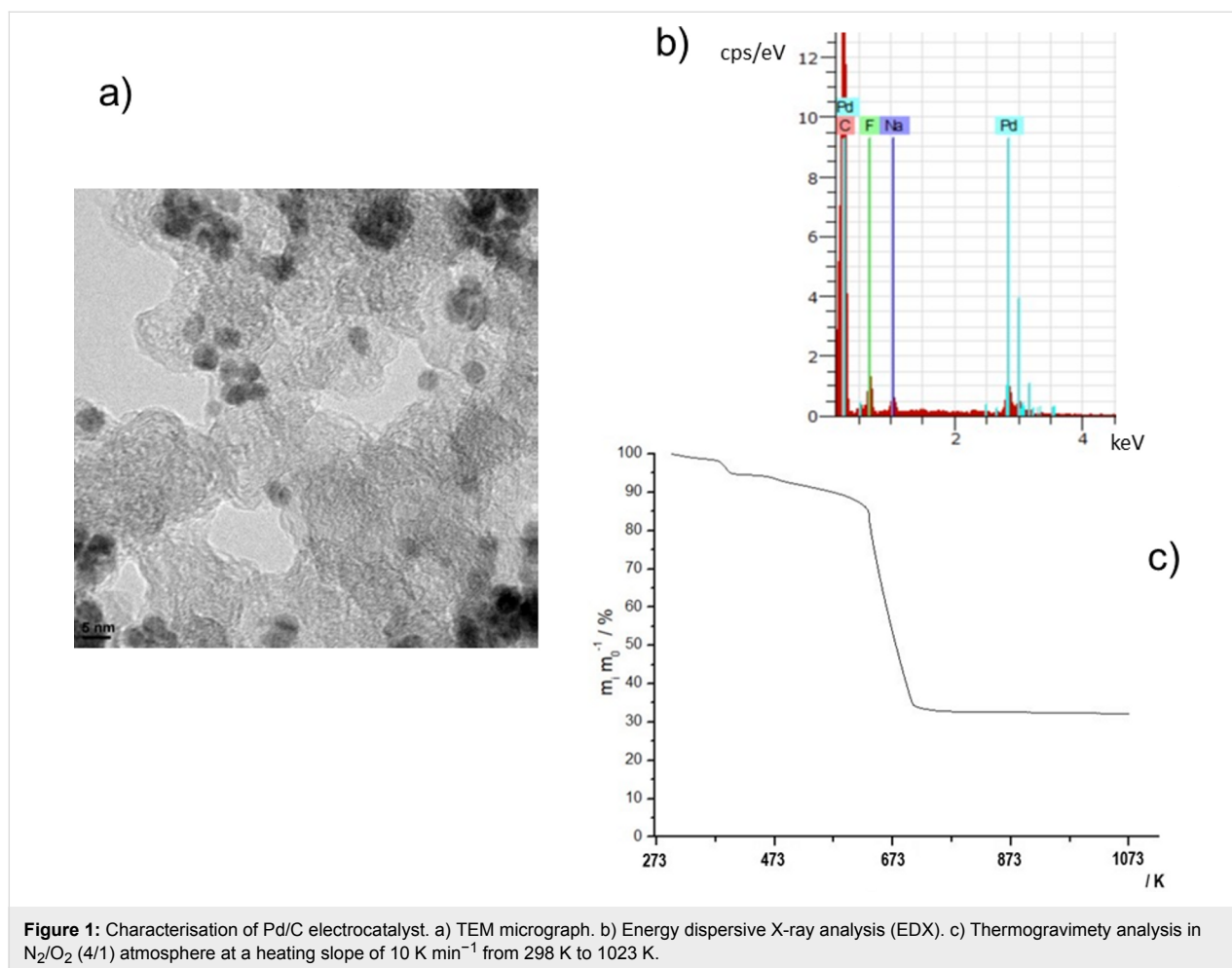
Figure 1: Characterisation of Pd/C electrocatalyst. a) TEM micrograph. b) Energy dispersive X-ray analysis (EDX). c) Thermogravimety analysis in N_2/O_2 (4/1) atmosphere at a heating slope of 10 K min^{-1} from 298 K to 1023 K.

were prepared and characterised by SEM and cyclic voltammetry. A Pd/C to Nafion ratio was established at 60:40 for each electrocatalytic layer irrespectively of the Pd loading in the electrocatalytic layer. Figure 2 depicts the SEM micrographics using back scattering electrons for both $Pd_{0.02}$/C/T and $Pd_{0.20}$/C/T electrodes (nomenclature described in the experimental section) at different magnifications. The SEM image for the highest electrocatalytic loading discloses a brighter appearance compared to the lowest one since backscattering electrons from high atomic weight (e.g., palladium) are brighter than lower atomic weight (e.g., carbon).

Apart from the SEM characterisation, the determination of the electrochemically active surface area (ESA) of the cathodic electrocatalytic layer is also crucial for the characterisation of both electrodes. In this regard, Figure 3 depicts the electrochemical behaviour of a $Pd_{0.20}$/C/T electrode in 0.5 M H_2SO_4 using cyclic voltammetry (CV) at a scan rate of 50 mV s^{-1} (potential interval of 0.1 and 1.2 V vs Ag/AgCl). The CV diagram shown in Figure 3 represents a typical pattern for the electrochemical behaviour of Pd bar electrode where a broad
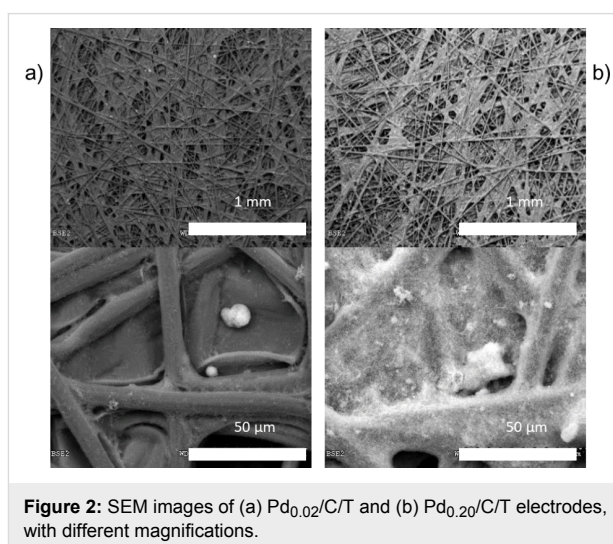

Figure 2: SEM images of (a) $Pd_{0.02}$/C/T and (b) $Pd_{0.20}$/C/T electrodes, with different magnifications.

anodic peak is associated to the oxidation of the Pd surface to PdO and then followed by a well-defined cathodic peak on the negative scan ascribed to the reduction of PdO to Pd [29]. From the coulombic charge integration of the cathodic peak on the

CV in Figure 3 (shadowed region) can be accurately calculated the ESA value and roughness factor, as defined in the experimental section. The ESA value is calculated according to Equation 1,

$$\text{ESA} = \frac{Q_{Pd}}{0.424 \cdot L_{Pd} \cdot A_{geom}} \qquad (1)$$

where Q_{Pd} (mC) is calculated from the coulombic charge integration from the cathodic peak after subtracting the double layer, L_{Pd} denotes the electrocatalytic loading expressed in mg of Pd per square centimetre of electrocatalytic layer, A_{geom} (cm^2) is the electrode geometric area and 0.424 refers to charge density expressed in mC per cm^2 of Pd [29]. On the other hand, the roughness factor rf is also calculated according to Equation 2.
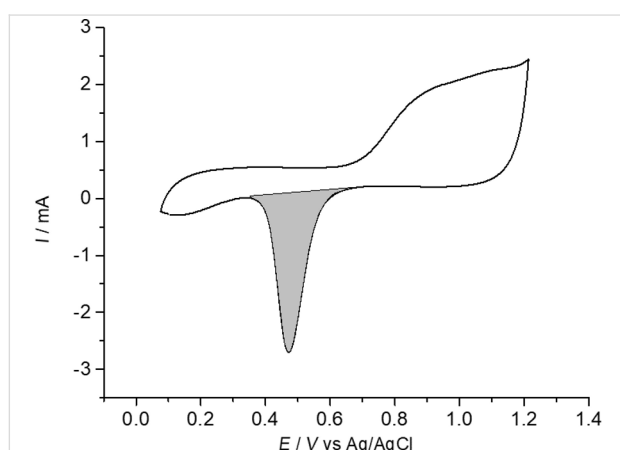
$$\text{rf} = \text{ESA} \cdot L_{Pd} \qquad (2)$$

Figure 3: Cyclic voltammetric behaviour of $Pd_{0.20}$/C/T electrode in 0.5 M H_2SO_4. Scan rate: 50 mV s^{-1}. Starting potential: 0.2 V vs Ag/AgCl. Positive scan.

Calculations of ESA and rf values were addressed for both $Pd_{0.02}$/C/T and $Pd_{0.20}$/C/T electrodes. It is worth noting that rf values denote real electrocatalytic surface area as a multiple factor of the theoretical geometric area. In this regard, rf values were 85 and 14 times the geometric area, whereas ESA values were 707 and 424 for $Pd_{0.02}$/C/T and $Pd_{0.20}$/C/T electrodes, respectively. The later ESA values indicate an increase of 67% of active surface area per weight unit, so the higher the electrocatalytic loading shown in a cathode electrocatalytic layer, the lower the electrochemically accessible surface per milligram. The above behaviour is likely attributed to a much thicker electrocatalytic layer for the $Pd_{0.20}$/C/T electrode compared to $Pd_{0.02}$/C/T electrode. Nonetheless, a thicker electrocatalytic layer is also detrimental for the accessibility of the electroactive species to the electrocatalytic metal surface, i.e., Pd nano-

particles, mostly due to the appearance of bottlenecks or blockage of network across the electrocatalytic layer, or likely some of these Pd nanoparticles could be covered up each other so those ones would be hidden.

Once Pd nanoparticle-based cathodes were manufactured and characterised, electrolytic hydrogenation of benzophenone in a cathodic process and hydrogen oxidation reaction as the anodic process was performed using a PEMER. Figure 4 describes each one of reactions involved in both cathodic and anodic processes and, also, the particulate elements of the electrochemical reactor.

Thus, preparative electrocatalytic hydrogenation of benzophenone was performed using a PEMER with $Pd_{0.02}$/C/T and $Pd_{0.20}$/C/T electrodes. We first investigated the influence of current density, i.e., 10, 15 and 20 mA cm^{-2}, on the electrochemical hydrogenation using a $Pd_{0.02}$/C/T electrode with a coulombic charge passed of 2 F (theoretical coulombic charge established by Faraday's Law by considering reaction of one mol of reagent). Figure 5 depicts the fractional conversion of benzophenone (expressed in percentage) versus the coulombic charge passed for all three current densities examined.

It should be noted that a higher fractional conversion of benzophenone of 25.8% is obtained for the lowest current density compared with values of 10.1% and 3.9% for current densities of 15 and 20 mA cm^{-2}, respectively (see Table 1). Our findings are highly expected accordingly to the steps involved in the electrochemical hydrogenation mechanisms (vide supra). In this regard, after formation of PdH_{ad}, the recombination rate of this "atomic active hydrogen" into diatomic hydrogen gas should be slower than the adsorption rate of the organic compound over the cathode in order to prompt electrocatalytic hydrogenation; consequently, a low current density should favour the hydrogenation process instead of diatomic hydrogen formation as competitive and side reaction by considering a slow PdH_{ad} formation rate of this.

HPLC analysis was performed for the identification and quantification of the benzophenone depletion and final product formation from the electrocatalytic hydrogenation at $Pd_{0.02}$/C/T electrode. An inspection of the chromatograms confirms the formation of two final products corresponding to diphenylmethanol (Ph_2CHOH) and diphenylmethane (Ph_2CH_2). Table 1 compiles fractional conversion of Ph_2CO (X_R), product yield of Ph_2CHOH and Ph_2CH_2 (η), selectivity of Ph_2CHOH (ξ) and cell voltage (ΔU_{cell}) for each current density over coulombic charge passed. It is worth noting that product yield for the Ph_2CHOH is higher at low current density with an almost linear increase as a function of coulombic charge passed. Moreover, it
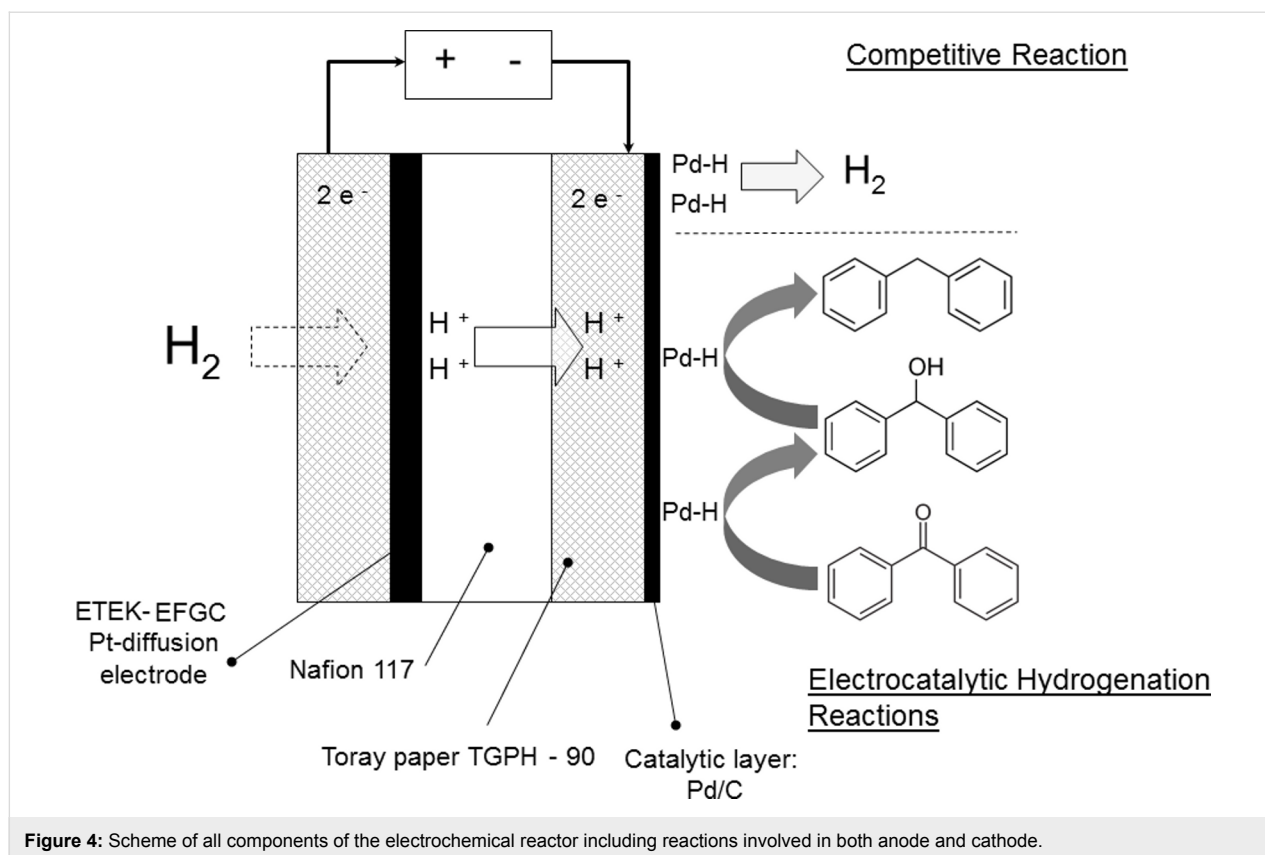
Figure 4: Scheme of all components of the electrochemical reactor including reactions involved in both anode and cathode.
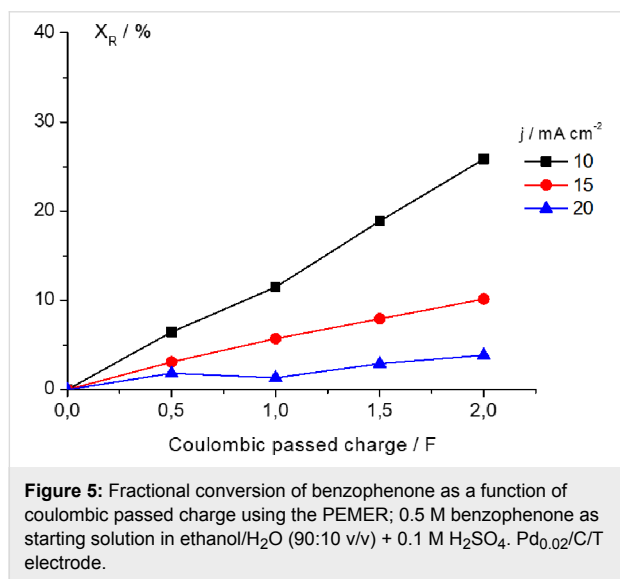

Figure 5: Fractional conversion of benzophenone as a function of coulombic passed charge using the PEMER; 0.5 M benzophenone as starting solution in ethanol/H$_2$O (90:10 v/v) + 0.1 M H$_2$SO$_4$. Pd$_{0.02}$/C/T electrode.

is noticed that the selectivity value generally over 90% is irrespective of the current density. Electrocatalytic hydrogenation of benzophenone was also performed using Pd$_{0.00}$/C/T electrodes, i.e., in the absence of the Pd electocatalyst, at 10 mA cm^{-2} demonstrated neither the electrochemical reduction of benzophenone nor the formation of alcohol or alkane derivatives.

Table 1 also depicts the average cell voltage from the electrocatalytic hydrogenation of benzophenone, with values of 0.2, 0.3 and 0.5 V for 10, 15 and 20 mA cm^{-2}, respectively. More precisely, Figure 6 plots cell voltage versus time at 10 mA cm^{-2}. In this case, a high cell voltage increase is observed from the open circuit voltage of around 0 V until the first stage of the electrocatalytic hydrogenation, followed by a cell voltage drop attributed to a decrease in IR drop of the membrane provoked by humidity lack of the membrane at either the anodic or cathodic sides when starting the electrocatalytic hydrogenation reaction. A similar variation of cell voltage versus time was also observed when using the rest of current densities.

Next we turn out to explore the influence of the Pd electrocatalytic loading on benzophenone conversion. Once again, electrocatalytic hydrogenation experiments were performed at constant current densities of 10, 15 and 20 mA cm^{-2} using a manufactured cathode with a Pd electrocatalytic loading of 0.2 mg cm^{-2} (Pd$_{0.20}$/C/T electrode). Results depicted in Figure 7 show again a higher benzophenone fractional conversion at lower current densities, as happened for the electrocatalytic hydrogenation using an electrode (Pd$_{0.02}$/C/T) with a 10 times lower Pd loading. Interestingly, benzophenone conversion performed at 15 and 20 mA cm^{-2} turned out to be slightly

Table 1: Fractional conversion (X_R), product yield for diphenylmethanol ($\eta_{Ph2CHOH}$) and diphenylmethane (η_{Ph2CH2}), selectivity for diphenylmethanol (ξ_{Ph2CH2}) versus coulombic charge passed at constant current densities of 10, 15 and 20 mA cm^{-2}. Pd$_{0.02}$/C/T electrode. Benzophenone (0.5 M) was used as starting solution in ethanol/water (90:10 v/v) + 0.1M H$_2$SO$_4$.

j		Q_{passed} [F]				ΔU_{cell}
[mA cm^{-2}]		0.5	1.0	1.5	2.0	[V]
10	X_R	6.5	11.5	18.9	25.8	0.2
	$\eta_{Ph2CHOH}$	4.1	9.2	16.9	22.4	
	η_{Ph2CH2}	0.9	1.1	1.6	1.6	
	$\xi_{Ph2CHOH}$	83	89	91	93	
15	X_R	3.1	5.7	7.9	10.1	0.3
	$\eta_{Ph2CHOH}$	3.7	5.4	7.4	9.9	
	η_{Ph2CH2}	0	0	0.3	0.4	
	$\xi_{Ph2CHOH}$	100	100	96	96	
20	X_R	1.8	1.3	2.9	3.9	0.5
	$\eta_{Ph2CHOH}$	0.9	1.7	2.5	3.0	
	η_{Ph2CH2}	0	0	0.3	0.4	
	$\xi_{Ph2CHOH}$	100	100	88	88	

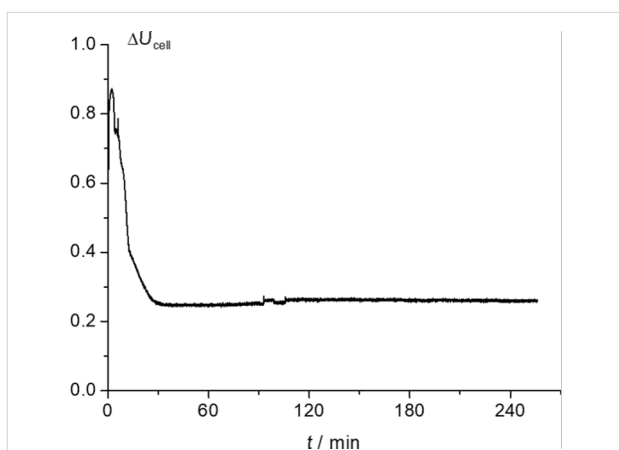**Figure 6:** Plot of cell voltage versus time obtained from a preparative electrosynthesis performed at 10 mA cm^{-2}, Pd$_{0.02}$/C/T electrode; 0.5 M benzophenone as starting solution in ethanol/water (90:10 v/v) plus 0.1 M H$_2$SO$_4$.
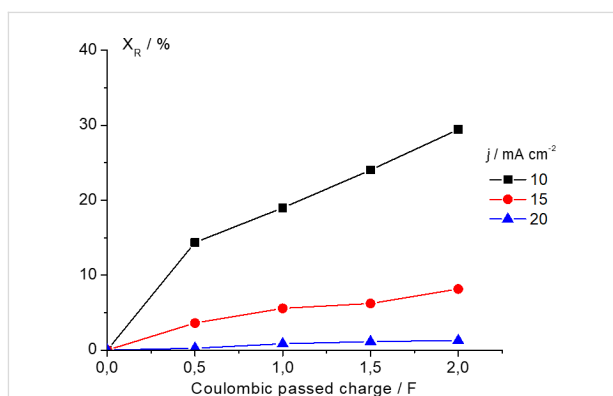

Figure 7: Fractional conversion of benzophenone as a function of coulombic charge passed; 0.5 M benzophenone as starting solution in ethanol/H$_2$O (90:10 v/v) plus 0.1 M H$_2$SO$_4$. Pd$_{0.20}$/C/T electrode.

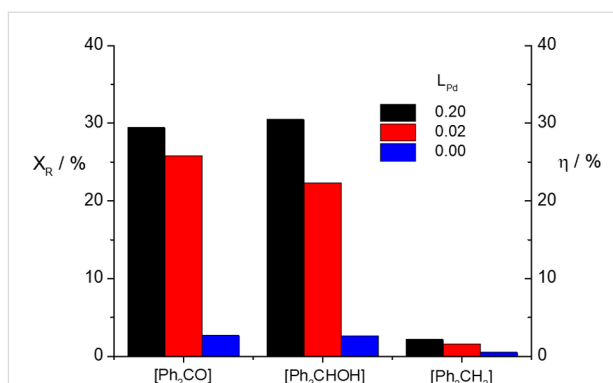**Figure 8:** Comparison of fractional conversion (X_R) and product yield (η) between Pd$_{0.02}$/C/T, Pd$_{0.20}$/C/T and Pd$_{0.00}$/C/T electrodes.

lower for the Pd$_{0.20}$/C/T electrode (vide infra). In this regard, Figure 8 shows the comparative results in terms of fractional conversion and product yield for both electrocatalytic hydrogenation reaction performed at Pd$_{0.02}$/C/T and Pd$_{0.20}$/C/T electrodes and no significantly electrocatalytic hydrogenation reaction at Pd$_{0.00}$/C/T electrode appears. In addition, the selectivity of diphenylmethanol is still over 90% irrespectively of the current density examined; the alcohol and alkane derivatives are also obtained, though prevailing the diphenylmethanol with high product yield (see Figure 8), being similar behaviour as that shown for the electrochemical hydrogenation using the Pd$_{0.02}$/C/T electrode.

The comparison of fractional conversion and product yield displayed in Figure 8 shows that the electrocatalytic hydrogenation of benzophenone is nearly irrespective of the Pd electrocatalytic loading. Indeed, one would respect a much higher fractional conversion of benzophenone when using the $Pd_{0.20}/C/T$ electrode. In other words, the higher Pd electrocatalytic loading, the higher adsorption of the organic molecule, and likely the higher reactivity of the adsorbed organic molecule with adsorbed hydrogen. At this point, we have defined a parameter, X_N, as fractional conversion normalised towards the electrochemically Pd accessible surface area, i.e., Pd accessible sites, according to Equation 3 shown below in order to shed light on the real effect of the Pd loading on the electrochemical hydrogenation of benzophenone.
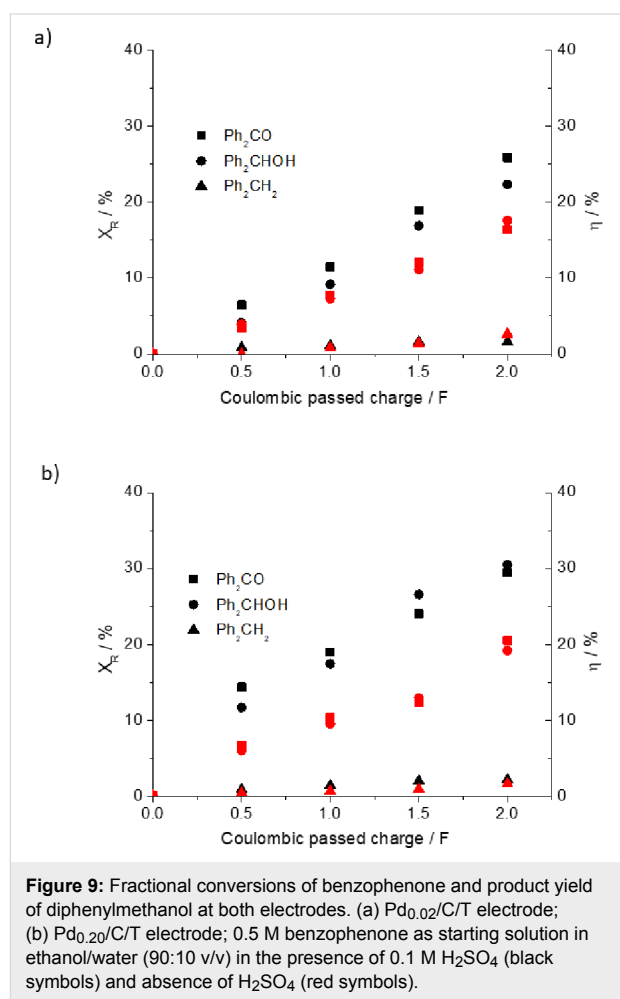
$$X_N = \frac{X_R}{rf \cdot A_{geom}} \qquad (3)$$

This parameter denotes the usefulness of electrocatalytic loading and is expressed as $\%~(cm^2~Pd)^{-1}$ where, X_R and rf have the usual meanings and A_{geom} corresponds to geometric area.

We have calculated the X_N value accordingly to the optimum current density of 10 mA cm^{-2} for both electrocatalytic loadings. These values are 0.073 and 0.014 for 0.02 and 0.2 (mg Pd) cm^{-2} respectively, confirming higher electrocatalytic usefulness for lower catalytic loading. By comparing Pd electrocatalytic loadings between 0.02 and 0.2, only 16% of the total accessible surface area in Pd electrocatalytic loading of 0.2 mg cm^{-2} resulted to be active to electrocatalytic hydrogenation of benzophenone. Accessibility problems of benzophenone molecules reaching electroactive sites within a thicker electrocatalytic layer are the most plausible explanation for getting a lower X_N value. Consequently, an increment of the electrocatalytic layer does not guarantee an enhancement of fractional conversion. For this reason, lower electrocatalytic loadings are the best approach to take into consideration.

Finally, the influence of acidic medium in catholyte solutions was explored to simplify the work-up of the crude mixture from the electrocatalytic hydrogenation of benzophenone. It is worth noticing that acidic medium is a parameter that must be taken into consideration in terms of selectivity for electrocatalytic hydrogenations of several organic compounds. In this regard, we performed the electrochemical hydrogenation of benzophenone in the absence of 0.1 M H_2SO_4 in order to investigate the contribution of hydronium ion formation from hydrogen oxidation reaction passing through the polymer electrolyte membrane as the sole hydronium ions source reaching the catholyte compartment. In doing so, the electrocatalytic hydrogenation of

benzophenone was performed at 10 mA cm^{-2} using both $Pd_{0.02}/C/T$ and $Pd_{0.20}/C/T$ electrodes in the absence of sulfuric acid. Figure 9 depicts the fractional conversions and product yields as a function of the coulombic charge passed for both electrodes in the absence and presence of 0.1 M H_2SO_4 for comparative purposes. Even though no changes were observed in terms of selectivity in the absence of the electrolyte, a remarkable fractional conversion decrease of around 10% can be calculated. As summary, the sole contribution of hydronium ions originating from the hydrogen oxidation reaction is not enough yet for an optimal performance of the electrocatalytic hydrogenation of benzophenone.

Figure 9: Fractional conversions of benzophenone and product yield of diphenylmethanol at both electrodes. (a) $Pd_{0.02}/C/T$ electrode; (b) $Pd_{0.20}/C/T$ electrode; 0.5 M benzophenone as starting solution in ethanol/water (90:10 v/v) in the presence of 0.1 M H_2SO_4 (black symbols) and absence of H_2SO_4 (red symbols).

Conclusion

The electrocatalytic hydrogenation of benzophenone has been performed at pre-pilot scale using a polymer electrolyte membrane electrochemical reactor (PEMER). The benzophenone conversion and diphenylmethanol and diphenylmethane yields are driven mostly by the current density used. Even though the lowest current density favours the benzophenone conversion and the alcohol yield, higher current density leads to a high

selectivity. In terms of Pd loading within the electrocatalytic layer, no significant difference is achieved with respect to fractional conversion and product yields, however, Pd accessible surface area per weight unit turns out to be enhanced for the lowest electrocatalytic loading, indicating a benzophenone accessibility to the Pd nanoparticulate electrocatalysts.

Hydrogen gas evolution reaction in the cathode compartment can be reused to feed a gas diffusion electrode for the hydrogen oxidation reaction. Moreover, in the absence of an acid medium as supporting electrolyte commonly used at the cathode compartment, the electrocatalytic hydrogenation is feasible by the sole supply of hydronium ions generated at the anode compartment coming from the hydrogen oxidation reaction.

Finally, it is worth noting that the hydrogen oxidation reaction was used as anodic process decreasing cell voltage of the process; besides, the use of hydrogen evolved at the cathode as competitive reaction must be considered as hydrogen source to partially feed the hydrogen anode.

Experimental

Benzophenone, diphenylmethanol, diphenylmethane, ethanol 96% (Sigma-Aldrich, Spain) were used without further purification. K_2PdCl_4 salt was purchased from Sigma-Aldrich (purity higher than 99%). Vulcan XC72R carbon material was purchased from Cabot Corporation. The other chemicals were purchased in the highest purity available and used as received. The solutions were prepared with doubly distilled water.

The synthesis of Pd nanoparticles was performed following a procedure previously used in our laboratory and described in the literature [27,28]. Briefly, a K_2PdCl_4 salt solution was reduced using $NaBH_4$ as reducing agent in a water-in-oil (w/o) microemulsion in the presence of polyethylene glycol hexadecyl ether, Brij@30 as capping agent and *n*-heptane as organic solvent (water/Brij@30/*n*-heptane). After precipitation and copiously washing with acetone and water, Pd nanoparticles were supported on Vulcan XC72R to get a nominal 30 wt % Pd loading (Pd/C electrocatalyst).

The cathode layer was prepared by air-brushing an electrocatalytic ink onto a Toray Paper TGPH-90 (carbonaceous composite paper supplied by Toray Industries Inc., thickness 280 μm). The electrocatalytic ink consisted of Pd nanoparticles supported in Vulcan XC72R 30 wt % dispersion in isopropanol containing a Nafion dispersion of 5 wt %. All electrodes have a Pd/C to Nafion ratio of 60:40 in the electrocatalytic layer with Pd loadings of 0.20 and 0.02 mg cm^{-2}. Cathodes were named as Pd$_x$/C/T where x stands for the Pd loading and T is the Toray paper support.

Morphology, size and dispersion of Pd nanoparticles in Pd/C were analysed by a transmission electron microscopy (TEM) using a JEOL JEM-2012 instrument with an accelerating voltage of 300 kV. The TEM was connected with an energy dispersion X-ray (EDX) for the analysis of the Pd nanoparticles. Thermogravimetric analysis (TGA) was performed using a Mettler Toledo model TGA/SDTA851 and /SF/1100 using a heating slope of 10 K min^{-1} from 298 K to 1023 K under a N_2:O_2 (4:1) atmosphere. For the characterisation of the Pd$_x$/C/T scanning electron microscopy (SEM) micrographs were obtained using a Hitachi S-3000N microscope with backscattered electron signal. Electrochemical surface characterisation of the distinct Pdx/C/T electrodes was explored by cyclic voltammetry (CV). CV measurements were performed using a PGSTAT30 Autolab system. A 0.5 cm × 1.0 cm Pd$_x$/C/T electrode acted as a working electrode (WE), the counter electrode was a platinum wire and an Ag/AgCl (3.0 M KCl) acted as reference electrode through a Luggin capillary. CV measurements were performed at room temperature and under argon atmosphere. CV curves were recorded between 0.1 and 1.2 V vs Ag/AgCl (3.0 M KCl) with a scan rate of 50 mV s^{-1} using a 0.5 M H_2SO_4 aqueous solution. The electrochemical accessible surface area (ESA) was defined as the Pd electrochemically active surface divided into the total Pd weight according to the total Pd loading, expressed in (cm^2 Pd) (mg Pd)$^{-1}$, while the roughness factor was defined as the Pd electrochemically active surface divided by the geometric total area, expressed in (cm^2 Pd) cm^{-2} (vide supra).

Electrosynthesis reactions were performed using a 25 cm^2 PEM single cell fuel cell (EFC-25-01 model from ElectroChem Inc.) acting as polymer electrolyte membrane electrochemical reactor (PEMER), as depicted in Figure 10. Such an electrochemical reactor consisted of (i) a Pd$_x$/C/T cathode, (ii) an ETEK gas diffusion-type EFGC (Pt/C/T) with a 40 wt % of Pt with respect to the amount of carbon, and a Pt electrocatalytic loading of 2.0 mg cm^{-2} as anode to carry out the hydrogen oxidation reaction, and, finally, (iii) a Nafion 117 cation exchange membrane in contact between both electrodes acting as solid polymer electrolyte.

The catholyte solutions for the electrochemical hydrogenation of benzophenone consisted of either (i) 0.5 M benzophenone in ethanol 96% /water (90:10 v/v) and 0.1 M H_2SO_4, or (ii) 0.5 M benzophenone in ethanol 96% /water (90:10 v/v) in the absence of the sulfuric acid electrolyte in order to explore the influence of the medium acidity upon the electrochemical hydrogenation.

A peristaltic pump Ismatel Reglo DIG MS/CA 2–8 provided a catholyte flow of 12 mL min^{-1} through the cathodic compartment and the total catholyte volume was 40 mL. At the same
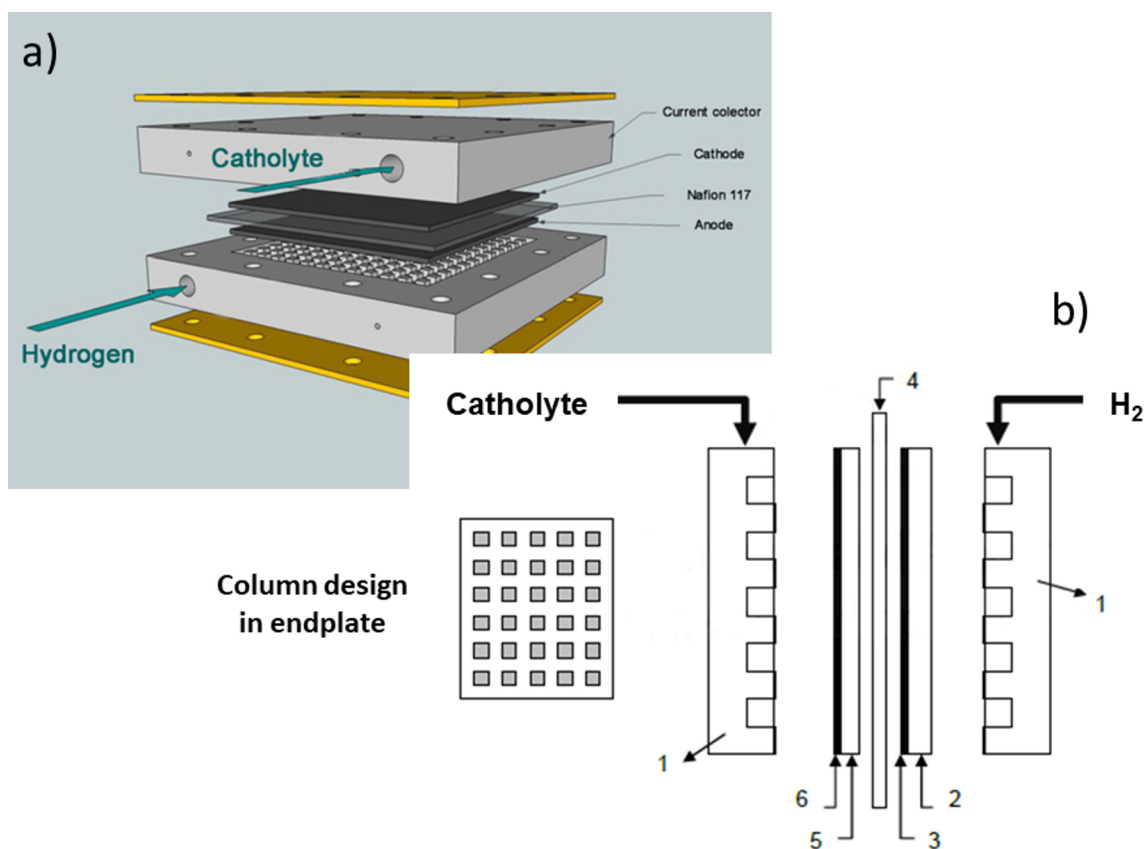
Figure 10: (a) General scheme of a PEMER; (b) itemisation of the main parts of PEMER: 1) endplates, 2) gas diffusion electrode, 3) Pt electrocatalytic layer, 4) polymer electrolyte membrane (solid polymer electrolyte), 5) carbonaceous support (Toray paper TGPH-90), 6) Pd/C electrocatalytic layer.

time, hydrogen (Praxair, purity: 99.999%) was fed to the anodic compartment at a flow rate of 50 mL min^{-1} as reactant in hydrogen oxidation reaction, using a MTS-module A-150 from ElectroChem Inc. Electrocatalytic hydrogenation reactions were carried out at constant current densities of 10, 15 and 20 mA cm^{-2} considering a projected geometric area of 25 cm^2 for both Pd$_{0.02}$/C/T and Pd$_{0.20}$/C/T electrodes using a potentiostat OrigaFlex OGF05A. Total coulombic charge passed was set at 2 Faradays for each experiment. The cell voltage was recorded during each experiment. All preparative electrochemical hydrogenations were carried out at room temperature. In this case, counter electrode plug was connected to reference electrode one and chronopotentiometries were performed registering cell voltage versus time.

The fractional conversion of benzopheneone and product yield and selectivity of final products from the electrocatalytic hydrogenation of benzophenone was examined as a function of current density and Pd loading in the electrocatalytic layer. On doing so, the catholyte solution was analysed by using a high-resolution liquid chromatograph (HPLC Agilent 1200) with a

Hypersil ODS column 4 × 250 mm, 5 μm particle size (Agilent Technologies). An acetonitrile/water (1:1 v/v, acetonitrile isocratic HPLC grade and water from Elix 3 Millipore system) was used as mobile phase. The flow rate was 1 mL min^{-1}; the injection volume was 100 μL and the working temperature was 303 K. Such experimental conditions provided linear calibration curves between 20 and 100 ppm with all benzophenone, diphenylmethanol and diphenylmethane standard organic solutions. Preparative electrosyntheses were given as fractional conversion (X_R) of benzophenone (Ph$_2$CO) and product yield (η) of diphenylmethanol (Ph$_2$CHOH) and diphenylmethane (Ph$_2$CH$_2$). Selectivity values (ξ) of diphenylmethanol and diphenylmethane were also calculated. For comparative purposes, a free-Pd electrocatalytic layer (Pd$_{0.00}$/C/T) cathode was also considered for the electrocatalytic hydrogenation of Ph$_2$CO.

Acknowledgements

ORCID® iDs

Cristina Mozo Mulero - https://orcid.org/0000-0002-6490-9710
Alfonso Sáez - https://orcid.org/0000-0002-2949-6711
Jesús Iniesta - https://orcid.org/0000-0003-4350-2169
Vicente Montiel - https://orcid.org/0000-0003-2353-2993

References

1. Chen, B.; Dingerdissen, U.; Krauter, J. G. E.;
   Lansink Rotgerink, H. G. J.; Möbus, K.; Ostgard, D. J.; Panster, P.;
   Riermeier, T. H.; Seebald, S.; Tacke, T.; Trauthwein, H. *Appl. Catal., A*
   2005, *280,* 17–46. doi:10.1016/j.apcata.2004.08.025
2. Rilander, P. N. *Hydrogenation Methods;* Academic Press, 1985; p 193.
3. Magnoux, P.; Lavaud, N.; Guisnet, M. *Top. Catal.* **2000,** *13,* 291–299.
   doi:10.1023/a:1009009727910
4. Yoshida, J.-i.; Kataoka, K.; Horcajada, R.; Nagaki, A. *Chem. Rev.*
   2008, *108,* 2265–2299. doi:10.1021/cr0680843
5. Cirtiu, C. M.; Brisach-Wittmeyer, A.; Ménard, H. *Catal. Commun.* **2007,**
   8, 751–754. doi:10.1016/j.catcom.2006.09.014
6. Coche, L.; Moutet, J. C. *J. Am. Chem. Soc.* **1987,** *109,* 6887–6889.
   doi:10.1021/ja00256a072
7. Moutet, J.-C. *Org. Prep. Proced. Int.* **1992,** *24,* 309–325.
   doi:10.1080/00304949209355892
8. Pintauro, P. N.; Bontha, J. R. *J. Appl. Electrochem.* **1991,** *21,* 799–804.
   doi:10.1007/bf01402817
9. Polcaro, A. M.; Dernini, M. S.; Palmas, S. *Electrochim. Acta* **1992,** *37,*
   365–367. doi:10.1016/0013-4686(92)85025-G
10. Polcaro, A. M.; Palmas, S.; Dernini, S. *Electrochim. Acta* **1993,** *38,*
    199–203. doi:10.1016/0013-4686(93)85129-M
11. Dabo, P.; Cyr, A.; Lessard, J.; Brossard, L.; Ménard, H. *Can. J. Chem.*
    1999, *77,* 1225–1229. doi:10.1139/v99-120
12. Laplante, F.; Brossard, L.; Ménard, H. *Can. J. Chem.* **2003,** *81,*
    258–264. doi:10.1139/v03-027
13. St-Pierre, G.; Chagnes, A.; Bouchard, N.-A.; Harvey, P. D.;
    Brossard, L.; Ménard, H. *Langmuir* **2004,** *20,* 6365–6373.
    doi:10.1021/la048977v
14. Cirtiu, C. M.; Hassani, H. O.; Bouchard, N.-A.; Rowntree, P. A.;
    Ménard, H. *Langmuir* **2006,** *22,* 6414–6421. doi:10.1021/la0519002
15. Cirtiu, C. M.; Brisach-Wittmeyer, A.; Ménard, H. *J. Catal.* **2007,** *245,*
    191–197. doi:10.1016/j.jcat.2006.10.010
16. Osa, T.; Matsue, T.; Yokozawa, A.; Yamada, T. *Denki Kagaku* **1986,**
    54, 484.
17. Osa, T.; Matsue, T.; Yokozawa, A.; Yamada, T. *Denki Kagaku* **1984,**
    52, 629.
18. Borup, R.; Meyers, J.; Pivovar, B.; Kim, Y. S.; Mukundan, R.;
    Garland, N.; Myers, D.; Wilson, M.; Garzon, F.; Wood, D.; Zelenay, P.;
    More, K.; Stroh, K.; Zawodzinski, T.; Boncella, J.; McGrath, J. E.;
    Inaba, M.; Miyatake, K.; Hori, M.; Ota, K.; Ogumi, Z.; Miyata, S.;
    Nishikata, A.; Siroma, Z.; Uchimoto, Y.; Yasuda, K.; Kimijima, K.-i.;
    Iwashita, N. *Chem. Rev.* **2007,** *107,* 3904–3951. doi:10.1021/cr050182l
19. Litster, S.; McLean, G. *J. Power Sources* **2004,** *130,* 61–76.
    doi:10.1016/j.jpowsour.2003.12.055
20. Smitha, B.; Sridhar, S.; Khan, A. A. *J. Membr. Sci.* **2005,** *259,* 10–26.
    doi:10.1016/j.memsci.2005.01.035
21. Montiel, V.; Sáez, A.; Expósito, E.; García-García, V.; Aldaz, A.
    Electrochem. Commun. **2010,** *12,* 118–121.
    doi:10.1016/j.elecom.2009.11.002
22. Sáez, A.; García-García, V.; Solla-Gullón, J.; Aldaz, A.; Montiel, V.
    Electrochem. Commun. **2013,** *34,* 316–319.
    doi:10.1016/j.elecom.2013.07.018
23. Sáez, A.; García-García, V.; Solla-Gullón, J.; Aldaz, A.; Montiel, V.
    Electrochim. Acta **2013,** *91,* 69–74.
    doi:10.1016/j.electacta.2012.12.097
24. Vilar, M.; Oliveira, J. L.; Navarro, M. *Appl. Catal., A* **2010,** *372,* 1–7.
    doi:10.1016/j.apcata.2009.09.041
25. Villalba, M.; Bossi, M. L.; Calvo, E. J. *Phys. Chem. Chem. Phys.* **2015,**
    17, 10086–10092. doi:10.1039/C5CP00225G
26. Villalba, M.; del Pozo, M.; Calvo, E. J. *Electrochim. Acta* **2015,** *164,*
    125–131. doi:10.1016/j.electacta.2015.02.113
27. Solla-Gullón, J.; Montiel, V.; Aldaz, A.; Clavilier, J. *J. Electrochem. Soc.*
    2003, *150,* E104–E109. doi:10.1149/1.1534600
28. Solla-Gullón, J.; Rodes, A.; Montiel, V.; Aldaz, A.; Clavilier, J.
    J. Electroanal. Chem. **2003,** *554–555,* 273–284.
    doi:10.1016/S0022-0728(03)00214-6
29. Fang, L.-l.; Tao, Q.; Li, M.-f.; Liao, L.-w.; Chen, D.; Chen, Y.-x.
    Chin. J. Chem. Phys. **2010,** *23,* 543–548.
    doi:10.1088/1674-0068/23/05/543-548

Electrochemical Corey–Winter reaction. Reduction of thiocarbonates in aqueous methanol media and application to the synthesis of a naturally occurring α-pyrone

Ernesto Emmanuel López-López[1], José Alvano Pérez-Bautista[2], Fernando Sartillo-Piscil[*2] and Bernardo A. Frontana-Uribe[*1,3]

Abstract

An electrochemical version of the Corey–Winter reaction was developed giving excellent results in aqueous methanol media (MeOH/H_2O (80:20) with AcOH/AcONa buffer 0.5 M as supporting electrolyte), using a reticulated vitreous carbon as cathode in a divided cell. The electrochemical version is much more environmentally friendly than the classical reaction, where a large excess of trialkyl phosphite as reducing agent and high temperatures are required. Thus, cathodic reduction at room temperature of two cyclic thiocarbonates (−1.2 to −1.4 V vs Ag/AgCl) afforded the corresponding alkenes, *trans*-6-(pent-1-enyl)-α-pyrone and *trans*-6-(pent-1,4-dienyl)-α-pyrone, which are naturally occurring metabolites isolated from *Trichoderma viride* and *Penicillium*, in high chemical yield and with excellent stereo selectivity.

Findings

The Corey–Winter reaction (also known as the Corey–Winter reductive olefination) is a chemical transformation that permits the conversion of 1,2-diols **A** into *E*-alkenes **C** via the forma- tion and reduction of a cyclic thiocarbonate intermediate **B** (Scheme 1) [1,2]. In general this reaction provides moderate to good yields, but the use of large quantities of toxic

and dangerous phosphorylated reductive reagents (e.g., trimethylphosphite employed as both reagent and solvent in the reaction) and the necessity of high temperatures, makes this synthetic protocol inappropriate for the stereospecific preparation of olefins in large scale [3]. Furthermore, the introduction of 1,3-dimethyl-2-phenyl-1,3,2-diazaphospholidine (**D**, Corey–Hopkins reagent) as the reductive reagent, has resulted in the development of a milder Corey–Winter protocol, which can be now carried out near to room temperature (Scheme 1) [4]. Despite this advantage, the low availability and high cost of this reagent [5] makes this reaction difficult to be used in industry.

Scheme 1: The Corey–Winter reaction in general.
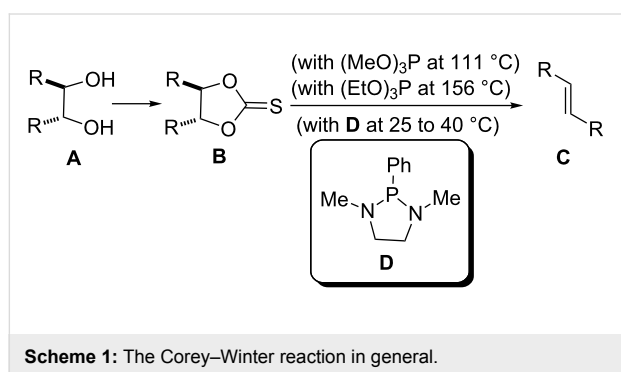
Previously, starting from the versatile chiron 7,3-lactone-xylo-furanose (**7,3-LXF**) [6], the first non-biological synthesis of chiral 6-pentyl-2*H*-pyran-2-ones **1–3** was reported by our research group [7]. These molecules proved to be enantiomers of metabolites isolated from *Trichoderma spp* and *Penicillium isolates*. Unfortunately, our efforts for obtaining the natural metabolite *trans*-6-(pent-1-enyl)-α-pyrone (**5**) (isolable from *Trichoderma viride* [8]) via a Corey–Winter reaction with the cyclic thiocarbonate **4** were unsuccessful (Scheme 2).
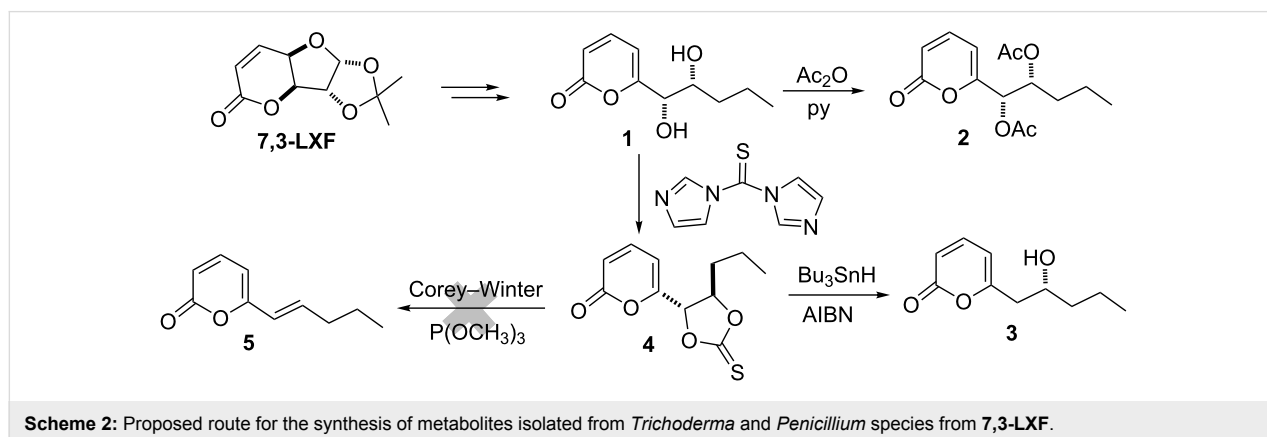
Electrochemical reactions are very useful in organic synthesis [9-14]. They possess unique features including the ability to
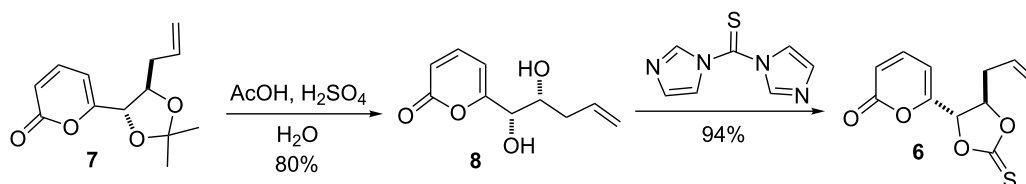
control the redox power [15], the substitution of large scale toxic or dangerous conventional redox reagents by sustainable and inexpensive electrical current [16-19], the ease with which umpolung reactivity is achieved [20-22], the access to unstable intermediates of great utility in organic synthesis [23-25], and in most of the cases, the use of mild reaction conditions. Importantly, they also represent a useful way to fulfilling important aspects of the green chemistry [26-28], making the synthetic pathways safer and more economical. Therefore, electrosynthetic reactions can be advantageous not only for solving synthetic problems where a redox step fails with a classical redox reagent, but also because the use of toxic-dangerous reagents is avoided [15,29,30]. Thus, a combination of the classical chemical approach with the electrochemical in a synthetic route can result in an improved final yield diminishing chemical waste [15,31].

Having in mind that the Corey–Winter reaction is in fact a reductive chemical process between the thiocarbonate moiety and the phosphorylated reagent, which oxidize P(III) to P(V), we anticipated that a cathodic reduction process applied to the same cyclic thiocarbonate **4** would provide the desired target molecule **5**. In this letter we report the electrochemical behavior of thiocarbonates **4** and **6** in aqueous methanol MeOH/H$_2$O (80:20) with 0.5 M AcOH/AcONa buffer as supporting electrolyte, as well as the results of several reductive electrolysis performed under green chemistry conditions.

Cyclic thiocarbonate **6** was prepared in two steps from pyrone dioxolane **7** [7]. Acid hydrolysis of **7** to 1,2-diol **8** followed by the reaction with 1,1'-thiocarbonyldiimidazole afforded thiocarbonate precursor **6** in high overall yield (Scheme 3). Compounds **6** and **8** were prepared in a similar manner as described in reference [7].

With thiocarbonates **4** and **6** in our hands, their electrochemical behavior was studied in the MeOH/H$_2$O media previously de-

Scheme 2: Proposed route for the synthesis of metabolites isolated from *Trichoderma* and *Penicillium* species from **7,3-LXF**.

Scheme 3: Preparation of thiocarbonate precursor **6** from pyrone dioxolane **7**.

scribed (Figure 1). This mixture of solvents has been used for the electrochemical preparation of anilines, hydroxylamines and nitroso compounds via the reduction of aromatic nitro derivatives [32,33], showing a convenient electrochemical window with graphitic electrodes (−1.75 to 1.25 V vs Ag/AgCl) and giving good environmental compatibility. Cyclic voltammetry of thiocarbonates **4** and **6** using a vitreous carbon electrode, showed two irreversible reduction peaks located at −1.18 and −1.6 V, respectively (Figure 1), indicating the possibility of reducing these compounds in two electrochemical steps under the selected conditions.

In order to determine which functional group is reduced, an electrolysis using 0.25 mmol of compound **4** was carried out under controlled potential after the first reduction peak ob-

served in cyclic voltammetry (−1.45V vs Ag/AgCl) in a divided (sintered glass) H-type cell fitted with a reticulated vitreous carbon cathode and a stainless steel anode (see Supporting Information File 1 for details). When 2.2 F/mol were consumed (ca. 1.5 h), TLC control of the electrolytic solution showed the total consumption of the starting material and the appearance of a less polar compound without other secondary compounds.

After reaction work-up, ^{1}H and ^{13}C NMR spectra of the extracted product were in full agreement with compound **5**, which was previously isolated from *Trichoderma viride* [8]. This fact let us to conclude that the thiocarbonate group was reduced selectively to the *trans*-alkene in a Corey–Winter-type reaction [2,3] giving the targeted structure **5** in 95% isolated yield (Scheme 4, Table 1, entry 1). The reaction occurred stereoselec-
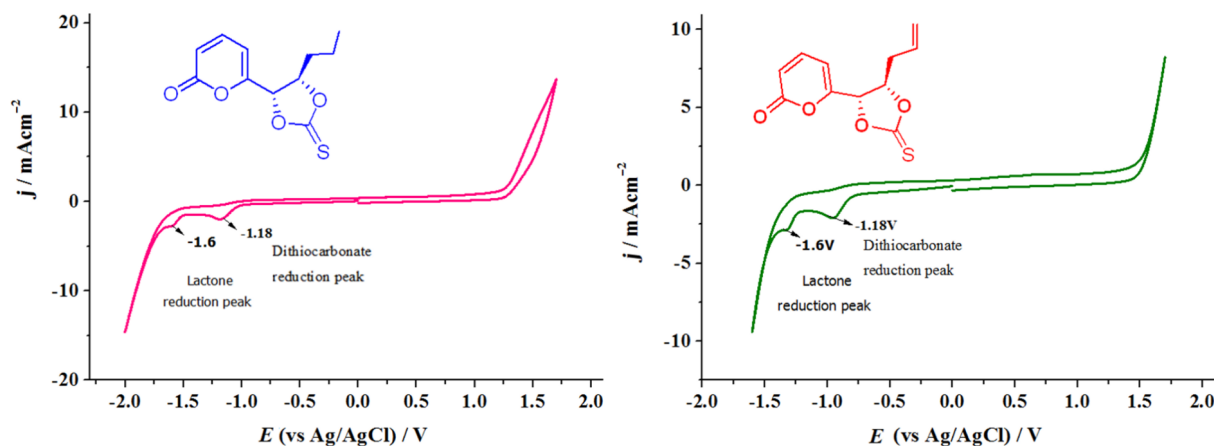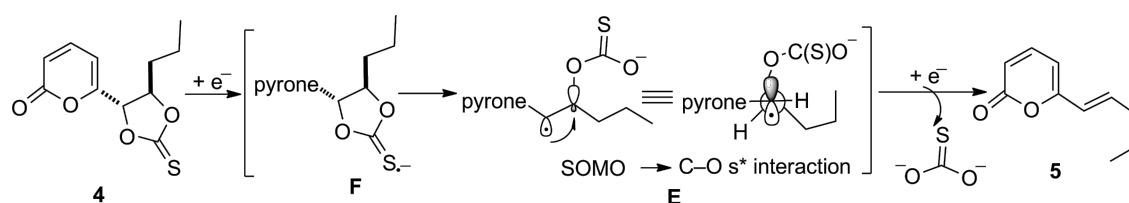

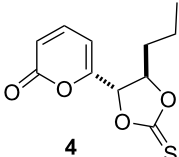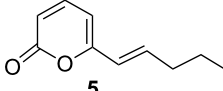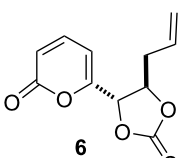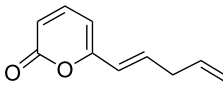**Figure 1:** Cyclic voltammetry of thiocarbonates **4** (left) and **6** (right); *c* = 1 × 10⁻³ M, N₂ bubbling 5 min, WE = vitreous carbon, CE = Pt wire, RE = Ag/AgCl in MeO/H₂O (80:20) in AcOH/AcONa buffer 0.5 M media.

Scheme 4: Putative reaction mechanism of the electrochemical Corey–Winter reaction.

Table 1: Electroreduction of thiocarbonates **4** and **6** in MeO/H$_2$O 80:20 with AcOH/AcONa buffer 0.5 M as electrolytic media.[a]

entry	thiocarbonate	conditions	product and yield %
1	**4** 0.25 mmol	potentiostatic electrolysis −1.45 V vs Ag/AgCl, 2.2 F/mol RVC cathode, 1,5 h	**5** 95–97[b] current efficiency: 90%
2	0.25 mmol	potentiostatic electrolysis −1.45 V vs Ag/AgCl, 2.2 F/mol graphite plate cathode, 1,5 h	80 current efficiency: 90%
3	0.25 mmol	galvanostatic electrolysis I = 15–25 mA[c] j = 7.5–12.5 mA/cm^2 [d] 2.5 F/mol, RVC cathode	95 current efficiency: 80%
4	**6** 0.25 mmol	potentiostatic electrolysis −1.2 vs Ag/AgCl, 2.2 F/mol RVC cathode, 1,5 h	**9** 94–97[b] current efficiency: 90%
5	0.25 mmol	galvanostatic electrolysis I = 15–25 mA[c] j = 7.5–12.5 mA/cm^2 [d] 2.5 F/mol, RVC cathode	93 current efficiency: 80%

[a]All the experiments were carried out with stainless steel as anode. The potentiostatic and galvanostatic experiments were carried out in a H-cell divided cell with 25 mL of electrolytic media per compartment. [b]Two reactions under the same conditions were carried out. [c]Lowest and highest current used for an efficient reaction; when the lowest is used the reaction takes 1 h to consume the starting material and with the highest 30 min are required. [d]A geometrical area of 2 cm^2 was used to calculate j; see Supporting Information File 1 for calculation details.

tively with no trace of *cis*-alkene isomer. The use of graphite electrodes instead of the reticulated vitreous carbon eroded the chemical yield to 80% (Table 1, entry 2). Cyclic voltammetry analysis of **4** showed a second reduction peak at −1.6 V (Figure 1), a value that agrees with that for reduction of the α,β-unsaturated ester functionality [34], which was not reduced under the reaction conditions.

The high stereospecificity of this electrochemical Corey–Winter-type reaction might be explained in terms of the stabilizing β-oxygen effect [35,36] of the radical intermediate **E**. This stereoelectronic interaction, which refers to the beneficial effect of β-oxygen substituents in radical deoxygenation [37], is dramatically favoured when the radical precursor group (or atom) is oriented antiperiplanar to the C−O bond via orbital interaction between the SOMO with the C−O σ* orbital [35]. Therefore, stabilization of intermediate **E**, which is formed by β-fragmentation of radical anion **F**, is maximum when is locked in an antiperiplanar conformation (Scheme 4). Therefore, this electrochemical reaction represents a promising way to produce *trans*-olefins from their respective thiocarbonates, overcoming thus the toxicity and safety issues of the classical Corey–Winter reaction.

When potential-controlled electrolysis (PCE) is used a particular functional group in a molecule, in this case the thiocarbonate vs the α,β-unsaturated ester, can be selectively reduced. Under PCE feasibility and affordability of the reaction are limited by the potentiostat, because this device is rarely available in an organic chemistry laboratory and it can be expensive to acquire it. In the other hand, current controlled electrolysis (CCE), where the electrode potential control is made indirectly by the experimental conditions, requires an ordinary and easy available direct current power source, therefore, reduction of compound **4** was attempted under CCE conditions. After a series of experiments, compound **5** was satisfactorily obtained using 25 mA (j = 12.5 mA/cm^2) with 95% yield using reticulated vitreous carbon in 30 min reaction in the aqueous methanol medium (Table 1, entry 3). The current efficiency decreases a little (80%) but remains in acceptable values for an attractive electrochemical reaction. This is due to the lack of potential control and when the concentration of the starting material decreases the electrode potential shifts to more negative values. The same potential controlled electrolysis protocol used for **4** was applied to the alkene thiocarbonate derivative **6**, but reducing it at −1.2 V vs Ag/AgCl, and likewise, quantitative chemical yield of the corresponding *E*-alkene **9** was obtained

(Table 1, entry 4). Also, the CCE of **6**, using the same current density previously optimized for compound **4**, gave **9** as the sole product in high yield (Table 1, entry 5). The reaction proceeds also with 15 mA (j = 7.5 mA/cm^2); however, the electrolysis occurs slowly (1 h), whereas at 25 mA (j = 12.5 mA/cm^2) the reaction is completed in 30 min; in both cases very good yields were obtained. When higher current density values for the electrolysis were used, TLC showed the formation of several byproducts. This indicates that the second reduction peak observed in cyclic voltammetry associated with the unsaturated ester function was reached.

There are several aspects of the reaction that are currently under study to generate a robust and general olefination electrochemical method via the thiocarbonate reduction; nevertheless, this letter shows for the first time the potential use of electrochemistry with this functional group using green reduction conditions. Application of this methodology to the synthesis of other biologically important products, the study of the reaction scope because other thiocarbonate derivatives seem to be not very reactive, as well as mechanistic details are under investigation and will be reported soon.

Conclusion

A new approach to convert thiocarbonates derived from 1,2-diols containing the 6-pentyl-2*H*-pyran-2-one framework to *trans*-alkenes by means of electrochemical reduction in an H-type separated cell was developed. The thiocarbonate functional group can be reduced using a vitreous carbon electrode in MeOH/H$_2$O 80:20 with AcOH/AcONa buffer 0.5 M as electrolytic media. We term this transformation as the "Electrochemical Corey–Winter (ECW) reaction". This new environmentally friendly process was used to synthetize a metabolite isolated from *Trichoderma viride* in high yield. Alkenes and α,β-unsaturated ester functionalities are stable under the electrolysis conditions. The reaction can be driven by both, controlled potential and constant current electrolysis with excellent results, which is convenient for application in organic chemistry laboratories.

Supporting Information

Supporting Information File 1

Experimental procedures and analytical data.
[https://www.beilstein-journals.org/bjoc/content/supplementary/1860-5397-14-41-S1.pdf]

ORCID® iDs

Fernando Sartillo-Piscil - https://orcid.org/0000-0002-4322-7534
Bernardo A. Frontana-Uribe - https://orcid.org/0000-0003-3796-5933

References

1. Corey, E. J.; Winter, R. A. E. *J. Am. Chem. Soc.* **1963,** *85,* 2677–2678. doi:10.1021/ja00900a043
2. Corey, E. J.; Carey, F. A.; Winter, R. A. E. *J. Am. Chem. Soc.* **1965,** *87,* 934–935. doi:10.1021/ja01082a057
3. Mergott, D. J. *Corey-Winter olefin synthesis.* In *Name Reactions for Functional Group Transformations;* Li, J. J.; Corey, E. J., Eds.; John Wiley & Sons: Hoboken, NJ, 2007; pp 354–362.
4. Corey, E. J.; Hopkins, B. *Tetrahedron Lett.* **1982,** *23,* 1979–1982. doi:10.1016/S0040-4039(00)87238-X
5. Discontinued in Aldrich; available with some distributors in Asia and Europe: 5.0 g per 124-161.20 Euros or 200-390 USD.
6. Ramirez, E.; Sánchez, M.; Meza-León, R. L.; Quintero, L.; Sartillo-Piscil, F. *Tetrahedron Lett.* **2010,** *51,* 2178–2180. doi:10.1016/j.tetlet.2010.02.094
7. Pérez-Bautista, J. A.; Meza-León, R. L.; Cruz-Gregorio, S.; Quintero, L.; Sartillo-Piscil, F. *Tetrahedron Lett.* **2016,** *57,* 4560–4562. doi:10.1016/j.tetlet.2016.08.089
8. Moss, M. O.; Jackson, R. M.; Rogers, D. *Phytochemistry* **1975,** *14,* 2706–2708. doi:10.1016/0031-9422(75)85255-1
9. Sperry, J. B.; Wright, D. L. *Chem. Soc. Rev.* **2006,** *35,* 605–621. doi:10.1039/B512308A
10. Yoshida, J.-i.; Kataoka, K.; Horcajada, R.; Nagaki, A. *Chem. Rev.* **2008,** *108,* 2265–2299. doi:10.1021/cr0680843
11. Waldvogel, S. R.; Janza, B. *Angew. Chem., Int. Ed.* **2014,** *53,* 7122–7123. doi:10.1002/anie.201405082
12. Horn, E. J.; Rosen, B. R.; Baran, P. S. *ACS Cent. Sci.* **2016,** *2,* 302–308. doi:10.1021/acscentsci.6b00091
13. Yan, M.; Kawamata, Y.; Baran, P. S. *Chem. Rev.* **2017,** *117,* 13230–13319. doi:10.1021/acs.chemrev.7b00397
14. Chiba, K.; Okada, Y. *Curr. Opin. Electrochem.* **2017,** *2,* 53–59. doi:10.1016/j.coelec.2017.03.014
15. Rosen, B. R.; Werner, E. W.; O'Brien, A. G.; Baran, P. S. *J. Am. Chem. Soc.* **2014,** *136,* 5571–5574. doi:10.1021/ja5013323
16. Anderson, L. A.; Redden, A.; Moeller, K. D. *Green Chem.* **2011,** *13,* 1652–1654. doi:10.1039/C1GC15207F
17. Francke, R.; Little, R. D. *Chem. Soc. Rev.* **2014,** *43,* 2492–2521. doi:10.1039/c3cs60464k
18. Broese, T.; Francke, R. *Org. Lett.* **2016,** *18,* 5896–5899. doi:10.1021/acs.orglett.6b02979
19. Nguyen, B. H.; Perkins, R. J.; Smith, J. A.; Moeller, K. D. *Beilstein J. Org. Chem.* **2015,** *11,* 280–287. doi:10.3762/bjoc.11.32
20. Little, D.; Moeller, K. D. *Electrochem. Soc. Interface* **2002,** 36–42.
21. Tang, F.; Chen, C.; Moeller, K. D. *Synthesis* **2007,** 3411–3420. doi:10.1055/s-2007-990835
22. Moeller, K. D. *Synlett* **2009,** 1208–1218. doi:10.1055/s-0028-1088126

23. Yoshida, J.-i.; Shimizu, A.; Ashikari, Y.; Morofuji, T.; Hayashi, R.; Nokami, T.; Nagaki, A. *Bull. Chem. Soc. Jpn.* **2015,** *88,* 763–775. doi:10.1246/bcsj.20150100

24. Shimizu, A.; Hayashi, R.; Ashikari, Y.; Nokami, T.; Yoshida, J.-i. *Beilstein J. Org. Chem.* **2015,** *11,* 242–248. doi:10.3762/bjoc.11.27

25. Zhao, H.-B.; Hou, Z.-W.; Liu, Z.-J.; Zhou, Z.-F.; Song, J.; Xu, H.-C. *Angew. Chem., Int. Ed.* **2017,** *56,* 587–590. doi:10.1002/anie.201610715

26. Steckhan, E.; Arns, T.; Heineman, W. R.; Hilt, G.; Hoormann, D.; Jörissen, J.; Kröner, L.; Lewall, B.; Pütter, H. *Chemosphere* **2001,** *43,* 63–73. doi:10.1016/S0045-6535(00)00325-8

27. Schäfer, H. J. *C. R. Chim.* **2011,** *14,* 745–765. doi:10.1016/j.crci.2011.01.002

28. Frontana-Uribe, B. A.; Little, R. D.; Ibanez, J. G.; Palma, A.; Vasquez-Medrano, R. *Green Chem.* **2010,** *12,* 2099–2119. doi:10.1039/c0gc00382d

29. Mihelcic, J.; Moeller, K. D. *J. Am. Chem. Soc.* **2004,** *126,* 9106–9111. doi:10.1021/ja048085h

30. Yin, B.; Inagi, S.; Fuchigami, T. *Beilstein J. Org. Chem.* **2015,** *11,* 85–91. doi:10.3762/bjoc.11.12

31. Palma, A.; Cárdenas, J.; Frontana-Uribe, B. A. *Green Chem.* **2009,** *11,* 283–293. doi:10.1039/B815745F

32. Frontana-Uribe, B. A.; Moinet, C. *Tetrahedron* **1998,** *54,* 3197–3206. doi:10.1016/S0040-4020(98)00058-1

33. Frontana-Uribe, B. A.; Moinet, C.; Toupet, L. *Eur. J. Org. Chem.* **1999,** 419–430. doi:10.1002/(SICI)1099-0690(199902)1999:2<419::AID-EJOC419>3.0. CO;2-V

34. Klemm, L. H.; Olson, D. R. *J. Org. Chem.* **1973,** *38,* 3390–3394. doi:10.1021/jo00959a034

35. Crich, D.; Beckwith, A. L. J.; Chen, C.; Yao, Q.; Davinson, I. G. E.; Longmore, R. W.; Anaya de Parrodi, C.; Quintero-Cortés, L.; Sandoval-Ramirez, J. *J. Am. Chem. Soc.* **1995,** *117,* 8757–8768. doi:10.1021/ja00139a008

36. Sánchez-Eleuterio, A.; Sandoval-Lira, J.; Garcia-Sánchez, J.; Monterrosas-Pérez, L.; Hernández-Pérez, J. M.; Quintero, L.; Sartillo-Piscil, F. *J. Org. Chem.* **2013,** *78,* 9127–9136. doi:10.1021/jo4012943

37. Barton, D. H. R.; Hartwig, W.; Motherwell, W. B. *J. Chem. Soc., Chem. Commun.* **1982,** 447–448. doi:10.1039/C39820000447

Investigating radical cation chain processes in the electrocatalytic Diels–Alder reaction

Yasushi Imada[1], Yohei Okada[2] and Kazuhiro Chiba[*1]

Abstract

Single electron transfer (SET)-triggered radical ion-based reactions have proven to be powerful options in synthetic organic chemistry. Although unique chain processes have been proposed in various photo- and electrochemical radical ion-based transformations, the turnover number, also referred to as catalytic efficiency, remains unclear in most cases. Herein, we disclose our investigations of radical cation chain processes in the electrocatalytic Diels–Alder reaction, leading to a scalable synthesis. A gram-scale synthesis was achieved with high current efficiency of up to 8000%. The reaction monitoring profiles showed sigmoidal curves with induction periods, suggesting the involvement of intermediate(s) in the rate determining step.

Introduction

Recently, radical ion reactivity has received great attention in the field of synthetic organic chemistry. The single electron transfer (SET) strategy is the key to generating radical ions, which provide powerful intermediates for bond formations. Photo- [1-6] and electrochemistry [7-12] are the most straightforward approaches to induce SET processes. Since the pioneering work by Ledwith [13-17], a chain process involving radical ions has constituted a unique mechanism for this class of reactions, which also has the potential for contributing to effec-

tive catalytic transformations. Although understanding the chain mechanism is a prerequisite to the rational design of new radical ion-based reactions, it remains unclear in most cases. In particular, only a handful of reports have mentioned the "length," also referred to as catalytic efficiency, of such radical ion chain processes. As an early example, Bauld estimated the chain lengths of cyclodimerizations of cyclohexadiene and *trans*-anethole (**1**) [18]. More recently, Yoon has established a straightforward method to estimate the chain length of photoredox processes

using the combination of quantum yield and luminescence quenching experiments [19]. With such an understanding in hand, radical ion chain processes could be further optimized to realize greener transformations.

We have been developing anodic cycloadditions [20-25] enabled by lithium perchlorate/nitromethane electrolyte solution [26], some of which were achieved with a catalytic amount of electricity. Such electrocatalytic cycloadditions should involve radical cation chain processes, meaning that the reaction is not only triggered by an oxidative SET at the surface of the electrode but also by an intermolecular SET process in bulk solution. We assumed that the catalytic efficiency of the reaction would be further improved through optimizing and/or tuning the conditions in order to facilitate the bulk SET processes. As recently demonstrated by Baran [27,28] and Waldvogel [29,30], electrochemical synthesis has also proven to be highly scalable as well as sustainable. The longer chain length, also referred to as a higher "current efficiency" in this context, would enhance such advantages of the electrochemical synthesis. It should also be noted that the mechanism of electrochemical reactions can easily be studied since the amount of electricity passed can be precisely controlled in a switchable manner. Described herein is a demonstration of excellent current efficiency and high productivity for the electrocatalytic Diels–Alder reaction.

Results and Discussion

The present work began by optimizing the SET-triggered Diels–Alder reaction of *trans*-anethole (**1**) and isoprene (**2**) as models (Scheme 1), which was first reported by Bauld [31] and was elegantly revisited by Yoon [32]. We also reported the electrochemical variation of the reaction [21,22], which was

found to go to completion with a catalytic amount of electricity. The desired Diels–Alder adduct **3** was obtained in 98% yield with less than 0.1 F/mol of electricity, suggesting that the current efficiency was up to 980%. The key step in the chain process should be the bulk SET between the starting *trans*-anethole (**1**) and the aromatic radical cation (**3**·+), triggering the catalytic cycle (Figure 1). The concentration of substrates must be balanced to lengthen the chain process, since a higher concentration of *trans*-anethole (**1**) is effective for the bulk SET, but it can also cause undesired self-dimerization. We intentionally stopped the reaction at 0.01 F/mol in order to highlight the difference between the concentrations used and then optimize them (Table 1).

Scheme 1: SET-triggered Diels–Alder reaction of *trans*-anethole (**1**) and isoprene (**2**).
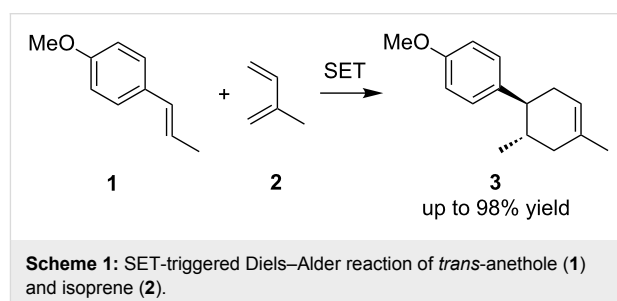
When a relatively lower concentration was used, the current efficiency was measured at 1300% (Table 1, entry 1). The termination of the radical cation chain process would be a reductive SET of the radical cations (**1**·+, **3**·+) at the cathode. Therefore, we tested higher concentrations of the substrates to facilitate the bulk SET processes. Gratifyingly, we were able to achieve increased current efficiencies when 100 mM and 300 mM concentrations of *trans*-anethole (**1**) were used (Table 1, entries 2 and 3). However, some dimerization of
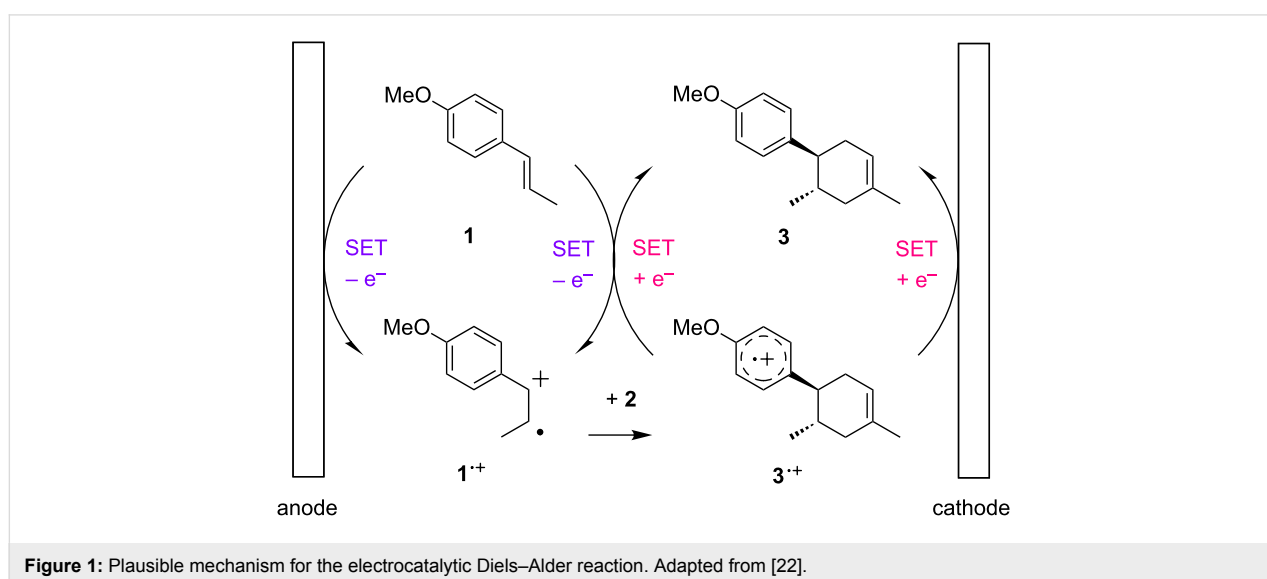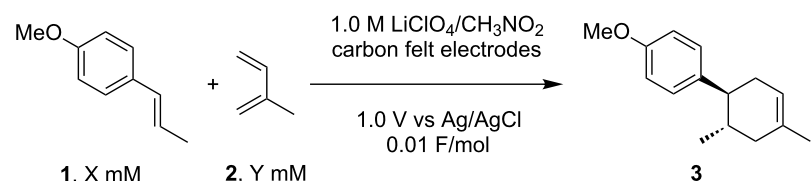

Figure 1: Plausible mechanism for the electrocatalytic Diels–Alder reaction. Adapted from [22].

Table 1: Optimization of the electrocatalytic Diels–Alder reaction.

Entry[a]	Conditions	Yield (%)[b], current efficiency (%)
1	X = 16, Y = 48	13, 1300
2	X = 100, Y = 300	58, 5800
3	X = 300, Y = 900	62, 6200
4	X = 300, Y = 3000	80, 8000

[a]All reactions were carried out in 10 mL of CH$_3$NO$_2$ at rt. [b]Yields were determined by ^{1}H NMR analysis using benzaldehyde as an internal standard.

trans-anethole (**1**) via the trapping of the radical cation (**1**$^{\cdot+}$) by neutral *trans*-anethole was also detected in both cases (Scheme 2). Since the undesired dimerization can decrease the current efficiency, we raised the amount of isoprene (**2**) from 3 to 10 equivalents in order to suppress it (Table 1, entry 4). As a result, the current efficiency reached up to 8000%, meaning that one electron was able to produce 80 molecules of the Diels–Alder adduct **3**.

With the optimized conditions (Table 1, entry 4) in hand, we monitored the reaction by gas chromatography mass spectrometry (GC–MS, Figure 2). Surprisingly, we found that only 0.015 F/mol was sufficient to complete the reaction and the Diels–Alder adduct **3** was obtained in 98% yield, suggesting that the current efficiency was up to 6533%. To the best of our knowledge, this is one of the highest current efficiencies in electrochemical synthesis in that one electron can run the radical cation chain process up to 65 times.

GC–MS monitoring showed a sigmoidal curve with an induction period. The monitoring was carried out in the presence of a large excess (10 equivalents) of isoprene (**2**), which might

follow pseudo-first order reaction kinetics. However, the observed induction period indicated that this was not the case and an intermediate(s) was involved in the rate determining step. This mechanism could be rationalized on the basis of a radical cation chain process since the concentrations of both starting *trans*-anethole (**1**) and the aromatic radical cation (**3**$^{\cdot+}$) would impact the overall reaction rate. Indeed, when the monitoring was carried out with a lower concentration of *trans*-anethole (**1**), no induction period was observed and the reaction required nearly a stoichiometric amount of electricity to complete (Figure 3).

We finally turned our attention to the scalability of the reaction. On the basis of the above discussed radical cation chain mechanism, even higher concentrations of the substrates would still be effective (Table 2). To our delight, a high current efficiency of around 5000% was maintained even at 1.0 M and 2.0 M concentrations of *trans*-anethole (**1**, Table 2, entries 1 and 2). However, 5.0 M was too concentrated and caused precipitation of the supporting electrolyte (Table 2, entry 3). To our satisfaction, up to 4.15 g of the Diels–Alder adduct (**3**) was isolated with 0.03 F/mol, giving a current efficiency of 3167% (Table 2,
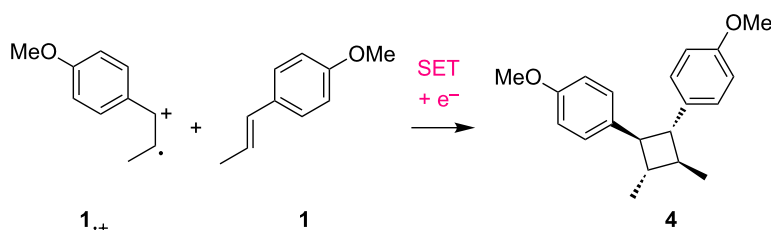
Scheme 2: Undesired dimerization of *trans*-anethole (**1**).
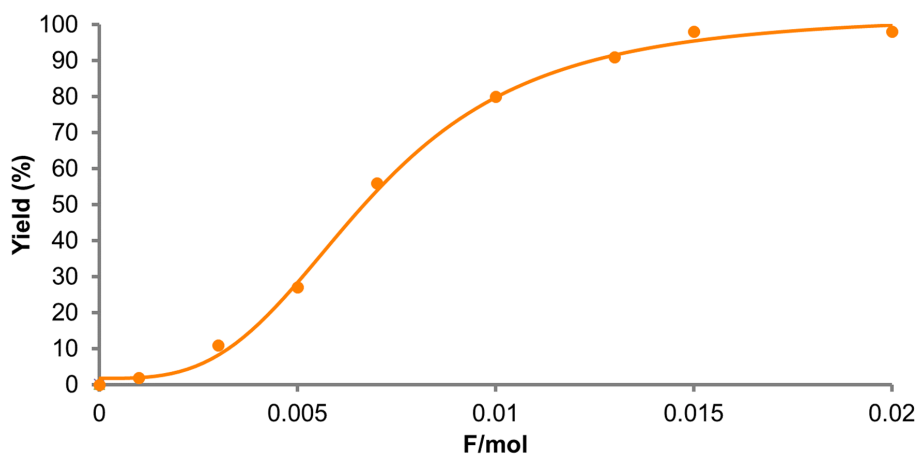
Figure 2: GC–MS monitoring of the electrocatalytic Diels–Alder reaction (**1**: 300 mM; **2**: 3000 mM).
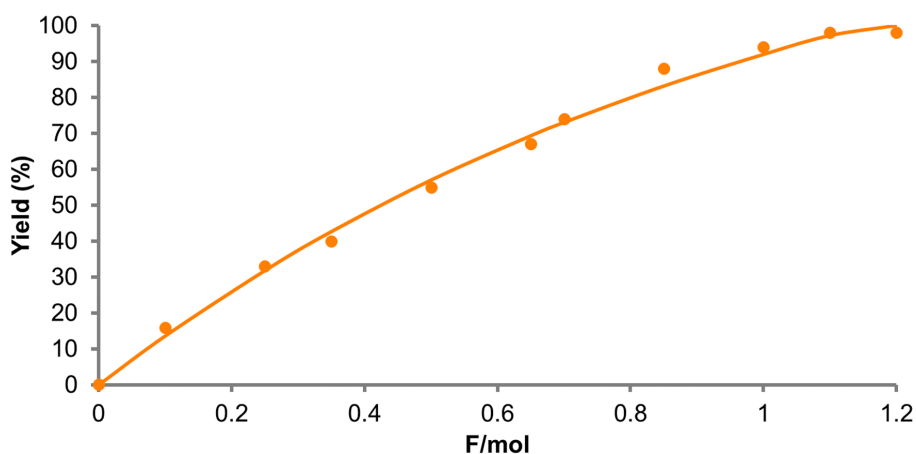
Figure 3: GC–MS monitoring of the electrocatalytic Diels–Alder reaction (**1**: 1 mM; **2**: 2000 mM).

Table 2: Optimization of the electrocatalytic Diels–Alder reaction.
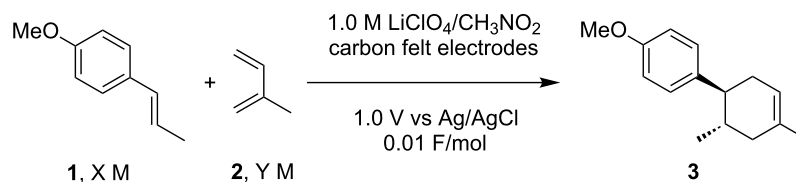
Entry[a]	Conditions	Yield (%)[b], current efficiency (%)
1	X = 1, Y = 3	55, 5500
2	X = 2, Y = 6	49, 4900
3	X = 5, Y = 15	2, 200
4	X = 2, Y = 6	95, 3167[c], 4.15 g

[a]All reactions were carried out in 10 mL of CH_3NO_2 at rt. [b]Yields were determined by ^1H NMR analysis using benzaldehyde as an internal standard. [c]0.03 F/mol was used.
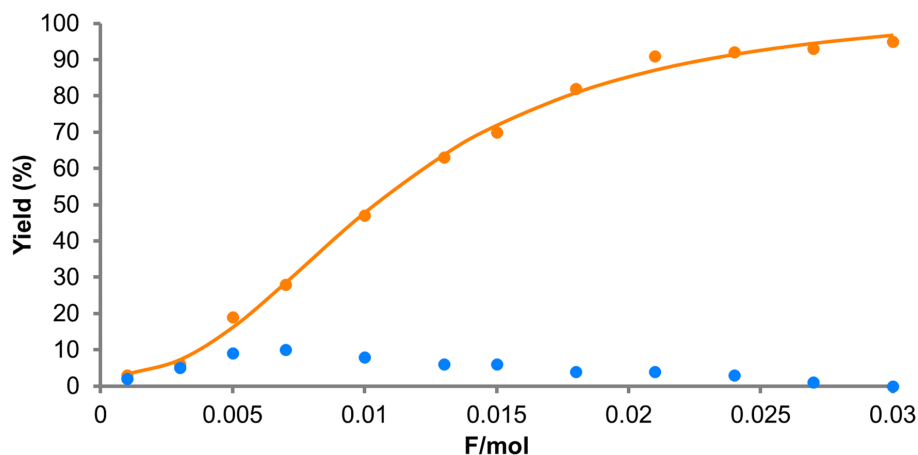
Figure 4: GC–MS monitoring of the electrocatalytic Diels–Alder reaction (**1**: 2 M; **2**: 6 M). Blue dots show the dimer **4**.

entry 4). Under these conditions, the undesired dimerization of *trans*-anethole (**1**) took place to give the dimer **4**. However, we found that the electrochemical radical cation Diels–Alder reaction was also possible from the dimer, whose photochemical version was reported by Yoon [33]. The reaction was monitored by GC–MS and also showed a sigmoidal curve (Figure 4).

Conclusion

In conclusion, we have optimized the reaction conditions for the electrocatalytic Diels–Alder reaction in order to improve the turnover number of the radical cation chain process, which resulted in a current efficiency of up to 8000%. To the best of our knowledge, this is one of the highest current efficiencies in electrochemical synthesis to date in that one electron can run the radical cation chain process up to 80 times. Taking advantage of this effective radical cation chain process, we also demonstrated that over 4 grams of the Diels–Alder adduct were obtained with high current efficiency. The reaction was monitored by GC–MS to show sigmoidal curves, suggesting the involvement of intermediate(s) in the rate determining step. Our findings described herein would lead to further design of SET-triggered radical ion-based reactions involving chain processes with high catalytic efficiency and productivity.

Supporting Information

Supporting Information File 1

Additional figure, general remarks, synthesis and characterization data, including copies of ^1H and ^{13}C NMR spectra.
[https://www.beilstein-journals.org/bjoc/content/supplementary/1860-5397-14-51-S1.pdf]

ORCID® iDs

Yohei Okada - https://orcid.org/0000-0002-4353-1595

References

1. Twilton, J.; Le, C.; Zhang, P.; Shaw, M. H.; Evans, R. W.; MacMillan, D. W. C. *Nat. Rev. Chem.* **2017**, *1*, No. 0052. doi:10.1038/s41570-017-0052
2. Prier, C. K.; Rankic, D. A.; MacMillan, D. W. C. *Chem. Rev.* **2013**, *113*, 5322–5363. doi:10.1021/cr300503r
3. Skubi, K. L.; Blum, T. R.; Yoon, T. P. *Chem. Rev.* **2016**, *116*, 10035–10074. doi:10.1021/acs.chemrev.6b00018
4. Schultz, D. M.; Yoon, T. P. *Science* **2014**, *343*, 1239176. doi:10.1126/science.1239176
5. Kärkäs, M. D.; Porco, J. A., Jr.; Stephenson, C. R. J. *Chem. Rev.* **2016**, *116*, 9683–9747. doi:10.1021/acs.chemrev.5b00760
6. Narayanam, J. M. R.; Stephenson, C. R. J. *Chem. Soc. Rev.* **2011**, *40*, 102–113. doi:10.1039/B913880N
7. Yoshida, J.-i.; Shimizu, A.; Hayashi, R. *Chem. Rev.* **2018**. doi:10.1021/acs.chemrev.7b00475
8. Yoshida, J.-i.; Kataoka, K.; Horcajada, R.; Nagaki, A. *Chem. Rev.* **2008**, *108*, 2265–2299. doi:10.1021/cr0680843
9. Yan, M.; Kawamata, Y.; Baran, P. S. *Chem. Rev.* **2017**, *117*, 13230–13319. doi:10.1021/acs.chemrev.7b00397
10. Horn, E. J.; Rosen, B. R.; Baran, P. S. *ACS Cent. Sci.* **2016**, *2*, 302–308. doi:10.1021/acscentsci.6b00091
11. Francke, R.; Little, R. D. *Chem. Soc. Rev.* **2014**, *43*, 2492–2521. doi:10.1039/c3cs60464k
12. Sperry, J. B.; Wright, D. L. *Chem. Soc. Rev.* **2006**, *35*, 605–621. doi:10.1039/b512308a
13. Bawn, C. E. H.; Ledwith, A.; Shih-Lin, Y. *Chem. Ind.* **1965**, 769–770.
14. Bell, F. A.; Crellin, R. A.; Fujii, H.; Ledwith, A. *J. Chem. Soc. D* **1969**, 251–252. doi:10.1039/c29690000251

15. Carruthers, R. A.; Crellin, R. A.; Ledwith, A. *J. Chem. Soc. D* **1969,** 252–253. doi:10.1039/c29690000252
16. Crellin, R. A.; Lambert, M. C.; Ledwith, A. *J. Chem. Soc. D* **1970,** 682–683. doi:10.1039/c29700000682
17. Ledwith, A. *Acc. Chem. Res.* **1972,** *5,* 133–139. doi:10.1021/ar50052a003
18. Lorenz, K. T.; Bauld, N. L. *J. Am. Chem. Soc.* **1987,** *109,* 1157–1160. doi:10.1021/ja00238a027
19. Cismesia, M. A.; Yoon, T. P. *Chem. Sci.* **2015,** *6,* 5426–5434. doi:10.1039/C5SC02185E
20. Okada, Y.; Chiba, K. *Chem. Rev.* **2018**. doi:10.1021/acs.chemrev.7b00400
21. Ozaki, A.; Yamaguchi, Y.; Okada, Y.; Chiba, K. *ChemElectroChem* **2017,** *4,* 1852–1855. doi:10.1002/celc.201700286
22. Okada, Y.; Yamaguchi, Y.; Ozaki, A.; Chiba, K. *Chem. Sci.* **2016,** *7,* 6387–6393. doi:10.1039/C6SC02117D
23. Okada, Y.; Shimada, K.; Kitano, Y.; Chiba, K. *Eur. J. Org. Chem.* **2014,** 1371–1375. doi:10.1002/ejoc.201301604
24. Yamaguchi, Y.; Okada, Y.; Chiba, K. *J. Org. Chem.* **2013,** *78,* 2626–2638. doi:10.1021/jo3028246
25. Okada, Y.; Nishimoto, A.; Akaba, R.; Chiba, K. *J. Org. Chem.* **2011,** *76,* 3470–3476. doi:10.1021/jo200490q
26. Imada, Y.; Yamaguchi, Y.; Shida, N.; Okada, Y.; Chiba, K. *Chem. Commun.* **2017,** *53,* 3960–3963. doi:10.1039/C7CC00664K
27. Kawamata, Y.; Yan, M.; Liu, Z.; Bao, D.-H.; Chen, J.; Starr, J. T.; Baran, P. S. *J. Am. Chem. Soc.* **2017,** *139,* 7448–7451. doi:10.1021/jacs.7b03539
28. Horn, E. J.; Rosen, B. R.; Chen, Y.; Tang, J.; Chen, K.; Eastgate, M. D.; Baran, P. S. *Nature* **2016,** *533,* 77–81. doi:10.1038/nature17431
29. Gütz, C.; Stenglein, A.; Waldvogel, S. R. *Org. Process Res. Dev.* **2017,** *21,* 771–778. doi:10.1021/acs.oprd.7b00123
30. Gütz, C.; Bänziger, M.; Bucher, C.; Galvão, T. R.; Waldvogel, S. R. *Org. Process Res. Dev.* **2015,** *19,* 1428–1433. doi:10.1021/acs.oprd.5b00272
31. Reynolds, D. W.; Bauld, N. L. *Tetrahedron* **1986,** *42,* 6189–6194. doi:10.1016/S0040-4020(01)88079-0
32. Lin, S.; Ischay, M. A.; Fry, C. G.; Yoon, T. P. *J. Am. Chem. Soc.* **2011,** *133,* 19350–19353. doi:10.1021/ja2093579
33. Ischay, M. A.; Ament, M. S.; Yoon, T. P. *Chem. Sci.* **2012,** *3,* 2807–2811. doi:10.1039/c2sc20658g

License and Terms

Stepwise radical cation Diels–Alder reaction via multiple pathways

Ryo Shimizu[1], Yohei Okada[2] and Kazuhiro Chiba[*1]

Abstract

Herein we disclose the radical cation Diels–Alder reaction of aryl vinyl ethers by electrocatalysis, which is triggered by an oxidative SET process. The reaction clearly proceeds in a stepwise fashion, which is a rare mechanism in this class. We also found that two distinctive pathways, including "direct" and "indirect", are possible to construct the Diels–Alder adduct.

Introduction

Umpolung, also known as polarity inversion, is a powerful approach in synthetic organic chemistry to trigger reactions that are otherwise difficult or impossible. In an umpolung reaction, the normal reactivity of the molecules being studied is reversed, e.g., electrophilicity is generated from a nucleophile. The single electron transfer (SET) process has been recognized as the most straightforward way to induce umpolung, which has recently been carried out by means of photo- [1-6] and electrochemical [7-12] approaches. A typical example involves an oxidative SET of an electron-rich and thus nucleophilic C–C double bond. The oxidative SET produces a radical cation species, which offers electrophilic reactivity for subsequent transformations. Enol ether radical cations are among the simplest members of

this class and thus have been widely used in synthetic organic chemistry [13-15].

The Diels–Alder reaction is a classic reaction, and one of the most powerful methods to construct six-membered ring systems. A "normal" Diels–Alder reaction must consider an electronic matching of the substrates, with an electron-rich diene and electron-deficient dienophile as the general combination. Although having both an electron-rich diene and dienophile is a less- or non-effective combination, oxidative SET has proven to be able to overcome this mismatch and such a strategy is well-known as a radical cation Diels–Alder reaction. The use of *trans*-anethole as a model electron-rich dienophile is

the representative example in this class. It was first reported by Bauld in 1986 [16] and was elegantly revisited by Yoon in 2011 [17] in the field of photoredox catalysis (Scheme 1). The reaction was further studied by Ferreira and Shores [18], followed by a unique mechanistic investigation by Rappé [19]. Although most recent examples of the radical cation Diels–Alder reaction have employed styrenes, the scope is not limited to such electron-rich dienophiles. Bauld and Yoon demonstrated that aryl vinyl ethers, enol ether equivalents, and aryl vinyl sulfides are also promising dienophiles for the reactions (Scheme 2) [17,20-25].

Scheme 1: Radical cation Diels–Alder reaction of *trans*-anethole [17].

Scheme 2: Radical cation Diels–Alder reactions of aryl vinyl ether and sulfides [17,25].
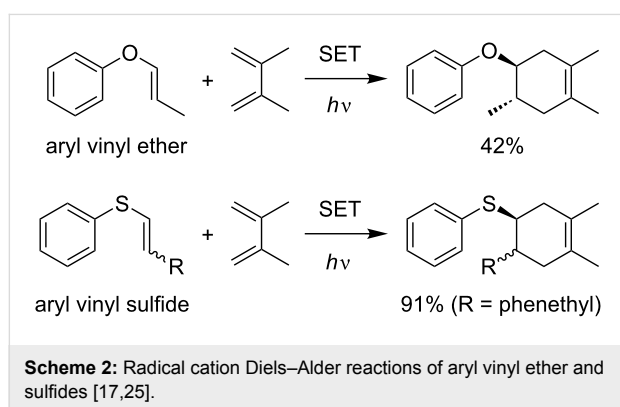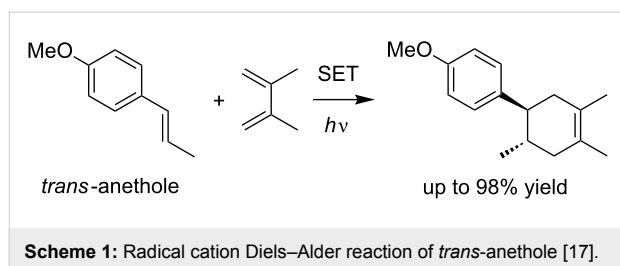
We have been developing oxidative SET-triggered cycloadditions of enol ethers by electrocatalysis [26-32] in lithium per-

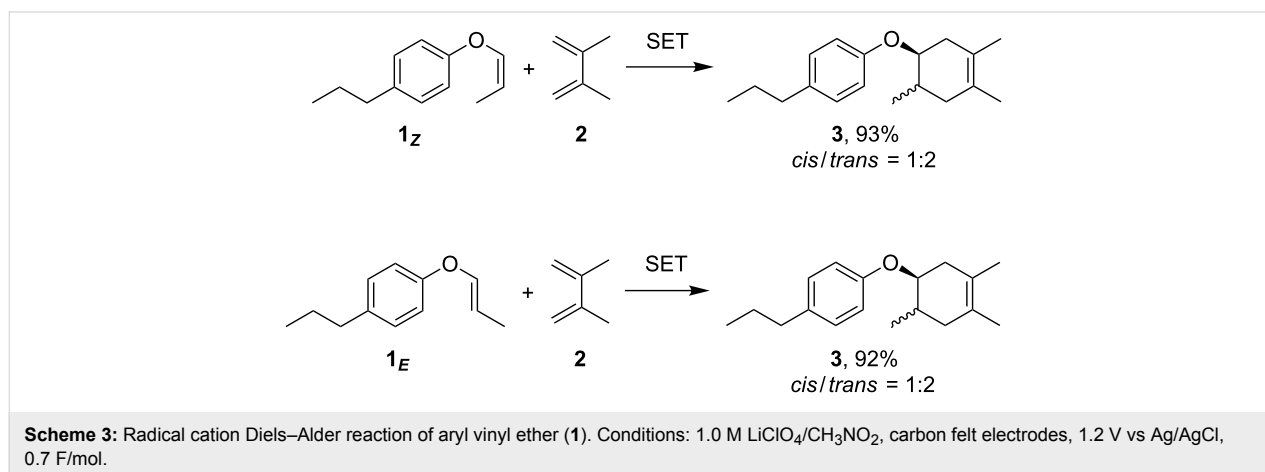chlorate/nitromethane electrolyte solution [33]. The reactions involve a radical cation chain process and are complete using a catalytic amount of electricity. During the course of our study, we discovered that radical cation Diels–Alder reactions are also possible by electrocatalysis, however, the scope was limited to styrenes [34]. Described herein is a stepwise radical cation Diels–Alder reaction of enol ethers by electrocatalysis, which proceeds via multiple unique pathways.

Results and Discussion

The present work began with the synthesis of the aryl vinyl ether **1** from *p*-propylphenol in 2 steps (Scheme S1 and Figure S1 in Supporting Information File 1). Both *E*- and *Z*-forms were readily purified by silica gel column chromatography. When the anodic oxidation of the *Z*-form **1$_Z$** was carried out in the presence of 2,3-dimethyl-1,3-butadiene (**2**), the corresponding Diels–Alder adduct **3** was obtained in excellent yield (Scheme 3). The reaction was completed using a catalytic amount of electricity and therefore should involve a radical cation chain process. Since Diels–Alder adduct **3** was an approximately *cis/trans* = 1:2 mixture, the reaction must proceed in a stepwise fashion. This stereochemistry was confirmed when the *E*-form **1$_E$** also gave the same synthetic outcome. Namely, the Diels–Alder adduct **3** was obtained as an approximately *cis/trans* = 1:2 mixture, indicating that the reaction was indeed stepwise.

When the reaction was carefully monitored by gas chromatography–mass spectrometry (GC–MS), we found that an adduct was generated in the early stage that was not the Diels–Alder product **3**. Therefore, we intentionally stopped the reaction after 0.1 F/mol of electricity had passed and attempted to identify the adduct. We found that it was a vinylcyclobutane **4**, whose formation was only observed in the early stage of the reaction and was completely consumed after 0.7 F/mol of electricity was passed (Scheme 4 and Figure 1). Vinylcyclobutanes are known

Scheme 3: Radical cation Diels–Alder reaction of aryl vinyl ether (**1**). Conditions: 1.0 M LiClO$_4$/CH$_3$NO$_2$, carbon felt electrodes, 1.2 V vs Ag/AgCl, 0.7 F/mol.
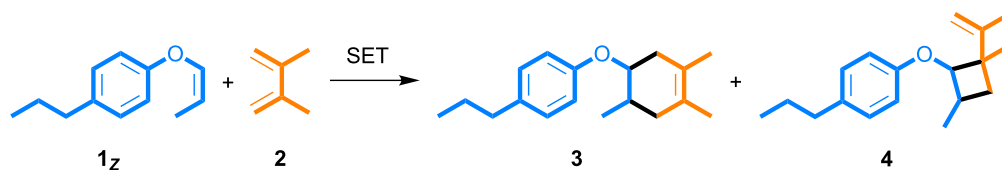
Scheme 4: Oxidative SET-triggered reaction of aryl vinyl ether **1**$_c$. Conditions: 1.0 M LiClO$_4$/CH$_3$NO$_2$, carbon felt electrodes, 1.2 V vs Ag/AgCl, 0.1 F/mol.
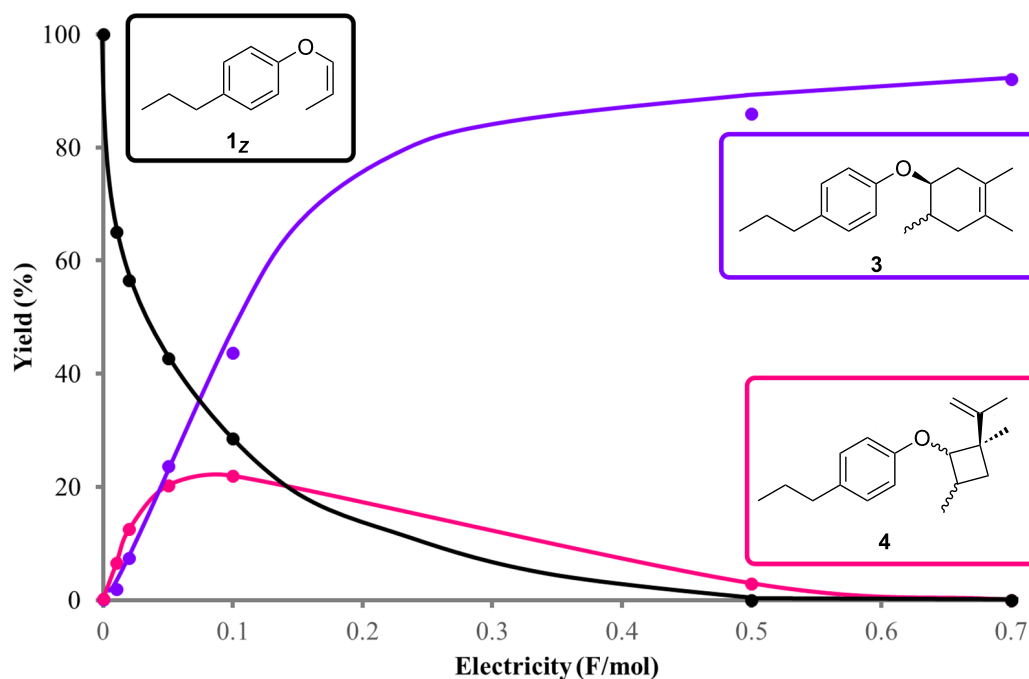
Figure 1: GC–MS Monitoring of the oxidative SET-triggered reaction of aryl vinyl ether **1**$_c$.

to rearrange to cyclohexenes via thermal and/or photochemical processes and therefore, we carried out the anodic oxidation of vinylcyclobutane **4** in the absence of 2,3-dimethyl-1,3-buta-diene (**2**, Scheme 5 and Supporting Information File 1, Figure S2). Interestingly, the rearrangement took place effectively to give Diels–Alder adduct **3** as an approximately *cis/trans* = 1:4 mixture, a significant difference from the synthetic outcome mentioned above (Scheme 3). Notably, no rearrangement was observed without electricity and the vinyl substituent was found to be essential for the transformation since no cyclohexane **6** was obtained from the cyclobutane **5** (Scheme 6). We also found that the Diels–Alder adduct **3** with an approximately *cis/trans* = 1:1 mixture was obtained in the early stage of the reaction (Supporting Information File 1, Figure S3).

Taken together, we can now propose a mechanism for the radical cation Diels–Alder reaction of the aryl vinyl ether **1**
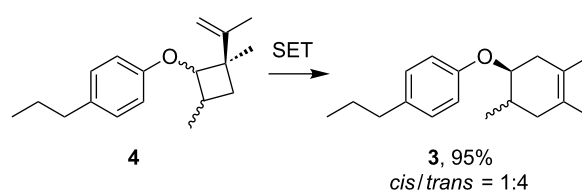
Scheme 5: Oxidative SET-triggered rearrangement of vinyl cyclo-butane **4**. Conditions: 1.0 M LiClO$_4$/CH$_3$NO$_2$, carbon felt electrodes, 1.2 V vs Ag/AgCl, 0.5 F/mol.

(Scheme 7). On the basis of the oxidation potentials, oxidative SET would selectively take place from the aryl vinyl ether **1** even in the presence of 2,3-dimethyl-1,3-butadiene (**2**) to generate the radical cation **1**$^{•+}$, in which the stereochemistry derived from the starting material is lost. Indeed, the anodic oxi-dation of either the *Z*- (**1**$_Z$) or the *E*-form (**1**$_E$) in the absence of

Scheme 6: Unsuccessful rearrangement of cyclobutanes. Conditions: 1.0 M LiClO$_4$/CH$_3$NO$_2$, carbon felt electrodes, a) no electricity, b)1.2 V vs Ag/AgCl, 0.1 F/mol.
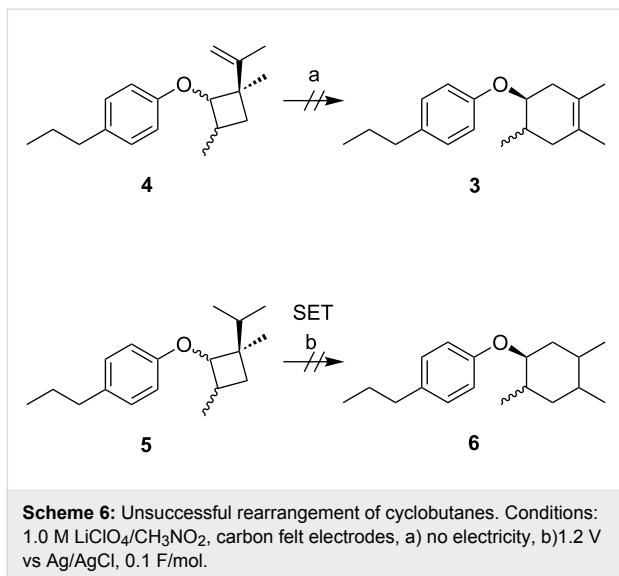
2,3-dimethyl-1,3-butadiene (**2**) led to isomerization. In other words, inversion of the configuration of the radical cation **1**$^{·+}$ proceeds readily, leading to a loss in stereoselectivity. The radical cation **1**$^{·+}$ is then trapped by 2,3-dimethyl-1,3-butadiene (**2**) to construct the acyclic radical cation intermediate **A**$^{·+}$, which is potentially converted into the aromatic radical cation with a six-membered ring (**3**$^{·+}$) or a four-membered ring (**4**$^{·+}$) via rapid intramolecular SET processes. It can be rationalized that the six-membered ring closure of the acyclic radical cation intermediate (**A**$^{·+}$) would be a stepwise process, leading to the Diels–Alder adduct **3** as an approximately *cis*/*trans* = 1:1 mix-

ture. However, since the oxidative SET-triggered rearrangement of the vinylcyclobutane **4** gives the Diels–Alder adduct **3** as an approximately *cis*/*trans* = 1:4 mixture, this should proceed via a different intermediate from the acyclic radical cation intermediate (**A**$^{·+}$). Here, we propose the cyclic radical cation intermediate **B**$^{·+}$ for the rearrangement, imparting stereoselectivity for the six-membered ring closure. The anodic oxidation of the Diels–Alder adduct **3** does not give either the retro-reaction product **1** or the vinylcyclobutane **4** and therefore, it seems that the overall transformation involves irreversible steps. Thus, the radical cation Diels–Alder reaction of aryl vinyl ether **1** effectively proceeds either via "direct" or "indirect" pathways, affording the corresponding adduct **3** in excellent yield.

Conclusion

In conclusion, we have demonstrated that the radical cation Diels–Alder reaction initiated by electrocatalysis in lithium perchlorate/nitromethane electrolyte solution is not limited to styrenes but was also effective for the aryl vinyl ether. While the mechanism is still controversial, most reported radical cation Diels–Alder reactions are highly stereoselective, even including stereospecific concerted examples. On the other hand, our current results clearly indicate that a stepwise mechanism is also effective for this class. Furthermore, the radical cation Diels–Alder reaction of the aryl vinyl ether is found to proceed via multiple unique pathways, including direct and indirect manners. Our findings described herein are beneficial to design novel SET-triggered cycloadditions, which are under development in our laboratory.

Scheme 7: Proposed mechanism for the radical cation Diels–Alder reaction of aryl vinyl ether **1**.
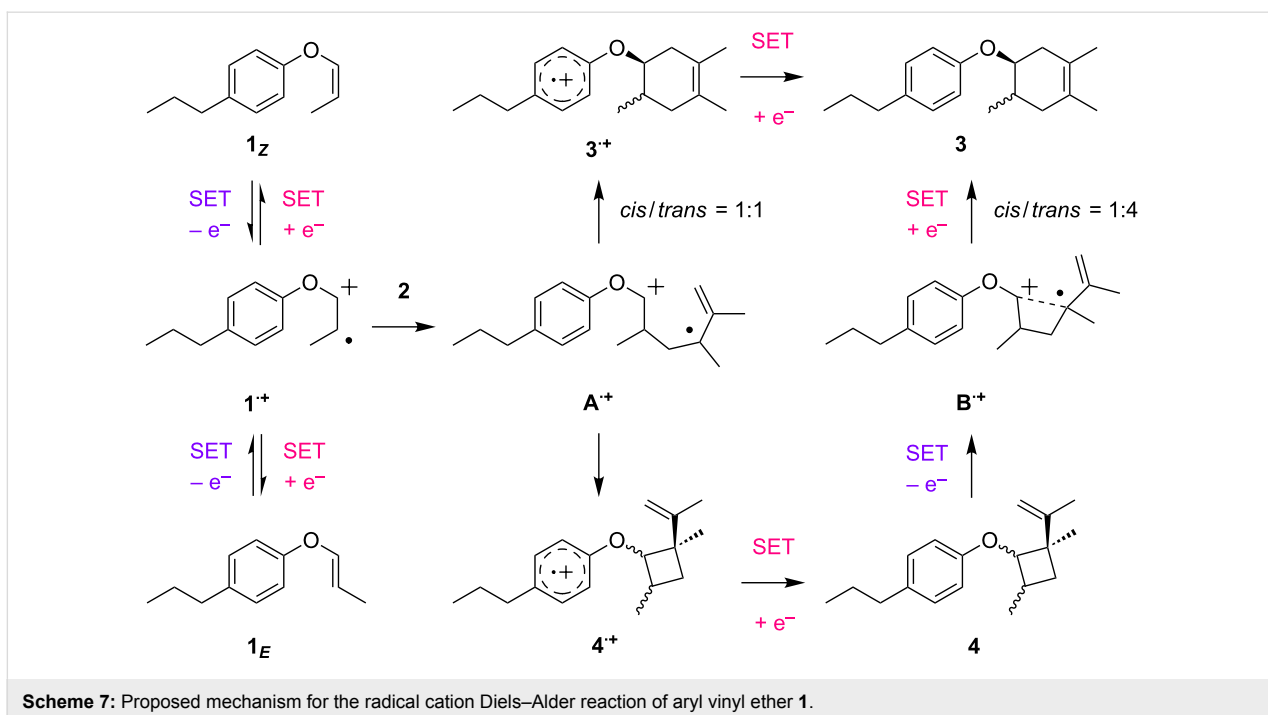
Supporting Information

Supporting Information File 1

Additional scheme and figures, general remarks, synthesis and characterization data, including copies of ^{1}H and ^{13}C NMR spectra.

[https://www.beilstein-journals.org/bjoc/content/supplementary/1860-5397-14-59-S1.pdf]

Acknowledgements

ORCID® iDs

Yohei Okada - https://orcid.org/0000-0002-4353-1595

References

1. Twilton, J.; Le, C.; Zhang, P.; Shaw, M. H.; Evans, R. W.; MacMillan, D. W. C. *Nat. Rev. Chem.* **2017,** *1,* No. 0052. doi:10.1038/s41570-017-0052
2. Prier, C. K.; Rankic, D. A.; MacMillan, D. W. C. *Chem. Rev.* **2013,** *113,* 5322–5363. doi:10.1021/cr300503r
3. Skubi, K. L.; Blum, T. R.; Yoon, T. P. *Chem. Rev.* **2016,** *116,* 10035–10074. doi:10.1021/acs.chemrev.6b00018
4. Schultz, D. M.; Yoon, T. P. *Science* **2014,** *343,* 1239176. doi:10.1126/science.1239176
5. Kärkäs, M. D.; Porco, J. A., Jr.; Stephenson, C. R. J. *Chem. Rev.* **2016,** *116,* 9683–9747. doi:10.1021/acs.chemrev.5b00760
6. Narayanam, J. M. R.; Stephenson, C. R. J. *Chem. Soc. Rev.* **2011,** *40,* 102–113. doi:10.1039/B913880N
7. Yoshida, J.-i.; Shimizu, A.; Hayashi, R. *Chem. Rev.* **2018**. doi:10.1021/acs.chemrev.7b00475
8. Yoshida, J.-i.; Kataoka, K.; Horcajada, R.; Nagaki, A. *Chem. Rev.* **2008,** *108,* 2265–2299. doi:10.1021/cr0680843
9. Yan, M.; Kawamata, Y.; Baran, P. S. *Chem. Rev.* **2017,** *117,* 13230–13319. doi:10.1021/acs.chemrev.7b00397
10. Horn, E. J.; Rosen, B. R.; Baran, P. S. *ACS Cent. Sci.* **2016,** *2,* 302–308. doi:10.1021/acscentsci.6b00091
11. Francke, R.; Little, R. D. *Chem. Soc. Rev.* **2014,** *43,* 2492–2521. doi:10.1039/c3cs60464k
12. Sperry, J. B.; Wright, D. L. *Chem. Soc. Rev.* **2006,** *35,* 605–621. doi:10.1039/b512308a
13. Feng, R.; Smith, J. A.; Moeller, K. D. *Acc. Chem. Res.* **2017,** *50,* 2346–2352. doi:10.1021/acs.accounts.7b00287
14. Moeller, K. D. *Synlett* **2009,** 1208–1218. doi:10.1055/s-0028-1088126
15. Tang, F.; Moeller, K. D. *Tetrahedron* **2009,** *65,* 10863–10875. doi:10.1016/j.tet.2009.09.028
16. Reynolds, D. W.; Bauld, N. L. *Tetrahedron* **1986,** *42,* 6189–6194. doi:10.1016/S0040-4020(01)88079-0
17. Lin, S.; Ischay, M. A.; Fry, C. G.; Yoon, T. P. *J. Am. Chem. Soc.* **2011,** *133,* 19350–19353. doi:10.1021/ja2093579
18. Stevenson, S. M.; Shores, M. P.; Ferreira, E. M. *Angew. Chem., Int. Ed.* **2015,** *54,* 6506–6510. doi:10.1002/anie.201501220
19. Higgins, R. F.; Fatur, S. M.; Shepard, S. G.; Stevenson, S. M.; Boston, D. J.; Ferreira, E. M.; Damrauer, N. H.; Rappé, A. K.; Shores, M. P. *J. Am. Chem. Soc.* **2016,** *138,* 5451–5464. doi:10.1021/jacs.6b02723
20. Reynolds, D. W.; Harirchian, B.; Chiou, H. S.; Marsh, B. K.; Bauld, N. L. *J. Phys. Org. Chem.* **1989,** *2,* 57–88. doi:10.1002/poc.610020108
21. Pabon, R. A.; Bellville, D. J.; Bauld, N. L. *J. Am. Chem. Soc.* **1984,** *106,* 2730–2731. doi:10.1021/ja00321a059
22. Harirchian, B.; Bauld, N. L. *J. Am. Chem. Soc.* **1989,** *111,* 1826–1828. doi:10.1021/ja00187a041
23. Aplin, J. T.; Bauld, N. L. *J. Chem. Soc., Perkin Trans. 2* **1997,** 853–855. doi:10.1039/a605317c
24. Harirchian, B.; Bauld, N. L. *Tetrahedron Lett.* **1987,** *28,* 927–930. doi:10.1016/S0040-4039(00)95876-3
25. Lin, S.; Lies, S. D.; Gravatt, C. S.; Yoon, T. P. *Org. Lett.* **2017,** *19,* 368–371. doi:10.1021/acs.orglett.6b03545
26. Okada, Y.; Chiba, K. *Chem. Rev.* **2018**. doi:10.1021/acs.chemrev.7b00400
27. Yamaguchi, Y.; Okada, Y.; Chiba, K. *J. Org. Chem.* **2013,** *78,* 2626–2638. doi:10.1021/jo3028246
28. Okada, Y.; Nishimoto, A.; Akaba, R.; Chiba, K. *J. Org. Chem.* **2011,** *76,* 3470–3476. doi:10.1021/jo200490q
29. Okada, Y.; Chiba, K. *Electrochim. Acta* **2011,** *56,* 1037–1042. doi:10.1016/j.electacta.2010.10.042
30. Okada, Y.; Akaba, R.; Chiba, K. *Org. Lett.* **2009,** *11,* 1033–1035. doi:10.1021/ol802984n
31. Arata, M.; Miura, T.; Chiba, K. *Org. Lett.* **2007,** *9,* 4347–4350. doi:10.1021/ol7019845
32. Chiba, K.; Miura, T.; Kim, S.; Kitano, Y.; Tada, M. *J. Am. Chem. Soc.* **2001,** *123,* 11314–11315. doi:10.1021/ja016885b
33. Imada, Y.; Yamaguchi, Y.; Shida, N.; Okada, Y.; Chiba, K. *Chem. Commun.* **2017,** *53,* 3960–3963. doi:10.1039/C7CC00664K
34. Okada, Y.; Yamaguchi, Y.; Ozaki, A.; Chiba, K. *Chem. Sci.* **2016,** *7,* 6387–6393. doi:10.1039/C6SC02117D

License and Terms

Anodic oxidation of bisamides from diaminoalkanes by constant current electrolysis

Tatiana Golub and James Y. Becker[*]

Abstract

In general, bisamides derived from diamines and involving 3 and 4 methylene groups as spacers between the two amide functionalities behave similar to monoamides upon anodic oxidation in methanol/LiClO$_4$ because both types undergo majorly mono- and dimethoxylations at the α-position to the N atom. However, in cases where the spacer contains two methylene groups only the anodic process leads mostly to CH$_2$–CH$_2$ bond cleavage to afford products of type RCONHCH$_2$OCH$_3$. Moreover, upon replacing LiClO$_4$ with Et$_4$NBF$_4$ an additional fragmentation type of product was generated from the latter amides, namely RCONHCHO. Also, the anodic process was found to be more efficient with C felt as the anode, and in a mixture of 1:1 methanol/acetonitrile co-solvents.

Introduction

It is well known that the anodic oxidation of amides involving a hydrogen atom at the α-position to the N atom could undergo alkoxylation, carboxylation and hydroxylation at this position [1-5] (Scheme 1). It has been found that anodic methoxylation of amides (and carbamates) can be utilized to form new carbon–carbon bonds [6,7] (Scheme 2). Furthermore, this anodic route could also be important from a synthetic point of view, affording ring-expansion [8-10] and annulation of rings [1,11,12] (Scheme 3).

Interestingly, in the case of anodic oxidation of aromatic amides of type Ph$_2$CHCONHAr, where no hydrogen atom is present at
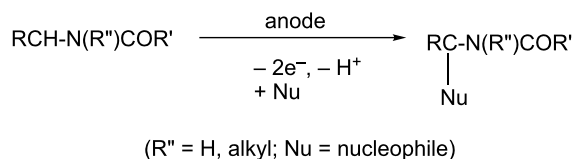
Scheme 1: Anodic oxidation of amides.
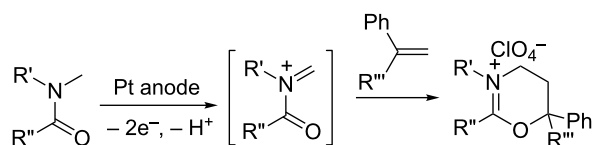
Scheme 2: Anodic oxidation of an amide in the presence of alkene.

Scheme 4: Anodic bond cleavages in amides of type $Ph_2CHCONHAr$.
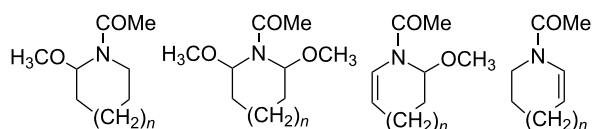
Scheme 5: Type of products obtained (*n* = 0, 1, 2).
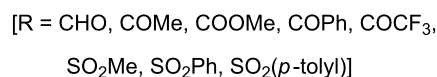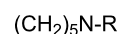
Scheme 6: Synthesized cyclic *N*-acyl and *N*-sulfonyl piperidines for electrolysis.

the α-position to the N atom, they undergo three types of bond cleavages (instead of the common substitution) [13] (Scheme 4).

Previously we investigated [14] the effect of the ring size (5-, 6-, and 7-membered) and the nature of the supporting electrolyte on the anodic methoxylation of *N*-acylazacycloalkanes at the α-position to the nitrogen. The outcome revealed the formation of four types of products of which two involve saturated and two unsaturated cyclic amides (Scheme 5).

The selectivity of the anodic process was found to be highly dependent on the electrolyte used, and to a lesser extent, on the substrate concentration. Notably the importance of the former parameter in electrolysis has been well documented [15,16].

More recently the effect of the functional group attached to the N atom in various piperidine derivatives (Scheme 6) on the anodic oxidation of 'cyclic amides' was explored in methanol under different experimental conditions [17]. The results indicate that this type of amides mostly undergo mono- and dimethoxylation at the α and α'-positions to the N atom. It was also found that the relative ratio among products was strongly dependent on the nature of the supporting electrolyte, the anode material and the substituent group attached to the N atom.

Amides and polyamides have been found as key units in many biologically active and pharmaceutical compounds. For instance, symmetrical and unsymmetrical bisamides derived from diamines are significant components as structural subunits for the construction of peptidomimetric frameworks [18] and as lubricants [19]. To the best of our knowledge nothing has been known so far about electrochemical properties of α,ω-bisamides derived from α,ω-diaminoalkanes. However, notably that the bisamide 3,5-diaza-2,6-heptanedione was obtained from *N*-methylacetamide by electrolysis on a Pt anode in water [20].

The present work describes the electrochemical behavior of eight synthesized bisamides (from diamines, Scheme 7) and the outcome from their preparative electrolysis (at constant current) under different experimental conditions, as a function of the length of spacer between the two amide functionalities.
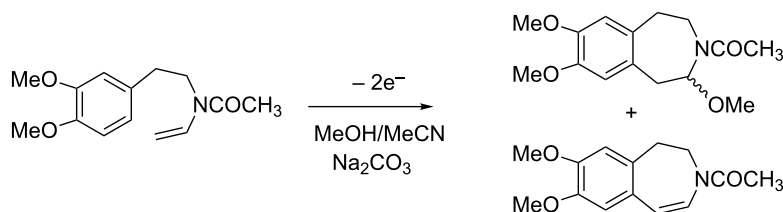
Scheme 3: Intramolecular cyclization via anodic oxidation of an eneamide.
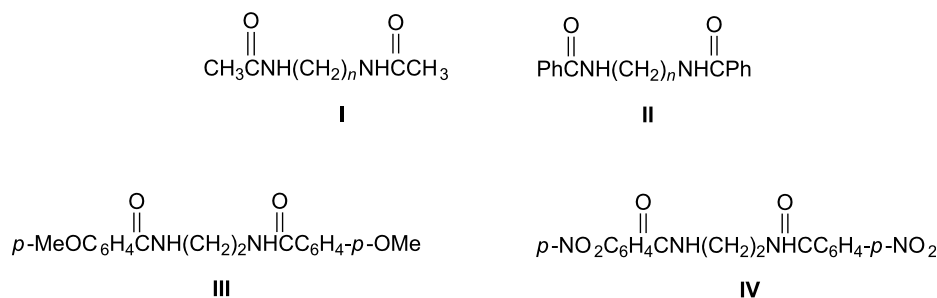
Scheme 7: Type of bisamides (derived from diamines) studied (*n* = 2, 3, 4).

Results and Discussion

The electrochemical properties of the bisamides described in Scheme 6 were studied by cyclic voltammetry and all of their redox potentials were found to be irreversible in acetonitrile. Their first oxidation potentials (in the range of 2.1–2.35 V vs Ag/AgCl) are summarized in Table 1. The first and second columns indicate that the longer the spacer the higher the oxidation potential. Also it is not surprising that the derivative with EWG (**IV**) is more difficult to oxidize than that with EDG (**III**). All bisamides derivatives exhibit one irreversible cathodic wave (not shown, at −2.2 to −2.4 V).

Constant current electrolysis (CCE) at a current density of 20 mA/cm^2 was carried out for all of the above synthesized bisamides under various experimental conditions, using different supporting electrolytes, anodes, and electricity consumption. Bisamide **II** (*n* = 3, will be designated as **II-3** hereafter) was arbitrarily chosen as a model compound for initial electrochemical studies. The spectrum of products obtained is described in Scheme 8. Except for the expected monomethoxylated **II-3a** and dimethoxylated **II-3b** products, fragmentation products (**II-3c**, **3d**, **3e**) were observed too.

Table 1: Oxidation potentials of α,ω-bisamides (Scheme 7) measured by cyclic voltammetry[a].

entry	$E_{p(ox)}$ (V)			
	I	**II**	**III**	**IV**
n = 2	2.10	2.13	2.17	2.33
n = 3	2.23	2.28		
n = 4	2.27	2.35		

[a]In CH$_3$CN/0.1 M LiClO$_4$; potentials are quoted versus Ag/AgCl reference electrode. Working electrode: glassy carbon disk (1.5 mm in diameter). Auxiliary electrode: a Pt wire.

Table 2 below summarizes the type of products and their relative ratios obtained from initial electrochemical oxidation of **II-3** under various experimental conditions. It appears that the selectivity and efficiency of the anodic process depends on both the anode material and electricity consumption (F/mol). Thus the oxidation of **II-3** on a C anode (Table 2, entries 1 and 2) is quite selective providing mostly mono-**II-3a** and dimethoxy-**II-3b** products in addition to ≈10% of methyl benzoate (**II-3d**) as a fragment. Notably that 20–30% of unreacted substrate
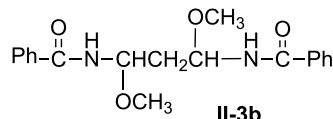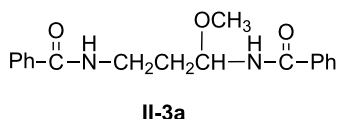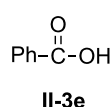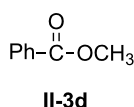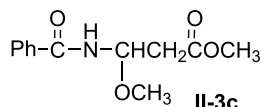
Scheme 8: Type of products obtained from anodic oxidation of **II-3**.

Table 2: The effects of anode material and electricity consumption on the results of anodic oxidation of substrate **II-3** in MeOH/LiClO$_4$[a].

entry	F/mol	anode material	products					unreacted substrate
			II-3a	**II-3b**	**II-3c**	methyl benzoate (**II-3d**)	benzoic acid (**II-3e**)	
1	5	C	40	18	–	12	–	30
2	10	C	27	40	5	9	–	19
3	5	Pt	26	8	–	21	10	35
4	10	Pt	20	40	5	5	20	10
5[b]	10	GC	43	12	–	5	3	36
6[c]	10	PbO$_2$	–	–	–	–	–	90
7[d]	10	DSA	–	–	–	–	–	≈100

[a]Yield of products was determined by ^{1}H NMR relative integration. [b]GC = glassy carbon. [c]Unidentified products (≈10%). [d]DSA = dimensionally stable anode, coated with oxides of Ru and Ir.

remains. An increase in electricity consumption (entries 2 vs 1) promotes the formation of the dimethoxy product **II-3b** over the monomethoxy one **II-3a**.

In comparison to the above results, oxidation of **II-3** on a Pt anode (Table 2, entries 3 and 4) affords similar products but with less selectivity because of the formation of an additional fragmentation product, benzoic acid (**II-3e**) in 10–20% yield. Other anodes were tested as well (Table 2, entries 5–7) at an electricity consumption of 10 F/mol. It appears that a GC anode favors the formation of the monomethoxy product **II-3a** whereas the anodes of PbO$_2$ and DSA are the worst because most of the substrate remained unreacted. Apparently at these two anodes the oxidation of the solvent methanol prevails.

Based on the results in Table 2 in which a C anode afforded better selectivity and efficiency compared to the other anodes studied, all other substrates outlined in Scheme 7 were oxidized at this anode and under the same conditions (namely, in methanol/LiClO$_4$, at 20 mA/cm^2, and with electricity consumption of

10 F/mol). The results are shown in Table 3. It appears that except for entries 5 and 6, the amounts of unreacted starting materials are considerably high (60–70%), indicating that the reaction is far from being efficient under these conditions, presumably because of favorable oxidation of the solvent methanol. Another reason for this observation could stem partially from the limited solubility of some of the substrates in this solvent (e.g., **II-2**, **III-2** and **IV-2**). The yield of total products is in the range of 30–80%, depending on the nature of the substituent attached to the carbonyl moiety, roughly in the order of: Ph > CH$_3$ > *p*-MeOC$_6$H$_4$, *p*-NO$_2$C$_6$H$_4$. In terms of type of products, they are mostly analogous to those described in Scheme 8 for **II-3**. However, it is obvious that in the case of anodic oxidation of substrates with *n* = 2, an additional new fragmented product (type **f**) was formed due to CH$_2$–CH$_2$ bond cleavage, which is exclusive for this type of bisamides (Scheme 9).

Obviously the fact that considerable amounts of starting materials were left unreacted (in most cases, except for Table 3, entries 5 and 6) has been dissatisfying and therefore, prompted

Table 3: Results of anodic oxidation of all substrates on a C rod anode in MeOH/LiClO$_4$. (10 F/mol; 20 mA/cm^2)[a].

entry	substrate	monomethoxy type '**a**'	dimethoxy type '**b**'	methoxylated amide type '**c**'	methyl benzoate '**d**'	RCONHCH$_2$OCH$_3$ '**f**'	unreacted substrate
1	**I-2** (*n* = 2)	10	–	–	–	25	65
2	**I-3** (*n* = 3)	30	10	–	–	–	60
3	**I-4** (*n* = 4)	5	30	–	–	–	65
4	**II-2**	9	–	–	5	23	63
5	**II-3**	27	40	5	9	–	19
6	**II-4**	26	27	–	17	–	30
7	**III-2**	15	–	–	–	15	70
8[b]	**IV-2**	–	–	–	–	10	65

[a]Relative yields of all products were determined by ^{1}H NMR integration. Analogous type of products (**a**–**d**) are described in Scheme 7. [b]PhCONH$_2$ was obtained in 10% yield along with 25% of unidentified products.
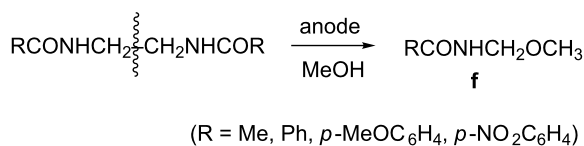
Scheme 9: Anodic splitting of C–C bond in bisamides in the presence of LiClO$_4$ electrolyte.
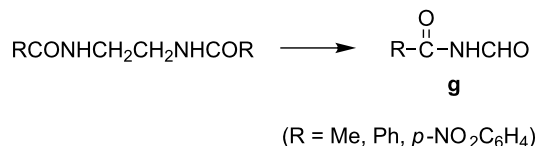
Scheme 10: Anodic splitting of C–C bond in bisamides in the presence of Et$_4$NBF$_4$ electrolyte.

us to change some parameters. At first, the LiClO$_4$ electrolyte was replaced by Et$_4$NBF$_4$ and the results are shown in Table 4. Clearly the bisamides with *n* = 2 afforded now, in addition to **f**, new fragmented products, aldehydes of type **g** (Scheme 10).

In addition, the relative yield of the fragmented products (**f** and **g,** both derived exclusively from bisamides with *n* = 2) increased considerably in the presence of this electrolyte. However, again, the amounts of unreacted starting materials were still significant in some cases.

The pronounced difference between the results obtained by the two electrolytes, namely affording '**f**' with LiClO$_4$, and '**g**' in addition to '**f**' with Et$_4$NBF$_4$, could stem from the different composition of the solution at the electrode surface (caused by different solvation of the electrolyte anion) than that of the bulk of the solution. Such a phenomenon was discussed in the literature previously [15,16,21]. For instance, Nyberg [16] already demonstrated the effect of ClO$_4^-$ vs BF$_4^-$ in the anodic oxidation of hexamethylbenzene in aqueous acetonitrile, and proposed that tetraflouroborate anion preferentially brought water into the anode surface giving high yield of ArCH$_2$OH (compared to ArCH$_2$NHCOMe with perchlorate). Therefore also in our case, the electro generated carbocation intermediate formed (RCONHCH$_2^+$) could meet with methanol (to form '**f**') or water (to form '**g**') preferentially at the electrode surface, dictating the ratio between products '**f**' and '**g**'.

In order to increase the solubility of the substrates with a limited one a mixture of MeOH/MeCN (1:1) was used, and in

parallel, the C rod anode was replaced with a C felt (that has a considerable larger surface area) in attempts to improve both efficiency and selectivity. The results are described in Table 5 and they show a pronounced difference compared to the ones in Table 4 because product yields are higher now (Table 5, entries 1, 4 and 5 show almost completion) even after consuming only 5 F/mol. In addition, although the spectrum of major products is similar in both tables, the weight of monomethoxylated products (51–56%, entries 2 and 5) and fragmented ones (of type **f**, 85–95%, entries 1 and 4) increased at the expense of consumed starting material (in all entries except for entry 8).

Previously (Table 3 vs Table 4) we observed a marked difference in results upon replacing LiClO$_4$ with Et$_4$NBF$_4$. Whereas in the former case mono- and dimethoxylated products were predominant, fragmentation products of type **f** and **g** became major in the latter case. Based on these observations a further attempt to improve the results outlined in Table 5 was conducted by employing similar conditions except for using Et$_4$NBF$_4$ (instead of LiClO$_4$) this time. Some selected substrates from Table 5 that left a considerable amount of unreacted starting material, namely **I-4**, **II-4**, **III-2** and **IV-2**, were chosen to be reoxidized under these modified conditions. The outcome described in Table 6 indicates that this approach was useful for one substrate only, **II-4**.

Mechanism

A mechanism of formation of mono- and dimethoxylated amides is well-documented in the published literature [1-6,14,17,23]. It is generally accepted that the initial electron

Table 4: Results of preparative electrolysis of selected bisamides in MeOH/Et$_4$NBF$_4$ (at C rod anode, 10F, 20 mA/cm^2)^a.

entry	substrate	monomethoxy type '**a**'	dimethoxy type '**b**'	RCONHCH$_2$OCH$_3$ '**f**'	RCONHC(O)H '**g**'	unreacted substrate
1	**I-2**	10	–	51	26	13
2	**I-3**	10	10	–	–	80
3	**I-4**	13	–	–	–	87
4	**II-2**	–	–	69	17	14
5	**III-2** (*p*-OMe)	–	–	23	–	77
6	**IV-2** (*p*-NO$_2$)	–	–	51	31	18

^{a}Yields were determined by ^{1}H NMR relative integration. Analogous type of products **a,b** are described in Scheme 7.

**Table 5:** Results[a] of anodic oxidation of bisamides on a C felt anode in MeOH/MeCN (1:1)/LiClO$_4$; 20 mA/cm^2; 5 F/mol).

entry	substrate	monomethoxy type 'a'	dimethoxy type 'b'	ester type 'd'	benzoic acid 'e'	RCONHCH$_2$OCH$_3$ 'f'	unreacted substrate
1	**I-2**	5	–	–	–	95	–
2	**I-3**	56	7	–	–	–[b]	34
3	**I-4**	20	30	–	–	–	50
4	**II-2**	–	–	15	–	85	–
5	**II-3**	51	24	8	5	(h)[c]	5
6	**II-4**	19	22	16	–	–	43
7	**III-2**	10	–	5	–	25	60
8	**IV-2**	–	–	5	5	5	85

[a]Yield are determined by ^{1}H NMR relative integration. Analogous type of products (type **a**, **b**, **d**, **e**) are described in Scheme 7. [b]Aldehyde (3%): MeCONHCH$_2$CH$_2$CHO (from, **I-3**) [22]. [c]Unsaturated bisamide (7%): PhCONHCH$_2$CH=CHNHCOPh (**II-3h**).

Table 6: Results of anodic oxidation of selected substrates on C felt anode in MeOH/MeCN (1:1)/Et$_4$NBF$_4$; 20 mA/cm^2; 5 F/mol.

entry	substrate	monomethoxy type 'a'	dimethoxy type 'b'	ester type 'd'	fragmented products	unreacted substrate
1	**I-4**	10	–	–	MeCONHCHO (**I-4g**, 5%)	85
2	**II-4**	12	74	8	–	6
3	**III-2** (*p*-OMe)	–	–	15	ArCONHCH$_2$OCH$_3$ (**III-2f**, 10%)	75
4	**IV-2** (*p*-NO$_2$)	–	–	31	–	69

transfer forms an iminium cation radical followed by deprotonation and further oxidation to generate an iminium ion/carbocation that undergoes methoxylation in methanol, as described in Scheme 11.
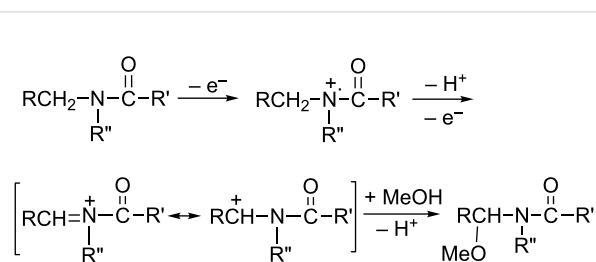
Scheme 11: A suggested mechanism for anodic methoxylation of amides.

Plausible mechanisms for the formation of various fragmentation products are described in Scheme 12.

Actually whenever benzoic acid or methyl benzoate were formed (top of Scheme 12), the corresponding aldehyde from the other part of the molecule was detected too and fully characterized.

Conclusion

In general, bisamides derived from diamines and involving 3 and 4 methylene groups as spacers between the two amide functionalities behave similar to monoamides upon anodic oxidation in methanol/LiCiO$_4$ because both types undergo majorly mono- and dimethoxylations at the α-position to the N atom. However, in cases where the spacer contains two methylene groups only the anodic process leads mostly to CH$_2$–CH$_2$ bond cleavage to afford products of type RCONHCH$_2$OCH$_3$. Moreover, upon replacing LiClO$_4$ with Et$_4$NBF$_4$ an additional fragmentation type of product was generated from the latter amides, namely RCONHCHO. Also, the anodic process was found to be more efficient with C felt as the anode, and in a mixture of 1:1 methanol/acetonitrile co-solvents.

Experimental
Materials

Reagents, electrolytes and solvents (all analytical grade) were supplied by various vendors, as mentioned in [23].

Preparation of bisamides **I–III**

All types of bisamides were prepared according to our own procedure by reacting the corresponding diamines (commercially available) with acetic anhydride, or benzoyl chloride or
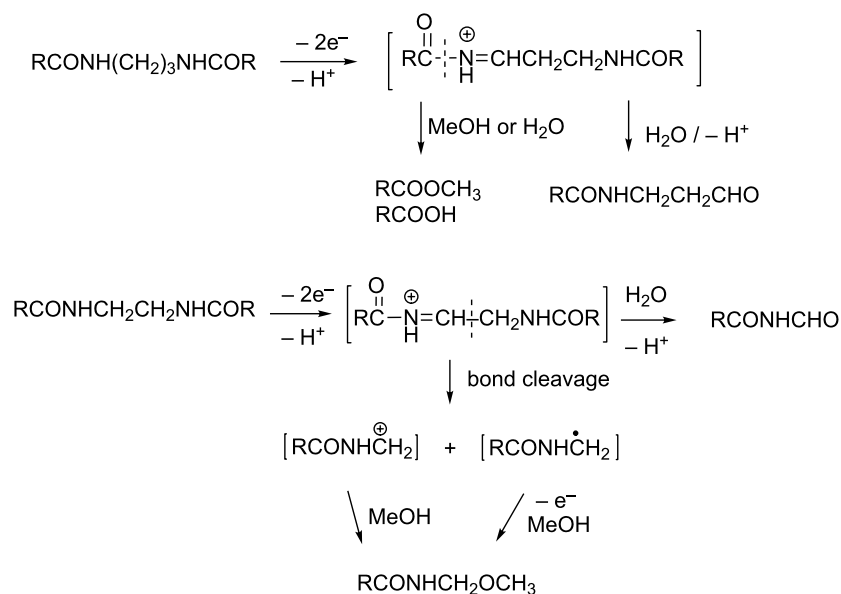
Scheme 12: Mechanisms of formation of fragmentation products.

4-methoxybenzoyl chloride. In a typical experiment, 30 mmol of a diamine (ethylenediamide, 1,3-diaminopropane or 1,4-diaminobutane) were introduced into a 500 mL Erlenmeyer flask with 50 mL of DCM and 20 mL of saturated aqueous bicarbonate solution. Then 70 mmol of acetic anhydride (or benzoyl chloride or 4-methoxybenzoyl chloride) were added dropwise by a separatory funnel to the diamine solution while stirring by a magnetic stirrer. Then the reaction mixture was filtered under vacuum and the solid residue was recrystallized from a mixture of ethyl acetate and water (9:1). The resulting white precipitate (except for the yellowish one derived from *p*-nitrobenzene derivative) was dried, weighed and verified by NMR spectra. The isolated yields of the bisamides were around 72–86%.

General methods

Instruments used in this study for ^{1}H NMR and ^{13}C NMR measurements, mass and IR spectra, high-resolution mass analyses, and cyclic voltammetry were described in [23].

Thin-layer chromatography (TLC) was carried out on aluminum sheets coated with aluminum oxide 60 F_{254} and silica gel 60 F_{254}. Retention time was evaluated by UV (for amides with benzene ring) or by using a general purpose stain of cerium molybdate [containing a mixture of $Ce(NH_4)_2(NO_3)_6$ - $(NH_4)_6Mo_7·4H_2O$ in H_2SO_4] for amides of type **I**. Preparative TLC was carried out by using 20 × 20 cm of glass plates coated with silica gel 60 F_{254}. Evaporation of solvents was performed at reduced pressure using a rotary evaporator.

Constant current electrolysis

Constant current electrolysis at preparative scale was performed at constant currents using a PAR Potentiostat/Galvanostat Model 273A, and a beaker-type undivided cell equipped with a C rod, C felt, PbO_2, GC, DSA or a Pt foil (immersed area of ≈5 cm^2) as the anode, and a Pt foil as the cathode. In a typical electrolysis α,ω-bisamides (1 mmol) were dissolved in methanol (or 1:1 methanol/acetonitrile, 25 mL) containing 0.1 M supporting electrolytes. Electrolysis took place at room temperature with a current density of 20 mA/cm^2 and was terminated after the desired consumption of electricity was passed (Tables 2–5). Then the reaction mixture was concentrated by rotary evaporator till all the solvents evaporated. The relative yield of products was determined by ^{1}H NMR integration. Notably this procedure of analyzing a mixture of products simultaneously and successfully is based on prior separation and characterization of the individual products in the mixture. Their previous separation was carried out either by silica gel column chromatography or preparative coated glass plates, using different mixtures of ethyl acetate (20–50%)/hexane or acetone/ethyl acetate, as eluent. Also since some of the products undergo facile hydrolysis/decomposition it is suggested that the analysis will be done immediately after terminating the electrolysis.

Characterization of products

See Supporting Information File 1 for spectral data and copies of ^{1}H and ^{13}C NMR spectra.

Supporting Information

Supporting Information File 1

Spectral data and copies of ^{1}H and ^{13}C NMR spectra.
[https://www.beilstein-journals.org/bjoc/content/
supplementary/1860-5397-14-72-S1.pdf]

Acknowledgments

References

1. Steckhan, E. Anodic oxidation of nitrogen-containing compounds. In *Organic Electrochemistry,* 4th ed.; Lund, H.; Hemmerich, O., Eds.; Ch. 15; Marcel Dekker, Inc.: NY, 2001; pp 570–602.
2. Grimshaw, J. *Electrochemical reactions and mechanisms in organic electrochemistry;* Ch. 8; Elsevier, 2000; pp 282–290.
3. Torii, S. *Electroorganic synthesis, Part 1: Oxidations;* Ch. 5.2; Kodansha VCH, 1985; pp 171–180.
4. Shono, T.; Matsumura, Y.; Tsubata, K.; Sugihara, Y.; Yamane, S.; Kanazawa, T.; Aoki, T. *J. Am. Chem. Soc.* **1982,** *104,* 6697–6703. doi:10.1021/ja00388a037
5. Shono, T.; Matsumura, Y.; Onomura, O.; Yamamoto, Y. *Tetrahedron Lett.* **1987,** *28,* 4073–4074. doi:10.1016/S0040-4039(01)83864-8
6. Genies, M. *Bull. Soc. Chim. Fr.* **1975,** 389–392.
7. Shono, T.; Hamaguchi, H.; Matsumura, Y. *J. Am. Chem. Soc.* **1975,** *97,* 4264–4268. doi:10.1021/ja00848a020
8. Wong, P. L.; Moeller, K. D. *J. Am. Chem. Soc.* **1993,** *115,* 11434–11445. doi:10.1021/ja00077a048
9. Moeller, K. D.; Rutledge, L. D. *J. Org. Chem.* **1992,** *57,* 6360–6363. doi:10.1021/jo00049a060
10. Moeller, K. D.; Rothfus, S. L.; Wong, P. L. *Tetrahedron* **1991,** *47,* 583–592. doi:10.1016/S0040-4020(01)87048-4
11. Okita, M.; Wakamatsu, T.; Mori, M.; Ban, Y. *Heterocycles* **1980,** *14,* 1089–1092. doi:10.3987/R-1980-08-1089
12. Okita, M.; Wakamatsu, T.; Ban, Y. *Heterocycles* **1983,** *20,* 401–404. doi:10.3987/R-1983-03-0401
13. Golub, T.; Becker, J. Y. *Org. Biomol. Chem.* **2012,** *10,* 3906–3912. doi:10.1039/c2ob06878h
14. Golub, T.; Becker, J. Y. *J. Electrochem. Soc.* **2013,** *160,* G3123–G3127. doi:10.1149/2.017307jes
15. Eberson, L.; Olofsson, B. *Acta Chem. Scand.* **1969,** *23,* 2355–2366. doi:10.3891/acta.chem.scand.23-2355
16. Nyberg, K. *J. Chem. Soc. D* **1969,** 774–775. doi:10.1039/c29690000774
17. Golub, T.; Becker, J. Y. *Electrochim. Acta* **2015,** *173,* 408–415. doi:10.1016/j.electacta.2015.04.133
18. Harichandran, G.; Amalraj, S. D.; Shanmugan, P. *Indian J. Chem.* **2011,** *50B,* 77–82.
19. Williams, J. B.; Geick, K. S.; Falter, J. A. *J. Vinyl Addit. Technol.* **1997,** *3,* 216–219. doi:10.1002/vnl.10194
20. Couch, D. E. *Electrochim. Acta* **1964,** *9,* 327–336. doi:10.1016/0013-4686(64)80040-2
21. Mayeda, E. A.; Miller, L. L. *Tetrahedron* **1972,** *28,* 3375–3380. doi:10.1016/0040-4020(72)88098-0
22. Kalisiak, J.; Trauger, S. A.; Kalisiak, E.; Morita, H.; Fokin, V. V.; Adams, M. W. W.; Sharpless, K. B.; Siuzdak, G. *J. Am. Chem. Soc.* **2009,** *131,* 378–386. doi:10.1021/ja808172n
23. Golub, T.; Becker, J. Y. *Electrochim. Acta* **2016,** *205,* 207–214. doi:10.1016/j.electacta.2016.04.074

License and Terms

BEILSTEIN JOURNAL OF ORGANIC CHEMISTRY

Electrochemically modified Corey–Fuchs reaction for the synthesis of arylalkynes. The case of 2-(2,2-dibromovinyl)naphthalene

Fabiana Pandolfi, Isabella Chiarotto and Marta Feroci[*]

Abstract

The electrochemical reduction of 2-(2,2-dibromovinyl)naphthalene in a DMF solution (Pt cathode) yields selectively 2-ethynyl-naphthalene or 2-(bromoethynyl)naphthalene in high yields, depending on the electrolysis conditions. In particular, by simply changing the working potential and the supporting electrolyte, the reaction can be directed towards the synthesis of the terminal alkyne (Et_4NBF_4) or the bromoalkyne ($NaClO_4$). This study allowed to establish that 2-(bromoethynyl)naphthalene can be converted into 2-ethynylnaphthalene by cathodic reduction.

Introduction

Terminal alkynes, due to the considerable triple-bond strength (839 kJ mol^{-1}), are characterized by a moderate thermo-dynamic reactivity [1]. Nevertheless, both the C–C triple bond and the terminal C–H bond can be efficiently and selectively activated by metal or metal-free catalysts. Therefore, terminal alkynes can be considered as raw material (thus an important resource).

The use of terminal alkynes, activated by catalysts, as building blocks or intermediates in the synthesis of a large number of chemicals is extensively summarized in recent reviews [1-3].

The recently published papers confirm the present interest in the chemistry of terminal alkynes, e.g., in the synthesis of sulfin-amides and isothiazoles [4], 1,3-enynes [5], α-monosubstituted propargylamines [6], 2-substituted pyrazolo[5,1-*a*]isoquin-olines [7], etc.

Terminal alkynes can be prepared by dehydrohalogenation of vicinal dihalides or vinyl bromides using sodium in ammonia or strong bases [8]. Alternatively, the compounds are accessible by homologation of aldehydes following the Bestmann modification of the Seyferth–Gilbert reaction, using in situ generated

dimethyl (diazomethyl)phosphonate [9,10]. Moreover, the aldehyde homologation to terminal alkynes can also be obtained using the Corey–Fuchs reaction [11]. This is a two-step reaction in which an aldehyde is at first converted into a 1,1-dibromoalkene with chain extension by one carbon atom through the reaction with carbon tetrabromide and triphenylphosphine (Scheme 1, reaction 1). The second step comprises the conversion of the 1,1-dibromoalkene into the corresponding alkyne by reaction with BuLi at −78 °C in THF (Scheme 1, reaction 2) [12].

Recently, a chemical modification of the second step of the Corey–Fuchs reaction was reported, in which the authors used Cs_2CO_3 as the base and performed the reaction in DMSO at 115 °C for 12 h [13]. Good to high yields of terminal alkynes were obtained (50–98%). Also DBU (4 equiv) in MeCN at room temperature is effective to carry out the second step of the Corey–Fuchs reaction, affording good to high yields of arylalkynes. In the latter reaction DBU acts both as base and as organocatalyst [14]. In all cases, an excess of a strong base or high temperature are necessary for the reaction to proceed. An overview on the importance of the Corey–Fuchs reaction for the synthesis of natural products has been pointed out by Heravi and co-workers recently [15].

As mentioned above the second step of the Corey–Fuchs reaction requires the cleavage of a C–Br bond. We thus envisaged if this could be achieved electrochemically via a selective cathodic cleavage of the C–Br bond. In this way, the reaction

could be performed under mild conditions and in the absence of reducing agents or bases in the reaction mixture.

Electrochemical methods can be considered an environmentally friendly technique: they rely on the use of practically massless electrons (which are not converted to byproducts) instead of stoichiometric amounts of redox reagents and frequently these reactions are carried out at room temperature and at atmospheric pressure, etc. [16-19].

The electrochemical behavior of halogenated compounds has been extensively investigated [20-22]. The cleavage of the C–halogen bond, yielding (via a radical intermediate) the corresponding carbanion and halogen anion, can be achieved by a bielectronic cathodic process (Scheme 2). The electrolysis is carried out at a suitable controlled potential, i.e., at a potential that is negative enough to achieve the selective fission of the envisaged C–halogen bond [23].

Therefore, the reactive species is an electrochemically generated carbanion and the outcome of the reaction strongly depends on the complex reactivity of this intermediate. Moreover, this reactivity is influenced by the reaction conditions, such as the solvent, supporting electrolyte, electroinactive substrates, temperature, working potential and amount of consumed charge [24].

Our group intensively investigated the electrochemical behavior of 1,1-dibromoalkenes by means of cyclic voltammetry and
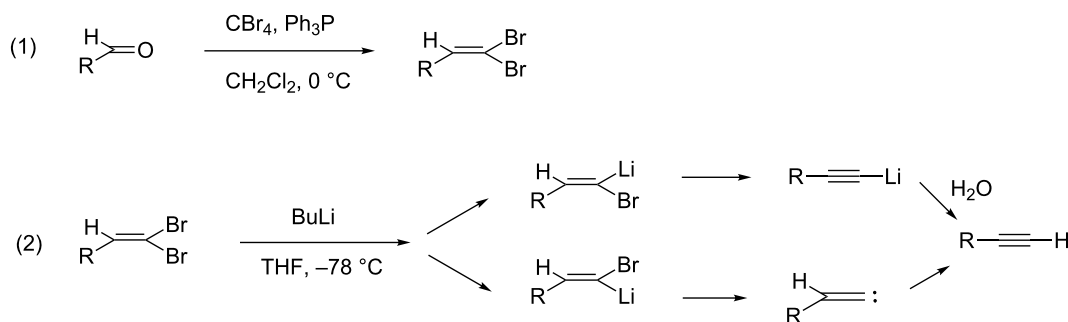
Scheme 1: The Corey–Fuchs reaction.
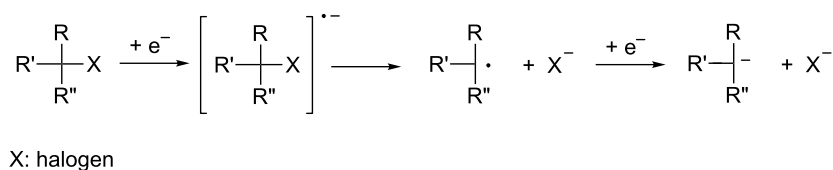
X: halogen

Scheme 2: Electrochemical reduction of a carbon–halogen bond.

electrolyses [25] and we reported the selective synthesis of vinyl bromides through the cathodic reduction of 1,1-dibromoalkenes in the presence of acetic acid. The electrolysis conditions in this transformation were optimized in order to avoid or minimize the formation of the terminal alkyne. The latter was obtained as the major product in the absence of a proton donor and its formation could be suppressed when performing the reaction with a Au cathode in acetonitrile (ACN) as the solvent and in the presence of an excess of acetic acid as the proton source. Under these conditions good yields of the vinyl bromides were obtained with preference of the Z-isomers (Scheme 3).

Scheme 3: Electrochemical synthesis of vinyl bromides [25].
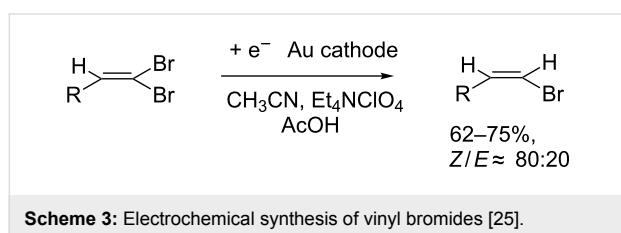
We have now reconsidered this investigation in order to obtain terminal alkynes and to avoid the formation of vinyl bromides. The scope of this paper is the determination of the electrolysis conditions for the transformation of 1,1-dibromoalkenes into the corresponding terminal alkynes, in order to carry out the second step of the Corey–Fuchs reaction under milder conditions.

2-Ethynylnaphthalene (**2a**) is a small molecule with a high and selective biological activity. In particular, this molecule has

been demonstrated to be a selective inactivator of cytochrome P-450 2B4 [26] and an inhibitor also of other cytochrome P-450 isoforms [27]. We thus decided to carry out our study using 2-(2,2-dibromovinyl)naphthalene (**1a**) as starting material for the synthesis of 2-ethynylnaphthalene (**2a,** Scheme 4).

Scheme 4: Scope of this work.
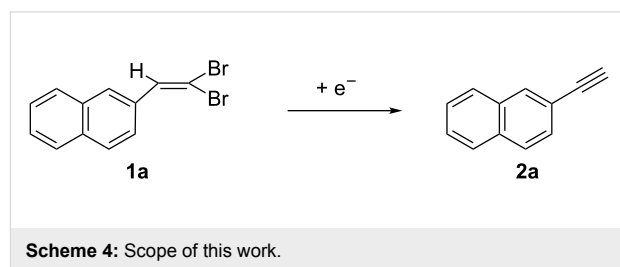
Results and Discussion

In our previous work [25], we found that the cathodic reduction of 2-(2,2-dibromovinyl)naphthalene (**1a**), carried out at the potential of the first voltammetric peak in ACN on a Au cathode and in the presence of an excess acetic acid, yielded the corresponding vinyl bromides (Scheme 3) in 75% yield (*Z/E* 82:18). The main product was 2-ethynylnaphthalene (**2a**, 65%) when the electrolysis was carried out in the absence of acetic acid as protonating agent (1.8 F consumed charge). Due to the importance of the latter product, we decided to reconsider this procedure in order to direct the synthesis towards the formation of the alkyne. We have therefore reconsidered the voltammetric behavior of **1a** at Pt, Ag and GC cathodes in DMF or ACN solutions (Figure 1).

Figure 1: Voltammetric curves of **1a** 0.020 mol dm^{-3}; Pt, glassy carbon (GC) or Ag cathode. v = 0.2 V s^{-1}, *T* = 25 °C; solvent left: DMF/Et$_4$NBF$_4$ 0.1 mol dm^{-3}; right: ACN/Et$_4$NBF$_4$ 0.1 mol dm^{-3}.
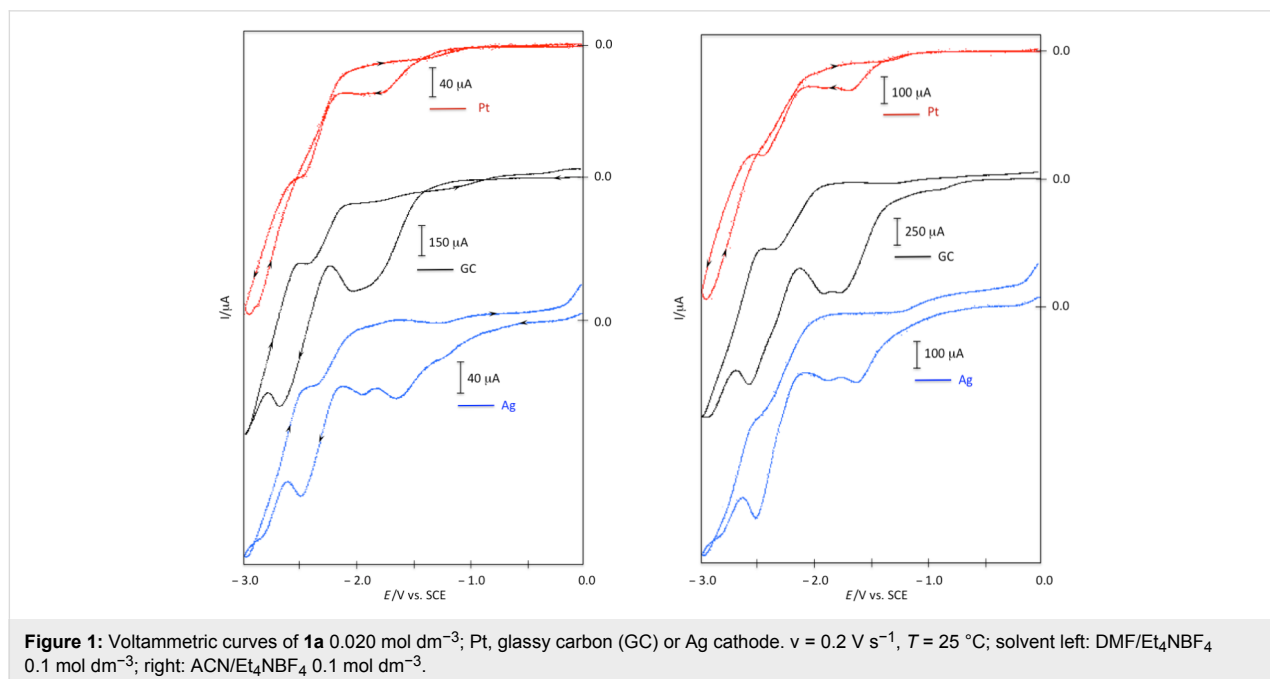
The voltammetric curves of **1a** show the presence of different reduction peaks which are affected by the solvent and by the electrode material (see peak potential Table S1 in Supporting Information File 1). These voltammograms (and the data reported in Supporting Information File 1, Table S1) evidence the catalytic effect of the silver cathode in the C–Br bond reduction (E_{p1} is quite less negative on Ag cathode) [28,29], although this effect is more evident in DMF than in ACN. In any voltammogram, the cathodic peak at the less negative potential should be related to the cleavage of the C–Br bond. In order to confirm this statement, we carried out a first electrolysis in acetonitrile on a Pt cathode at the controlled potential of −1.75 V vs SCE, corresponding to the first reduction wave of **1a** (Table 1, entry 1). The current flow was stopped after the disappearance of **1a** (6.0 F). The only product was the expected alkyne **2a** (Scheme 4) with 69% yield. This result was in accordance with what reported in our previous work using a Au cathode (but with a much lower current efficiency – probably due to side

reactions – when compared to the result obtained using a Au cathode in the previous paper) [25].

In order to ascertain the role of the solvent in this electrosynthesis, we carried out an electrolysis in DMF instead of ACN on a Pt cathode at the controlled potential of −2.00 V vs SCE, corresponding to the first reduction wave of **1a** (Table 1, entry 2). The current flow was stopped after the disappearance of **1a** (3.0 F). Also in this case the only product was the expected alkyne **2a** with a higher yield (80%).

An increase in the charge did not lead to an increase of the yield (81%, Table 1, entry 3). When the working potential was increased to −1.75 V and the electrolysis was stopped after the total consumption of **1a** (1.5 F), a mixture of products was obtained (Scheme 5 and Table 1, entry 4). In particular, a large amount (48%) of the brominated alkyne **3a** was isolated, along with traces of hydrogenated alkene **4a**. In order to confirm the

Table 1: Electrochemical synthesis of 2-ethynylnaphthalene (**2a**). Electrolysis conditions optimization (Scheme 5).[a]

entry	cathode	*E* or *I*[b]	F[c]	products (%)[d]			
				2a	**3a**	**4a**	**5a**
1[e]	Pt	−1.75 V	6.0	69	–	–	–
2	Pt	−2.00 V	3.0	80	–	traces	traces
3	Pt	−2.00 V	4.0	81	–	traces	–
4	Pt	−1.75 V	1.5	25	48	4	traces
5[f]	Pt	−1.75 V	2.3	27	–	–	58[g]
6	Pt	10 mA/cm^2	3.0	46	–	41	–
7	Pt	5 mA/cm^2	3.0	29	–	39	–
8	GC	−1.70 V	0.6	5	7	–	7
9	Ag	−1.80 V	3.0	72	–	6	–
10	Ag	−2.10 V	3.0	65	–	15	2
11[h]	Pt	−2.20 V	2.0	7	89	–	–
12[h]	Pt	−2.20 V	3.0	43	38	–	–

[a]Electrolysis conditions: divided cell, 5.0 mL of DMF (catholyte)/0.1 mol dm^{-3} Et$_4$NBF$_4$ containing **1a** (0.5 mmol), rt, N$_2$ atmosphere. Anolyte: 2.0 mL same solvent. Working electrode: as in Table; anode: Pt; reference electrode: modified SCE (see Supporting Information File 1). The electrolyses were stopped after total consumption of starting **1a**. [b]Controlled potential electrolyses: working potential *E* (Volts) reported vs SCE. Controlled current electrolyses: working current density *I* (mA/cm^2) reported. [c]Amount of charge: number of Faradays. [d]Isolated yields, with respect to starting **1a**. [e]ACN instead of DMF as solvent. [f]3 Equivalents of acetic acid were present in the catholyte during electrolysis. [g]Mixture of isomers: *Z/E* = 69:31. [h]NaClO$_4$ instead of Et$_4$NBF$_4$ as supporting electrolyte.
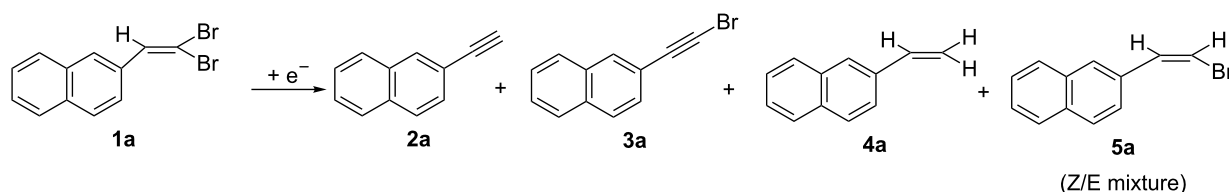
Scheme 5: Possible products from the electrolysis of 2-(2,2-dibromovinyl)naphthalene (**1a**).

effect of the presence of a proton donor, acetic acid was added to the solution and the electrolysis was carried out at the first cathodic peak potential (Table 1, entry 5). After 2.3 F (total consumption of starting material), the alkyne **2a** was isolated in 27% yield, while the major product was bromoalkene **5a** (mixture of *Z* and *E* isomers) in 58% yield. This result is very similar to what we reported in our previous work [25].

Also the electrochemical methodology has a dramatic effect on the products of the cathodic reduction of **1a**. In fact, carrying out the electrolysis under controlled current conditions (Table 1, entry 6) equimolar amounts of desired alkyne **2a** and of vinyl derivative **4a** (Scheme 5) were obtained when a current density of 10 mA/cm² was used, while lowering the current density to 5 mA/cm² did not alter significantly the reaction outcome (Table 1, entry 6 vs 7).

It is well known that the electrode material could influence the outcome of an electrosynthesis, so we carried out electrolyses of **1a** using a glassy carbon cathode (Table 1, entry 8) and a silver cathode (Table 1, entry 9). In both cases the working potential was that of the first reduction wave. In the case of glassy carbon, the electrolysis could not be terminated as the current flow stopped very early [30]. When a silver cathode was used, a good yield of desired alkyne **2a** was obtained (72%), along with a small amount of hydrogenated alkene **4a** (6%). In order to increase the yield of alkyne **2a** (and as **2a** reduction potential is much more negative, vide infra), we carried out a cathodic reduction of **1a** on a silver cathode at the second reduction wave potential (Table 1, entry 10). In this last case, the selectivity of the reaction dropped and a notable amount of hydrogenated alkene **4a** was obtained (15%), along with a lower yield of alkyne **2a** (65%).

The effect of a different supporting electrolyte was evaluated by substitution of Et₄NBF₄ with NaClO₄. Also in this case the electrolysis was stopped after the complete consumption of starting **1a** (Table 1, entry 11). The change in supporting electrolyte led to a complete change in products. In fact, a very high yield of 2-(bromoethynyl)naphthalene (**3a**) was obtained (89%), along with only 7% of 2-ethynylnaphthalene (**2a**) after 2.0 F. Increasing the consumed charge to 3.0 F under the same experimental conditions, an equimolar mixture of bromoalkyne **3a** and alkyne **2a** was obtained, confirming the possibility of obtaining **2a** by cathodic reduction of **3a** (Table 1, entry 11 vs 12).

In order to better understand the electrochemical behavior of dibromoalkene **1a**, we carried out the voltammetric analysis of all isolated products (see Supporting Information File 1). The first cathodic peak potential of 2-(bromoethynyl)naphthalene (**3a**, Scheme 5) is very close to the first cathodic peak potential

of 2-(2,2-dibromovinyl)naphthalene (**1a**), irrespective of the solvent and working electrode material. This renders impossible a selective cathodic reduction of **1a** in the presence of **3a**. The voltammetric behavior of 2-ethynylnaphthalene (**2a**) shows only one reduction peak at a potential that is quite more negative than the first cathodic peak of **1a** and **3a**, respectively, and corresponding to the third reduction peak of **1a** and to the second of **3a**. Also in this case the potential value is independent of the solvent and working electrode material. This voltammetric analysis shows that the cathodic reduction of both **1a** and **3a** could lead to the formation of the desired alkyne **2a**.

To ascertain this hypothesis and to get information on the nature of the intermediates of the electrochemical process, we carried out the electrosynthesis under the optimized experimental conditions reported in Table 1, entry 2, analyzing the catholyte during the electrolysis. The yields of electrolysis products **2a** and **3a** were reported as a function of the number of Faraday (Figure 2).

Figure 2: Variation of the amounts of **1a**, **2a**, and **3a** with the number of Faradays of **1a**.
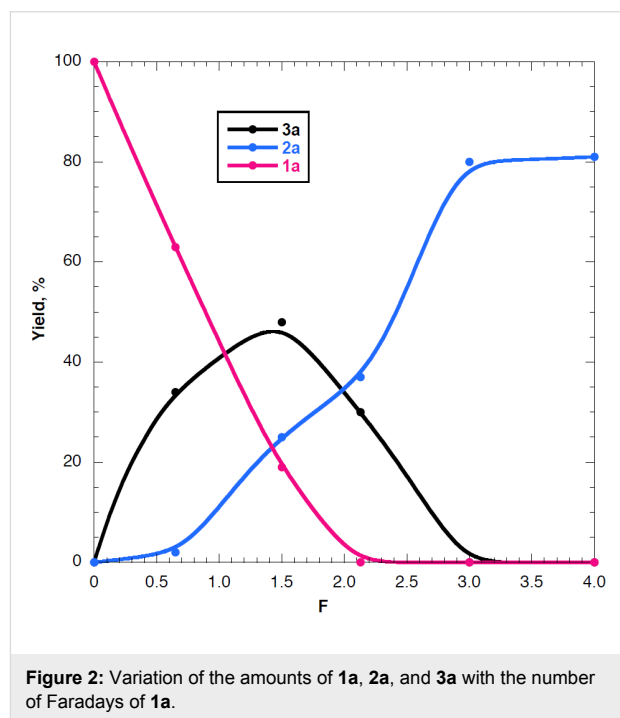
The results of this last investigation (curves reported in Figure 2) show that i) the concentration of **1a** decreases and that of **2a** increases with increasing charge; ii) dibromoalkene **1a** is completely reduced after a consumption of 2.0 F, i.e., a value of charge near the theoretical value for the bielectronic reduction of a C–Br bond; iii) after a consumption of 2.0 F the yield of alkyne **2a** is 40% versus a yield of 80% after 3.0 F; iv) the analysis of the solution during the electrolysis shows the presence of bromoalkyne **3a**.

The concentration of **3a** initially increases and subsequently decreases upon increasing the charge; bromoalkyne **3a** is absent in the final solution. The maximum yield of **3a**, close to 50%, is reached after the consumption of about 1.5 F.

Bromoalkyne **3a** and alkyne **2a** seem to be strictly related. In fact, the increase of **3a** corresponds to the decrease of starting **1a**, while the subsequent decrease of **3a** corresponds to the increase of **2a**. In addition the analysis of the electrolyzed solutions shows the presence of only a trace amount of vinyl bromide **5a**. Note that vinyl bromide **5a** is cathodically active at the working potential (see Supporting Information File 1). The overall analysis allows suggesting a mechanistic hypothesis (Scheme 6).

The bielectronic cathodic reduction of dibromoalkene **1a** leads to the cleavage of one C–Br bond and the formation of the corresponding vinyl anion (Scheme 6, reaction 1). An equilibrium of proton exchange between this electrogenerated carbanion and parent **1a** yields vinylbromide **5a** and a second vinyl anion (Scheme 2, reaction 2), which is converted to bromoalkyne **3a** by bromide elimination. Vinyl bromide **5a** can be cathodically reduced to 2-vinylnaphthalene (**4a**) or eliminate HBr to yield alkyne **2a**.

Bromoalkyne **3a** then can be reduced at the electrode to yield alkyne **2a**. The presence of a proton donor (Table 1, entry 5) increases the yield of **5a** and substitutes **1a** (as proton donor) in reaction 2 (Scheme 6).

The anion generated by cathodic reduction of dibromoalkene **1a** (Scheme 2, reaction 1) can also eliminate bromide (as reported in literature [31]), yielding the corresponding carbene (Scheme 2, reaction 2). This carbene can undergo a rearrangement to yield alkyne **2a**. According to the mechanism shown in Scheme 6, the formation of bromoalkyne **3a** competes with the formation of **2a** in reaction 2 and its rate of formation is comparable to that of **2a**. Since its reduction potential is close to that of **1a** (see Supporting Information File 1, Table S1 and Figure S2), it is further reduced to the alkyne **2a** (reaction 3 in Scheme 6) during the electrolysis.

The various possible ways described in Scheme 6 are highly influenced by the reaction conditions. When the supporting electrolyte is NaClO$_4$ instead of Et$_4$NBF$_4$, a different mechanism seems to be operative. In fact, following reactions (1) and (2) in Scheme 6, a maximum yield of 50% of **3a** can be obtained. It is thus possible that when using NaClO$_4$ an electrogenerated base (OH$^-$) is formed, due to the reduction of water
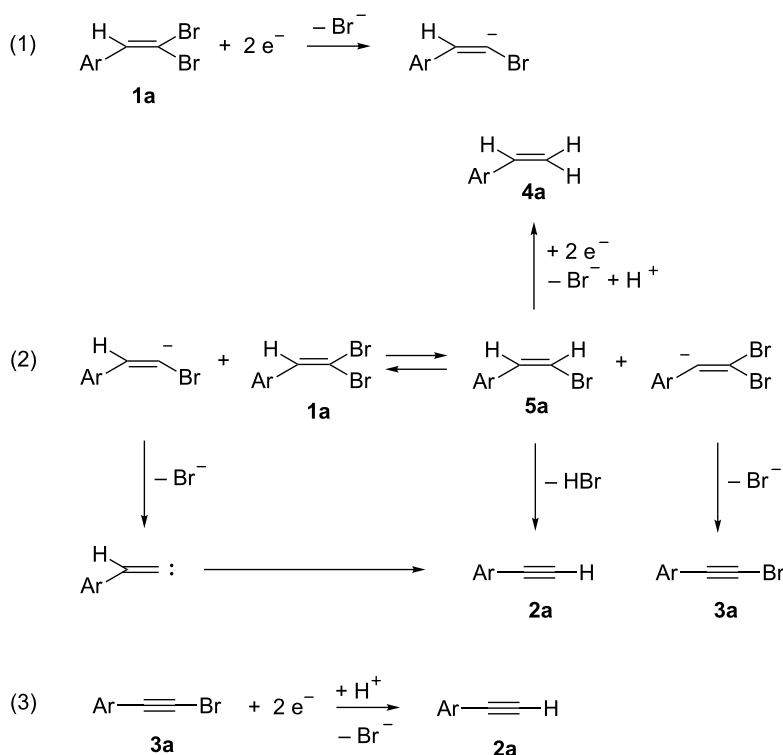
Scheme 6: Mechanistic hypothesis for the synthesis of alkyne **2a** and bromoalkyne **3a** from 2-(2,2-dibromovinyl)naphthalene (**1a**). Alkene configurations are not defined.

and this base converts **1a** to **3a**. In fact, the Na$^+$ cation is highly hydrophilic while the Et$_4$N$^+$ cation is hydrophobic. Thus, in DMF/NaClO$_4$ the double layer would be constituted by the strongly solvated Na$^+$(H$_2$O)$_n$, while in DMF/Et$_4$NBF$_4$, the double layer would be free of water. On Pt, a low hydrogen overvoltage material, it is then conceivable that the reduction of water to dihydrogen and hydroxide anions would be faster than the reduction of **1a**. The overall reaction would be a one-electron process catalyzed by water reduction (Scheme 7) [32].
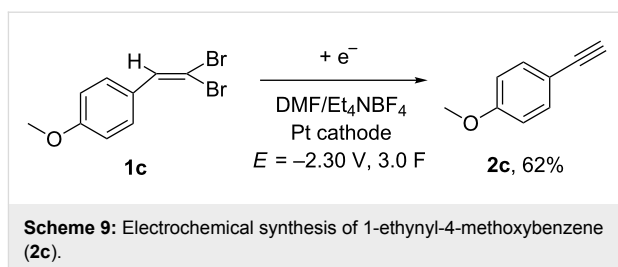
It is thus possible by selecting the electrolysis conditions to synthesize selectively 2-ethynylnaphthalene (**2a**, Table 1, entry 2) or 2-(bromoethynyl)naphthalene (**3a**, Table 1, entry 11) in high yields.

Finally, to test the general applicability of the proposed electrochemical methodology, we submitted to electrolysis (under the optimized conditions reported in Table 1, entry 2), 3-(2,2-dibromovinyl)-9-ethyl-9*H*-carbazole (**1b**, Scheme 8). In fact, the corresponding alkyne **2b** is an important intermediate in the synthesis of molecules for organic electronics (e.g., organic light-emitting diodes [33] and organic field-effect transistors [34]). The voltammetric analysis showed a behavior similar to that of **1a** (see Supporting Information File 1) and thus the electrolysis was carried out at the second wave potential. 9-Ethyl-3-ethynyl-9*H*-carbazole (**2b**) was obtained in 77% yield.

Similarly, when starting from 1-(2,2-dibromovinyl)-4-methoxybenzene (**1c**), the corresponding terminal alkyne **2c** was obtained in 62% yield (Scheme 9).

Scheme 9: Electrochemical synthesis of 1-ethynyl-4-methoxybenzene (**2c**).

towards different products simply by changing the electrolysis parameters (potential, solvent, supporting electrolyte, amount of charge, additives, etc.) and making use of electrons (as green, cheap, no byproduct-forming reagents) renders electrosynthesis attractive for organic chemists.

In particular, this work reported the selective synthesis of 2-ethynylnaphthalene or 2-(bromoethynyl)naphthalene in high yields by the cathodic reduction of 2-(2,2-dibromovinyl)naphthalene. The electrolyses were carried out in DMF solution (Pt cathode) under potentiostatic conditions; if the potential was fixed at −2.00 V (vs SCE) and the supporting electrolyte was Et$_4$NBF$_4$, and 2-ethynylnaphthalene was obtained in 80% yield after 3.0 F, while using NaClO$_4$ as salt and a potential of −2.20 V 2-(bromoethynyl)naphthalene was obtained in 89% yield after 2.0 F. We also demonstrated that 2-(bromoethynyl)naphthalene can be cathodically converted to 2-ethynylnaphthalene. The extension of the method to two other substrates was successfully demonstrated. This methodology allows carrying out the second step of the Corey–Fuchs reaction under milder experimental conditions.

Conclusion

The electrochemical methodology is shown to be a useful tool in organic synthesis. The possibility to direct the reaction

Experimental

Electrolyses. Constant potential or current electrolyses were performed under a nitrogen atmosphere at 25 °C using an Amel
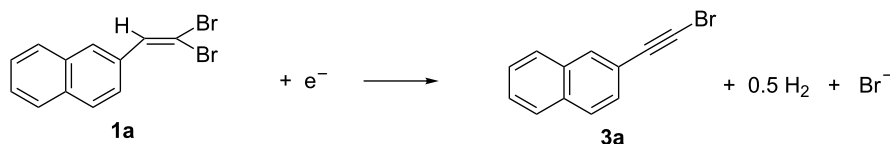
Scheme 7: Possible reaction using NaClO$_4$ as supporting electrolyte.
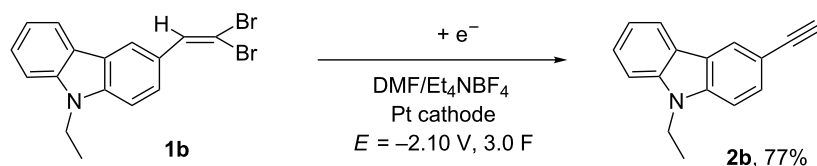
Scheme 8: Electrochemical synthesis of 9-ethyl-3-ethynyl-9*H*-carbazole (**2b**).

2053 potentiostat-galvanostat equipped with an Amel 731 integrator. All experiments were carried out in a divided glass cell separated through a porous glass plug filled with a layer of gel (i.e., methyl cellulose 0.5 vol % dissolved in DMF/Et$_4$NBF$_4$, 1.0 mol dm^{-3}). Pt spirals (apparent area 0.8 cm^2) were used as both cathode and anode, unless otherwise specified. Catholyte: 5 mL of DMF/0.1 M Et$_4$NBF$_4$; anolyte: 2 mL of the same solvent of catholyte. 2,2-Dibromovinylnaphthalene (0.5 mmol) was present in the catholyte during electrolysis. The number of Coulombs and the electrolysis potential/current were varied as reported in the text. At the end of the electrolysis, the catholyte was poured in an excess of water and extracted with petroleum ether 40–60 (3 × 20 mL). Flash column chromatography (eluent: petroleum ether/ethyl acetate from 100:0 to 90:10) gave purified products.

Supporting Information

Supporting Information File 1
Detailed experimental procedures, NMR spectra and cyclic voltammetries.
[https://www.beilstein-journals.org/bjoc/content/supplementary/1860-5397-14-76-S1.pdf]

Acknowledgements

ORCID® iDs
Fabiana Pandolfi - https://orcid.org/0000-0002-5972-851X
Isabella Chiarotto - https://orcid.org/0000-0001-7165-3226
Marta Feroci - https://orcid.org/0000-0002-3673-6509

References

1. Lei, J.; Su, L.; Zeng, K.; Chen, T.; Qiu, R.; Zhou, Y.; Au, C.-T.; Yin, S.-F. *Chem. Eng. Sci.* **2017,** *171,* 404–425. doi:10.1016/j.ces.2017.05.021
2. Chinchilla, R.; Nájera, C. *Chem. Rev.* **2014,** *114,* 1783–1826. doi:10.1021/cr400133p
3. Ackermann, L. *Acc. Chem. Res.* **2014,** *47,* 281–295. doi:10.1021/ar3002798
4. Rodríguez, M. R.; Beltrán, Á.; Mudarra, Á. L.; Álvarez, E.; Maseras, F.; Díaz-Requejo, M. M.; Pérez, P. J. *Angew. Chem., Int. Ed.* **2017,** *56,* 12842–12847. doi:10.1002/anie.201705664
5. Islas, R. E.; Cárdenas, J.; Gaviño, R.; García-Ríos, E.; Lomas-Romero, L.; Morales-Serna, J. A. *RSC Adv.* **2017,** *7,* 9780–9789. doi:10.1039/c6ra28855c
6. Takano, S.; Kochi, T.; Kakiuchi, F. *Chem. Lett.* **2017,** *46,* 1620–1623. doi:10.1246/cl.170754
7. Liu, H.; Lu, L.; Hua, R. *Tetrahedron* **2017,** *73,* 6428–6435. doi:10.1016/j.tet.2017.09.037
8. Campbell, K. N.; Campbell, B. K. *Org. Synth.;* Coll. Vol. 4; 1963; pp 763–766.
9. Müller, S. G.; Liepold, B.; Roth, G. J.; Bestmann, H. J. *Synlett* **1996,** 521–522. doi:10.1055/s-1996-5474
10. Roth, G. J.; Liepold, B.; Müller, S. G.; Bestmann, H. J. *Synthesis* **2004,** 59–62. doi:10.1055/s-2003-44346
11. Corey, E. J.; Fuchs, P. L. *Tetrahedron Lett.* **1972,** *13,* 3769–3772. doi:10.1016/S0040-4039(01)94157-7
12. Sahu, B.; Muruganantham, R.; Namboothiri, I. N. N. *Eur. J. Org. Chem.* **2007,** 2477–2489. doi:10.1002/ejoc.200601137
13. Zhao, M.; Kuang, C.; Yang, Q.; Cheng, X. *Tetrahedron Lett.* **2011,** *52,* 992–994. doi:10.1016/j.tetlet.2010.12.071
14. Morri, A. K.; Thummala, Y.; Doddi, V. R. *Org. Lett.* **2015,** *17,* 4640–4643. doi:10.1021/acs.orglett.5b02398
15. Heravi, M. M.; Asadi, S.; Nazari, N.; Lashkariani, M. B. *Curr. Org. Chem.* **2015,** *19,* 2196–2219. doi:10.2174/1385272819666150619174010
16. Steckhan, E.; Arns, T.; Heineman, W. R.; Hilt, G.; Hoormann, D.; Jörissen, J.; Kröner, L.; Lewall, B.; Pütter, H. *Chemosphere* **2001,** *43,* 63–73. doi:10.1016/S0045-6535(00)00325-8
17. Frontana-Uribe, B. A.; Little, R. D.; Ibanez, J. G.; Palma, A.; Vasquez-Medrano, R. *Green Chem.* **2010,** *12,* 2099–2119. doi:10.1039/C0GC00382D
18. Schäfer, H. J. *C. R. Chim.* **2011,** *14,* 745–765. doi:10.1016/j.crci.2011.01.002
19. Horn, E. J.; Rosen, B. R.; Baran, P. S. *ACS Cent. Sci.* **2016,** *2,* 302–308. doi:10.1021/acscentsci.6b00091
20. Casanova, J.; Reddy, V. P. Electrochemistry of the carbon−halogen bond. In *The Chemistry of Functional Groups, Supplement D2;* Patai, S.; Rappoport, Z., Eds.; Wiley: New York, 1995; pp 1003–1067.
21. Peters, D. G. Oxidation and reduction of halogen-containing compounds. In *Encyclopedia of Electrochemistry;* Schäfer, H. J., Ed.; Wiley-VCH Verlag GmbH: Weinheim, Germany, 2004; Vol. 8, pp 217–233.
22. Torii, S. Electroreduction of Halogenated Compounds. *Electroorganic Reduction Synthesis;* Wiley-VCH Verlag GmbH: Weinheim, Germany, 2006; Vol. 1, pp 331–432.
23. Peters, D. G. In *Organic Electrochemistry,* 5th ed.; Hammerich, O.; Speiser, B., Eds.; Taylor & Francis, LLC: London, 2016; pp 941–980.
24. Martin, E. T.; McGuire, C. M.; Mubarak, M. S.; Peters, D. G. *Chem. Rev.* **2016,** *116,* 15198–15234. doi:10.1021/acs.chemrev.6b00531
25. Feroci, M.; Orsini, M.; Palombi, L.; Sotgiu, G.; Inesi, A. *Electrochim. Acta* **2004,** *49,* 635–640. doi:10.1016/j.electacta.2003.09.018
26. Strobel, S. M.; Szklark, G. D.; He, Y. Q.; Foroozesh, M.; Alworth, W. L.; Roberts, E. S.; Hollenberg, P. F.; Halpert, J. R. *J. Pharmacol. Exp. Ther.* **1999,** *290,* 445–451.
27. Beebe, L. E.; Roberts, E. S.; Fornwald, L. W.; Hollenberg, P. F.; Alworth, W. L. *Biochem. Pharmacol.* **1996,** *52,* 1507–1513. doi:10.1016/S0006-2952(96)00525-4
28. Mubarak, M. S.; Peters, D. G. *Curr. Opin. Electrochem.* **2017,** *2,* 60–66. doi:10.1016/j.coelec.2017.03.001
29. Gennaro, A.; Isse, A. A.; Mussini, P. R. In *Organic Electrochemistry,* 5th ed.; Hammerich, O.; Speiser, B., Eds.; Taylor & Francis, LLC: London, 2016; pp 917–940.
30. The use of glassy carbon (GC) as cathode was not possible probably due to adsorption of material on the electrode surface, which led to electrical insulation.

31. Abbas, S.; Hayes, C. J.; Worden, S. *Tetrahedron Lett.* **2000,** *41,* 3215–3219. doi:10.1016/S0040-4039(00)00353-1

32. We are grateful to a referee for suggesting this mechanistic hypothesis.

33. Li, Y.-P.; Fan, X.-X.; Wu, Y.; Zeng, X.-C.; Wang, J.-Y.; Wei, Q.-H.; Chen, Z.-N. *J. Mater. Chem. C* **2017,** *5,* 3072–3078. doi:10.1039/c7tc00382j

34. Kato, S.-i.; Noguchi, H.; Kobayashi, A.; Yoshihara, T.; Tobita, S.; Nakamura, Y. *J. Org. Chem.* **2012,** *77,* 9120–9133. doi:10.1021/jo3016538

Polysubstituted ferrocenes as tunable redox mediators

Sven D. Waniek, Jan Klett[*], Christoph Förster[*] and Katja Heinze[*]

Abstract

A series of four ferrocenyl ester compounds, 1-methoxycarbonyl- (**1**), 1,1'-bis(methoxycarbonyl)- (**2**), 1,1',3-tris(methoxycarbonyl)- (**3**) and 1,1',3,3'-tetrakis(methoxycarbonyl)ferrocene (**4**), has been studied with respect to their potential use as redox mediators. The impact of the number and position of ester groups present in **1–4** on the electrochemical potential $E_{1/2}$ is correlated with the sum of Hammett constants. The $\mathbf{1/1^+}$–$\mathbf{4/4^+}$ redox couples are chemically stable under the conditions of electrolysis as demonstrated by IR and UV–vis spectroelectrochemical methods. The energies of the C=O stretching vibrations of the ester moieties and the energies of the UV–vis absorptions of **1–4** and $\mathbf{1^+}$–$\mathbf{4^+}$ correlate with the number of ester groups. Paramagnetic ^{1}H NMR redox titration experiments give access to the chemical shifts of $\mathbf{1^+}$–$\mathbf{4^+}$ and underline the fast electron self-exchange of the ferrocene/ferrocenium redox couples, required for rapid redox mediation in organic electrosynthesis.

Introduction

Since its discovery, ferrocene (FcH) has been established as versatile redox-active building block [1-3]. Ferrocene can be reversibly oxidized to the 17 valence electron ferrocenium cation (FcH$^+$) at a useful electrochemical potential (FcH/FcH$^+$ +630 mV vs NHE; +380 mV vs SCE in CH$_3$CN) [4]. The 0/+ redox couple of ferrocene and its derivatives possesses high electron self-exchange rates $k_{ex} = 10^6$–10^7 M^{-1} s^{-1}, remarkably independent on the electrolyte and solvent [5,6]. Both, the ferrocene/ferrocenium and the decamethylferrocene/decamethylferrocenium redox couples are well established as internal reference redox systems for electrochemical analyses in non-aqueous media [7-10]. Important requirements for redox

couples with respect to useful applications are: (i) Both components of the redox couple should be soluble. (ii) Homogeneous and heterogeneous electron-transfer (ET) reactions should be fast. (iii) Both components should be stable under the electrolysis conditions and should not react irreversibly with any component of the supporting electrolyte [8]. In general, the redox mediators used as redox catalysts in indirect organic electrosyntheses should comprise the same characteristics [11-14]. A mediator is a reversible redox couple with a fast ET between itself and the electrode (heterogeneous) and between itself and the substrate (homogeneous). The benefit of the presence of a mediator is the switch of the sluggish heterogeneous electron

transfer between electrode and substrate to a rapid homoge-neous redox reaction between mediator and substrate. Further, the mediator's redox potential must be below or above of that of the substrate for oxidation or reduction processes, respectively. This avoids the often kinetically hindered direct ET between electrode and substrate and diminishes overoxidation or overre-duction of the substrate.

Redox-active ferrocenyl derivatives find application in redox flow batteries [15], with water soluble (ferrocenylmethyl)am-monium salts acting as catholytes. Ferrocene dicarboxylic acid has been described as mediator for the voltammetric determina-tion of glutathione in hemolized erythrocytes [16]. (Substituted) ferrocenium salts were successfully employed as single-elec-tron transfer (SET) reagents in organic syntheses [17-28]. Tuning of the electrochemical potential of substituted ferrocen-ium salts promoted a selective oxidative bicyclization reaction under mild conditions (Scheme 1a) [27]. Ferrocene and decamethylferrocene act as redox catalysts in Meerwein aryl-ation reactions [29], borylations of arenediazonium salts [30]

Scheme 1: Selected transformations with ferrocene/ferrocenium as SET reagents (a) [27], catalyzed (b,c) [29-31] and mediated transformations (d–f) [34-36] by the ferrocene/ferrocenium redox couple.
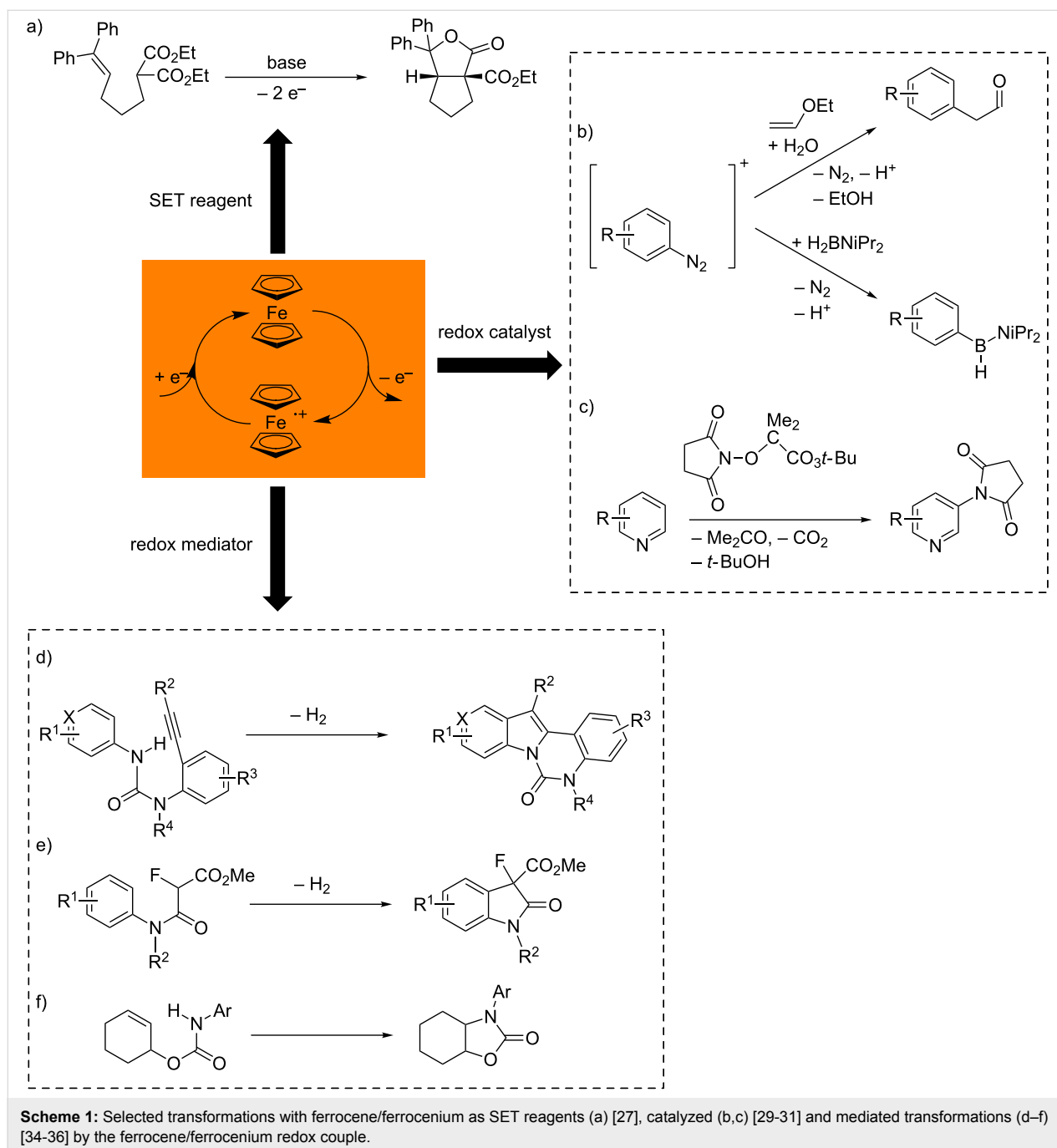
and in C–H imidation reactions of (hetero)arenes [31] (Scheme 1b,c). Ferrocene has been used as redox mediator for the electrochemical modification of carbon surfaces via electrochemical oxidation of carboxylates [32,33], as mediator for dehydrogenative coupling reactions [34,35] and for olefin hydroamidations [36] (Scheme 1d–f).

For potential applications of ferrocene derivatives as redox mediators or SET reagents, it is crucial to adjust the electrochemical potential to the potential of the substrate. The electrochemical potential of the ferrocene/ferrocenium redox couple strongly depends on the number and types of substituents [27,37-44]. One major drawback of changing the substituents is the dramatic change in chemical reactivity of ferrocene derivatives, e.g., ligand substitutions, apart from the solely intended tuning of the redox potential. A single class of ferrocene compounds with similar chemical and physical characteristics, yet covering a broad range of electrochemical potentials should circumvent this problem. To increase the ferrocene/ferrocenium potential, electron-withdrawing substituents are required. Mono-, 1,1'-diesters and a single 1,1',3-triester of ferrocene are known [45-53]. Elegant routes to 1,1',3-tris(methoxycarbonyl)-ferrocene and 1,1',3,3'-tetrakis(methoxycarbonyl)ferrocene were developed only very recently [54], complementing the series of methyl esters of ferrocene carboxylic acids **1**–**4** (Scheme 2) [45-52].

The extremely bulky and electron-poor pentakis(methoxycarbonyl)cyclopentadienyl ligand gives a pseudo octahedral high-spin iron(II) complex **5**, instead of forming a stable classical low-spin sandwich complex, precluding its application as redox mediator (Scheme 2) [55,56].

Ferrocenyl esters **1**–**4** are synthetically accessible via the acids of **1** [45,46], **2** [57], **3** and **4** [54] in a direct selective metalation

of ferrocene [54,57-60], quenching with carbon dioxide, followed by esterification [45-48,54]. The 1,1'-disubstituted ferrocene **2** can also be obtained by direct coordination of the respective substituted cyclopentadienyl ligand (CpR) to iron(II) [49]. An alternative route to the mono-, 1,1'-di- and 1,1',3-tricarboxylic acids of ferrocene is the oxidation of the respective acetylferrocenes [47,48,53]. Ferrocene carboxylic acid is also available via basic hydrolysis of ferrocenyl aryl ketones [61]. Together with the redox potentials of ferrocene, **1** and **2**, the hitherto unknown electrochemical potentials of **3** and **4** should cover a wide potential range. This will meet the requirements of different substrates for the potential application of **1**–**4** and their ferrocenium ions as selective redox mediators or SET reagents. Apart from the redox potentials of the redox mediators FcH and **1**–**4**, the stability of the 18 and 17 valence electron species as well as their solubility and the availability of spectroscopic probes to monitor reaction progress and stability are important issues. These fundamental aspects will be addressed in this study.

Herein, a detailed study of the properties of **1**–**4** and their ferrocenium ions 1^+–4^+ in solution is reported including electrochemical methods (cyclic voltammetry and square wave voltammetry; CV, SWV) and covering investigations regarding the stability of 1–$4/1^+$–4^+ by spectroelectrochemical methods (UV–vis, IR) [62-68]. In addition, the mediators $1/1^+$–$4/4^+$ are probed by paramagnetic NMR spectroscopic methods [69-73]. The results are supported with (time-dependent) density functional theoretical (TD)-DFT methods.

Results and Discussion
Electrochemistry of esters 1–4
The esters **1**–**4** were studied by cyclic and square wave voltammetry in 0.1 M CH$_2$Cl$_2$ solutions of [*n*-Bu$_4$N][B(C$_6$F$_5$)$_4$], using platinum working and counter electrodes. All esters **1**–**4** show
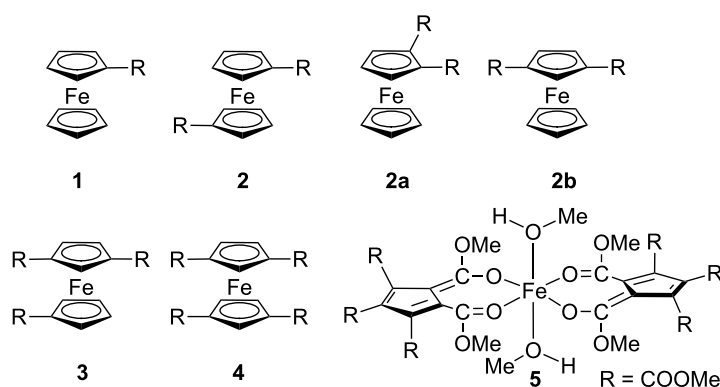
Scheme 2: Methyl esters of ferrocene carboxylic acids **1** [45,46], **2** [47-49], **2a** [50], **2b** [51,52], **3**, **4** [54] and pseudo octahedral high-spin iron(II) complex **5** with pentakis(methoxycarbonyl)cyclopentadienyl ligands [55,56].

an essentially reversible behaviour for the ferrocene/ferrocenium oxidation process (Figure 1, Figure S1, Supporting Information File 1). The electrochemical potentials cover a wide range, $E_{1/2}$ = 260–900 mV vs FcH/FcH$^+$ (Figure 1, Table 1).

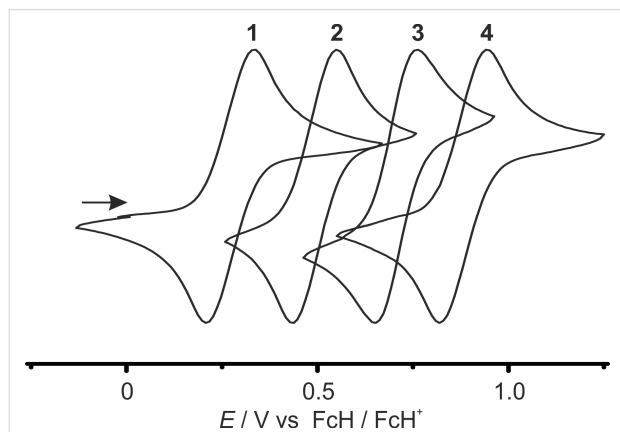**Figure 1:** Normalized cyclic voltammograms for anodic sweeps of **1–4** in CH_2Cl_2/[n-Bu$_4$N][B(C_6F_5)$_4$] (scan rate 100 mV s^{-1}).

Table 1: Electrochemical data of esters **1–4** and sum of Hammett substituent constants $\sigma_p{}^a$ and $\sigma_m{}^a$.

	$E_{1/2}$ [mV]^b	$\sum\sigma_{p/m}$	$\sum\sigma_p$
1	260	σ_p = 0.45	0.45
2	495	2 σ_p = 0.90	0.90
3	700	2 σ_p + σ_m = 1.27	1.35
4	900	2 σ_p + 2 σ_m = 1.64	1.80

$^a\sigma_p$ = 0.45, σ_m = 0.37 for COOMe substituent [74]. ^{b}vs FcH/FcH$^+$.

The oxidation potential of the tetraester **4** is very high with $E_{1/2}$ = 900 mV. To the best of our knowledge, higher oxidation potentials (vs FcH/FcH$^+$) have been observed only for 1,1',2,2',4,4'-hexakis(pentafluorophenyl)ferrocene (940 mV in CH_2Cl_2) [40], 1,1',2,2',3,3'-hexakis(pentafluorophenyl)ferrocene (951 mV in CH_2Cl_2) [40], decachloroferrocene (E_p = 1246 mV in MeCN) [37], 1,1',2-tri(formyl)ferrocene (910 mV in CH_2Cl_2 at −40 °C) [38] and 1,1',2,2'-tetra(formyl)ferrocene (1145 mV in CH_2Cl_2 at −40 °C) [38]. The latter three are only irreversibly oxidized at room temperature precluding any application as mediators. The data are in full accordance with the increasing electron-withdrawing character of the cyclopentadienyl ligands from **1** to **4**. The position of the ester groups has a slight influence on the electrochemical potential. 1- or 1'-substitution with a methoxycarbonyl group raises the potential by ca. 250 mV (FcH → **1**, **1** → **2**), while substitution in 3- and 3'-position has only a smaller impact with an increase of the potential by ca. 200 mV (**2** → **3**, **3** → **4**). According to Lever et al. [39], the calculated electrochemical pa-

rameters E_L(L) for 1-(methoxycarbonyl)cyclopentadienyl and 1,3-bis(methoxycarbonyl)cyclopentadienyl ligands amount to E_L(L$_1$) = 250 mV and E_L(L$_2$) = 450 mV vs FcH/FcH$^+$, respectively. Indeed, the electrochemical potential $E_{1/2}$ = 700 mV of **3** perfectly corresponds to the sum E_L(L$_1$) + E_L(L$_2$) = 700 mV. Consequently, the ligand contributions to the electrochemical potential of substituted cyclopentadienyl complexes are essentially additive for **1–4**.

This characteristic relationship is supported by correlating the electrochemical data with the Hammett substituent constants [37,39,74,75]. Typically, the $E_{1/2}$ data of substituted ferrocenes correlate linearly with the sum $\sum\sigma_p$ of the Hammett values σ_p of *para*-substituents [37,39,74].

For esters **1–4**, the electrochemical potentials $E_{1/2}$ (vs FcH/FcH$^+$) versus sum of Hammett values $\sum\sigma_p$ did not give a satisfactory linear relation. Within this approach, the relative positions of ester groups and hence their different electronic influence to the electrochemical potential is not considered. The influence of a methoxycarbonyl substituent in 1- or 1'-position is indeed best described with σ_p = 0.45 [75]. On the other hand, substituents in the 3- or 3'-position require using σ_m = 0.37 [75] for *meta*-substituents, to give an excellent linear correlation of $E_{1/2}$ with $\sum\sigma_{p/m}$ (Figure 2, Table 1).
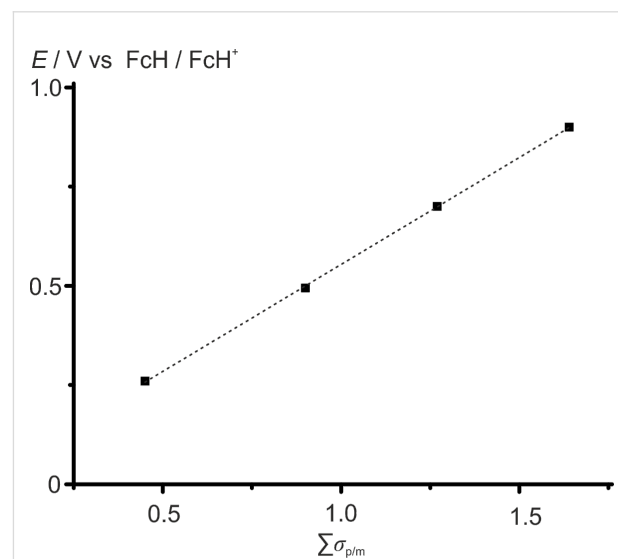
Figure 2: Electrochemical potentials $E_{1/2}$ (vs FcH/FcH$^+$) of esters **1–4** versus sum of Hammett values $\sum\sigma_{p/m}$ with linear regression ($E_{1/2}$ = 0.539 V · $\sum\sigma_{p/m}$ + 0.015 V, R^2 = 0.9999).

The generalizable use of σ_p and especially σ_m to include the effect on the relative positions of substituents for $E_{1/2}$ of polysubstituted ferrocenes has to be further validated with other series of polysubstituted ferrocenes.

IR spectroelectrochemistry of esters **1–4**

In the attenuated total reflection (ATR) IR spectra of solid samples of esters **1–4**, several overlapping bands for the C=O stretching vibrations of the ester substituents are observed between 1678 and 1730 cm^{-1} (Figure 3a, Figures S2–S6, Table S1, Supporting Information File 1). DFT calculations (B3LYP, def2-TZVP, RIJCOSX, ZORA, CPCM (CH$_2$Cl$_2$)) on di-, tri- and tetraesters **2–4** suggest an intramolecular coupling of the C=O vibrations of the ester moieties substantiating the number of observed bands (Table S1, Supporting Information File 1). Furthermore, crystal packing effects with intermolecular C=O···H–C interactions, differing in strengths, can be responsible for the occurrence of distinguishable C=O bands [54,76,77]. For example, two different molecules of monoester **1** are present in the asymmetric unit of the solid-state structure [76], leading to different C=O stretching vibration bands (Figure 3a).

In contrast to the solid-state IR spectra, only a single broad C=O band is observed for **1–4** in solution (Figure 3, Figure 4, Figures S7–S14, Supporting Information File 1). In the series **1–4**, the C=O bands shift to higher wavenumbers in solution $\tilde{v}_{CO}$ = 1712–1724 cm^{-1} with increasing number of electron-withdrawing COOMe groups (Figure 3b). The DFT calculated IR spectra with unscaled energies of the C=O vibrations $\tilde{v}_{max(CO)}$ = 1710–1724 cm^{-1} fully support these findings (Table S1, Figures S15–S22, Supporting Information File 1).

Figure 4: IR spectroelectrochemical oxidation of **3** to **3$^+$** in CH$_2$Cl$_2$/[*n*-Bu$_4$N][B(C$_6$F$_5$)$_4$] (C=O stretching vibration region, 0.4–1.1 V vs Ag pseudo reference electrode).
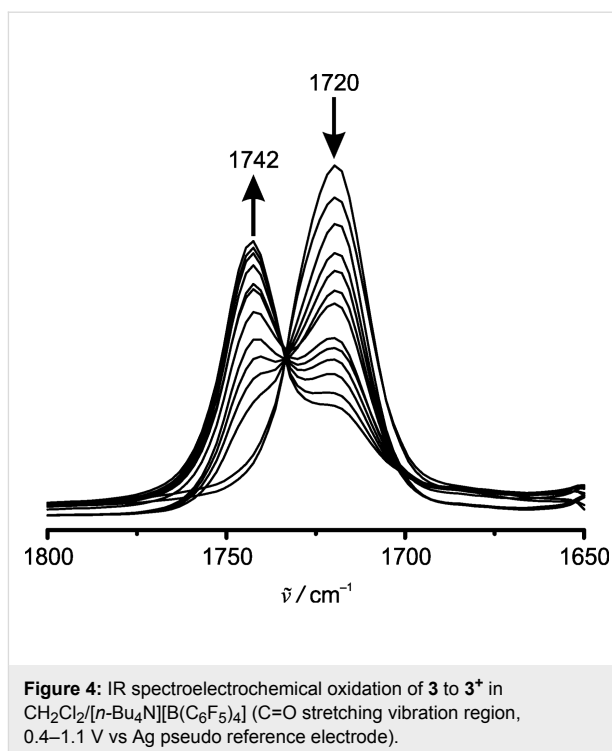
Compounds **1–4** can be reversibly oxidized to **1$^+$–4$^+$** in dichloromethane and [*n*-Bu$_4$N][B(C$_6$F$_5$)$_4$] as supporting electrolyte in an IR spectroelectrochemical (SEC) cell, confirming

Figure 3: a) Partial ATR IR spectra (transmission normalized, C=O stretching vibration region) of solids **1–4**. b) Partial spectroelectrochemical IR spectra (absorption normalized, C=O stretching vibration region) of mixtures of the **1/1$^+$–4/4$^+$** redox couples in dichloromethane/[*n*-Bu$_4$N][B(C$_6$F$_5$)$_4$].
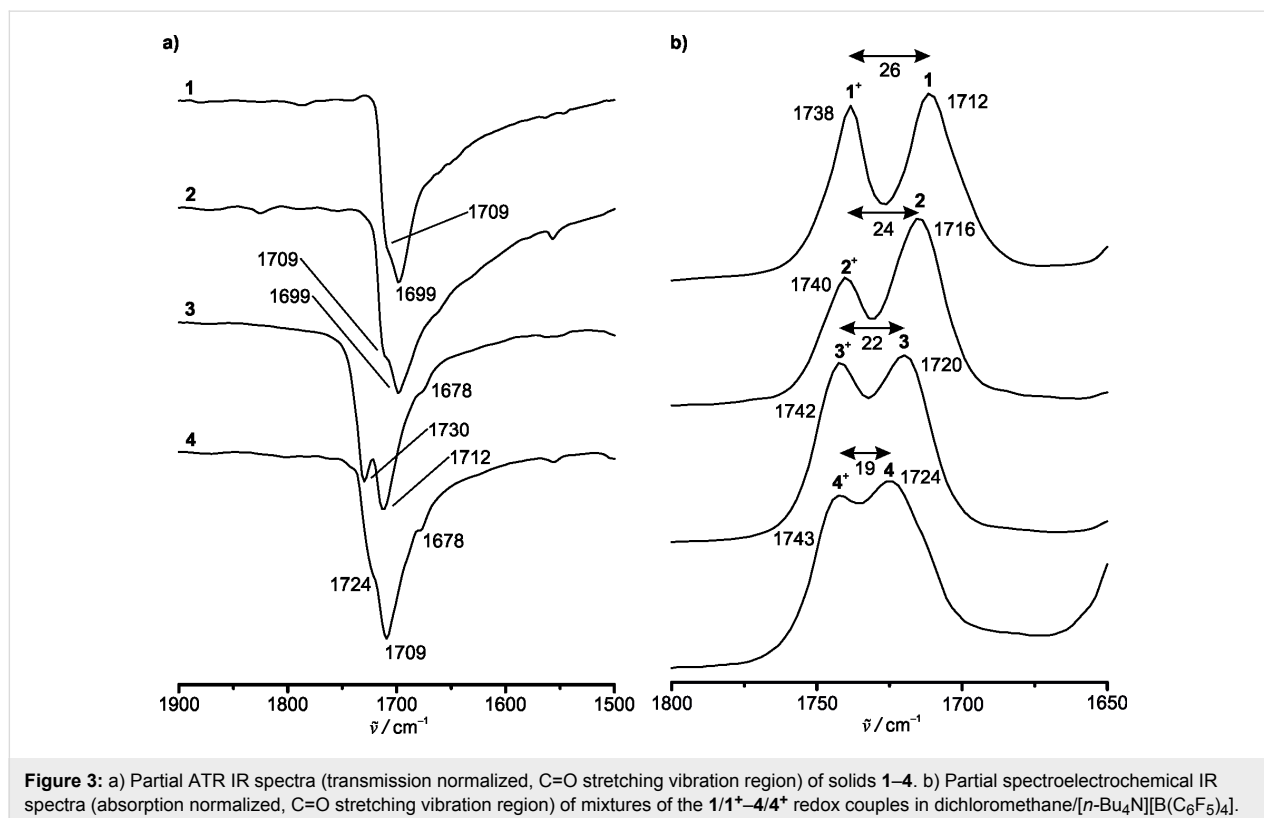
the chemical stability of the ferrocenyl esters under the conditions of electrolysis (Figure 3b, Figure 4, Figures S7–S14, Table S1, Supporting Information File 1).

Triester **3** and tetraester **4** cannot be quantitatively oxidized to **3⁺** and **4⁺** in the SEC cell up to a potential of 1.1 V and 1.4 V, respectively, probably due to a fast diffusion of **3** and **4** to the anode in the beam path (Figure 4, Figures S11–S14, Supporting Information File 1). In addition, precipitation of some poorly soluble [**4**][**X**] also occurs. During oxidation to the respective ferrocenium cations, the C=O stretching vibration bands of **1–4** decrease in intensity, while the C=O bands of **1⁺–4⁺** appear, crossing in clean isosbestic points. Expectedly, the C=O stretching vibrations of **1⁺–4⁺** are shifted to higher wavenumbers by 26–19 cm⁻¹ ($\tilde{v}_{CO}$ = 1738–1743 cm⁻¹) with an increasing electron-withdrawing character of the Cp ligands. The substituent effect is attenuated by the positive charge at the iron atom in **1⁺–4⁺** ($\Delta\tilde{v}_{CO}$ = 5 cm⁻¹), compared to **1–4** ($\Delta\tilde{v}_{CO}$ = 12 cm⁻¹), respectively (Figure 3b, Table S1, Figures S7–S14, Supporting Information File 1) [78]. The unscaled

energies of the DFT calculated C=O bands of **1⁺–3⁺** fit very well to the experimental observations of **1⁺–3⁺** (Figures S7–S12, S16, S18, S20, Table S1, Supporting Information File 1). Unexpectedly, the calculated $\tilde{v}_{CO}$ data of **4⁺** are significantly lower than the experimental ones, which remain unexplained at the moment.

For all redox couples of the ferrocenyl esters, the C=O stretching vibration delivers a useful in operando probe substantiating the stability of the redox mediator and enabling quantification of both redox partners and hence estimation of the actual concentration-dependent redox potential in solution.

UV–vis spectroelectrochemistry of esters 1–4

Analogous to the IR-SEC experiments, the esters **1–4** were also probed by UV–vis-SEC investigations. The UV–vis spectra of **1–4** recorded in dichloromethane show the ferrocene ligand field absorption band at λ_{max} = 444, 449, 455 and 457 nm, which is typically around λ_{max} ≈ 440–490 nm [66,70,79,80] (Figure 5a).
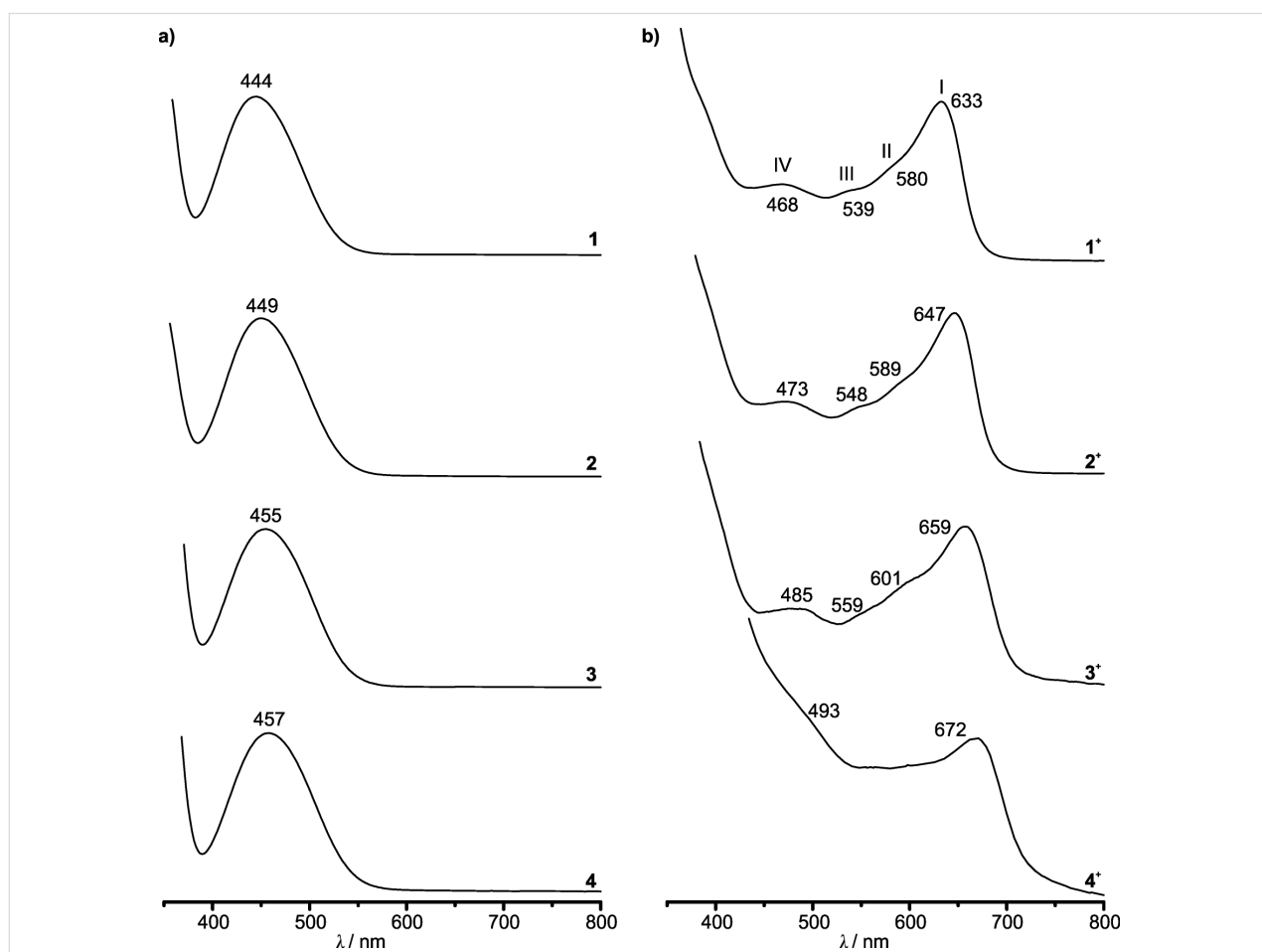
Figure 5: a) Normalized UV–vis spectra of **1–4** in CH_2Cl_2. b) Normalized UV–vis absorptions of **1⁺–4⁺** in $CH_2Cl_2/[n\text{-}Bu_4N][B(C_6F_5)_4]$ after spectroelectrochemical oxidation of **1–4**.

The energy of the absorption bands decreases almost linearly with the number *n* of the electron-withdrawing COOMe substituents for **1**–**4** (Figure 6a).

Figure 6: Absorption energy *E* of ferrocene bands of **1**–**4** (a) and energies of the low energy absorption maxima at around $\lambda_{max} \approx 630$–670 nm of **1**$^+$–**4**$^+$ (b) versus number of methoxycarbonyl substituents *n* with regression lines
a) $E = -222$ cm$^{-1} \cdot n + 22700$ cm^{-1}, $R^2 = 0.9824$;
b) $E = -303$ cm$^{-1} \cdot n + 16100$ cm^{-1}, $R^2 = 0.9991$.
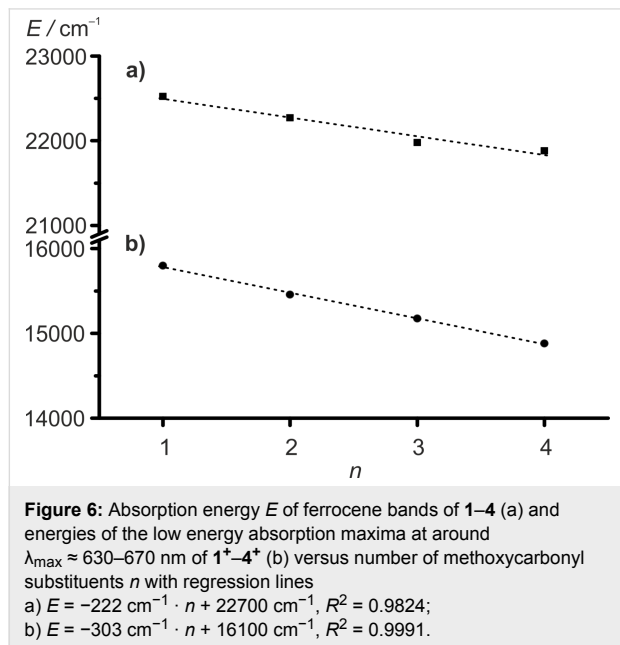
The reversible oxidation of **1**–**4** in UV–vis-SEC experiments in CH$_2$Cl$_2$/[*n*-Bu$_4$N][B(C$_6$F$_5$)$_4$] is monitored by the decreasing band intensity of the ferrocene absorption and the appearance of a set of four partially resolved characteristic ferrocenium absorptions (bands I–IV) responsible for the blue color (Figure 5b and Figure 7, Figures S23–S31, Supporting Information File 1).

Figure 7: UV–vis spectroelectrochemical oxidation of **3** in CH$_2$Cl$_2$/[*n*-Bu$_4$N][B(C$_6$F$_5$)$_4$] (0–1.1 V vs Ag pseudo reference electrode).
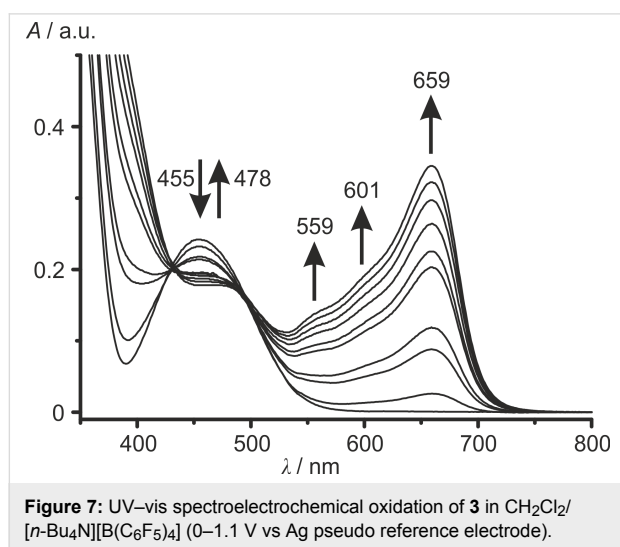
Isosbestic points indicate clean conversions of **1** $\rightarrow$ **1**$^+$, **2** $\rightarrow$ **2**$^+$ and **3** $\rightarrow$ **3**$^+$, respectively. For example, this set of bands and

shoulders (sh) IV–I is observed at $\lambda_{max} = 485$ nm (IV), $\lambda_{sh} = 559$ nm (III), 601 nm (II) and $\lambda_{max} = 659$ nm (I) for **3**$^+$. During oxidation of **4** to **4**$^+$, isosbestic points between the absorption bands of **4** and **4**$^+$ cannot be observed (Figures S29 and S30, Supporting Information File 1). Probably, precipitation of the poorly soluble tetraester **4**$^+$ could be responsible for this effect, as already suggested for the IR-SEC experiments of **4**/**4**$^+$. On the other hand, isosbestic points are observed in the UV–vis spectra upon re-reduction of **4**$^+$ to **4** (Figure S31, Supporting Information File 1). The energy of the absorptions of the ferrocenium cations **1**$^+$–**4**$^+$ decreases with the electron-withdrawing nature of the Cp ligands in the series **1**$^+$–**4**$^+$, similar to the vis absorption maxima of the neutral ferrocenes **1**–**4**. For the prominent band I of the cations **1**$^+$–**4**$^+$, a linear and stronger dependency of the energy on the number *n* of methoxycarbonyl substituents can be found than for the ligand field band of the ferrocenes **1**–**4** (Figure 6b). The lowest energy band (band I) in the UV–vis spectra of **1**$^+$–**4**$^+$ is assigned to ligand-to-metal charge transfer (LMCT) transitions [79,81-83]. The bands II–IV are assigned to mainly d–d transitions [79]. TD-DFT calculations on the B3LYP, def2-TZVP, RIJCOSX, ZORA, CPCM (CH$_2$Cl$_2$) level do not give satisfactory results concerning energy, number of bands and oscillator strength of electronic transitions (Figures S32–S35, Supporting Information File 1). The poor agreement of TD-DFT calculated electronic spectra of metallocenes and derivatives with experimental data has been noted before. Improvements have been achieved by testing different functionals [84,85] and by including vibrational distortions of the ferrocene geometry into the calculations [86]. Nevertheless, the LMCT character of the prominent band I is confirmed by the calculations. The intensity of band I scales with the amount of the corresponding ferrocenium ion present and consequently the actual potential in solution can be estimated by UV–vis spectroscopy.

NMR spectroscopy of esters 1–4 and 1$^+$–4$^+$

In contrast to typical organic paramagnetic redox mediators, the relaxation properties of proton nuclei of paramagnetic ferrocenium derivatives allow the observation of reasonable sharp resonances [87]. The fast electron self-exchange of the ferrocene/ferrocenium redox couple and derivatives on the NMR timescale leads to the observation of resonances with averaged chemical shifts δ in the ^{1}H NMR spectra of ferrocene/ferrocenium mixtures [5,6,70-72]. The molar fraction of FcH/FcH$^+$ can be calculated from the averaged ^{1}H NMR resonance frequencies of a mixture and the known resonance frequencies of FcH and FcH$^+$, respectively [6]. This relation gives $\chi_P = (\delta - \delta_D)/(\delta_P - \delta_D)$ for the molar fraction of the paramagnetic species, expressed in the chemical shift scale with δ_D being the chemical shift of the diamagnetic species, δ_P being the

resonance of the paramagnetic species and δ being the averaged chemical shift of the mixture.

The detection of the resonances of $1/1^+$–$4/4^+$ should allow for determining the ratio of $1:1^+$–$4:4^+$ by in situ NMR experiments. Thus, titration of **1**–**4** with Magic Green, tris(2,4-dibromophenyl)ammoniumyl hexachloroantimonate [10], as a strong oxidant ($E_{1/2}$ = 1140 mV in MeCN vs FcH/FcH$^+$) in CD$_2$Cl$_2$ under NMR monitoring shows that the Cp proton resonances broaden upon oxidation and shift to lower field, while the methyl proton resonances of the ester substituents shift to higher field and remain much sharper (Figure 8, Table 2, Figures S36–S38, Supporting Information File 1).

In some cases, e.g., 3^+, the different Cp protons can still be distinguished in spite of the broadened resonances (Figure 8). The broadening is much more severe for the Cp proton resonances, while the methyl proton resonances are still rather sharp allowing the discrimination and assignment of the different methyl protons of 3^+ (Figure 8).

With an increasing number of ester groups, the proton resonances of the mono- and disubstituted Cp ligands and of the methyl groups shift to lower field for **1**–**4** (CpR: **1** → **2** → **3**, CpR$_2$: **3** → **4**), while for 1^+–4^+, the Cp ligand proton resonances shift to lower field and the methyl proton resonances shift to higher field (CpR: 1^+ → 2^+ → 3^+, CpR$_2$: 3^+ → 4^+).

This substituent effect is larger for the paramagnetically shifted resonances of 1^+–4^+ than for the diamagnetic complexes **1**–**4**.

In CD$_3$CN, the treatment of **3** with Magic Green led to the disappearance of the resonances of **3**. However, paramagnetically shifted resonances of 3^+ are absent suggesting that the initially formed 3^+ undergoes further reactions with the coordinating solvent CD$_3$CN (Figure S39, Supporting Information File 1). This finding underscores that the solvent has to be carefully chosen with respect to the mediated reaction and stability of the mediator.

From the observed ^{1}H NMR chemical shifts – either of the cyclopentadienyl or methyl resonances – the relative concentrations of the ferrocene and ferrocenium ion can be extracted, again allowing the estimation of the actual potential in solution by spectroscopic techniques.

Conclusion

Ferrocenyl esters **1**–**4** with one to four ester substituents are reversibly oxidized to the respective ferrocenium cations 1^+–4^+, spanning a broad electrochemical potential range from 260 mV for **1** to 900 mV for **4** vs the ferrocene/ferrocenium redox couple. The electrochemical potentials $E_{1/2}$ of **1**–**4** correlate linearly with the sum of Hammett substituent parameters $\sum\sigma_{p/m}$. However, the position of ester substituents has to be taken into account by employing σ_p for 1- and 1'-substituents and σ_m for
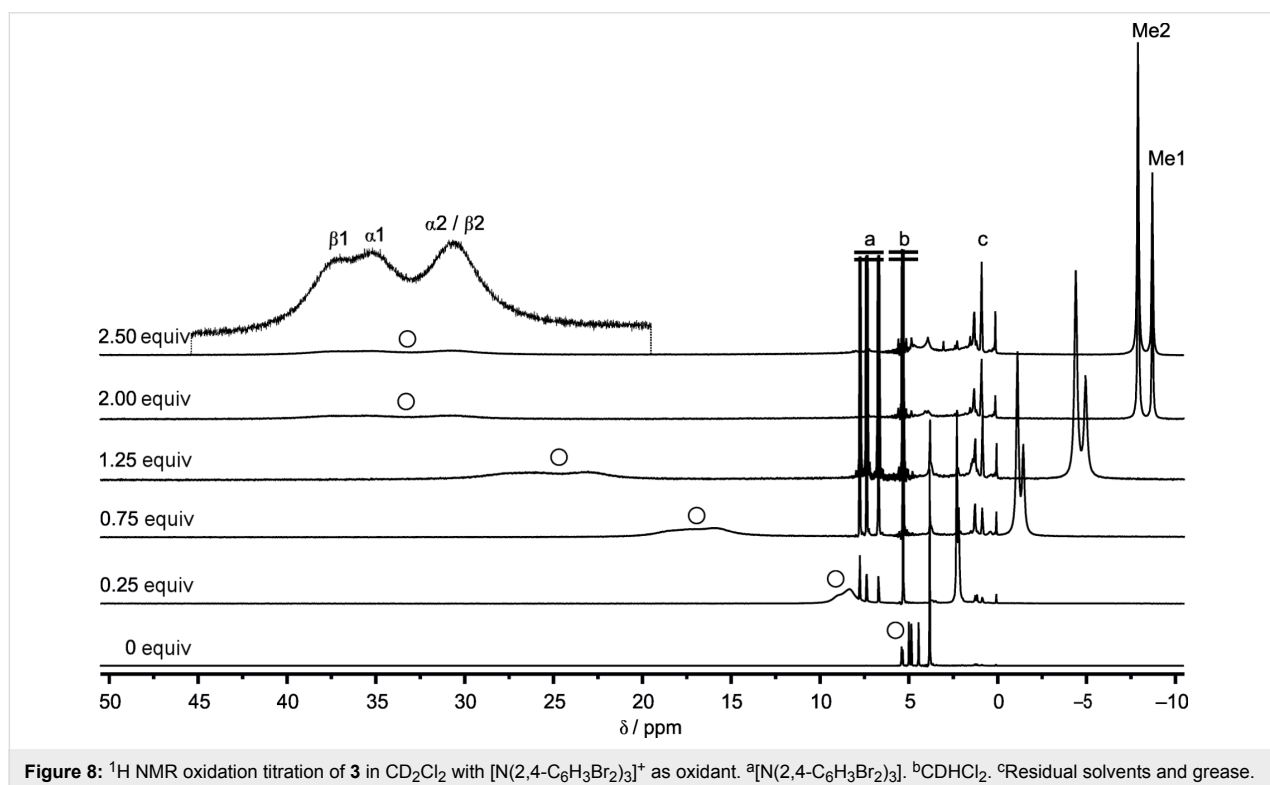

Figure 8: ^{1}H NMR oxidation titration of **3** in CD$_2$Cl$_2$ with [N(2,4-C$_6$H$_3$Br$_2$)$_3$]$^+$ as oxidant. ^{a}[N(2,4-C$_6$H$_3$Br$_2$)$_3$]. ^{b}CDHCl$_2$. ^{c}Residual solvents and grease.

Table 2: ^{1}H NMR data (δ [ppm])^a of **1–4** and **1^+–4^+** in CD$_2$Cl$_2$.

	H^{Cp}	H$^{\alpha1}$/H$^{\beta1}$	H$^{\alpha2}$/H$^{\beta2}$	H^{Me1}	H^{Me2}
1	4.20	4.40/4.77		3.76	
1^+	37.0	30.1/32.3		−8.34	
2		4.42/4.79		3.78	
2^+		34.0^b		−8.51	
3		4.43/4.84	4.97/5.39	3.79	3.80
3^+		35.3/37.5	30.7^b	−8.75	−7.94
4			4.98/5.42		3.87
4^+			33.6^b		−8.26

^{a}Numbering scheme:

^{b}Only a single broad resonance.

3- and 3'-substituents, respectively. Complexes **1–4** and **1^+–4^+** are stable under conditions of electrolysis (CH$_2$Cl$_2$, [*n*-Bu$_4$N][B(C$_6$F$_5$)$_4$]) as demonstrated by IR and UV–vis spectroelectrochemical experiments and ^{1}H NMR spectroscopy. The C=O stretching vibrations of the ester substituents as characteristic probes in the IR spectra are consistently shifted to higher energies from **1** to **4** and from **1^+** to **4^+**. Upon oxidation of **1–4** to **1^+–4^+** in solution, the ferrocene bands in the UV–vis spectra of **1–4** at λ_{max} = 444–457 nm and the LMCT bands of **1^+–4^+** at λ_{max} = 633–672 nm bathochromically shift linearly with increasing number of ester groups. The ^{1}H NMR paramagnetic chemical shifts of **1^+–4^+** have been determined by redox titration experiments.

With all the data in hand, the molar fraction of the ester-substituted redox couples **1/1^+–4/4^+** can be accessed a) from the C=O stretching vibrations of the ester groups, b) the ferrocenium CT bands or c) from the averaged ^{1}H NMR chemical shifts of the Cp or ester methyl protons. Ongoing investigations focus on the spectroscopic monitoring of **1–4** as redox mediators in selected electrosynthetic transformations.

Experimental

Dichloromethane, CD$_2$Cl$_2$ and CD$_3$CN were distilled from calcium hydride. Electrochemical experiments were carried out on a BioLogic SP-50 voltammetric analyzer using a platinum working electrode, a platinum wire as counter electrode, and a 0.01 M Ag/AgNO$_3$ CH$_3$CN electrode as reference electrode. The measurements were carried out at a scan rate of 100 mV s^{-1} for cyclic voltammetry experiments and 100 mV s^{-1} for square wave voltammetry experiments using 0.1 M [*n*-Bu$_4$N][B(C$_6$F$_5$)$_4$] as supporting electrolyte and 0.001 M of the sample in dichloromethane. Potentials are given relative to the ferrocene/ferrocenium couple.

Spectroelectrochemical experiments were performed using a Specac omni-cell liquid transmission cell with CaF$_2$ windows equipped with a Pt-gauze working electrode, a Pt-gauze counter electrode and an Ag wire as pseudo-reference electrode, melt-sealed in a polyethylene spacer (approximate path length 0.5 mm) in dichloromethane (68, 35, 13, 2 mM solutions of **1–4** in CH$_2$Cl$_2$, containing 0.1 M [*n*-Bu$_4$N][B(C$_6$F$_5$)$_4$]) [88]. UV–vis/near-IR spectra were recorded on a Varian Cary 5000 spectrometer using 1.0 cm cells (Hellma, Suprasil). IR spectra were recorded on a Bruker Alpha FTIR spectrometer with ATR unit, containing a diamond crystal.

NMR spectra were recorded on a Bruker Avance DRX 400 spectrometer at 400.31 MHz (^{1}H) at 25 °C. All resonances are reported in ppm versus the solvent signal as internal standard: CD$_2$Cl$_2$ (^{1}H, δ = 5.32 ppm), CD$_3$CN (^{1}H, δ = 1.94 ppm) [89].

DFT calculations were carried out using the ORCA program package (version 4.0.1) [90]. All calculations were performed using the B3LYP functional [91-93] and employ the RIJCOSX approximation [94,95]. Relativistic effects were calculated at the zeroth order regular approximation (ZORA) level [96]. The ZORA keyword automatically invokes relativistically adjusted basis sets. To account for solvent effects, a conductor-like screening model (CPCM) modeling dichloromethane was used in all calculations [97]. Geometry optimizations and TD-DFT calculations (50 vertical transitions) were performed using Ahlrichs' split-valence triple-ξ basis set def2-TZVP which comprises polarization functions for all non-hydrogen atoms [98,99]. The presence of energy minima was checked by numerical frequency calculations. Explicit counterions and/or solvent molecules were not taken into account.

Supporting Information

The Supporting Information file contains square wave voltammograms, IR and UV–vis spectra of the spectroelectrochemical experiments, (TD)-DFT calculated IR and UV–vis spectra, a table with IR data, ^{1}H NMR spectra of the oxidation titration experiments and Cartesian coordinates of DFT calculated structures of **1–4**.

Supporting Information File 1
Mediators measured and calculated spectra, IR data and Cartesian coordinates.
[https://www.beilstein-journals.org/bjoc/content/supplementary/1860-5397-14-86-S1.pdf]

Acknowledgements

ORCID® iDs

Jan Klett - https://orcid.org/0000-0002-0055-5335
Katja Heinze - https://orcid.org/0000-0003-1483-4156

References

1. Togni, A.; Hayashi, T. *Ferrocenes;* Wiley-VCH Verlag GmbH: Weinheim, Germany, 1994.
2. Štěpnička, P., Ed. *Ferrocenes. Ligands, materials and biomolecules;* J. Wiley: Chichester, England, 2008.
3. Astruc, D. *Eur. J. Inorg. Chem.* **2017,** 6–29. doi:10.1002/ejic.201600983
4. Pavlishchuk, V. V.; Addison, A. W. *Inorg. Chim. Acta* **2000,** *298,* 97–102. doi:10.1016/S0020-1693(99)00407-7
5. Yang, E. S.; Chan, M.-S.; Wahl, A. C. *J. Phys. Chem.* **1980,** *84,* 3094–3099. doi:10.1021/j100460a025
6. Nielson, R. M.; McManis, G. E.; Safford, L. K.; Weaver, M. J. *J. Phys. Chem.* **1989,** *93,* 2152–2157. doi:10.1021/j100342a086
7. Gagne, R. R.; Koval, C. A.; Lisensky, G. C. *Inorg. Chem.* **1980,** *19,* 2854–2855. doi:10.1021/ic50211a080
8. Gritzner, G.; Kuta, J. *Pure Appl. Chem.* **1984,** *56,* 461–466. doi:10.1351/pac198456040461
9. Noviandri, I.; Brown, K. N.; Fleming, D. S.; Gulyas, P. T.; Lay, P. A.; Masters, A. F.; Phillips, L. *J. Phys. Chem. B* **1999,** *103,* 6713–6722. doi:10.1021/jp991381+
10. Connelly, N. G.; Geiger, W. E. *Chem. Rev.* **1996,** *96,* 877–910. doi:10.1021/cr940053x
11. Steckhan, E. *Angew. Chem., Int. Ed. Engl.* **1986,** *25,* 683–701. doi:10.1002/anie.198606831
12. Francke, R.; Little, R. D. *Chem. Soc. Rev.* **2014,** *43,* 2492–2521. doi:10.1039/c3cs60464k
13. Wiebe, A.; Gieshoff, T.; Möhle, S.; Rodrigo, E.; Zirbes, M.; Waldvogel, S. R. *Angew. Chem., Int. Ed.* **2018,** *57,* 2–28. doi:10.1002/anie.201711060
14. Jiang, Y.; Xu, K.; Zeng, C. *Chem. Rev.* **2018,** in press. doi:10.1021/acs.chemrev.7b00271
15. Ding, Y.; Yu, G. *Angew. Chem., Int. Ed.* **2017,** *56,* 8614–8616. doi:10.1002/anie.201701254
16. Raoof, J. B.; Ojani, R.; Karimi-Maleh, H.; Hajmohamadi, M. R.; Biparva, P. *Anal. Methods* **2011,** *3,* 2637–2643. doi:10.1039/c1ay05031a
17. Jahn, U. *J. Org. Chem.* **1998,** *63,* 7130–7131. doi:10.1021/jo981180m
18. Langer, T.; Illich, M.; Helmchen, G. *Synlett* **1996,** *1996,* 1137–1139. doi:10.1055/s-1996-5668
19. Jahn, U.; Müller, M.; Aussieker, S. *J. Am. Chem. Soc.* **2000,** *122,* 5212–5213. doi:10.1021/ja000565v
20. Jahn, U.; Hartmann, P.; Dix, I.; Jones, P. G. *Eur. J. Org. Chem.* **2001,** 3333–3355. doi:10.1002/1099-0690(200109)2001:17<3333::aid-ejoc3333>3.0.co;2-a
21. Pigge, F. C.; Coniglio, J. J.; Rath, N. P. *J. Org. Chem.* **2004,** *69,* 1161–1168. doi:10.1021/jo035058l
22. Sibi, M. P.; Hasegawa, M. *J. Am. Chem. Soc.* **2007,** *129,* 4124–4125. doi:10.1021/ja069245n
23. Goddard, J.-P.; Gomez, C.; Brebion, F.; Beauvière, S.; Fensterbank, L.; Malacria, M. *Chem. Commun.* **2007,** 2929–2931. doi:10.1039/b705284g
24. Richter, J. M.; Whitefield, B. W.; Maimone, T. J.; Lin, D. W.; Castroviejo, M. P.; Baran, P. S. *J. Am. Chem. Soc.* **2007,** *129,* 12857–12869. doi:10.1021/ja074392m
25. Krygowski, E. S.; Murphy-Benenato, K.; Shair, M. D. *Angew. Chem., Int. Ed.* **2008,** *47,* 1680–1684. doi:10.1002/anie.200704830
26. Jahn, U.; Dinca, E. *Chem. – Eur. J.* **2009,** *15,* 58–62. doi:10.1002/chem.200802139
27. Khobragade, D. A.; Mahamulkar, S. G.; Pospíšil, L.; Císařová, I.; Rulíšek, L.; Jahn, U. *Chem. – Eur. J.* **2012,** *18,* 12267–12277. doi:10.1002/chem.201201499
28. Holan, M.; Pohl, R.; Císařová, I.; Klepetářová, B.; Jones, P. G.; Jahn, U. *Chem. – Eur. J.* **2015,** *21,* 9877–9888. doi:10.1002/chem.201500424
29. Chernyak, N.; Buchwald, S. L. *J. Am. Chem. Soc.* **2012,** *134,* 12466–12469. doi:10.1021/ja305660a
30. Marciasini, L. D.; Richy, N.; Vaultier, M.; Pucheault, M. *Adv. Synth. Catal.* **2013,** *355,* 1083–1088. doi:10.1002/adsc.201200942
31. Foo, K.; Sella, E.; Thomé, I.; Eastgate, M. D.; Baran, P. S. *J. Am. Chem. Soc.* **2014,** *136,* 5279–5282. doi:10.1021/ja501879c
32. Hernández-Muñoz, L. S.; Fragoso-Soriano, R. J.; Vázquez-López, C.; Klimova, E.; Ortiz-Frade, L. A.; Astudillo, P. D.; González, F. J. *J. Electroanal. Chem.* **2010,** *650,* 62–67. doi:10.1016/j.jelechem.2010.09.006
33. Hernández-Muñoz, L. S.; Galano, A.; Astudillo-Sánchez, P. D.; Abu-Omar, M. M.; González, F. J. *Electrochim. Acta* **2014,** *136,* 542–549. doi:10.1016/j.electacta.2014.04.189
34. Hou, Z.-W.; Mao, Z.-Y.; Zhao, H.-B.; Melcamu, Y. Y.; Lu, X.; Song, J.; Xu, H.-C. *Angew. Chem., Int. Ed.* **2016,** *55,* 9168–9172. doi:10.1002/anie.201602616
35. Wu, Z.-J.; Xu, H.-C. *Angew. Chem., Int. Ed.* **2017,** *56,* 4734–4738. doi:10.1002/anie.201701329
36. Zhu, L.; Xiong, P.; Mao, Z.-Y.; Wang, Y.-H.; Yan, X.; Lu, X.; Xu, H.-C. *Angew. Chem., Int. Ed.* **2016,** *55,* 2226–2229. doi:10.1002/anie.201510418
37. Brown, K. N.; Gulyas, P. T.; Lay, P. A.; McAlpine, N. S.; Masters, A. F.; Phillips, L. *J. Chem. Soc., Dalton Trans.* **1993,** 835–840. doi:10.1039/DT9930000835
38. Hildebrandt, A.; Khalyfeh, K. A.; Schaarschmidt, D.; Korb, M. *J. Organomet. Chem.* **2016,** *804,* 87–94. doi:10.1016/j.jorganchem.2015.12.027
39. Lu, S.; Strelets, V. V.; Ryan, M. F.; Pietro, W. J.; Lever, A. B. P. *Inorg. Chem.* **1996,** *35,* 1013–1023. doi:10.1021/ic950620e
40. Thornberry, M. P.; Slebodnick, C.; Deck, P. A.; Fronczek, F. R. *Organometallics* **2000,** *19,* 5352–5369. doi:10.1021/om000798v
41. Rhode, C.; Lemke, J.; Lieb, M.; Metzler-Nolte, N. *Synthesis* **2009,** *2009,* 2015–2018. doi:10.1055/s-0029-1216812
42. Nieto, D.; Bruña, S.; Montero-Campillo, M. M.; Perles, J.; González-Vadillo, A. M.; Méndez, J.; Mo, O.; Cuadrado, I. *Chem. Commun.* **2013,** *49,* 9785–9787. doi:10.1039/c3cc44619k
43. Sünkel, K.; Weigand, S.; Hoffmann, A.; Blomeyer, S.; Reuter, C. G.; Vishnevskiy, Y. V.; Mitzel, N. W. *J. Am. Chem. Soc.* **2015,** *137,* 126–129. doi:10.1021/ja511588p
44. Inkpen, M. S.; Du, S.; Hildebrand, M.; White, A. J. P.; Harrison, N. M.; Albrecht, T.; Long, N. J. *Organometallics* **2015,** *34,* 5461–5469. doi:10.1021/acs.organomet.5b00811

45. Benkeser, R. A.; Goggin, D.; Schroll, G. *J. Am. Chem. Soc.* **1954,** *76,* 4025–4026. doi:10.1021/ja01644a047

46. Witte, P.; Lal, T. K.; Waymouth, R. M. *Organometallics* **1999,** *18,* 4147–4155. doi:10.1021/om990083w

47. Woodward, R. B.; Rosenblum, M.; Whiting, M. C. *J. Am. Chem. Soc.* **1952,** *74,* 3458–3459. doi:10.1021/ja01133a543

48. Sonoda, A.; Moritani, I. *J. Organomet. Chem.* **1971,** *26,* 133–140. doi:10.1016/S0022-328X(00)80600-2

49. Petrov, A. R.; Jess, K.; Freytag, M.; Jones, P. G.; Tamm, M. *Organometallics* **2013,** *32,* 5946–5954. doi:10.1021/om4004972

50. Werner, G.; Butenschön, H. *Eur. J. Inorg. Chem.* **2017,** 378–387. doi:10.1002/ejic.201600766

51. Hisatome, M.; Tachikawa, O.; Sashō, M.; Yamakawa, K. *J. Organomet. Chem.* **1981,** *217,* C17–C20. doi:10.1016/S0022-328X(00)86033-7

52. Kasahara, A.; Izumi, T.; Yoshida, Y.; Shimizu, I. *Bull. Chem. Soc. Jpn.* **1982,** *55,* 1901–1906. doi:10.1246/bcsj.55.1901

53. Deschenaux, R.; Kosztics, I.; Nicolet, B. *J. Mater. Chem.* **1995,** *5,* 2291–2295. doi:10.1039/jm9950502291

54. Klett, J. *Chem. – Eur. J.* **2018,** in press. doi:10.1002/chem.201800608.

55. Bruce, M. I.; Skelton, B. W.; Wallis, R. C.; Walton, J. K.; White, A. H.; Williams, M. L. *J. Chem. Soc., Chem. Commun.* **1981,** 428–430. doi:10.1039/C39810000428

56. Bruce, M. I.; Walton, J. K.; Williams, M. L.; Patrick, J. M.; Skelton, B. W.; White, A. H. *J. Chem. Soc., Dalton Trans.* **1983,** 815–821. doi:10.1039/dt9830000815

57. Rausch, M. D.; Ciappenelli, D. J. *J. Organomet. Chem.* **1967,** *10,* 127–136. doi:10.1016/S0022-328X(00)81725-8

58. Sanders, R.; Mueller-Westerhoff, U. T. *J. Organomet. Chem.* **1996,** *512,* 219–224. doi:10.1016/0022-328X(95)05914-B

59. Bishop, J. J.; Davison, A.; Katcher, M. L.; Lichtenberg, D. W.; Merrill, R. E.; Smart, J. C. *J. Organomet. Chem.* **1971,** *27,* 241–249. doi:10.1016/S0022-328X(00)80571-9

60. Butler, I. R.; Cullen, W. R.; Ni, J.; Rettig, S. J. *Organometallics* **1985,** *4,* 2196–2201. doi:10.1021/om00131a023

61. Reeves, P. C. *Org. Synth.* **1977,** *56,* 28. doi:10.15227/orgsyn.056.0028

62. Kaim, W.; Klein, A. *Spectroelectrochemistry;* Royal Society of Chemistry: Cambridge, 2008.

63. Kaim, W.; Fiedler, J. *Chem. Soc. Rev.* **2009,** *38,* 3373–3382. doi:10.1039/b504286k

64. Siebler, D.; Linseis, M.; Gasi, T.; Carrella, L. M.; Winter, R. F.; Förster, C.; Heinze, K. *Chem. – Eur. J.* **2011,** *17,* 4540–4551. doi:10.1002/chem.201002101

65. Neidlinger, A.; Ksenofontov, V.; Heinze, K. *Organometallics* **2013,** *32,* 5955–5965. doi:10.1021/om400498h

66. Kienz, T.; Förster, C.; Heinze, K. *Organometallics* **2014,** *33,* 4803–4812. doi:10.1021/om500052k

67. Hüttinger, K.; Förster, C.; Heinze, K. *Chem. Commun.* **2014,** *50,* 4285–4288. doi:10.1039/C3CC46919K

68. Preiß, S.; Melomedov, J.; Wünsche von Leupoldt, A.; Heinze, K. *Chem. Sci.* **2016,** *7,* 596–610. doi:10.1039/C5SC03429A

69. Bertini, I.; Luchinat, C.; Parigi, G. *Solution NMR of paramagnetic molecules. Applications to metallobiomolecules and models. Current methods in inorganic chemistry 2,* 1st ed.; Elsevier, 2001.

70. Siebler, D.; Förster, C.; Gasi, T.; Heinze, K. *Organometallics* **2011,** *30,* 313–327. doi:10.1021/om1010808

71. Siebler, D.; Förster, C.; Heinze, K. *Dalton Trans.* **2011,** *40,* 3558–3575. doi:10.1039/c0dt01528h

72. Förster, C.; Veit, P.; Ksenofontov, V.; Heinze, K. *Chem. Commun.* **2015,** *51,* 1514–1516. doi:10.1039/C4CC08868A

73. Preiß, S.; Förster, C.; Otto, S.; Bauer, M.; Müller, P.; Hinderberger, D.; Haeri, H. H.; Carella, L.; Heinze, K. *Nat. Chem.* **2017,** *9,* 1249–1255. doi:10.1038/nchem.2836

74. Gubin, S. P. *Pure Appl. Chem.* **1970,** *23,* 463–488. doi:10.1351/pac197023040463

75. Hansch, C.; Leo, A.; Taft, R. W. *Chem. Rev.* **1991,** *91,* 165–195. doi:10.1021/cr00002a004

76. Beck,, W.; Woisetschläger, O. E.; Mayer, P. *Z. Kristallogr. - New Cryst. Struct.* **2001,** *216,* 403–404. doi:10.1524/ncrs.2001.216.14.425

77. Cetina, M.; Jukić, M.; Rapic, V.; Golobic, A. *Acta Crystallogr., Sect. C: Struct. Chem.* **2003,** *59,* m212–m214. doi:10.1107/S0108270103008503

78. For the redox couple **4/4+**, an additional shoulder at $\tilde{\nu}_{CO}$ = 1710 cm^{-1} is observed during oxidation (Figure S13, Supporting Information File 1). The intensity of this shoulder also increases upon re-reduction (Figure S14, Supporting Information File 1) and hence is tentatively assigned to the C=O stretching vibration of solid **4** (Figure 3a), as a consequence of precipitation due to the lower solubility of **4** in CH_2Cl_2.

79. Gray, H. B.; Sohn, Y. S.; Hendrickson, N. *J. Am. Chem. Soc.* **1971,** *93,* 3603–3612. doi:10.1021/ja00744a011

80. Yamaguchi, Y.; Ding, W.; Sanderson, C. T.; Borden, M. L.; Morgan, M. J.; Kutal, C. *Coord. Chem. Rev.* **2007,** *251,* 515–524. doi:10.1016/j.ccr.2006.02.028

81. Sohn, Y. S.; Hendrickson, D. N.; Gray, H. B. *J. Am. Chem. Soc.* **1970,** *92,* 3233–3234. doi:10.1021/ja00713a079

82. Hendrickson, D. N.; Sohn, Y. S.; Duggan, D. M.; Gray, H. B. *J. Chem. Phys.* **1973,** *58,* 4666–4675. doi:10.1063/1.1679029

83. Fulara, J.; Filipkowski, K.; Maier, J. P. *J. Phys. Chem. C* **2017,** *121,* 10694–10697. doi:10.1021/acs.jpcc.6b10391

84. Li, Y. L.; Han, L.; Mei, Y.; Zhang, J. Z. H. *Chem. Phys. Lett.* **2009,** *482,* 217–222. doi:10.1016/j.cplett.2009.10.026

85. Yáñez-S, M.; Moya, S. A.; Zúñiga, C.; Cárdenas-Jirón, G. *Comput. Theor. Chem.* **2017,** *1118,* 65–74. doi:10.1016/j.comptc.2017.08.032

86. Salzner, U. *J. Chem. Theory Comput.* **2013,** *9,* 4064–4073. doi:10.1021/ct400322v

87. Bluemel, J.; Hebendanz, N.; Hudeczek, P.; Koehler, F. H.; Strauss, W. *J. Am. Chem. Soc.* **1992,** *114,* 4223–4230. doi:10.1021/ja00037a028

88. Krejčík, M.; Daněk, M.; Hartl, F. *J. Electroanal. Chem. Interfacial Electrochem.* **1991,** *317,* 179–187. doi:10.1016/0022-0728(91)85012-E

89. Fulmer, G. R.; Miller, A. J. M.; Sherden, N. H.; Gottlieb, H. E.; Nudelman, A.; Stoltz, B. M.; Bercaw, J. E.; Goldberg, K. I. *Organometallics* **2010,** *29,* 2176–2179. doi:10.1021/om100106e

90. Neese, F. *Wiley Interdiscip. Rev.: Comput. Mol. Sci.* **2012,** *2,* 73–78. doi:10.1002/wcms.81

91. Becke, A. D. *J. Chem. Phys.* **1993,** *98,* 5648–5652. doi:10.1063/1.464913

92. Lee, C.; Yang, W.; Parr, R. G. *Phys. Rev. B* **1988,** *37,* 785–789. doi:10.1103/PhysRevB.37.785

93. Miehlich, B.; Savin, A.; Stoll, H.; Preuss, H. *Chem. Phys. Lett.* **1989,** *157,* 200–206. doi:10.1016/0009-2614(89)87234-3

94. Neese, F.; Wennmohs, F.; Hansen, A.; Becker, U. *Chem. Phys.* **2009,** *356,* 98–109. doi:10.1016/j.chemphys.2008.10.036

95. Izsák, R.; Neese, F. *J. Chem. Phys.* **2011,** *135,* 144105. doi:10.1063/1.3646921

96. Pantazis, D. A.; Chen, X.-Y.; Landis, C. R.; Neese, F. *J. Chem. Theory Comput.* **2008,** *4,* 908–919. doi:10.1021/ct800047t

97. Sinnecker, S.; Rajendran, A.; Klamt, A.; Diedenhofen, M.; Neese, F. *J. Phys. Chem. A* **2006,** *110,* 2235–2245. doi:10.1021/jp056016z

98. Weigend, F.; Ahlrichs, R. *Phys. Chem. Chem. Phys.* **2005,** *7,* 3297–3305. doi:10.1039/b508541a

99. Weigend, F. *Phys. Chem. Chem. Phys.* **2006,** *8,* 1057–1065. doi:10.1039/b515623h

Stereoselective nucleophilic addition reactions to cyclic *N*-acyliminium ions using the indirect cation pool method: Elucidation of stereoselectivity by spectroscopic conformational analysis and DFT calculations

Koichi Mitsudo[1], Junya Yamamoto[1], Tomoya Akagi[1], Atsuhiro Yamashita[1], Masahiro Haisa[1], Kazuki Yoshioka[1], Hiroki Mandai[1], Koji Ueoka[2], Christian Hempel[2], Jun-ichi Yoshida[2] and Seiji Suga[*1]

Address:
[1]Division of Applied Chemistry, Graduate School of Natural Science and Technology, Okayama University, 3-1-1 Tsushima-naka, Kita-ku, Okayama 700-8530, Japan and [2]Department of Synthetic Chemistry and Biological Chemistry, Graduate School of Engineering, Kyoto University, Nishikyo-ku, Kyoto 615-8510, Japan

Email:
Seiji Suga[*] - suga@cc.okayama-u.ac.jp

* Corresponding author

Abstract

In this study, six-membered *N*-acyliminium ions were generated by the "indirect cation pool" method and reacted with several nucleophiles. These reactions afforded disubstituted piperidine derivatives with high diastereoselectivities and good to excellent yields. The conformations of the obtained *N*-acyliminium ions were studied by low temperature NMR analyses and DFT calculations and were found to be consistent with the Steven's hypothesis.

Introduction

Cyclic amines are significant key motifs in pharmaceutical and natural products because a variety of compounds bearing those moieties exhibit physiological and pharmacological activities [1-3]. As many of these compounds feature asymmetric carbon atoms at the α-position of the cyclic amine, the stereoselective carbon–carbon bond formation at this position is of great importance from the perspective of drug discovery [4,5]. Meanwhile the "cation pool" method can realize the generation and accumulation of highly reactive cationic species such as *N*-acyl-

iminium ions in relatively high concentrations by low temperature electrolysis [6-10]. The *N*-acyliminium ions thus generated can directly react with a variety of carbon nucleophiles to very efficiently yield carbon–carbon bond-formation products. In addition, this research lead to the development of an indirect cation pool method that enables the creation of the cation pool by reacting a cation precursor having a C–S bond with an electrochemically generated $ArS(ArSSAr)^+$ as the cation-generating reagent. For example, a pool of alkoxycarbenium ions

can be rapidly generated by the reaction of thioacetals and ArS(ArSSAr)$^+$ (Ar = *p*-FC$_6$H$_4$, Scheme 1) [11].

The cation pool method is advantageous over the conventional Lewis acid promoted generation of carbocation species because the reactive cationic species can be detected by spectroscopy such as NMR and IR measurements. For this research, the reaction of six-membered *N*-acyliminium ions having a substituent in the 4-, 5-, or 6-position were generated by the indirect cation pool method and examined in the reaction with several nucleophiles to give the disubstituted piperidine derivatives in an excellent diastereoselective manner (Scheme 1). This result inspired us to investigate the stereochemistry of the *N*-acyliminium ions by means of NMR spectroscopy, which is challenging to achieve without using cation pool methods. The current report presents the diastereoselective synthesis of disubstituted piperidine derivatives by the indirect cation pool method and the elucidation of the stereoselectivity based on both NMR analyses of the cyclic *N*-acyliminium ions and DFT calculations.

Results and Discussion

N-Acyliminium ions obtained from *N*-Boc-piperidines are attractive intermediates because they easily can be transformed to a variety of alkaloids having a piperidine skeleton. In our preliminary study, we found the indirect cation pool method suit-

able for the generation and accumulation of *N*-acyliminium ions. Therefore, the reaction of *N*-Boc-4-phenyl-2,3,4,5-tetrahydropyridin-1-ium (**C1**) derived from precursor **1a** and ArS(ArSSAr)$^+$ (Ar = *p*-FC$_6$H$_4$) generated by the low temperature electrolysis was first performed with several nucleophiles (Table 1). The starting **1a** and other *N*-acyliminium ion precursors were synthesized by the modified Beak's protocol [12] (see Supporting Information File 1). As observed in our previous studies, the Boc protecting group was found not suitable for the direct cation pool method due to its cleavage by protic acid generated during the electrolysis of the cation precursor. However, it can be utilized in the indirect cation pool method as diaryldisulfides are the exclusive side products formed during carbocation generation. Thus, the reaction of acyliminium ion **C1** with Me$_3$Al afforded *trans*-1-(*tert*-butoxycarbonyl)-2-methyl-4-phenylpiperidine (**2aa**) in a good yield and virtually complete diastereoselectivity (*cis/trans* = <1:99). Similarly, the reaction of **C1** with diethylzinc or allyltributylstannane gave piperidine derivatives **2ab** and **2ac** with high yields and *trans*-selectivity (Table 1, entries 2 and 3). Also, the introduction of phenyl or cyano groups in the piperidine core proceeded in a highly regioselective manner and good to high yields (Table 1, entries 4 and 5).

Next, we examined the reaction of *N*-Boc-4-methyl-2,3,4,5-tetrahydropyridin-1-ium (**C2**) with nucleophiles (Table 2).
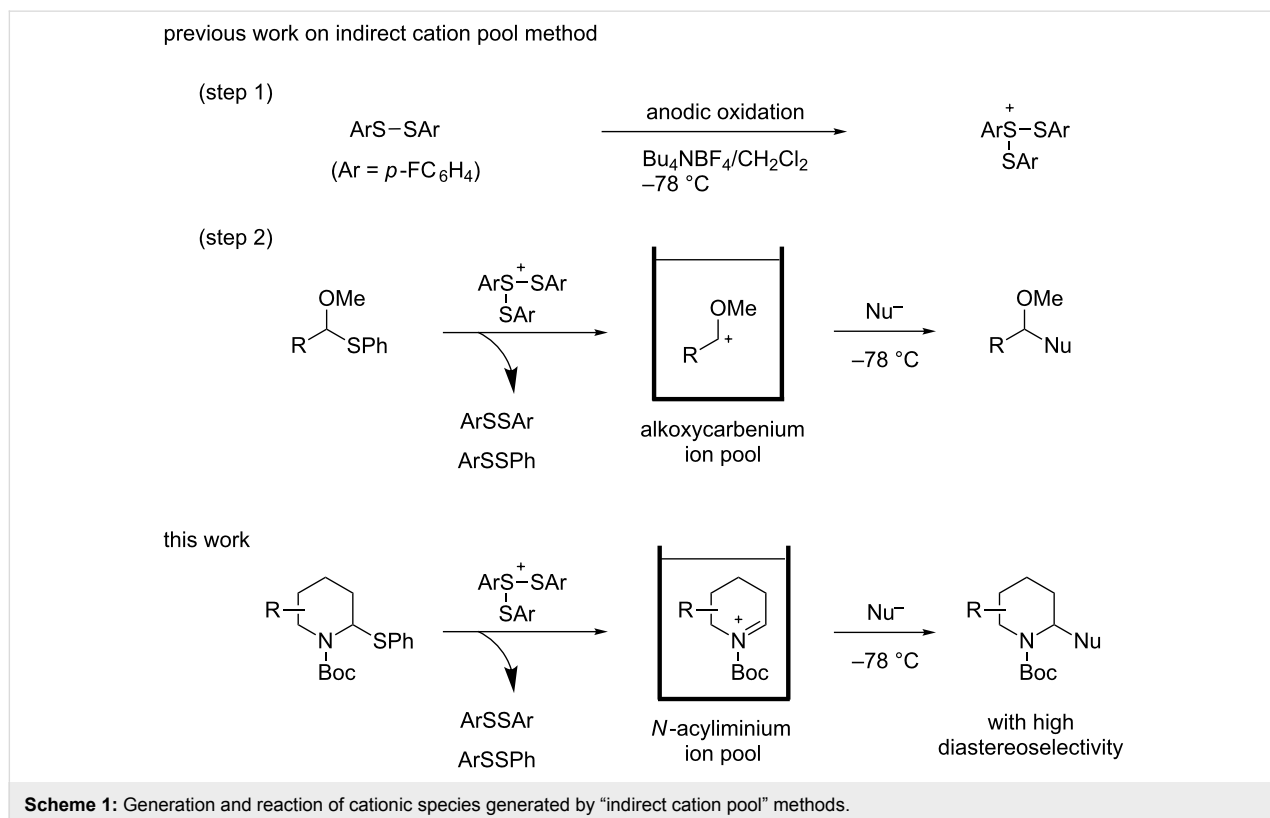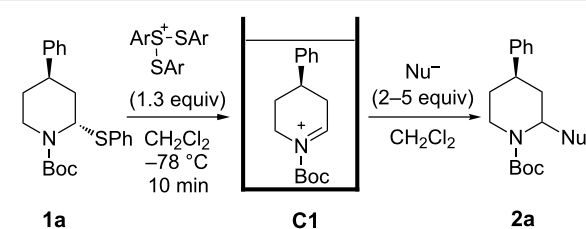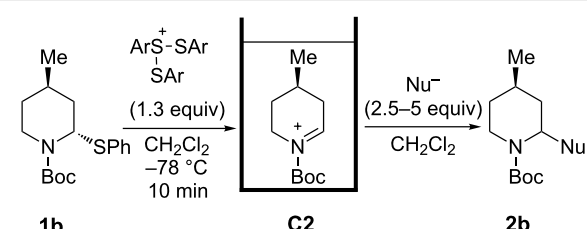

Scheme 1: Generation and reaction of cationic species generated by "indirect cation pool" methods.

Table 1: Reaction of *N*-acyliminium ion **C1** with several nucleophiles.

1a → (ArS⁺–SAr / SAr, 1.3 equiv, CH₂Cl₂, −78 °C, 10 min) → **C1** → (Nu⁻, 2–5 equiv, CH₂Cl₂) → **2a**

entry	Nu⁻	2	yield (%)[a]	*cis/trans*[b]
1	Me₃Al (5.0 equiv)	**2aa**	85	<1:99
2	Et₂Zn (2.5 equiv)	**2ab**	89	3:97
3	(allyl)SnBu₃ (3.0 equiv)	**2ac**	>99	<1:99
4	PhMgBr (2.0 equiv)	**2ad**	87	15:85
5	TMSCN (5.0 equiv)	**2ae**	99	<1:99

[a]Isolated yield. [b]Determined by GC analysis.

Table 2: Reaction of *N*-acyliminium ion **C2** with several nucleophiles.

1b → (ArS⁺–SAr / SAr, 1.3 equiv, CH₂Cl₂, −78 °C, 10 min) → **C2** → (Nu⁻, 2.5–5 equiv, CH₂Cl₂) → **2b**
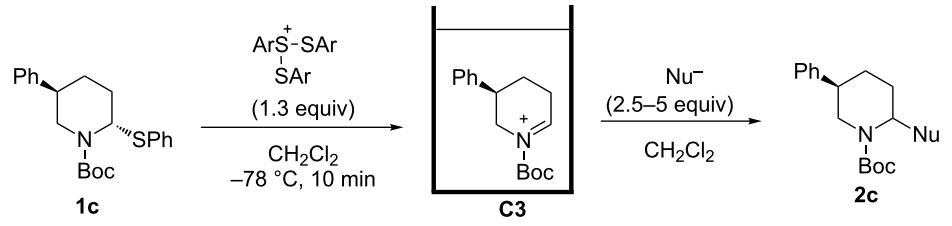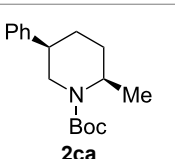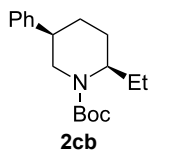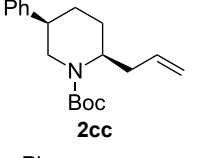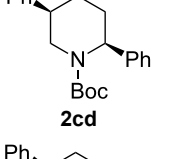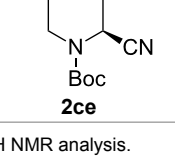
entry	Nu⁻	2	yield (%)[a]	*cis:trans*[b]
1	Me₃Al (2.5 equiv)	**2ba**	86	<1:99
2	Et₂Zn (5.0 equiv)	**2bb**	95	<1:99
3	(allyl)SnBu₃ (2.5 equiv)	**2bc**	95	<1:99
4	PhMgBr (2.5 equiv)	**2bd**	93	3:97
5	TMSCN (5.0 equiv)	**2be**	89	<1:99

[a]Isolated yield. [b]Determined by GC analysis.

Both, the reactivity and diastereoselectivity of the reactions were similar to those of **C1** and the disubstituted piperidine derivatives **2ba–be** were obtained in good to high yields with excellent diastereoselectivities.

Then, the reaction of 5-phenyl-substituted *N*-acyliminium cation **C3** was performed (Table 3). Interestingly, all reactions led to the 2,5-disubstituted piperidine derivatives **2ca–ce** in very good yields and high *cis*-selective manner. A similar trend is observed for the reactions of the 5-methyl-substituted cation **C4**

and all products **2da–dc** were obtained in high to excellent *cis*-diastereoselectivities (Table 4).

The tendency of the reactions of the 6-phenyl-substituted *N*-acyliminium cation **C5** with nucleophiles was slightly different compared to those of **C1–C4** (Table 5). The reactions proceeded in a *cis*-selective manner, however, the selectivity was not high except in case of product **2ed** (Table 5, entry 4). The low yield of **2ed** was due to the generation of an enamine as a byproduct. While the reason of the low selectivity has not

Table 3: Reaction of *N*-acyliminium ion **C3** with several nucleophiles.

entry	Nu⁻	2	yield (%)[a]	cis:trans[b]
1[c]	Me₃Al (2.5 equiv)	**2ca**	89	94:6
2	Et₂Zn (2.5 equiv)	**2cb**	99	96:4
3[c]	(allyl)SnBu₃ (2.5 equiv)	**2cc**	97	98:2
4	PhMgBr (2.5 equiv)	**2cd**	97	96:4[c]
5	TMSCN (5.0 equiv)	**2ce**	96	98:2

[a]Isolated yield. [b]Determined by GC analysis. [c]Determined by ¹H NMR analysis.

been clear, it is probably due to steric repulsion between the phenyl and Boc groups. A distortion of the Boc group in **C5** was also suggested by DFT calculation (see Supporting Information File 1). The reaction of 6-methyl-substituted *N*-acyliminium cation **C6** bearing a methyl group, which is smaller than a phenyl group, gave the corresponding *cis*-products with high diastereoselectivities (Table 6).

As mentioned, the reaction between the cyclic *N*-acyliminium ions **C1–C6** and several nucleophiles proceeded diastereoselectively. To clarify the reason of the observed selectivity, ¹H NMR analyses of **C1–C6** were performed at low temperature (Figures 1–3, see also Supporting Information File 1). All protons on the piperidine ring in **C1** (H^a–H^h) have been assigned by H–H COSY (Figure 1). In addition, the signal of

H^d (3.10 ppm) exhibited an axial–axial coupling (*J* > 10 Hz) and 7.1% ROE was observed between H^d and H^g. These results suggest that H^d adopts an axial and the phenyl group a pseudo-equatorial position at low temperature.

The low temperature NMR analysis of **C3**, which has a phenyl group at 5-position, was next performed and the ¹H NMR spectrum is depicted in Figure 2. An axial–axial coupling between H^e and H^f was observed, suggesting that these two protons were located at axial positions. This result indicates that the phenyl group of **C3** was located in the pseudo-equatorial position.

The conformation of **C5**, an *N*-acyliminium ion bearing a phenyl group in the 6-position, was also examined by NMR analy-
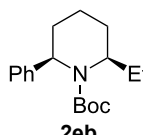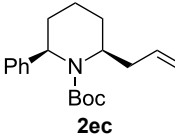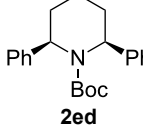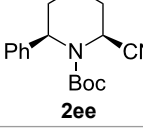
Table 4: Reaction of *N*-acyliminium ion **C4** with several nucleophiles.

entry	Nu⁻	**2**	yield (%)[a]	*cis*:*trans*[b]
1	Me₃Al	**2da**	73	98:2
2	Et₂Zn	**2db**	82	95:5
3	(allyl)SnBu₃	**2dc**	90	98:2
4	PhMgBr	**2dd**	83	91:9
5	TMSCN	**2de**	98	96:4

[a]Isolated yield. [b]Determined by GC analysis.

Table 5: Reaction of *N*-acyliminium ion **C5** with several nucleophiles.

entry	Nu⁻	**2**	yield (%)[a]	*cis*:*trans*[b]
1	Me₃Al	**2ea**	40	63:37

Table 5: Reaction of *N*-acyliminium ion **C5** with several nucleophiles. (continued)

2	Et₂Zn	**2eb**	90	76:24
3	(allyl)SnBu₃	**2ec**	94	72:28
4	PhMgBr	**2ed**	56	92:8
5	TMSCN	**2ee**	85	64:36

^aIsolated yield. ^bDetermined by GC analysis.

Table 6: Reaction of *N*-acyliminium ion **C6** with several nucleophiles.
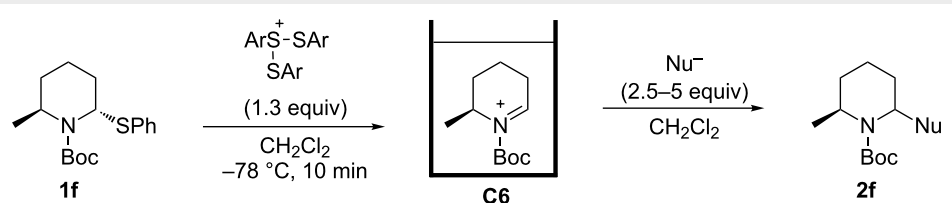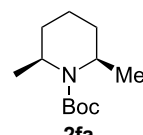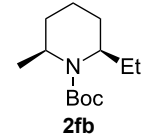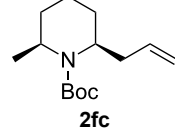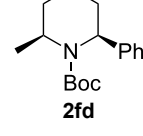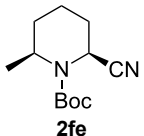

entry	Nu⁻	2	yield (%)ᵃ	*cis:trans*ᵇ
1	Me₃Al	**2fa**	49	82:18
2	Et₂Zn	**2fb**	46	96:4
3	(allyl)SnBu₃	**2fc**	87	96:4
4	PhMgBr	**2fd**	87	96:4

Table 6: Reaction of *N*-acyliminium ion **C6** with several nucleophiles. (continued)

| 5 | TMSCN | **2fe** | 90 | >99:1 |

^aIsolated yield. ^bDetermined by GC analysis.
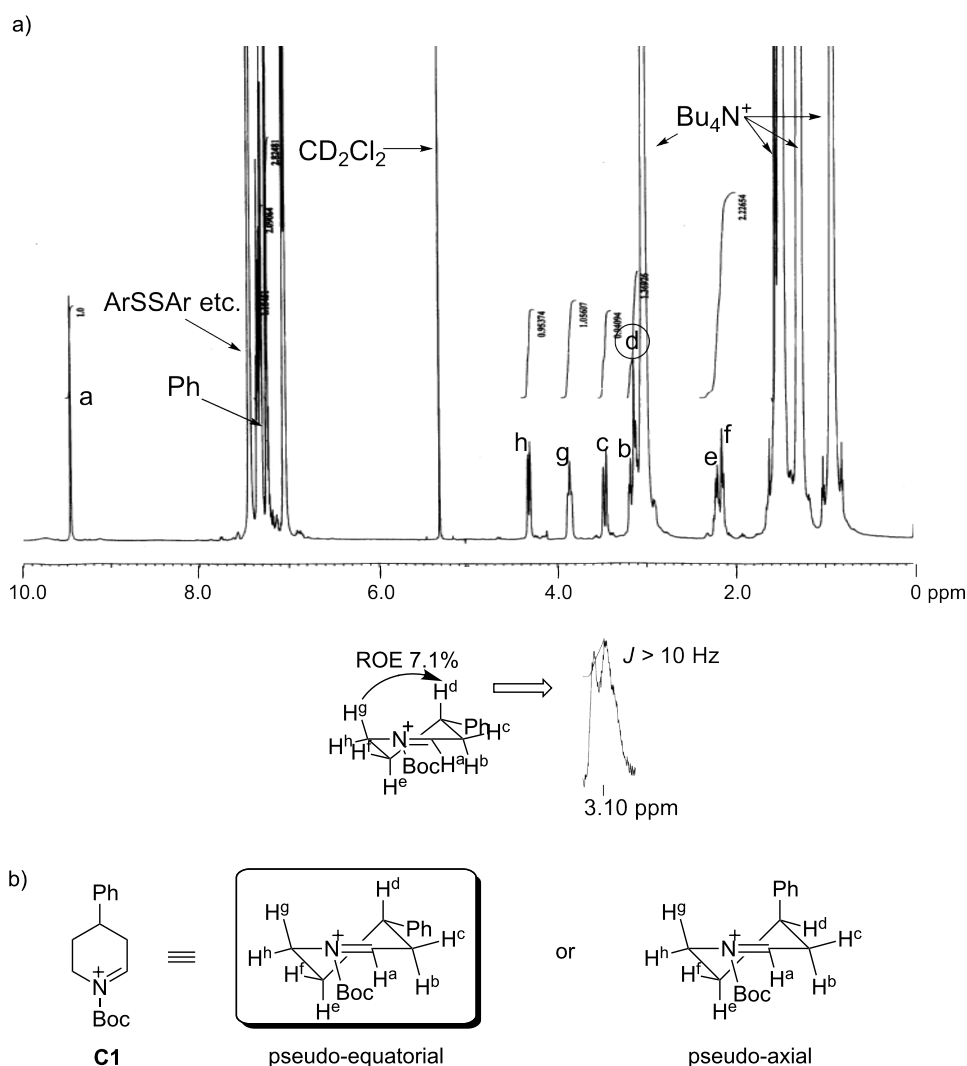
Figure 1: (a) ¹H NMR of *N*-acyliminium ion **C1** in CD₂Cl₂ at −80 °C (600 MHz). (b) Preferred conformation of **C1**.

sis (Figure 3). The signal of H^f was observed as a triplet due to the axial–axial coupling with H^e and the geminal coupling with H^g, and these results indicate that the phenyl group of **C5** is placed in the pseudo-axial position. The low temperature NMR measurements of *N*-acyliminium ions **C2**, **C4**, and **C6** were also performed. The conformations of **C2** and **C6** were similar to those of **C1** and **C5**, respectively (**C2**: pseudo-equatorial, **C6**: pseudo-axial). Although the conformation of **C4** could not be determined by the NMR analysis, the conformation is assumed to be similar to that of **C3** (pseudo-equatorial), because both ions led to similar stereoselectivities in the reactions with nucleophiles. As mentioned, the conformation of *N*-acyl-iminium cation **C1**–**C4** was pseudo-equatorial and that of **C5** and **C6** was pseudo-equatorial (Figure 4).
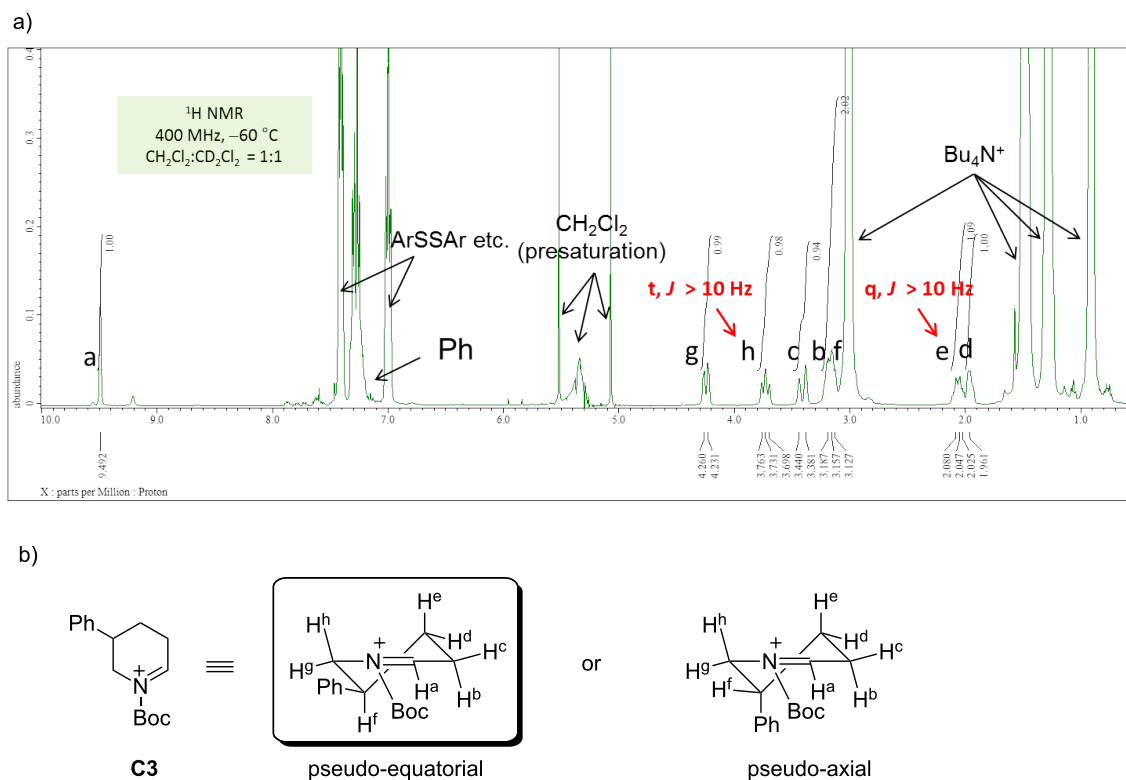
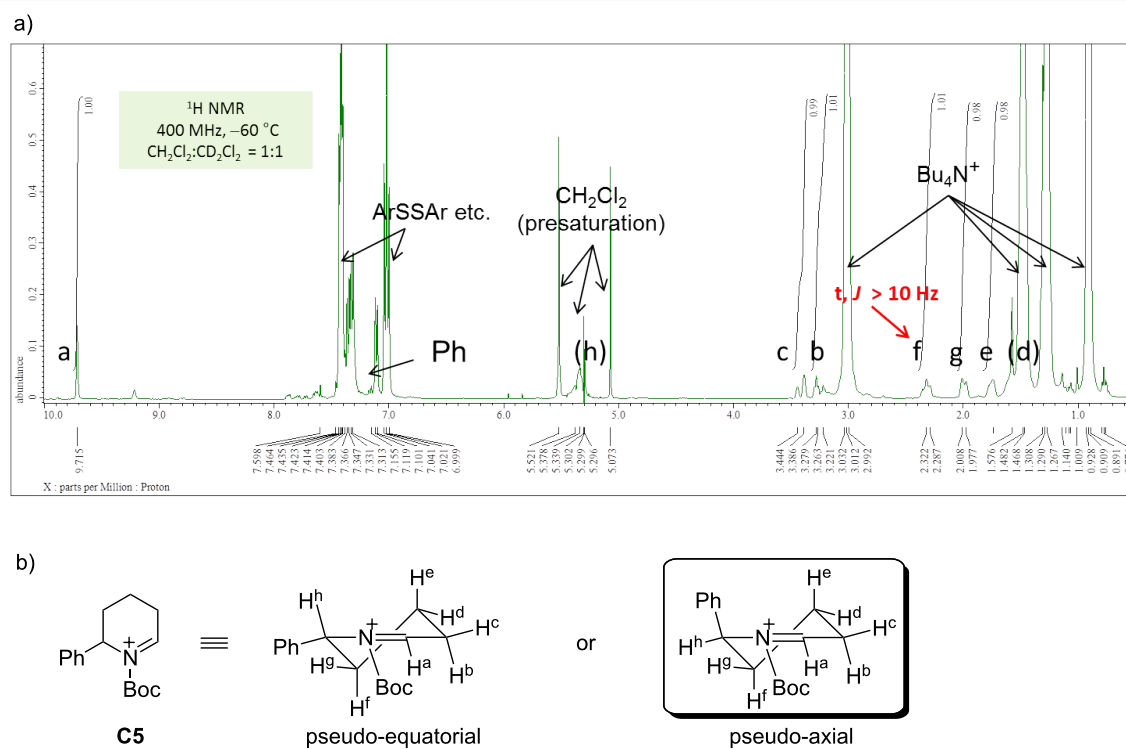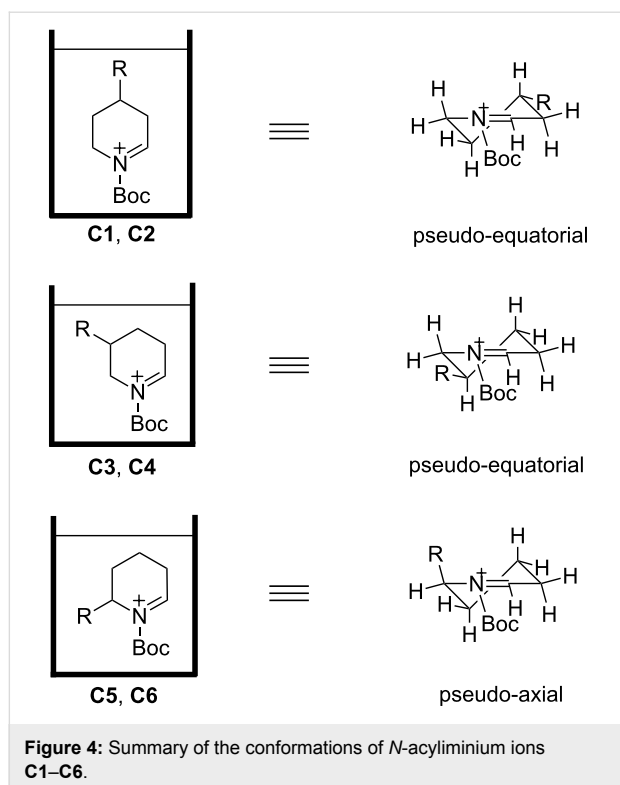**Figure 2:** (a) ^{1}H NMR spectrum of **C3** in CD$_2$Cl$_2$ at −60 °C (400 MHz). (b) Preferred conformation of **C3**.
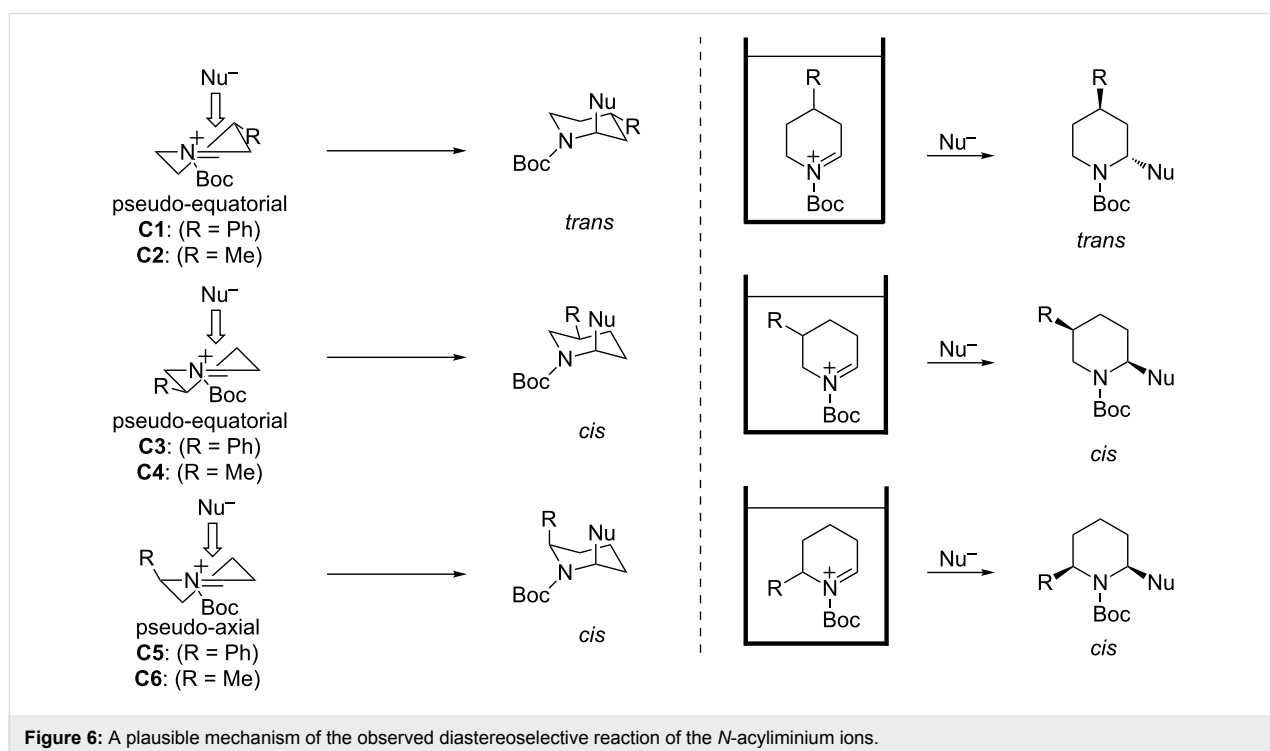

Figure 3: (a) ^{1}H NMR spectrum of **C5** in CD$_2$Cl$_2$ at −60 °C (400 MHz). (b) Preferred conformation of **C5**.

Figure 4: Summary of the conformations of *N*-acyliminium ions **C1–C6**.

It is commonly assumed that the diastereoselectivity of the disubstituted piperidine derivatives **2a–f** was influenced by the conformation of the *N*-acyliminium ions **C1–C6**. In this context Stevens proposed that the conformation of the six-membered

N-acyliminium ion would be a half-chair form and that the attack of the nucleophile proceeds from that side that generates a stable chair form product, because an attack from another side would lead to a more unstable product with a twist form [13]. As a close study, Woerpel reported a diastereoselective substitution reaction for synthesizing disubstituted tetrahydropyrans via six-membered oxocarbenium ions generated in situ from tetrahydropyran acetals [14]. If the Stevens' hypothesis is true, a nucleophilic reaction with **C1**, having a pseudo-equatorial phenyl group, should give a *trans*-2,4-disubstituted product (Figure 5). Similarly, acyliminium ions **C3** and **C5** should give the *cis*-2,5- or *cis*-2,6-disubstituted piperidine derivatives, respectively. These explanations are consistent with above mentioned conformational analyses results, and the hypothesis was in agreement with the experimental results (Figure 6).

Figure 5: Stevens' hypothesis on the tendency of the addition of nucleophiles to *N*-acyliminium ions. The substituent at the nitrogen atom is omitted for clarity.

Figure 6: A plausible mechanism of the observed diastereoselective reaction of the *N*-acyliminium ions.
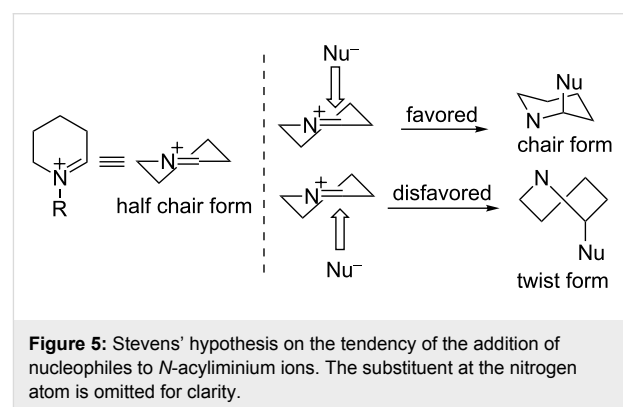
To obtain further insight in the conformation of the cyclic *N*-acyliminium ions, DFT calculations of **C1**–**C6** were performed (Figure 7). First, Δ*G* of pseudo-equatorial and pseudo-axial conformations of **C1** was calculated at the B3LYP/6-31G(d) level of theory. The pseudo-equatorial conformation of **C1** was more stable than the pseudo-axial conformation by 1.27 kcal/mol. Similarly, DFT calculations of **C3** and **C5** were performed, and the results show that the pseudo-equatorial conformation of **C3** and the pseudo-axial conformation of **C5** were more stable than the other conformations, respectively. The more stable conformations that the calculations implied are consistent with the conformations determined by the low temperature NMR analyses, and the DFT calculations suggest that

the preferred conformations of **C2**, **C4**, and **C6** were similar to those of **C1**, **C3**, and **C5**.

Conclusion

In this study, we presented an efficient method for the highly diastereoselective synthesis of disubstituted piperidine derivatives through the reaction of *N*-acyliminium ions with nucleophiles. The starting *N*-acyliminium ions were generated by the indirect cation pool method and their conformations were confirmed by low temperature NMR analyses for the first time. The experimental results were fully consistent with DFT calculations. The correlation between the stereochemistry of the *N*-acyliminium ions and the reaction products is in agreement
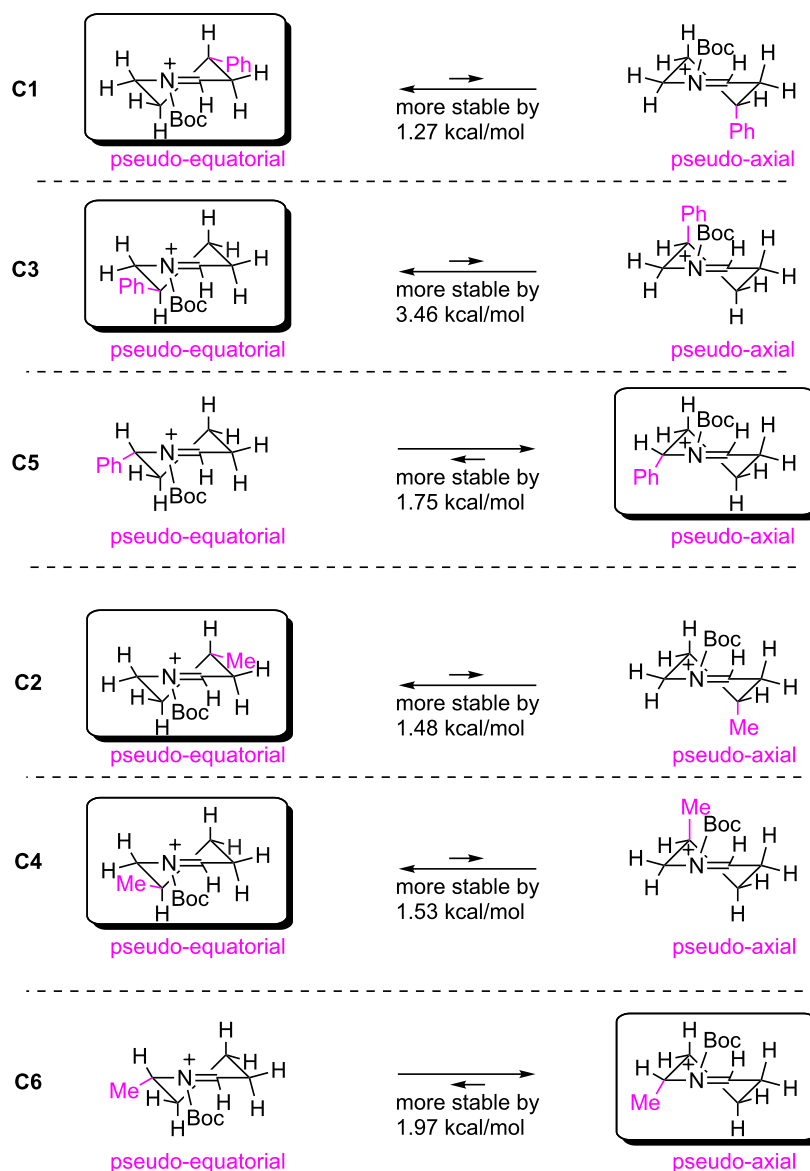

Figure 7: Comparison of Δ*G* for the pseudo-equatorial and pseudo-axial conformations of **C1**–**C6** at the B3LYP/6-31G(d) level.

with common interpretation and further synthetic applications and more detailed investigations of the reaction mechanism are in progress in our laboratory.

Supporting Information

Supporting Information File 1
Experimental details, ORTEP drawings of **1a**, **1b**, **1d**–**1f**, theoretical calculations of **C1**–**C6**, and NMR spectra of all new compounds and **C1**–**C6**.
[https://www.beilstein-journals.org/bjoc/content/supplementary/1860-5397-14-100-S1.pdf]

Supporting Information File 2
X-ray structure analysis data for **1a** (CCDC-1813600), **1b** (CCDC-1813582), **1d** (CCDC-1813594), **1e** (CCDC-1813595), **1f** (CCDC-1813596). These data can be obtained free of charge from The Cambridge Crystallographic Data Centre via http://www.ccdc.cam.ac.uk/data_request/cif.
X-ray analysis of **1a**–**f**.
[https://www.beilstein-journals.org/bjoc/content/supplementary/1860-5397-14-100-S2.cif]

ORCID® iDs
Koichi Mitsudo - https://orcid.org/0000-0002-6744-7136
Hiroki Mandai - https://orcid.org/0000-0001-9121-3850
Jun-ichi Yoshida - https://orcid.org/0000-0001-8439-2272

References
1. Alvarez-Buill, J.; Vaquero, J. J.; Barluenga, J., Eds. *Modern Heterocyclic Chemistry;* Wiley-VCH: Weinheim, 2011.
2. Galliford, C. V.; Scheidt, K. A. *Angew. Chem., Int. Ed.* **2007,** *46,* 8748. doi:10.1002/anie.200701342
3. Carroll, F. I.; Dolle, R. E. *ChemMedChem* **2014,** *9,* 1638. doi:10.1002/cmdc.201402142
4. McLaughlin, N. P.; Evans, P.; Pines, M. *Bioorg. Med. Chem.* **2014,** *22,* 1993. doi:10.1016/j.bmc.2014.02.040
5. Källström, S.; Leino, R. *Bioorg. Med. Chem.* **2008,** *16,* 601. doi:10.1016/j.bmc.2007.10.018
6. Yan, M.; Kawamata, Y.; Baran, P. S. *Chem. Rev.* **2017,** *117,* 13230. doi:10.1021/acs.chemrev.7b00397
7. Waldvogel, S. R.; Janza, B. *Angew. Chem., Int. Ed.* **2014,** *53,* 7122. doi:10.1002/anie.201405082
8. Matsumoto, K.; Suga, S.; Yoshida, J.-i. *Org. Biomol. Chem.* **2011,** *9,* 2586. doi:10.1039/c0ob01070g
9. Yoshida, J.-i.; Kataoka, K.; Horcajada, R.; Nagaki, A. *Chem. Rev.* **2008,** *108,* 2265. doi:10.1021/cr0680843
10. Yoshida, J.-i.; Suga, S. *Chem. – Eur. J.* **2002,** *8,* 2650. doi:10.1002/1521-3765(20020617)8:12<2650::AID-CHEM2650>3.0.CO;2-S
11. Suga, S.; Matsumoto, K.; Ueoka, K.; Yoshida, J.-i. *J. Am. Chem. Soc.* **2006,** *128,* 7710. doi:10.1021/ja0625778
12. Beak, P.; Lee, W.-K. *Tetrahedron Lett.* **1989,** *30,* 1197. doi:10.1016/S0040-4039(00)72714-6
13. Stevens, R. V. *Acc. Chem. Res.* **1984,** *17,* 289. doi:10.1021/ar00104a005
14. Ayala, L.; Lucero, C. G.; Romero, J. A. C.; Tabacco, S. A.; Woerpel, K. A. *J. Am. Chem. Soc.* **2003,** *125,* 15521. doi:10.1021/ja037935a

Spectroelectrochemical studies on the effect of cations in the alkaline glycerol oxidation reaction over carbon nanotube-supported Pd nanoparticles

Dennis Hiltrop[1], Steffen Cychy[1], Karina Elumeeva[2], Wolfgang Schuhmann[2] and Martin Muhler[*1]

Address:
[1]Laboratory of Industrial Chemistry, Ruhr-Universität Bochum, Universitätsstr. 150, 44780 Bochum, Germany and [2]Analytical Chemistry - Center for Electrochemical Sciences (CES), Ruhr-Universität Bochum, Universitätsstr. 150, 44780 Bochum, Germany

Email:
Martin Muhler[*] - muhler@techem.rub.de

* Corresponding author

Abstract

The effects of the alkali cations Na^+ and K^+ were investigated in the alkaline electrochemical oxidation of glycerol over Pd nanoparticles (NPs) deposited on functionalized carbon nanotubes (CNTs). The electrocatalytic activity was assessed by cyclic voltammetry revealing a lower overpotential of glycerol oxidation for nitrogen-functionalized Pd/NCNTs compared with oxygen-functionalized Pd/OCNTs. Whereas significantly lower current densities were observed for Pd/OCNT in NaOH than in KOH in agreement with stronger non-covalent interactions on the Pd surface, Pd/NCNT achieved an approximately three-times higher current density in NaOH than in KOH. In situ electrochemistry/IR spectroscopy was applied to unravel the product distribution as a function of the applied potential in NaOH and KOH. The IR spectra exhibited strongly changing band patterns upon varying the potential between 0.77 and 1.17 V vs RHE: at low potentials oxidized C_3 species such as mesoxalate and tartronate were formed predominantly, and with increasing potentials C_2 and C_1 species originating from C–C bond cleavage were identified. The tendency to produce carbonate was found to be less pronounced in KOH. The less favored formation of highly oxidized C_3 species and of carbonate is deduced to be the origin of the lower current densities in the cyclic voltammograms (CVs) for Pd/NCNT in KOH. The enhanced current densities in NaOH are rationalized by the presence of Na^+ ions bound to the basic nitrogen species in the NCNT support. Adsorbed Na^+ ions can form complexes with the organic molecules, presumably enhanced by the chelate effect. In this way, the organic molecules are assumed to be bound more tightly to the NCNT support in close proximity to the Pd NPs facilitating their oxidation.

Introduction

The conversion of biomass to biofuels is a promising process for carbon-neutral energy conversion [1]. First-generation biofuels such as bioethanol or biodiesel are produced from starch, sugar or oils and fats [2,3]. The transesterification of oils and fats produces glycerol as a byproduct, which requires further processing to reduce the costs of biofuels [4]. The comparably high energy density of glycerol of 5965 Wh L^{-1} assuming its total oxidation to CO_2 suggests its utilization in fuel cells (FCs) converting chemical into electrical energy [5]. In alkaline FCs (AFCs) and proton exchange membrane FCs (PEMFCs), H_2 and O_2 are converted to H_2O, heat and electricity. Since the development of anion exchange membranes the research interest in AFCs has increased again, because AFCs have several advantages over PEMFCs such as faster kinetics of the oxygen reduction reaction at the cathode, greater longevity and the possible adaption of less precious metals due to the alkaline electrolyte [6,7]. In direct alkaline alcohol FCs (DAAFCs) electricity is generated by oxidizing small organic molecules. A direct alkaline methanol FC was already tested in 1965 oxidizing methanol over a Pt catalyst in highly alkaline medium [8]. Alcohols such as ethanol and glycerol are valuable and non-toxic substrates for DAAFCs, too. However, the higher chemical complexity of the alcohols complicates the total oxidation reaction, because numerous intermediates occur that need to be oxidized efficiently without poisoning the catalyst.

Another important utilization of glycerol is the electrosynthesis of fine chemicals. It is a highly suitable precursor for valuable chemicals such as DL-glyceric acid, mesoxalic acid and 1,3-dihydroxyacetone (DHA). These products are conventionally obtained by oxidation using rather unselective oxidants. Especially DHA is of great interest due to its use in the cosmetic industry, as a precursor for further value-added fine chemicals [9] and as a monomer for biopolymers like polyesters and polyurethanes [4]. The route to higher functionalized products starting from glycerol via electrosynthesis offers several advantages compared with thermal gas-phase oxidation processes. In the aqueous environment low temperatures and pressures are applied allowing a higher control of selectivity. Moreover, additional parameters such as pH value, the nature of the ions and the concentration of glycerol in the liquid phase can be tuned in liquid-phase processes [4].

Monitoring of electrocatalytic reactions is challenging as all products are dissolved in the electrolyte. High-performance liquid or ion chromatography and differential electrochemical mass spectrometry provide information about the nature of dissolved and chemically stable products [10,11]. A rather direct view on the reaction is provided by infrared (IR) spectroscopy. Specifically designed experimental cells focus the IR beam on the working electrode surface through a thin electrolyte layer probing vibrations of adsorbed intermediates and products [12]. Highly active catalysts converting glycerol to carbonate consume 20 hydroxide ions per glycerol molecule in the thin electrolyte layer, which leads to a substantial local pH drop and cannot be fully compensated by OH$^-$ diffusion from the bulk into the thin layer. This pH drop further complicates the identification of products, because the product selectivity may change as a function of pH as demonstrated by Wang et al. [13] on a Pd disk electrode for ethylene glycol electrooxidation. For glycerol, a similar study was conducted by Ferreira et al. [14] on PdRh electrodeposits showing that the glycerol oxidation route follows a pathway involving the consumption rather than production of H_2O once the initially present OH$^-$ ions are consumed. Finally, the structural similarity of the possible oxidation products makes the assignment of occurring IR bands to certain species challenging. Glycerol oxidation was studied over different catalytically active metals, such as Au [15], AuAg/C [16], Pt [17,18], Au/C [19,20], Pt/C [20,21], Pd/C [20], PdAu/C [22], PdNi/C, PdAg/C [23] and PtBi/C [21] in alkaline medium using IR spectroscopy for product identification.

Strmcnik et al. [24] investigated the effect of different alkali ions using LiOH, NaOH, KOH and CsOH on the observed currents in the hydrogen oxidation, oxygen reduction and methanol oxidation reactions over Pt single crystal, polycrystalline Pt and Pt/C electrodes. They proposed two different adsorbate structures of hydrated alkali metal cations on the electrode, either via a hydrogen bonding between hydrating water and two OH$_{ad}$ groups (1) or direct ion–dipole interactions between two OH$_{ad}$ and the cation (2). The formation of the structures (1) or (2) was correlated to the hydration energies (ΔH_M) of the cations. Highly charged species with a high ΔH_M like Li$^+$ were considered more likely to form structure (2), because the cation–OH$_{ads}$ interaction is stronger than for cations with a low ΔH_M like Cs$^+$. A high surface coverage with such clusters was assumed to inhibit the adsorption and movement of reactants on the electrode surface accounting for the activity trends Li$^+$ < Na$^+$ < K$^+$ < Cs$^+$ in the investigated reactions [24].

This study gave rise to further investigations on the impact of ions on electrochemical reactions. Studies of the cation effect on Au electrodes are scarce [25,26], as the majority of reports employ Pt electrodes. In acidic medium the influence of Cs$^+$ and Na$^+$ on the specific adsorption of OH, O and H on polycrystalline Pt was investigated [27] as well as the cation influence on the water electrolysis on Pt(111) [28] and Ir(111)/oxide electrodes [29]. Different Pt single crystal surfaces [30] and other electrochemical reactions such as CO [30], formate [31] and ethylene glycol oxidation [32,33] were studied as well.

Especially for these more complex oxidation reactions of small organic molecules, studies of the cation impact on the formed products are rather scarce. Sitta et al. [32] revealed an analogous trend as Strmcnik et al. [24], i.e., increasing current densities for ethylene glycol electrooxidation over Pt in the order $Li^+ < Na^+ < K^+$. They used IR spectroscopy to determine the nature of the formed products and identified carbonate and oxalate as the main products in addition to traces of glycolate and CO. By comparing the ratio of the integrated band intensities for oxalate and carbonate they concluded that C–C bond scission is influenced by the cation in the electrolyte by blocking surface sites that are required for the carbon bond cleavage.

To the best of our knowledge, there are no studies focusing on the cation effect on the glycerol electrooxidation reaction using Pd-based materials. With respect to FC applications and the electrosynthesis of fine chemicals it is important to extend the knowledge about this effect. In this study we used Pd nanoparticles (NPs) deposited on functionalized carbon nanotubes (Pd/xCNT, x = N or O) for catalyzing the glycerol oxidation reaction (GOR). Pd/NCNT has been investigated recently in the ethanol electrooxidation reaction in alkaline medium reaching high specific current densities of about 500 A g^{-1}_{Pd} [34]. The Pd/OCNTs of this study differ from the Pd/OCNTs used here by an additional He treatment of the oxygen-functionalized CNTs to improve the comparability of the catalysts due to the same thermal treatment. Cyclic voltammetry was used to determine the glycerol oxidation activity of the catalysts, and electrochemistry coupled with attenuated total reflection IR (ATR–IR) spectroscopy was performed to determine the product distribution in the thin electrolyte layer between the working electrode and the ATR crystal. The band assignment was supported by reference measurements under identical conditions.

Results and Discussion
Electrochemical glycerol oxidation
Figure 1 shows cyclic voltammograms (CVs) of the two catalysts obtained in 1 M KOH containing 1 M glycerol. In the forward scan the peak labeled p1 occurs due to the oxidation of glycerol on the Pd^0 NPs, which is inhibited at $E > 0.9$ V vs

RHE by PdO formation. In the reverse scan, the oxide layer is reduced back to Pd^0 at around 0.8 V vs RHE. The oxidative current densities at $E < 0.8$ V vs RHE are then caused by the oxidation of freshly adsorbing glycerol as well as oxidation of still adsorbed species from the forward scan (p2). Quantitative information extracted from the CVs in NaOH and KOH is summarized in Table 1.
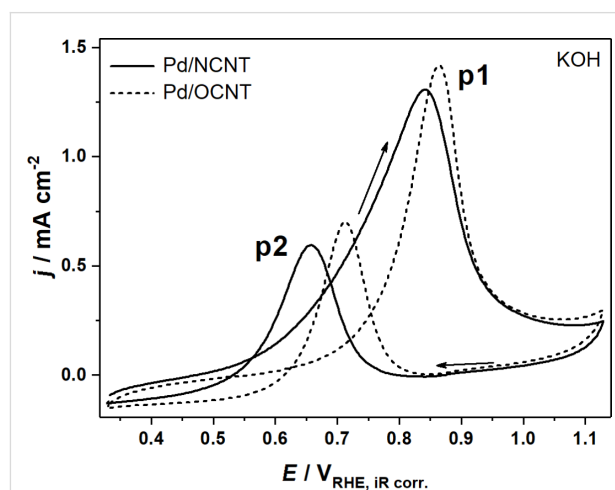

Figure 1: CVs of the electrooxidation of 1 M glycerol over Pd/NCNT and Pd/OCNT in 1 M KOH at 1000 rpm at a scan rate 0.01 V s^{-1}.

The CVs illustrate the differences between the two catalysts. For Pd/NCNT peak p1 is much broader and the peak potentials (E_{p1} and E_{p2}) are found at lower anodic potentials (−29 and −52 mV vs RHE on average) compared with Pd/OCNT. Although the peak current densities are almost equal, the catalytic activity towards glycerol oxidation is higher for Pd/NCNT, as the reaction starts at lower anodic overpotentials. This activity relation is in good agreement with studies applying these catalysts in ethanol electrooxidation and olefin hydrogenation [34,35].

Analogous CV experiments were also carried out in NaOH and the obtained CVs are shown in Figure 2. The current densities recorded for Pd/OCNT are significantly lower in NaOH compared with KOH in agreement with the results reported by

Table 1: Peak potentials E_{p1} and E_{p2}, peak current densities j_{p1} and j_{p2}, and peak charges Q_{p1} and Q_{p2} extracted from the CVs shown in Figure 1 and Figure 2.

	Pd/OCNT		Pd/NCNT	
	KOH	NaOH	KOH	NaOH
E_{p1}, E_{p2} [V] vs RHE	0.86, 0.71	0.88, 0.71	0.84, 0.66	0.84, 0.66
j_{p1}, j_{p2} [mA cm^{-2}]	1.42, 0.70	0.55, 0.19	1.31, 0.59	3.08, 1.74
Q_{p1}, Q_{p2} [C]	17.3, 7.09	6.80, 2.16	26.0, 7.58	62.5, 25.6

Strmcnik et al. [24]. Surprisingly, the current densities for Pd/NCNT are enhanced by a factor of approximately 2.4 without significant changes in peak potentials and shapes. Obviously, the peak potentials and shapes depend on the structural properties of the catalyst, whereas the changes in j_{p1} and j_{p2} are caused by the nature of the cation in the electrolyte.

Figure 2: CVs of the electrooxidation of 1 M glycerol over Pd/NCNT-NH$_3$ and Pd/OCNT-He in 1 M NaOH at 1000 rpm at a scan rate 0.01 V s^{-1}.
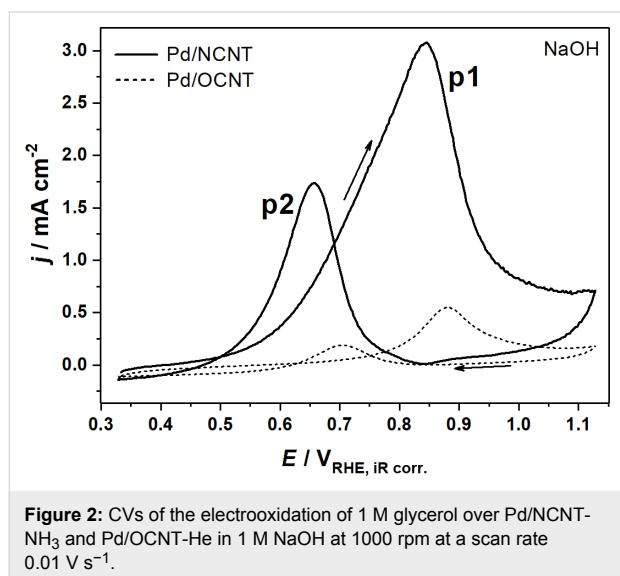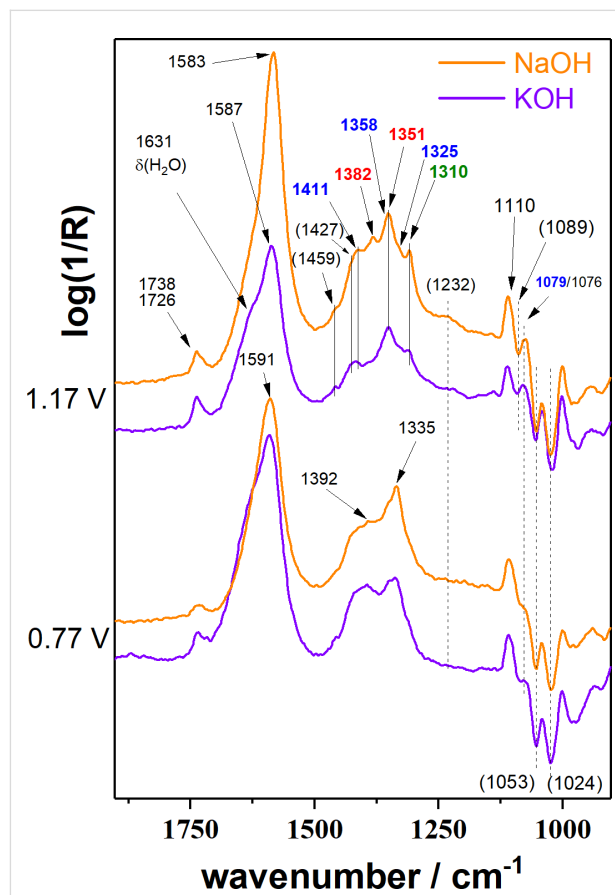
The higher catalytic activity of the metallic Pd NPs supported on NCNTs in heterogeneous gas-phase catalysis has been explained by an electronic effect due to the electron-donating effect of the embedded nitrogen species [35]. Pd^0 is also considered the active site in glycerol electrooxidation, and the observed lower overpotential may originate from the same interaction with the nitrogen-doped support. Furthermore, the thermal treatment of the oxygen-functionalized CNTs in He reduces the number of acidic groups on the surface leading to a higher degree of hydrophobicity of the OCNT support lowering the coverage of adsorbed glycerol. A combination of these properties may explain the lower activity of Pd/OCNT, but it does not provide a straightforward explanation for the observed higher current densities for Pd/NCNT in NaOH compared with KOH considering the non-covalent interactions proposed by Strmcnik et al. [24].

In situ FTIR spectroscopy

The reaction products in NaOH and KOH solutions formed over Pd/NCNT were identified by IR spectroscopy (Figure 3, Table 2) using a cell that allows to adjust the distance between the electrode surface and the IR window (d_{TL}) [36]. The distance d_{TL} was adjusted to 28 μm to minimize the impact of local pH changes ensuring bulk-like reaction conditions in the thin layer (Supporting Information File 1, Figure S1). At 0.77 V vs RHE the spectra in NaOH and KOH appear to be quite simi-

lar. The most pronounced difference is the intense band at 1335 cm^{-1} in NaOH. A shoulder at 1351 cm^{-1} found in both electrolytes is assigned to the $\nu_s(COO^-)$ vibration of formate [37]. We assign the band at 1335 cm^{-1} to a highly oxidized C$_3$ species like tartronate and mesoxalate [15], although in literature this signal is also often attributed to 1,3-dihydroxyacetone (DHA) [20,21,38,39]. Our reference experiments with DHA (Supporting Information File 1, Figure S3) exclude this assignment, because no band was found at 1335 cm^{-1} [15,16]. Further bands caused by DHA would occur at 1738 ($\nu(C=O)$), 1056 and 1003 cm^{-1}, of which only the first can be identified. The intensity is generally weak and found to decrease with higher potential suggesting that it is either less formed or more easily further oxidized.

Figure 3: Comparison of IR spectra recorded at 0.77 and 1.17 V vs RHE (further potentials are shown in Supporting Information File 1, Figure S2) for Pd/NCNT after electrooxidation of 1 M glycerol for 14.7 min in 0.1 M of NaOH or KOH, respectively (d_{TL} = 28 μm).

The assignment to tartronate or mesoxalate is additionally supported by the presence of bands at 1110 and 1725 cm^{-1} (shoulder of the band at 1738 cm^{-1}). Hydroxypyruvate (1383, 1215 cm^{-1} [15]) is tentatively excluded as no sharp band intensity is found. The intense slightly asymmetric band around

Table 2: Wavenumbers of identified species found in the IR spectra. Wavenumbers in italics originate from homemade reference experiments, other species were identified using refs. [15,16] if not indicated differently.

identified species	molecular structure	wavenumber[a] [cm^{-1}]
methanol	H_3COH	*1110*
formate		*1382, 1351*
carbonate	CO_3^{2-}	*1390*
glycolate, glycerate		*1411* (sh), *1358* (sh), *1325* (sh)
oxalate		*1310*
glyoxal, glyoxylate		1076 [13]
glycerol		(*1112*, *1044*)
tartronate, mesoxalate		1725 (sh), 1335, 1110
DHA		*1738* (*1056*, *1003*)

[a]"sh" is an abbreviation for "shoulder"; wavenumbers in brackets indicate expected bands that were not identified in the IR spectra.

1590 cm^{-1} cannot be assigned to a single species, because most of the possible products contain one or more carboxylic groups. In addition, there is the overlap with the H_2O bending mode ($\delta(H_2O)$) at $\approx$1631 cm^{-1}. The negative signals at 1053 and 1024 cm^{-1} indicate the consumption of a compound but do not correspond to the ν(C–O) bands of glycerol (1105, 1060 cm^{-1}) rendering their assignment difficult.

Upon increasing the applied potential to 1.17 V vs RHE, the IR spectra in both NaOH and KOH change. The band at 1335 cm^{-1} is hardly visible anymore, but additional bands are identified and assigned to δ(HCO) of formate (1382 cm^{-1}, only in NaOH) [37] and oxalate (1310 cm^{-1}) [15,16]. Glycerate and glycolate are presumably also present. Both contain one fully oxidized terminal C atom and by cleaving the C–C bond in glycerate, glycolate can be obtained. Thus, the easiest differentiation would be by a ν(C–O) band at around 1125 cm^{-1} [15]. This band is not found, but glycolate bands (wavenumbers in blue in Figure 3) [15] are present as shoulders indicating that glycerate is either oxidized further too fast to be observed or glycolate is

generated from a different species like tartronate after C–C cleavage. A weak band at 1076 cm^{-1} could indicate glyoxal or glyoxylate that are only found at higher potentials as intermediate species towards oxalate [13].

The product assignment clearly indicates that increasing potentials favor C–C bond cleavage. Bond scission is likely to proceed via highly oxidized C_3 species that are prone to undergo C–C scission more easily as the carbon atoms become positively charged with increasing number of oxygen atoms in the molecule. An additional indicator is the band at 1110 cm^{-1} already assigned to mesoxalate or tatronate. It is observed that its IR intensity is slightly higher at 1.17 V vs RHE. Because C_3 species are less favored at higher potentials, this band has to be at least partly caused by another species. A reasonable assignment is the ν(C–O) vibration of a methoxy group. For instance, the glycerate-to-glycolate conversion generates a methoxy species for each converted molecule. For the NaOH electrolyte this band is increasing with more anodic potential supporting this hypothesis.

The generation of C$_1$ species further suggests the production of carbonate (1390 cm^{-1} [15]). Its contribution seems to be rather weak at 0.77 V vs RHE, whereas the spectra recorded at 1.17 V vs RHE show a contribution. Especially the spectrum in KOH shows a strong lack of intensity in this region in comparison to the spectrum in NaOH. The conclusions drawn from the IR spectra help to explain the CV results. The last oxidation step of glycerol to carbonate via three formate species involves almost 43% of the transferable number of electrons per mole of glycerol. Thus, the lack of band intensity in the carbonate region in KOH in combination with the generally lower IR band intensities indicate an overall lower degree of glycerol conversion and extent of oxidation producing carbonate as final product.

The surface coverage of solvated Na$^+$ clusters on the Pd NPs is supposed to be higher than for the corresponding K$^+$ clusters and thus should hinder the adsorption/oxidation of glycerol leading to lower currents also for Pd/NCNT [24]. It has to be pointed out that a non-linearity of this cation effect has already been found for Au electrodes in the case of ethanol and methanol oxidation [26] and H$_2$O electrolysis in alkaline media [28]. In our case using CNT-supported Pd NPs, the observed cation-related activity trend suggests another reason due to the differently functionalized CNT surfaces. Gosselink et al. [40] reported on the beneficial role of increased surface polarity of carbon nanofibers introduced by oxygen groups in the deoxygenation of stearic acid over Pd NPs deposited in addition on this support. They identified a favorable mode of adsorption of the stearic acid via the carboxylic group for high support polarity instead of a flat adsorption mode for low support polarity [40]. The upright adsorption mode facilitates the deoxygenation due to the close contact with the Pd NPs pointing to the importance of metal-support interactions [40].

A similar adsorption-induced effect may be present in glycerol oxidation over Pd/NCNT in NaOH due to the more favorable interaction of Na$^+$ with the basic nitrogen species in the CNT surface acting as ligands. Also the oxygen-containing functional groups in glycerol and the various intermediates can act as ligands resulting in a high affinity to the complexing Na$^+$ ions on the NCNT support. Thus, oxidation over the Pd NPs is facilitated, because the organic species are kept close to the catalytically active Pd NPs. As a result, highly oxidized products are formed leading to higher current densities. The chelate effect is assumed to strengthen the binding of the oxygen-functionalized molecules acting as polydentate ligands. We plan to extend our experimental series to LiOH and CsOH and to apply Pd NPs deposited on non-functionalized CNTs and Pd film electrodes to provide additional support for the postulated beneficial role of Na$^+$ surface complexes on NCNTs.

Conclusion

The effects of the alkali cations Na$^+$ and K$^+$ on the electrochemical oxidation of glycerol were investigated over Pd nanoparticles supported on carbon nanotubes. The CNTs used as support for the Pd NPs were either oxygen- or nitrogen-functionalized. Cyclic voltammetry showed that the achieved current densities were higher in KOH than in NaOH solution for Pd/OCNT in agreement with the theory of weaker non-covalent interactions on the Pd surface in KOH. Pd/NCNT was electrocatalytically more active as shown by the lower anodic onset potential achieving slightly higher current densities in KOH compared with Pd/OCNT. In contrast, significantly higher current densities in NaOH were observed for Pd/NCNT. The product distribution determined by ATR–IR spectroscopy at constant potentials revealed significant differences considering the relative production of species. The IR spectra recorded in NaOH indicate the presence of more strongly oxidized products including C–C bond scission. More specific, in KOH less IR intensity in the carbonate band region was found in agreement with the lower current densities observed during the CV experiments. It is claimed that the Na$^+$ cations interact with the nitrogen-functionalized CNTs more strongly forming complexes with the organic molecules, presumably enhanced by the chelate effect. In this way, the organic molecules are assumed to be bound more tightly to the NCNT support in close proximity to the catalytically active Pd NPs facilitating their oxidation.

Experimental
Catalysts
The preparation of the two catalysts Pd/NCNT and Pd/OCNT has been published elsewhere [34,35,41]. In brief, the oxygen- and subsequent nitrogen-functionalization of the purified and washed CNTs (Baytubes C 150 P, washed in 1.5 M HNO$_3$) was performed by HNO$_3$ vapor treatment at 473 K for 48 h. Then, the obtained O-functionalized CNTs were exposed to 10 vol % of NH$_3$/He at 673 K for 6 h to obtain NCNTs. The O-functionalized CNTs were additionally heated in He at 673 K for 6 h (OCNTs). The Pd NPs were deposited from a colloidal method, dried at 333 K for 12 h, reduced in 10 vol % H$_2$/He (100 mL min^{-1}) for 2 h and cooled to room temperature in He. The catalysts possess a weight load of <1 wt %.

Electrochemistry
The electrochemical characterization of Pd/NCNT and Pd/OCNT was performed in a conventional three-electrode set-up using 0.11 cm^2 glassy carbon electrodes as working electrode, a Ag/AgCl/3 M KCl as reference and a Pt mesh as counter electrode. The working electrodes were polished to a mirror finish using grinding papers and alumina suspensions of different grain sizes. Prior to each experiment, the glassy car-

bon surface was repolished using a 0.05 μm Al_2O_3 suspension and ultrasonicated in H_2O before a new catalyst layer was deposited. The catalyst ink was prepared according to a final concentration of 5 mg/mL using 49:49:2 vol % H_2O/ethanol/ Nafion. An aliquot of the catalyst ink was drop-cast on the glassy carbon electrode achieving a loading of 210 μg cm^{-2} and dried in air at ambient conditions. The catalyst-covered electrodes were initially conditioned in a potential range from 0.33 to 1.13 V vs RHE in Ar-saturated 1 M of alkali base + 1 M of glycerol for 10 cycles at a scan rate of 0.1 V s^{-1} and an electrode rotation rate of 1000 rpm. The uncompensated electrolyte resistance was determined by electrochemical impedance spectroscopy performed at open circuit potential without electrode rotation before glycerol oxidation was monitored using a scan rate of 0.01 V s^{-1} for one cycle. The results were repeated to ensure reproducibility. The potential was applied by a Metrohm Autolab potentiostat and is reported versus the reversible hydrogen electrode scale.

Spectroelectrochemistry

FTIR experiments were performed in a spectroelectrochemical cell described in detail in ref. [36]. In brief, it combines ATR–IR spectroscopy with electrochemical techniques in a thin electrolyte layer configuration, where the thickness of the thin layer is tunable in the micrometer range by an implemented micrometer screw. The Bruker Tensor 27 FTIR spectrometer was equipped with an A530/P reflection unit, a liquid nitrogen mercury cadmium telluride detector and was constantly purged with dried air. All IR experiments were performed in Ar-saturated 0.1 M alkali base containing 1 M glycerol using a Ge internal reflection element. The active electrode area was slightly increased to 0.5 cm^2 to increase the IR band intensity of the generated species by covering a substantial part of the internal reflection element. The electrode preparation and catalyst deposition were performed in the same manner as for the other experiments yielding a comparable surface loading. If not otherwise mentioned, all IR spectra were recorded in the range from 4000 to 700 cm^{-1} with a resolution of 4 cm^{-1} and correspond to the average of 200 individual interferograms (≈90s) after automatic subtraction of the reference spectrum recorded with the same number of IR scans. The spectra are shown as log(1/reflection) with generated and consumed species pointing upwards and downwards, respectively, with respect to the reference spectrum. Spectra acquisition was controlled using the Opus 7.2 software. The constant sample potentials that were applied during the spectroelectrochemical experiments were modulated by a Metrohm Autolab PGSTAT204 potentiostat using the Nova 1.11.2 software. Reference spectra were recorded without adapting any electrochemical equipment. The compounds DHA, glyceric acid, carbonate, formate, oxalate, glycerol and methanol were diluted in 0.1 M KOH at a concentration of 0.05 M and several spectra were recorded to check for chemical stability in alkaline medium.

Supporting Information

Supporting Information File 1
Additional spectra.
[https://www.beilstein-journals.org/bjoc/content/
supplementary/1860-5397-14-120-S1.pdf]

ORCID® iDs

Wolfgang Schuhmann - https://orcid.org/0000-0003-2916-5223
Martin Muhler - https://orcid.org/0000-0001-5343-6922

References

1. Brandt, A.; Hallett, J. P.; Leak, D. J.; Murphy, R. J.; Welton, T. *Green Chem.* **2010,** *12,* 672–679. doi:10.1039/b918787a
2. Ramirez, J. A.; Brown, R. J.; Rainey, T. J. *Energies (Basel, Switz.)* **2015,** *8,* 6765–6794. doi:10.3390/en8076765
3. Haas, M. J.; McAloon, A. J.; Yee, W. C.; Foglia, T. A. *Bioresour. Technol.* **2006,** *97,* 671–678. doi:10.1016/j.biortech.2005.03.039
4. Simões, M.; Baranton, S.; Coutanceau, C. *ChemSusChem* **2012,** *5,* 2106–2124. doi:10.1002/cssc.201200335
5. Soloveichik, G. L. *Beilstein J. Nanotechnol.* **2014,** *5,* 1399–1418. doi:10.3762/bjnano.5.153
6. Antolini, E.; Gonzalez, E. R. *J. Power Sources* **2010,** *195,* 3431–3450. doi:10.1016/j.jpowsour.2009.11.145
7. McLean, G. F.; Niet, T.; Prince-Richard, S.; Djilali, N. *Int. J. Hydrogen Energy* **2002,** *27,* 507–526. doi:10.1016/S0360-3199(01)00181-1
8. Badwal, S. P. S.; Giddey, S.; Kulkarni, A.; Goel, J.; Basu, S. *Appl. Energy* **2015,** *145,* 80–103. doi:10.1016/j.apenergy.2015.02.002
9. Hekmat, D.; Bauer, R.; Fricke, J. *Bioprocess Biosyst. Eng.* **2003,** *26,* 109–116. doi:10.1007/s00449-003-0338-9
10. Kwon, Y.; Koper, M. T. M. *Anal. Chem.* **2010,** *82,* 5420–5424. doi:10.1021/ac101058t
11. Schnaidt, J.; Heinen, M.; Denot, D.; Jusys, Z.; Behm, R. J. *J. Electroanal. Chem.* **2011,** *661,* 250–264. doi:10.1016/j.jelechem.2011.08.011
12. Ye, J.-Y.; Jiang, Y.-X.; Sheng, T.; Sun, S.-G. *Nano Energy* **2016,** *29,* 414–427. doi:10.1016/j.nanoen.2016.06.023
13. Wang, L.; Meng, H.; Shen, P. K.; Bianchini, C.; Vizza, F.; Wei, Z. *Phys. Chem. Chem. Phys.* **2011,** *13,* 2667–2673. doi:10.1039/c0cp01913e
14. Ferreira, R. S., Jr.; Giz, M. J.; Camara, G. A. *J. Electroanal. Chem.* **2013,** *697,* 15–20. doi:10.1016/j.jelechem.2013.03.007
15. de Souza, N. E.; Gomes, J. F.; Tremiliosi-Filho, G. *J. Electroanal. Chem.* **2017,** *800,* 106–113. doi:10.1016/j.jelechem.2016.08.019

16. Gomes, J. F.; Garcia, A. C.; Gasparotto, L.; de Souza, N. E.; Ferreira, E. B.; Pires, C.; Tremiliosi-Filho, G. *Electrochim. Acta* **2014,** *144,* 361–368. doi:10.1016/j.electacta.2014.08.035

17. Gomes, J. F.; Martins, C. A.; Giz, M. J.; Tremiliosi-Filho, G.; Camara, G. A. *J. Catal.* **2013,** *301,* 154–161. doi:10.1016/j.jcat.2013.02.007

18. Garcia, A. C.; Kolb, M. J.; van Nierop y Sanchez, C.; Vos, J.; Birdja, Y. Y.; Kwon, Y.; Tremiliosi-Filho, G.; Koper, M. T. M. *ACS Catal.* **2016,** *6,* 4491–4500. doi:10.1021/acscatal.6b00709

19. Bott-Neto, J. L.; Garcia, A. C.; Oliveira, V. L.; de Souza, N. E.; Tremiliosi-Filho, G. *J. Electroanal. Chem.* **2014,** *735,* 57–62. doi:10.1016/j.jelechem.2014.10.010

20. Simões, M.; Baranton, S.; Coutanceau, C. *Appl. Catal., B* **2010,** *93,* 354–362. doi:10.1016/j.apcatb.2009.10.008

21. González-Cobos, J.; Baranton, S.; Coutanceau, C. *J. Phys. Chem. C* **2016,** *120,* 7155–7164. doi:10.1021/acs.jpcc.6b00295

22. Geraldes, A. N.; Silva, D. F.; Silva, J. C. M.; Souza, R. F. B.; Spinacé, E. V.; Neto, A. O.; Linardi, M.; Santos, M. C. *J. Braz. Chem. Soc.* **2014,** *25,* 831–840. doi:10.5935/0103-5053.20140044

23. Holade, Y.; Morais, C.; Servat, K.; Napporn, T. W.; Kokoh, K. B. *ACS Catal.* **2013,** *3,* 2403–2411. doi:10.1021/cs400559d

24. Strmcnik, D.; Kodama, K.; van der Vliet, D.; Greeley, J.; Stamenkovic, V. R.; Marković, N. M. *Nat. Chem.* **2009,** *1,* 466–472. doi:10.1038/nchem.330

25. Angelucci, C. A.; Varela, H.; Tremiliosi-Filho, G.; Gomes, J. F. *Electrochem. Commun.* **2013,** *33,* 10–13. doi:10.1016/j.elecom.2013.03.039

26. Nakamura, M.; Nakajima, Y.; Kato, K.; Sakata, O.; Hoshi, N. *J. Phys. Chem. C* **2015,** *119,* 23586–23591. doi:10.1021/acs.jpcc.5b07878

27. Berkes, B. B.; Inzelt, G.; Schuhmann, W.; Bondarenko, A. S. *J. Phys. Chem. C* **2012,** *116,* 10995–11003. doi:10.1021/jp300863z

28. Tymoczko, J.; Colic, V.; Ganassin, A.; Schuhmann, W.; Bandarenka, A. S. *Catal. Today* **2015,** *244,* 96–102. doi:10.1016/j.cattod.2014.07.007

29. Ganassin, A.; Colic, V.; Tymoczko, J.; Bandarenka, A. S.; Schuhmann, W. *Phys. Chem. Chem. Phys.* **2015,** *17,* 8349–8355. doi:10.1039/c4cp04791e

30. Stoffelsma, C.; Rodriguez, P.; Garcia, G.; Garcia-Araez, N.; Strmcnik, D.; Marković, N. M.; Koper, M. T. M. *J. Am. Chem. Soc.* **2010,** *132,* 16127–16133. doi:10.1021/ja106389k

31. Previdello, B. A. F.; Machado, E. G.; Varela, H. *RSC Adv.* **2014,** *4,* 15271–15275. doi:10.1039/C4RA00769G

32. Sitta, E.; Batista, B. C.; Varela, H. *Chem. Commun.* **2011,** *47,* 3775–3777. doi:10.1039/c0cc05353h

33. Sitta, E.; Nagao, R.; Kiss, I. Z.; Varela, H. *J. Phys. Chem. C* **2015,** *119,* 1464–1472. doi:10.1021/jp5105505

34. Hiltrop, D.; Masa, J.; Maljusch, A.; Xia, W.; Schuhmann, W.; Muhler, M. *Electrochem. Commun.* **2016,** *63,* 30–33. doi:10.1016/j.elecom.2015.11.010

35. Chen, P.; Chew, L. M.; Kostka, A.; Muhler, M.; Xia, W. *Catal. Sci. Technol.* **2013,** *3,* 1964–1971. doi:10.1039/c3cy00097d

36. Hiltrop, D.; Masa, J.; Botz, A. J. R.; Lindner, A.; Schuhmann, W.; Muhler, M. *Anal. Chem.* **2017,** *89,* 4367–4372. doi:10.1021/acs.analchem.6b03732

37. Rotzinger, F. P.; Kesselman-Truttmann, J. M.; Hug, S. J.; Shklover, V.; Grätzel, M. *J. Phys. Chem. B* **2004,** *108,* 5004–5017. doi:10.1021/jp0360974

38. Zalineeva, A.; Serov, A.; Padilla, M.; Martinez, U.; Artyushkova, K.; Baranton, S.; Coutanceau, C.; Atanassov, P. B. *Appl. Catal., B* **2015,** *176–177,* 429–435. doi:10.1016/j.apcatb.2015.04.037

39. Zalineeva, A.; Baranton, S.; Coutanceau, C. *Electrochim. Acta* **2015,** *176,* 705–717. doi:10.1016/j.electacta.2015.07.073

40. Gosselink, R. W.; Xia, W.; Muhler, M.; de Jong, K. P.; Bitter, J. H. *ACS Catal.* **2013,** *3,* 2397–2402. doi:10.1021/cs400478q

41. Dong, W.; Chen, P.; Xia, W.; Weide, P.; Ruland, H.; Kostka, A.; Köhler, K.; Muhler, M. *ChemCatChem* **2016,** *8,* 1269–1273. doi:10.1002/cctc.201501379

License and Terms

Cobalt–metalloid alloys for electrochemical oxidation of 5-hydroxymethylfurfural as an alternative anode reaction in lieu of oxygen evolution during water splitting

Jonas Weidner[‡1], Stefan Barwe[‡1], Kirill Sliozberg[1], Stefan Piontek[2], Justus Masa[1], Ulf-Peter Apfel[2,3] and Wolfgang Schuhmann[*1]

Abstract
The electrochemical water splitting commonly involves the cathodic hydrogen and anodic oxygen evolution reactions (OER). The oxygen evolution reaction is more energetically demanding and kinetically sluggish and represents the bottleneck for a commercial competitiveness of electrochemical hydrogen production from water. Moreover, oxygen is essentially a waste product of low commercial value since the primary interest is to convert electrical energy into hydrogen as a storable energy carrier. We report on the anodic oxidation of 5-hydroxymethylfurfural (HMF) to afford the more valuable product 2,5-furandicarboxylic acid (FDCA) as a suitable alternative to the oxygen evolution reaction. Notably, HMF oxidation is thermodynamically more favorable than water oxidation and hence leads to an overall improved energy efficiency for H_2 production. In addition, contrary to the "waste product O_2", FDCA can be further utilized, e.g., for production of polyethylene 2,5-furandicarboxylate (PEF), a sustainable polymer analog to polyethylene terephthalate (PET) and thus represents a valuable product for the chemical industry with potential large scale use. Various cobalt–metalloid alloys (CoX; X = B, Si, P, Te, As) were investigated as potential catalysts for HMF oxidation. In this series, CoB required 180 mV less overpotential to reach a current density of 55 mA cm^{-2} relative to OER with the same electrode. Electrolysis of HMF using a CoB modified nickel foam electrode at 1.45 V vs RHE achieved close to 100% selective conversion of HMF to FDCA at 100% faradaic efficiency.

Introduction

Energy production from renewable sources continues to contribute to a significant growing share of current and future energy requirements. However, the intermittency of renewable energy sources renders it a necessity to develop new technologies to convert and store surplus energy, which can be made accessible on demand [1]. Energy storage in hydrogen as a highly versatile energy carrier, which can be inexhaustibly obtained from water, is very appealing [2]. For the conversion of renewable energy into storable hydrogen, electrochemical water splitting turns out to be among the most promising approaches. However, this reaction is energy intensive, especially due to sluggish kinetics and high overpotential of the oxygen evolution reaction (OER) leading to a low energy conversion efficiency [3].

Importantly, the oxygen that is produced as an inevitable by-product possesses comparatively low economic value with respect to the energy demand of its production. Thus, replacing the OER by a thermodynamically and/or kinetically more favorable anode reaction is desirable in order to increase the energy efficiency of the hydrogen production and hence to facilitate the development of large scale electrochemical hydrogen production. Advantageously, the oxidation of an alternative substrate at the anode, for example a biomass-derived fuel, allows to generate high value products besides hydrogen concomitantly with an increase in energy conversion efficiency during electrolysis [4]. Alternative anode products replacing oxygen evolution could be produced in new generation electrolyzers (see Scheme 1) [5].

According to the report of the US Department of Energy from 2004, the fructose-derived hydroxymethylfurfural (HMF) and its oxidation product 2,5-furandicarboxylic acid (FDCA) are bio-refinery based chemicals for a "green" chemical industry [6-8]. FDCA was suggested to replace, e.g., terephthalic acid as building block for the formation of polyamides, polyesters, and polyurethanes [6]. Especially, the polymer polyethylene terephthalate (PET), a perpetually used polymer, could be substituted by FDCA-based polyethylene 2,5-furandicarboxylate (PEF) produced via a green chemical synthetic route. Thus, HMF oxidation would lead to a product of high economic value and ecological relevance [9].

Classically, the oxidation of HMF is performed by means of homogeneous and heterogeneous catalysis [10,11]. The conversion of HMF to FDCA via homogeneous catalysis, however, suffers from two main drawbacks. Firstly, the yield in FDCA is relatively low due to poor oxidation selectivity. Secondly, the recycling of the catalysts and the purification of FDCA from the reaction mixtures is time-consuming and costly. Heterogeneous
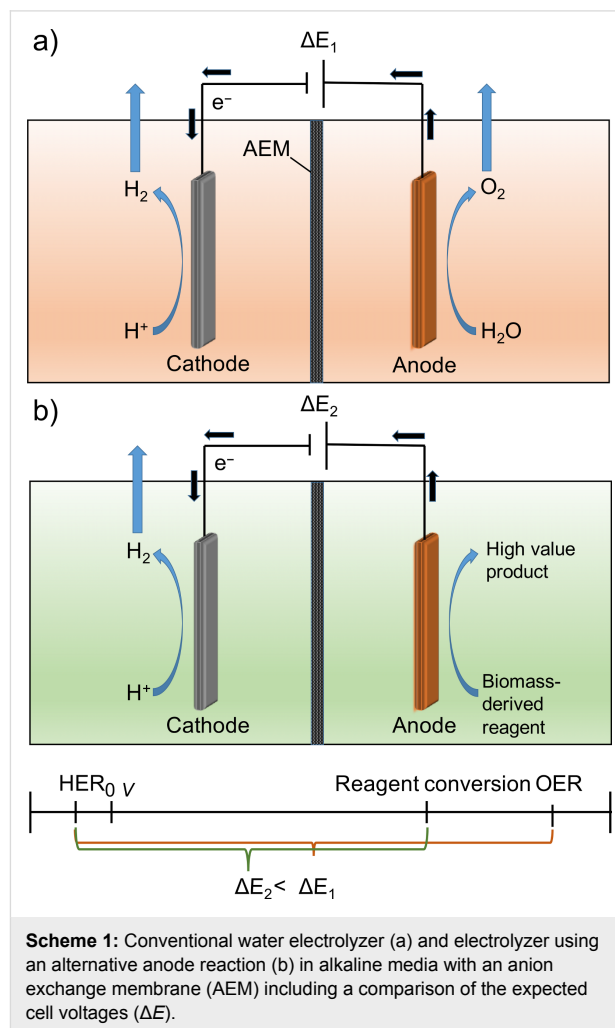
Scheme 1: Conventional water electrolyzer (a) and electrolyzer using an alternative anode reaction (b) in alkaline media with an anion exchange membrane (AEM) including a comparison of the expected cell voltages (ΔE).

catalysts are more easily separated from the reaction solution and can therefore be reused for further oxidation of HMF. Noble metal catalysts such as Pt [12-16], Au [16-20], Pd [16,21-23], and Ru [24] are frequently employed as heterogeneous catalysts for the oxidation of HMF. However, the high cost of the noble metal catalysts has aroused interest in transition metal catalysts and alternative methods for the oxidation of HMF. The electrochemical oxidation of HMF to FDCA was first reported in 1991 by Grabowski and co-workers [25]. Here, HMF was selectively converted to FDCA in NaOH (1.0 M) as electrolyte using a nickel oxide/hydroxide anode achieving a yield of 71% [25]. Strasser and Vuyyuru observed the degradation of HMF to humin type products in highly alkaline solutions and proposed a lower working pH value (<13) for electrocatalytic HMF oxidation. However, using a Pt electrode at pH 10, only sluggish FDCA formation in trace amounts was achieved (below 1%) [26]. This result highlights the need for highly efficient catalysts to enhance the oxidation of HMF to FDCA at high pH values. Li and co-workers studied the electro-

chemical oxidation of HMF on carbon black supported monometallic Pd/C and Au/C, and bimetallic Pd-Au/C catalysts [27]. Their studies revealed that the reaction pathway was influenced by the type of catalyst and the applied potential [27]. Furthermore, Choi and Cha found that the overpotential required to initiate HMF oxidation was considerably decreased by introducing 2,2,6,6-tetramethylpiperidine-1-oxyl (TEMPO) as an electron mediator to the electrolyte [4]. Despite promising results in synthesizing FDCA, this method suffers from the high cost of TEMPO, which had to be added in 1.5 equivalents relative to HMF [4]. The elaborate separation of TEMPO from FDCA appeared to be an additional disadvantage [24]. Recently, Sun and co-workers reported the electrochemical oxidation of HMF using various non-precious cobalt and nickel based bifunctional HER/OER water splitting electrocatalysts, namely CoP on copper foam, Ni_2P and Ni_3S_2 on nickel foam, in a one compartment batch type electrochemical reactor [5,28,29]. We recently reported on the synthesis and application of alloys of cobalt with boron and phosphorus as exceptionally active bifunctional HER/OER catalysts for water splitting. Inspired by these results, we herein report on the application of different cobalt–metalloid alloys (Co–X; X = B, Si, P, As and Te) for the electrochemical HMF oxidation. With the exception of CoP, all tested materials were to the best of our knowledge not described before for the electrochemical HMF oxidation. Screening of the various cobalt–metalloid alloys supported on Ni RDE electrodes revealed CoB to be the most efficient HMF oxidation catalyst. Using a CoB modified Ni foam as anode material, and Ni foam as the cathode in a continuous flow reactor with an anion exchange membrane separating the anodic and cathodic compartments, a faradaic efficiency of 100% for HMF oxidation, 100% selectivity to FDCA with a yield of 94% was observed.

Results and Discussion
Catalyst screening

Replacing the O_2 evolution reaction with an alternative energetically less demanding and more facile process leading to a more valuable product is an appealing approach for increasing the competitiveness of the electrochemical hydrogen production. 5-Hydroxymethylfurfural (HMF) is a biomass-derived compound that can be converted to economically more valuable 2,5-furandicarboxylic acid (FDCA) via electrochemical oxidation at a comparatively lower potential than that required for water oxidation. Suitable catalysts are, however, required to achieve a selective oxidation of HMF to FDCA with a high conversion yield. We recently demonstrated that the modification of cobalt with boron and phosphorus alters the electronic and lattice properties of elemental cobalt leading to significant enhancement of its activity for the oxygen evolution reaction (OER) and the hydrogen evolution reaction (HER). We therefore envi-

sioned that modification of cobalt with other metalloid elements, that is, cobalt–metalloid alloys (CoX; X = B, Si, P, As and Te), could likewise lead to an enhanced electrocatalysis for reactions other than the OER and the HER. To this end, alloys of cobalt with boron, silicon, phosphorus, arsenic and tellurium were screened for their electrocatalytic activity for HMF oxidation. A detailed synthetic procedure to afford cobalt boride (CoB) and cobalt phosphide (CoP) was published previously together with a detailed material characterization [30-33]. CoAs as well as CoTe was synthesized at 1100 °C from the elements in sealed glass ampules. In contrast to CoAs and CoTe, Co_2Si was not accessible via a similar high-temperature synthesis from the elements and was obtained by salt metathesis from Mg_2Si and $CoCl_2$ at 400 °C under inert conditions. Characterization of the materials was performed using powder XRD (Figure 1). For Co_2Si, the observed reflexes correlate well with those observed for PXRD patterns generated from single crystalline Co_2Si (PDF04-0847) with only little contribution of metallic Co [34]. To further confirm the composition of this material, we performed energy-dispersive X-ray spectroscopy (EDS) to elucidate the structural composition of the material. EDS unequivocally revealed a Co:Si ratio of 2:1 and further supported the formation of Co_2Si (Supporting Information File 1, Figure S1). In contrast to Co_2Si, CoAs and CoTe are identified as the phase pure arsenide [35] (ICDD 00-052-0774) and telluride [36] (pdf 00-034-0420), respectively (Figure 1).
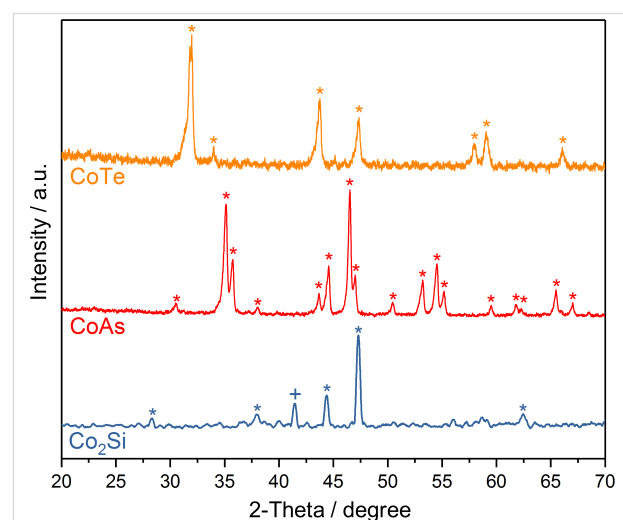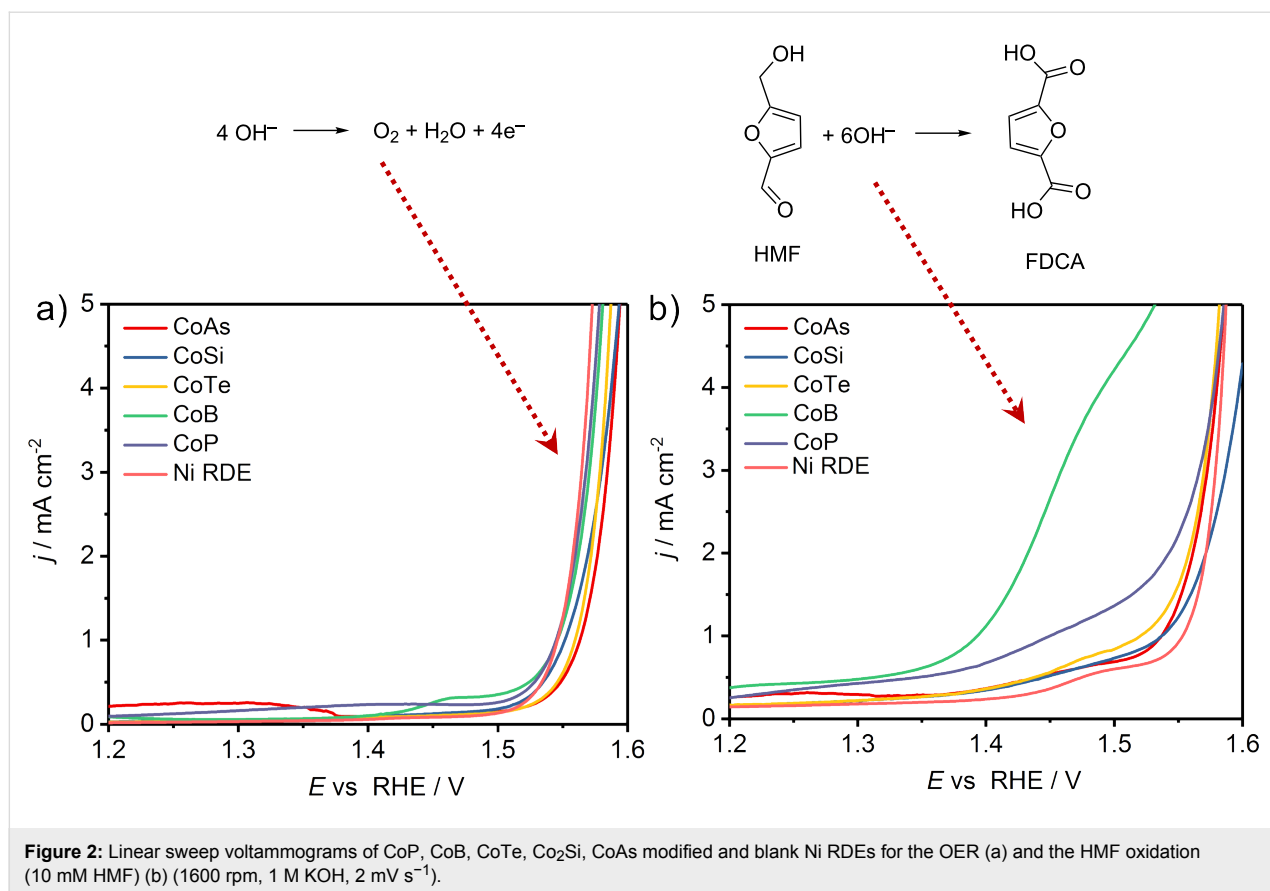

Figure 1: XRD patterns of Co_2Si, CoTe, CoAs. Cobalt is indicated by (+) and signals corresponding to the desired materials are indicated by (*).

An initial screening of the catalysts with respect to their catalytic HMF oxidation activity was performed by potentiodynamic rotating disk electrode (RDE) voltammetry in 1.0 M KOH, in the absence (Figure 2a) and presence of HMF (10 mM, Figure 2b). Linear sweep voltammograms (LSVs) in the

Figure 2: Linear sweep voltammograms of CoP, CoB, CoTe, Co$_2$Si, CoAs modified and blank Ni RDEs for the OER (a) and the HMF oxidation (10 mM HMF) (b) (1600 rpm, 1 M KOH, 2 mV s^{-1}).

absence of HMF show similar activity toward the OER for all the tested materials. However, there is an apparent contribution of the nickel substrate to the measured OER activity. On the contrary, a pure Ni electrode did not show any significant HMF oxidation in the investigated potential window and hence any increased HMF oxidation current is considered to be due to the activity of the catalyst materials. LSVs recorded in the presence of HMF revealed an increase in the measured current density at substantially lower anodic potentials, and exhibited a plateau-like behavior, which is especially pronounced for CoAs, CoSi and CoTe. In the case of CoB and CoP, the HMF oxidation current merged with the OER current and a shoulder-like feature rather than a plateau was observed. This feature is, however, significantly more pronounced in case of CoB. A comparison of the features shown in Figure 2a and 2b indicates that the OER is negligible in the potential window between 1.2 V to 1.5 V vs RHE, where HMF oxidation is facilitated by all investigated catalyst materials. However, parallel O$_2$ evolution at slow rates cannot be fully excluded.

For a comparison of the HMF oxidation activity of the investigated catalysts, two performance criteria were taken into account, namely, the current density achieved at a potential of 1.45 V vs RHE, a potential where the contribution of OER ac-

tivity is negligibly small, and the potential necessary to attain a current density of 1 mA cm^{-2}. The CoB electrocatalyst achieved a current density of 2.69 mA cm^{-2} at 1.45 V and delivered 1.0 mA cm^{-2} at 1.39 V. The overpotential for HMF oxidation is thus decreased by 160 mV as compared to the OER displaying the same current density and using the same electrode. In the series of materials tested, CoB is the most active electrocatalyst for the oxidation of HMF. A detailed comparison of the activities of all investigated CoX-based catalysts (X = B, Si, P, As and Te) is highlighted in Table 1.

HMF oxidation in a continuous flow reactor

The surprisingly high HMF oxidation activity of CoB made it especially interesting to further study the product distribution and FDCA yield in a continuous mode. For this, a flow reactor was employed which contains two nickel foam (NF) electrodes separated by an anion exchange membrane (Supporting Information File 1, Figure S2). The NF anode (1 cm × 1 cm) was modified with CoB by means of spray coating while pure NF was used as cathode material. The photographs in Figure S3 (Supporting Information File 1) show the contrast of the bare NF and the CoB-modified NF, while Figure S4 (Supporting Information File 1) shows scanning electron (SEM) micrographs of CoB-modified NF.

Table 1: A comparison of the OER and HMF oxidation activity of CoB, CoP, CoAs, Co$_2$Si and CoTe modified Ni RDEs (data taken from LSVs of Figure 2).

	Current density [mA cm^{-2}] @ 1.45 V vs RHE (no HMF)	Current density [mA cm^{-2}] @ 1.45 V vs RHE (10 mM HMF)	Potential [vs RHE, V] @ 1 mA cm^{-2} (no HMF)	Potential [vs RHE, V] @ 1 mA cm^{-2} (10 mM HMF)
CoAs	0.11	0.54	1.56	1.54
Co$_2$Si	0.13	0.52	1.55	1.54
CoTe	0.10	0.57	1.56	1.52
CoB	0.26	2.69	1.55	1.39
CoP	0.23	1.00	1.54	1.45
Ni electrode	0.08	0.37	1.55	1.55

The initially smooth NF surface (Figure 3a,b) appears rough with nanometer sized agglomerates of CoB nanoparticles after the spray-coating process (Figure 3c,d; Supporting Information File 1, Figure S4). The current density (normalized to the geometric area of NF) at 1.45 V vs RHE reached 55 mA cm^{-2} during the oxidation of HMF, while a 180 mV more anodic potential was necessary to achieve the same current density during OER in the absence of HMF (Figure 3e). The LSV recorded in the absence of HMF shows a pre-OER oxidation peak at around 1.40 V to 1.45 V vs RHE originating from a convolution of Ni and Co oxidation processes from the NF substrate and from the catalyst, respectively [32]. Evidently, as already

seen during RDE voltammetry the presence of HMF allowed an oxidation process to occur prior to the OER.

However, neither the degree of oxidation, product distribution nor the reaction pathway for HMF oxidation can be resolved from voltammograms. Constant potential electrolysis at 1.45 V vs RHE was performed and product analysis at various time points during electrolysis was conducted by means of high-performance liquid chromatography (HPLC) to monitor the oxidation of HMF to FDCA. The current density vs time transient (Supporting Information File 1, Figure S5) shows a rapid decrease of the measured current density within the first minutes,
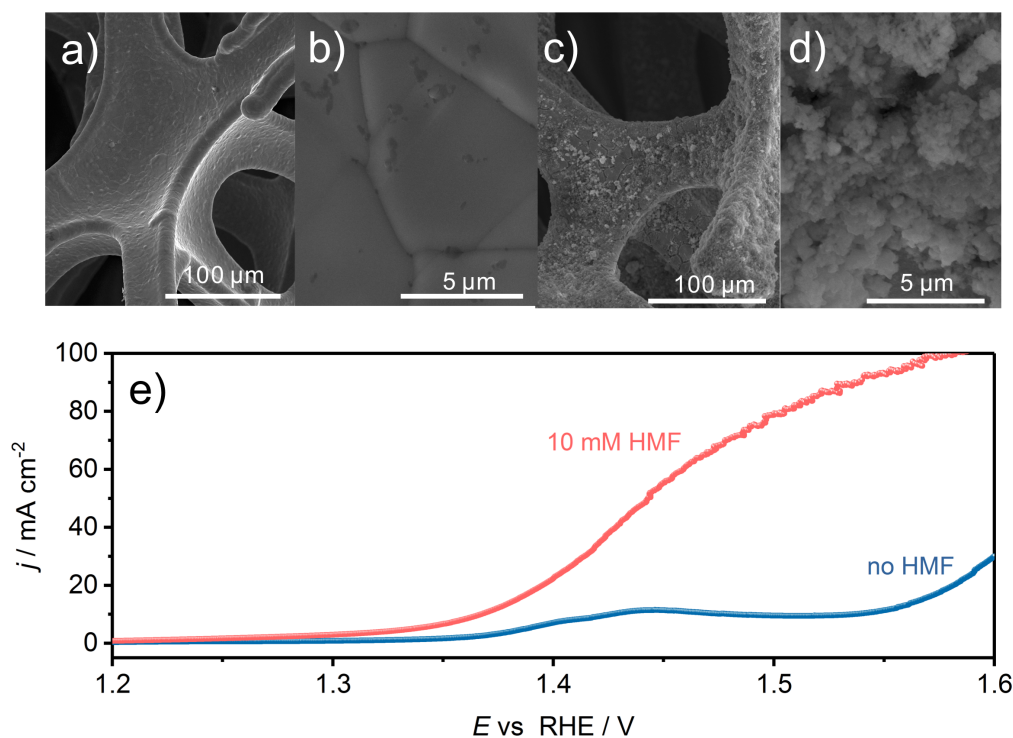
Figure 3: SEM micrographs of bare (a, b) and CoB-modified (c, d) NF with 1000× or 20000× magnification, respectively. e) LSVs of CoB modified NF in the absence and presence of HMF (10 mM) in the flow reactor (1 M KOH, 2 mV s^{-1}, 18 mL min^{-1}).

approaching zero current after approximately 1 h, indicating complete HMF conversion. The consumed charge shows a corresponding steep rise with a change in the slope after about 40 min of electrolysis. The continuous increase of charge after a steady current associated with HMF oxidation was attained is attributed to the underlying OER that already proceeds at 1.45 V vs RHE, however, at a very low reaction rate. Complete (100%) HMF conversion requires 6 Faradays or 58 C for 10 mL of a 10 mM HMF solution. In this case, 58.8 C or 6.1 Faradays were transferred after 60 min of electrolysis further pointing towards complete conversion of HMF.

High-performance liquid chromatography product analysis

HPLC was employed to qualitatively and quantitatively determine the conversion of HMF and all potential side products. HMF oxidation starts with oxidation of either the alcohol or the aldehyde leading to the dialdehyde 2,5-diformylfuran (DFF) or

to 5-hydroxymethyl-2-furancarboxylic acid (HMFCA), respectively (Figure 4a). Subsequent oxidation of DFF and HMFCA leads to 5-formyl-2-furancarboxylic acid (FFCA) and finally to FDCA. The chromatograms revealed signal changes especially at retention times of 2.87 and 6.54 min, which correspond to FDCA and HMF, respectively. The intensity of the HMF signal at 6.54 min decreased gradually with time until it disappeared finally after 70 min of electrolysis, indicating complete oxidation of HMF. Correspondingly, the FDCA signal at 2.87 min increased steadily with time reaching a steady state after 60 min of electrolysis. Minor signals from HMFCA and FFCA were observed at retention times of 3.69 and 3.95 min, respectively, while DFF with a retention time of 7.82 min could only be observed during the first 30 min of HMF electrolysis as a very small peak (Figure 4b).

Besides qualitative observation of the products and intermediates of HMF oxidation, HPLC was employed for quantification
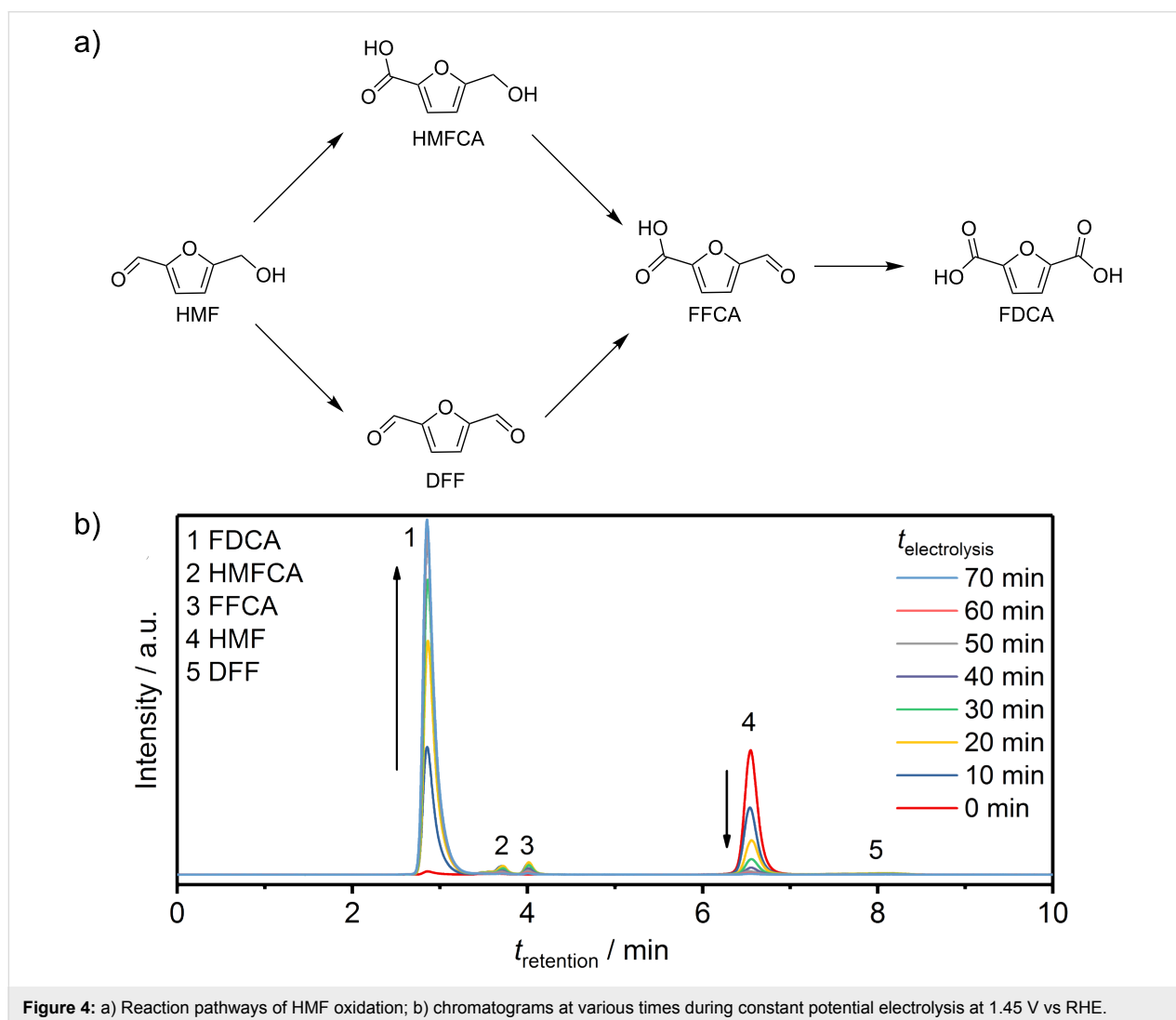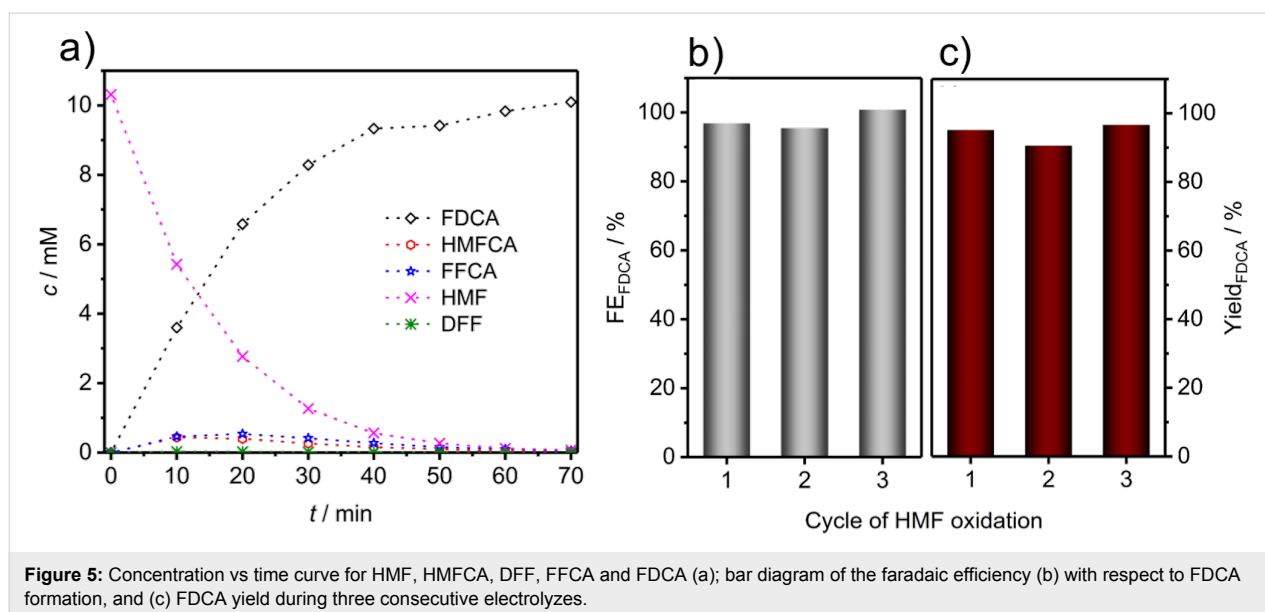

Figure 4: a) Reaction pathways of HMF oxidation; b) chromatograms at various times during constant potential electrolysis at 1.45 V vs RHE.

of the intermediates and products at various electrolysis times (Figure 5a). For this, calibration was performed using standard solutions of pure HMF, FDCA and the reaction intermediates (for further information see Supporting Information File 1, Figure S7). The results revealed complete conversion of HMF to FDCA with a faradaic efficiency of 98 ± 2%, thus confirming that the OER is negligible during electrochemical oxidation of the HMF at 1.45 V. According to our HPLC results, HMFCA was the more pronounced intermediate as compared to DFF, which could be due to rapid transformation of DFF to FFCA or slow formation of DFF. Nevertheless, the results clearly indicate that the oxidation of HMF proceeds via both possible pathways forming DFF as well as HMFCA as intermediates, which are then further oxidized to FFCA and finally FDCA. The yield of FDCA was determined to be 94 ± 3% for three consecutive electrolysis cycles, although the faradaic efficiency and thus the selectivity was close to 100%. HMF is known to decompose into humin type structures at a pH value higher than 12 [26]. Nevertheless, a high pH value is necessary to accelerate HMF conversion [37]. HPLC analysis of 10 mM HMF in 1 M KOH without any applied potential revealed an about 10%/h degradation of HMF into electrochemically inactive humins (Supporting Information File 1, Figure S8), which can then obviously not be transformed into FDCA. This explains the determined faradaic efficiency of 98 ± 2% with a yield of 94 ± 3% for the conversion of the fraction of HMF which was not decomposed at the high pH value. Importantly, the HMF degradation rate decreased under electrochemical HMF oxidation conditions. The catalyst modified electrodes showed a high stability and could be used for multiple successive electrolysis cycles with a reproducible HMF to FDCA conversion (Figure 5b,c; Supporting Information File 1, Figure S9). In each cycle, HMF was fully

converted to FDCA with a faradaic efficiency of close to 100%. Unlike the OER, the oxidation of HMF does not lead to bubble formation and thus does not induce high physical stress on the catalyst coating. Therefore, the catalyst coating stays intact even after several cycles of HMF electrolysis (Supporting Information File 1, Figure S10). In conclusion, HMF oxidation is not only more energy efficient than the OER but the employed electrodes and catalyst films certainly suffer less deactivation.

Conclusion

An alternative, energetically less demanding anode reaction forming a more valuable product in lieu of the oxygen evolution reaction is presented. The oxidation of the bio-refinery product HMF in a flow reactor led to selective formation of the corresponding dicarboxylic acid FDCA with a faradaic efficiency of close to 100%. FDCA is an industrially relevant chemical that can be used for the production of polymers with a potential large-scale application. Thus, HMF oxidation at the anode as a complementary reaction to cathodic hydrogen evolution does not only form a product of added value but also leads to a significant decrease of the overpotential necessary to achieve a certain current density as compared to the OER. While HMF tends to decompose in highly alkaline solutions, its electrochemical oxidation is kinetically more favorable and leads to a competition between HMF decomposition and its transformation into FDCA. However, although 10% of HMF decompose within 1 h when stored in 1 M KOH, electrolysis of a 10 mM solution of HMF in 1 M KOH employing CoB as electrocatalyst suppressed this decomposition and afforded high FDCA yields of 94 ± 3%. It is therefore evident that the catalyst is capable to selectively oxidize HMF to FDCA with only minor losses due to decomposition. Further research and opti-

Figure 5: Concentration vs time curve for HMF, HMFCA, DFF, FFCA and FDCA (a); bar diagram of the faradaic efficiency (b) with respect to FDCA formation, and (c) FDCA yield during three consecutive electrolyzes.

mization of the electrocatalyst could enhance the kinetics of the HMF oxidation and minimize its decomposition even further.

Experimental

All chemicals were of analytical grade and used without further purification. All aqueous solutions were prepared using ultra-pure Milli-Q water (SG Water). KOH was purchased from Carl Roth. HMF, DFF, HMFCA, FFCA and FDCA were from Sigma-Aldrich. Pure elements (Co, As, Te) were supplied by Sigma-Aldrich, Merck, and Alfa Aesar with high purities. All high temperature steps were performed in a tubular furnace in 10 mm quartz ampules evacuated to a pressure of 4×10^{-2} mbar. Nickel foam (99.5% purity) used as electrode material was purchased from Goodfellow.

Catalyst preparation
Cobalt silicide, Co$_2$Si. CoCl$_2$ (0.50 g) and Mg$_2$Si (0.15 g) were thoroughly mixed and heated to 400 °C. Subsequently, the mixture was hold isothermal at this temperature for 24 h. The mixture was then allowed to slowly cool to room temperature. The obtained solid was then ground to give a fine powder that was washed with water and dried in vacuum.

Cobalt arsenide, CoAs. A mixture of cobalt (440 mg) and arsenic (560 mg) was heated to 700 °C. The temperature was hold for 3 h followed by a heating step to 1100 °C with an isothermal step for 20 h. The mixture was subsequently cooled to room temperature to give CoAs.

Cobalt telluride, CoTe. Cobalt telluride was synthesized from the elements Co (0.948 g) and tellurium (2.052 g). The ampule was heated to 800 °C followed by an isothermal step for 2 h. The mixture was then heated to 1100 °C and hold for 15 h. Subsequently, the bulk material was cooled down by switching off the furnace. The product was obtained in form of a purple metallic ingot.

Electrochemical measurements
Electrode preparation
Nickel RDEs (∅ = 3 mm) were polished successively with 1 μm and 0.05 μm alumina polishing paste. Polished electrodes were drop coated with a catalyst ink containing 5 mg mL^{-1} solid catalyst material suspended in a water/ethanol (1:1 v/v) mixture. The catalyst suspension was sonicated for 20 min in order to be homogeneous prior to electrode preparation. After drying in air, the final loading of catalyst material on the electrode was 210 μg cm^{-2}.

Nickel foam electrodes were modified by means of spray coating. The NF electrodes were cleaned by immersing in concentrated HCl for 5 min prior the spray-coating process.

Residual acid was subsequently removed by washing with water, ethanol and acetone. Clean NF was spray-coated from a stirred suspension of catalyst material (2.5 mg mL^{-1}) in a water/ethanol (1:1 v/v) mixture. During the spray coating, the NF electrodes were heated to 80 °C in order to facilitate fast solvent evaporation. The final catalyst loading on NF was ≈1 mg cm$^{-2}_{\text{geom.}}$.

Rotating disk electrode measurements
Each measurement was conducted with an Autolab III potentiostat/galvanostat (Metrohm) attached to an Autolab rotator (Metrohm). The experiments were performed in a three-electrode configuration using aqueous 1 M KOH as electrolyte. HMF oxidation was performed using a 10 mM HMF in 1 M KOH solution. A Pt mesh served as counter electrode (CE), and a Ag/AgCl/3 M KCl was used as reference electrode (RE). The potential was converted to the reversible hydrogen electrode (RHE) according to Equation 1:

$$E_{\text{RHE}} = E_{\text{Ag/AgCl}} + 0.059 \text{ V} \cdot \text{pH} + E^0_{\text{Ag/AgCl}} \qquad (1)$$

The pH value of the 1 M KOH was determined by means of a pH electrode for high alkaline solutions (Dr. Kornder Anlagen-und Messtechnik, Germany) to be 14.

RDE measurements were performed at a rotation speed of 1600 rpm. In order to correct the potential for the uncompensated electrolyte resistance, electrochemical impedance spectroscopy (EIS) was performed at the open circuit potential at perturbation frequencies between 10 kHz and 200 Hz with an amplitude of 10 mV$_{\text{pp}}$. Catalyst conditioning was performed by running 20 cyclic voltammograms between 0 V and 0.5 V vs Ag/AgCl/3 M KCl at a scan rate of 100 mV s^{-1}. Linear sweep voltammograms (LSVs) in a potential range between 0 V and 0.7 V vs Ag/AgCl/3 M KCl at a scan rate of 2 mV s^{-1} were performed to determine the HMF oxidation activity.

Flow reactor measurements
Flow reactor measurements were performed using a VMP-3 potentiostat (Bio-logic) in a specifically designed two compartment flow cell setup shown in Figure S2 (Supporting Information File 1). Two separated electrolyte circuits were used for the anode and the cathode compartment. Experiments were conducted in three-electrode configuration using aqueous 1 M KOH as electrolyte solution containing 10 mM HMF. The WE compartment and the CE compartment were separated by a PEEK reinforced anion exchange membrane (Fumatech). The CE consisted of two stacked unmodified Ni foams (1 cm × 1 cm) and a Hg/HgO/1 M KOH electrode served as RE. Catalyst modified NF (1 cm × 1 cm) was used as the WE.

The potential was converted to the RHE scale according to Equation 2:

$$E_{\text{RHE}} = E_{\text{Hg/HgO}} + 0.059 \text{ V} \cdot \text{pH} + E^0_{\text{Hg/HgO}} \qquad (2)$$

The pH value of the 1 M KOH was determined by means of a pH electrode for high alkaline solutions (Dr. Kornder Anlagen- und Messtechnik, Germany) to be 14.

The electrolyte solution was pumped through the cell with a flow rate of 18 mL min^{-1}. Before each measurement an EIS was recorded to determine the uncompensated electrolyte resistance and the potential was corrected accordingly. The conditioning of the catalyst was performed by cyclic voltammetry with 20 cycles between 0.97 V vs RHE and 1.43 V vs RHE with a scan rate of 100 mV s^{-1}. The LSVs were measured between 0.97 V vs RHE and 1.65 V vs RHE with a scan rate of 2 mV s^{-1}. Constant potential electrolysis was done at 1.45 V vs RHE with a total electrolyte volume of 10 mL in the anode electrolyte reservoir and a HMF concentration of 10 mM. Before and after each electrolysis CVs consisting of one cycle between 0.97 V vs RHE and 1.58 V vs RHE with a scan rate of 2 mV s^{-1} were recorded.

HPLC analysis

The HPLC system consists of a Knauer pump, a Merck Hitachi L-4250 UV–vis detector, and a Shim-pack GWS C18 column from Shimadzu. Calibration for HMF, HMFCA, DFF, FFCA, and FDCA was conducted with a flow rate of 5 mL min^{-1} using an eluent consisting of 70 vol % 5 mM ammonium formate solution and 30 vol % methanol. The UV detector was recording the absorbance of the different compounds using a single wavelength of 265 nm. Ten μL of sample solutions were diluted with 490 μL of water. A volume of three times the volume of the injection loop (10 μL) was injected.

Conversion of HMF, product yield and faradaic efficiency were calculated according to Equations 3–5, respectively

$$\text{HMF conversion } (\%) = \left[n(\text{HMF consumed})/n(\text{HMF initial}) \right] \times 100 \qquad (3)$$

$$\text{product yield } (\%) = \left[n(\text{product})/n(\text{HMF initial}) \right] \times 100 \qquad (4)$$

$$\text{faradaic efficiency } (\%) = \left[n(\text{FDCA formed})/\left(\text{charge}/(6 \times \text{F}) \right) \right] \times 100 \qquad (5)$$

with F being the Faraday constant (96 485 C mol^{-1}) and *n* the mol of reactant calculated from the concentration measured by HPLC.

HPLC analysis of HMF decomposition

The decomposition of HMF in alkaline solution was measured in a stirred 1 M KOH solution in the presence of 10 mM HMF at 20 °C. Samples were taken directly after the addition of HMF, after 10, 30, 60, 100, and 120 min. The samples were injected into the HPLC system after dilution with 990 μL water.

Physical characterization
X-ray diffractometry

XRD data were obtained using a Panalytical X'PERT Pro MPD X-ray diffractometer with a Cu Kα radiation source (λ = 1.5418 Å) in the 2θ = 20–80° range.

Scanning electron microscopy

SEM images were taken using a Quanta ED FEG scanning electron microscope (FEI). The SEM was operated at 20 kV.

Supporting Information

Supporting Information File 1
Additional figures and chromatograms.
[https://www.beilstein-journals.org/bjoc/content/supplementary/1860-5397-14-121-S1.pdf]

ORCID® iDs

Stefan Barwe - https://orcid.org/0000-0001-7333-3808
Justus Masa - https://orcid.org/0000-0002-8555-5157
Ulf-Peter Apfel - https://orcid.org/0000-0002-1577-2420
Wolfgang Schuhmann - https://orcid.org/0000-0003-2916-5223

References

1. Dincer, I. *Renewable Sustainable Energy Rev.* **2000,** *4,* 157–175. doi:10.1016/S1364-0321(99)00011-8
2. Chu, S.; Majumdar, A. *Nature* **2012,** *488,* 294–303. doi:10.1038/nature11475

3. Jiao, Y.; Zheng, Y.; Jaroniec, M.; Qiao, S. Z. *Chem. Soc. Rev.* **2015,** *44,* 2060–2086. doi:10.1039/C4CS00470A
4. Cha, H. G.; Choi, K.-S. *Nat. Chem.* **2015,** *7,* 328–333. doi:10.1038/nchem.2194
5. You, B.; Liu, X.; Jiang, N.; Sun, Y. *J. Am. Chem. Soc.* **2016,** *138,* 13639–13646. doi:10.1021/jacs.6b07127
6. Bozell, J. J.; Petersen, G. R. *Green Chem.* **2010,** *12,* 539–554. doi:10.1039/b922014c
7. Eerhart, A. J. J. E.; Faaij, A. P. C.; Patel, M. K. *Energy Environ. Sci.* **2012,** *5,* 6407–6422. doi:10.1039/c2ee02480b
8. van Putten, R.-J.; van der Waal, J. C.; de Jong, E.; Rasrendra, C. B.; Heeres, H. J.; de Vries, J. G. *Chem. Rev.* **2013,** *113,* 1499–1597. doi:10.1021/cr300182k
9. Kwon, Y.; Schouten, K. J. P.; van der Waal, J. C.; de Jong, E.; Koper, M. T. M. *ACS Catal.* **2016,** *6,* 6704–6717. doi:10.1021/acscatal.6b01861
10. Saha, B.; Dutta, S.; Abu-Omar, M. M. *Catal. Sci. Technol.* **2012,** *2,* 79–81. doi:10.1039/C1CY00321F
11. Hansen, T. S.; Sádaba, I.; García-Suárez, E. J.; Riisager, A. *Appl. Catal., A* **2013,** *456,* 44–50. doi:10.1016/j.apcata.2013.01.042
12. Ait Rass, H.; Essayem, N.; Besson, M. *Green Chem.* **2013,** *15,* 2240–2251. doi:10.1039/c3gc40727f
13. Ait Rass, H.; Essayem, N.; Besson, M. *ChemSusChem* **2015,** *8,* 1206–1217. doi:10.1002/cssc.201403390
14. Siankevich, S.; Savoglidis, G.; Fei, Z.; Laurenczy, G.; Alexander, D. T. L.; Yan, N.; Dyson, P. J. *J. Catal.* **2014,** *315,* 67–74. doi:10.1016/j.jcat.2014.04.011
15. Miao, Z.; Wu, T.; Li, J.; Yi, T.; Zhang, Y.; Yang, X. *RSC Adv.* **2015,** *5,* 19823–19829. doi:10.1039/C4RA16968A
16. Davis, S. E.; Houk, L. R.; Tamargo, E. C.; Datye, A. K.; Davis, R. J. *Catal. Today* **2011,** *160,* 55–60. doi:10.1016/j.cattod.2010.06.004
17. Miao, Z.; Zhang, Y.; Pan, X.; Wu, T.; Zhang, B.; Li, J.; Yi, T.; Zhang, Z.; Yang, X. *Catal. Sci. Technol.* **2015,** *5,* 1314–1322. doi:10.1039/C4CY01060D
18. Cai, J.; Ma, H.; Zhang, J.; Song, Q.; Du, Z.; Huang, Y.; Xu, J. *Chem. – Eur. J.* **2013,** *19,* 14215–14223. doi:10.1002/chem.201301735
19. Villa, A.; Schiavoni, M.; Campisi, S.; Veith, G. M.; Prati, L. *ChemSusChem* **2013,** *6,* 609–612. doi:10.1002/cssc.201200778
20. Gupta, N. K.; Nishimura, S.; Takagaki, A.; Ebitani, K. *Green Chem.* **2011,** *13,* 824–827. doi:10.1039/c0gc00911c
21. Liu, B.; Ren, Y.; Zhang, Z. *Green Chem.* **2015,** *17,* 1610–1617. doi:10.1039/C4GC02019G
22. Mei, N.; Liu, B.; Zheng, J.; Lv, K.; Tang, D.; Zhang, Z. *Catal. Sci. Technol.* **2015,** *5,* 3194–3202. doi:10.1039/C4CY01407C
23. Zhang, Z.; Zhen, J.; Liu, B.; Lv, K.; Deng, K. *Green Chem.* **2015,** *17,* 1308–1317. doi:10.1039/C4GC01833H
24. Zhang, Z.; Deng, K. *ACS Catal.* **2015,** *5,* 6529–6544. doi:10.1021/acscatal.5b01491
25. Grabowski, G.; Lewkowski, J.; Skowroński, R. *Electrochim. Acta* **1991,** *36,* 1995. doi:10.1016/0013-4686(91)85084-K
26. Vuyyuru, K. R.; Strasser, P. *Catal. Today* **2012,** *195,* 144–154. doi:10.1016/j.cattod.2012.05.008
27. Chadderdon, D. J.; Xin, L.; Qi, J.; Qiu, Y.; Krishna, P.; More, K. L.; Li, W. *Green Chem.* **2014,** *16,* 3778–3786. doi:10.1039/C4GC00401A
28. Jiang, N.; You, B.; Boonstra, R.; Terrero Rodriguez, I. M.; Sun, Y. *ACS Energy Lett.* **2016,** *1,* 386–390. doi:10.1021/acsenergylett.6b00214
29. You, B.; Jiang, N.; Liu, X.; Sun, Y. *Angew. Chem., Int. Ed.* **2016,** *55,* 9913–9917. doi:10.1002/anie.201603798
30. Ganem, B.; Osby, J. O. *Chem. Rev.* **1986,** *86,* 763–780. doi:10.1021/cr00075a003
31. Masa, J.; Weide, P.; Peeters, D.; Sinev, I.; Xia, W.; Sun, Z.; Somsen, C.; Muhler, M.; Schuhmann, W. *Adv. Energy Mater.* **2016,** *6,* 1502313. doi:10.1002/aenm.201502313
32. Masa, J.; Barwe, S.; Andronescu, C.; Sinev, I.; Ruff, A.; Jayaramulu, K.; Elumeeva, K.; Konkena, B.; Roldan Cuenya, B.; Schuhmann, W. *ACS Energy Lett.* **2016,** *1,* 1192–1198. doi:10.1021/acsenergylett.6b00532
33. Barwe, S.; Andronescu, C.; Vasile, E.; Masa, J.; Schuhmann, W. *Electrochem. Commun.* **2017,** *79,* 41–45. doi:10.1016/j.elecom.2017.04.014
34. Liang, Y.-H.; Yu, S.-Y.; Hsin, C.-L.; Huang, C.-W.; Wu, W.-W. *J. Appl. Phys.* **2011,** *110,* 074302. doi:10.1063/1.3643007
35. Lyman, P. S.; Prewitt, C. T. *Acta Crystallogr., Sect. B: Struct. Sci.* **1984,** *40,* 14–20. doi:10.1107/S0108768184001695
36. Guo, J.; Shi, Y.; Chu, Y.; Ma, T. *Chem. Commun.* **2013,** *49,* 10157–10159. doi:10.1039/c3cc45698f
37. Nam, D.-H.; Taitt, B. J.; Choi, K.-S. *ACS Catal.* **2018,** *8,* 1197–1206. doi:10.1021/acscatal.7b03152

Direct electrochemical generation of organic carbonates by dehydrogenative coupling

Tile Gieshoff[1,2], Vinh Trieu[3], Jan Heijl[4] and Siegfried R. Waldvogel[*1,2]

Full Research Paper

Address:
[1]Institute of Organic Chemistry, Johannes Gutenberg University Mainz, Duesbergweg 10-14, 55128 Mainz, Germany, [2]Graduate School Materials Science in Mainz, Staudingerweg 9, 55128 Mainz, Germany, [3]Covestro AG, Kaiser-Wilhelm-Allee 60, 51373 Leverkusen, Germany and [4]Covestro NV, Haven 507 - Scheldelaan 420, 2040 Antwerpen, Belgium

Email:
Siegfried R. Waldvogel[*] - waldvogel@uni-mainz.de

* Corresponding author

Abstract

Organic carbonates are an important source for polycarbonate synthesis. However, their synthesis generally requires phosgene, sophisticated catalysts, harsh reaction conditions, or other highly reactive chemicals. We present the first direct electrochemical generation of mesityl methyl carbonate by C–H activation. Although this reaction pathway is still challenging concerning scope and efficiency, it outlines a new strategy for carbonate generation.

Introduction

Polycarbonates are high-performance polymeric materials with versatile applications in various fields with economic impact, e.g., construction, food, and pharmaceutical industry [1]. For their technical large-scale production, organic carbonates like diphenyl carbonate (DPC) or dimethyl carbonate (DMC) are key intermediates. Processes for the carbonate generation have been investigated since the 1950s [2]. Although the use of these starting materials is straightforward and unobjectionable at first sight, their generation usually requires highly reactive chemicals. This comes with disadvantages in high safety require-

ments for handling these chemicals, such as ethylene oxide and phosgene [3]. Alternative approaches to carbonate generation are oxidative carbonylations or dehydrative condensations based on alcohols as starting materials (Figure 1) [4-6]. However, both alternatives do not compete with the phosgene approach, since catalyst, excessive amounts of reagents, or harsh reaction conditions are necessary and provide rather low yields. Contemporary research also focuses on the incorporation of carbon dioxide by catalytic polymer formation with less reactive epoxides (other than ethylene oxide) [7-10].

**Figure 1:** Current non-phosgene approaches to organic carbonates.
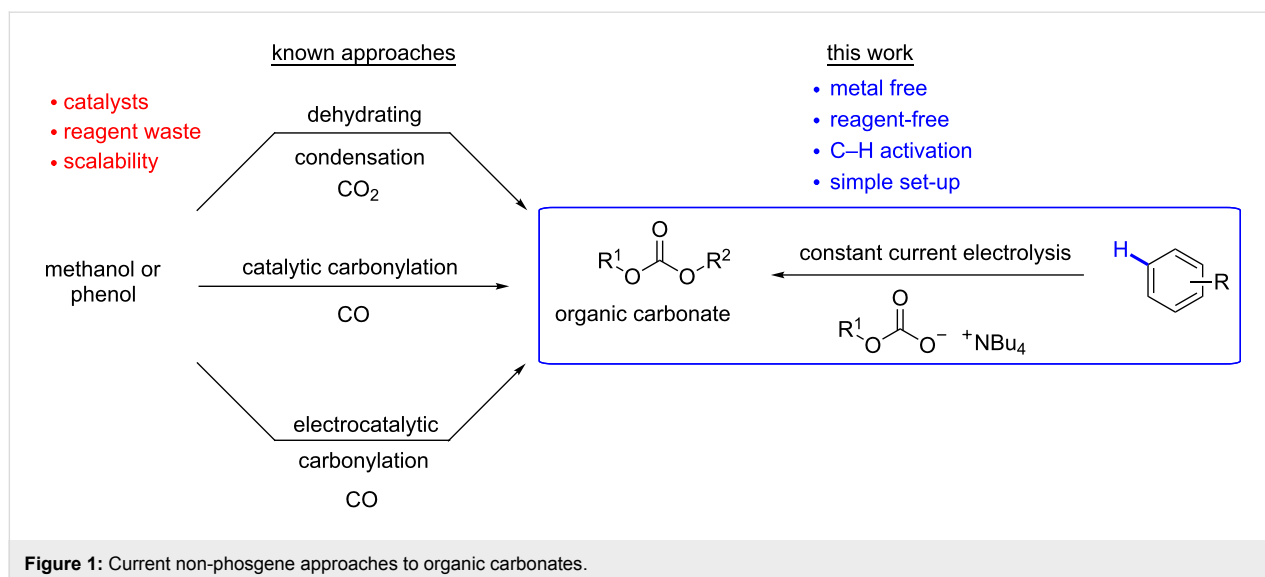
Electrochemistry has the capability to access products by extra-ordinary reaction pathways. Electric current is an inexpensive reagent and inherently safe reaction set-ups ensure a resource saving and applicable technology [11,12]. Several groups developed interesting protocols to use electrochemistry for carbonate generation, but these approaches suffer from complex electrolysis set-ups and lack in scalability [13-20].

In this context, we decided to focus onto a novel electrochemical method for the generation of organic carbonates using inexpensive starting materials without the necessity of catalysts. Generally, alcohols serve as starting materials for the DPC and DMC synthesis. However, efficiency increases if non-functionalized aromatic compounds serve as feedstock. Boron-doped diamond (BDD) as electrode material has the capability to convert simple aromatic systems by direct C–H activation [21-27]. In contrast, other typical anode materials such as graphite, glassy carbon, or platinum tend to lead to electrode fouling when applying high positive potentials [28-30]. In combination with easily accessible carbonate sources, we tried to establish a new dehydrogenative approach to organic carbonates. Here, the study on the first direct electrochemical generation of organic carbonates by dehydrogenative coupling is presented.

Results and Discussion

Within initial experiments the anodic electrolysis of benzene in an aqueous media with metal carbonate salts was investigated. Due to the challenging combination of both, benzene and carbonate source in sufficient concentration within the electrolyte, first experiments were not successful. Benzene exhibits a solubility in water of 1.74 g/L [31]. However, upon addition of carbonates this solubility decreased to trace levels. Moreover, twofold functionalization of carbonate salts is challenging,

because the stability of mono-functionalized intermediates is questionable. Therefore, we switched to an organic acetonitrile-based electrolyte system. Acetonitrile tolerates highly positive potential regimes, which are necessary for C–H activation of non-functionalized arenes. Since simple metal-based carbonate salts are not sufficiently soluble in organic media, the choice of carbonate source is crucial. Therefore, tetrabutylammonium methyl carbonate was employed. The solubility in acetonitrile is attributed to the tetrabutylammonium counterion. Its preparation is very simple by direct treatment of carbon dioxide with the methoxide alkylammonium salt (Scheme 1) [32]. Since this carbonate source is blocked at one end, the mono-functionalization is sufficient for product generation. Although mixed carbonates will be generated with this carbonate source, the products are also applicable in polycarbonate synthesis, as current non-phosgene diphenyl carbonate technology employs a disproportionation of such mixed carbonates [33].

Scheme 1: Preparation of tetrabutylammonium methyl carbonate by direct carbon dioxide incorporation.
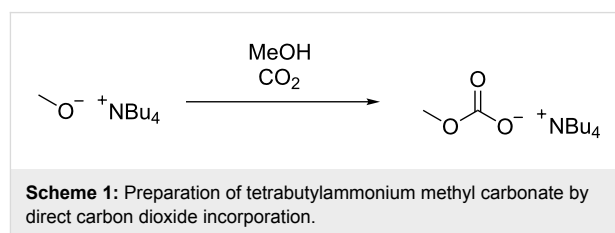
Electrolysis experiments were conducted in undivided 5 mL beaker-type cells. Initial studies with benzene as the aromatic compound in acetonitrile in the presence of the described methyl carbonate salt did not result in the desired organic carbonate. Polymerization of the benzene was most likely and quinoide products were generated due to water traces in the commercially available acetonitrile. In order to investigate the

potential functionalization of a side chain, xylene was tested. In contrast to benzene, traces of two compounds were detected by GC–MS analysis with a matching molar mass for a mono-functionalized product. A comparison with reference material revealed that these signals refer to the core and side-chain functionalization of xylene with a strong preference for the initially targeted functionalization at the core. However, only traces were observed, and no material could be isolated. We assumed that the presence of different aromatic positions lowered the selectivity of the reaction. We changed to mesitylene as the arene, since it exhibits equivalent aromatic positions for carbonate functionalization. This approach enabled a selective process and led to sufficient conversion for further studies. By optimization studies, we were able to produce 21% of the organic carbonate according to ^{1}H NMR analysis on a 0.5 mmol scale (Scheme 2). Similar to the conversion of xylene, we also detected a weak signal of the corresponding side-chain functionalized product. Within our studies, we observed that only acetonitrile as solvent and BDD as anode material led to a successful conversion. Other electrodes and solvents (see Supporting Information File 1) indicated no traces of product in accordance with the high potential range accessible with this electrolyte–electrode combination. Loss of material occurs due to oligomerization of mesitylene and the co-generation of mesityl aldehyde and mesityl acetamide.

According to cyclovoltammetric measurements (see Supporting Information File 1), it is most likely that mesitylene is oxidized

Scheme 2: Direct generation of mesityl methyl carbonate by dehydrogenative functionalization.
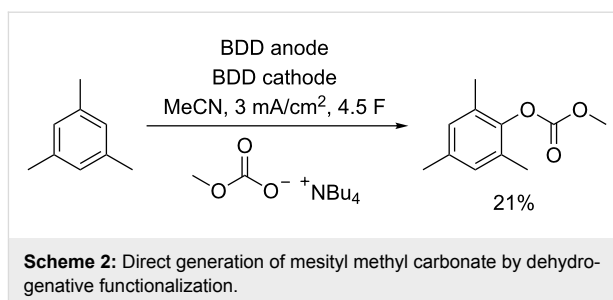
prior to the tetrabutylammonium methyl carbonate. However, oxidation potentials are close to each other, which might lower the efficiency of the conversion. Tetrabutylammonium methyl carbonate serves as nucleophile and supporting electrolyte in this system. Although this unification is a straightforward approach, it can complicate aspects like optimization. Variation of the concentration revealed that only a very small concentration window ($\approx$0.1 M) enables product generation in our set-up. Increased concentrations of the carbonate nucleophile, which might be beneficial at first sight, led to no conversion. Similar results emerged within scale-up, when a significant effect of the electrode distance occurred (Figure 2).

To generate a sufficient amount of material for work-up studies, we conducted conversions in 25 mL beaker-type cells. However, neither product formation nor conversion were observed. Since all parameters were constant except the electrode distance, which increased from 0.5 cm (set-up A) to 1.0 cm

Figure 2: Influence of the electrode distance; [a] ^{1}H NMR yield; [b] isolated yield.
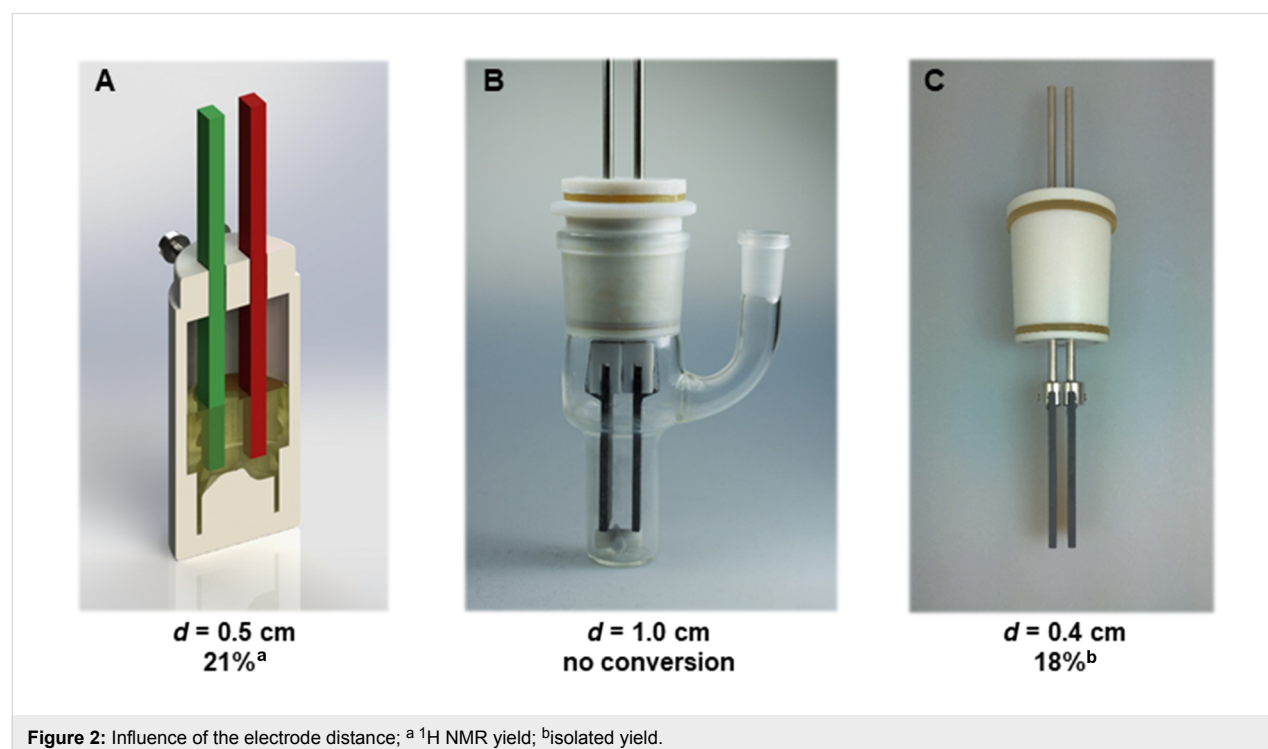
(set-up B), we repeated these experiments with a lower electrode distance of 0.4 cm (set-up C, Figure 2). This latter variation afforded selective conversion and an isolated yield of 18%. Separation of the product was achieved with a short-path distillation. A possible rationale for these effects is the sensitive influence of the carbonate nucleophile, which serves as nucleophile and supporting electrolyte. However, this behaviour is currently inexplicable for us and its elucidation is still in progress.

Within our studies on a potential scope of aromatic compounds, the symmetric 1,3,5-threefold substitution pattern showed best selectivity according to GC–MS measurements. Since the nucleophilic attack is controlled by sterics, non-symmetric substitution patterns gave weak signals and product mixtures. Generally, the nucleophilicity of carbonates is limited and therefore, the choice of suitable arenes is crucial. Heterofunctionalizations like fluoro, chloro, and methoxy groups are generally accepted, but it depends on the substitution pattern. The sensitive interplay of inefficient oxidation at highly positive oxidation potentials and the oligomerization tendency of electron-rich arenes limit the scope (see Supporting Information File 1).

Conclusion

The first direct electrochemical generation of organic carbonates by dehydrogenative coupling at arenes was established. Even though this ambitious method is currently restricted to mesitylene, efforts are being made to develop an electrolysis protocol, which allows better conversions and higher yields. Nevertheless, the present results indicate that with BDD anodes this electro-conversion should be feasible in a general context, and might open the door to further direct installation of oxygen functionalization onto aromatic substrates.

Supporting Information

Supporting Information File 1

Synthesis protocols, analytical data, GC chromatograms, MS spectra, and NMR spectra.
[https://www.beilstein-journals.org/bjoc/content/supplementary/1860-5397-14-135-S1.pdf]

Acknowledgements

ORCID® iDs

Vinh Trieu - https://orcid.org/0000-0002-1831-0221
Jan Heijl - https://orcid.org/0000-0001-6111-2119
Siegfried R. Waldvogel - https://orcid.org/0000-0002-7949-9638

References

1. LeGrand, D. G.; Bendler, J. T., Eds. *Handbook of polycarbonate science and technology;* Marcel Dekker: New York, NY, 2000.
2. Schnell, H.; Bottenbruch, L.; Krimm, H. Verfahren zur Herstellung thermoplastischer Kunststoffe. Ger. Patent DE1953F0013040, Oct 17, 1953.
3. Kim, W. B.; Joshi, U. A.; Lee, J. S. *Ind. Eng. Chem. Res.* **2004,** *43,* 1897–1914. doi:10.1021/ie034004z
4. Sakakura, T.; Kohno, K. *Chem. Commun.* **2009,** 1312–1330. doi:10.1039/b819997c
5. Keller, N.; Rebmann, G.; Keller, V. *J. Mol. Catal. A: Chem.* **2010,** *317,* 1–18. doi:10.1016/j.molcata.2009.10.027
6. Yalfani, M. S.; Lolli, G.; Wolf, A.; Mleczko, L.; Müller, T. E.; Leitner, W. *Green Chem.* **2013,** *15,* 1146–1149. doi:10.1039/c3gc36877g
7. Jutz, F.; Buchard, A.; Kember, M. R.; Fredriksen, S. B.; Williams, C. K. *J. Am. Chem. Soc.* **2011,** *133,* 17395–17405. doi:10.1021/ja206352x
8. Kember, M. R.; Buchard, A.; Williams, C. K. *Chem. Commun.* **2011,** *47,* 141–163. doi:10.1039/C0CC02207A
9. Langanke, J.; Wolf, A.; Hofmann, J.; Böhm, K.; Subhani, M. A.; Müller, T. E.; Leitner, W.; Gürtler, C. *Green Chem.* **2014,** *16,* 1865–1870. doi:10.1039/C3GC41788C
10. Chapman, A. M.; Keyworth, C.; Kember, M. R.; Lennox, A. J. J.; Williams, C. K. *ACS Catal.* **2015,** *5,* 1581–1588. doi:10.1021/cs501798s
11. Wiebe, A.; Gieshoff, T.; Möhle, S.; Rodrigo, E.; Zirbes, M.; Waldvogel, S. R. *Angew. Chem., Int. Ed.* **2018,** *57,* 5594–5619. doi:10.1002/anie.201711060
12. Möhle, S.; Zirbes, M.; Rodrigo, E.; Gieshoff, T.; Wiebe, A.; Waldvogel, S. R. *Angew. Chem., Int. Ed.* **2018,** *57,* 6018–6041. doi:10.1002/anie.201712732
13. Figueiredo, M. C.; Trieu, V.; Eiden, S.; Koper, M. T. M. *J. Am. Chem. Soc.* **2017,** *139,* 14693–14698. doi:10.1021/jacs.7b08208
14. Kanega, R.; Ogihara, H.; Yamanaka, I. *Res. Chem. Intermed.* **2015,** *41,* 9497–9508. doi:10.1007/s11164-015-1975-8
15. Kanega, R.; Hayashi, T.; Yamanaka, I. *ACS Catal.* **2013,** *3,* 389–392. doi:10.1021/cs300725j
16. Murayama, T.; Hayashi, T.; Kanega, R.; Yamanaka, I. *J. Phys. Chem. C* **2012,** *116,* 10607–10616. doi:10.1021/jp300809s
17. Zhang, L.; Niu, D.; Zhang, K.; Zhang, G.; Luo, Y.; Lu, J. *Green Chem.* **2008,** *10,* 202–206. doi:10.1039/B711981J
18. Yuan, D.; Yan, C.; Lu, B.; Wang, H.; Zhong, C.; Cai, Q. *Electrochim. Acta* **2009,** *54,* 2912–2915. doi:10.1016/j.electacta.2008.11.006
19. Yuan, X.; Lu, B.; Liu, J.; You, X.; Zhao, J.; Cai, Q. *J. Electrochem. Soc.* **2012,** *159,* E183–E186. doi:10.1149/2.049212jes
20. Garcia-Herrero, I.; Cuéllar-Franca, R. M.; Enríquez-Gutiérrez, V. M.; Alvarez-Guerra, M.; Irabien, A.; Azapagic, A. *ACS Sustainable Chem. Eng.* **2016,** *4,* 2088–2097. doi:10.1021/acssuschemeng.5b01515
21. Waldvogel, S. R.; Mentizi, S.; Kirste, A. *Top. Curr. Chem.* **2012,** *320,* 1–31. doi:10.1007/128_2011_125

22. Elsler, B.; Schollmeyer, D.; Dyballa, K. M.; Franke, R.; Waldvogel, S. R. *Angew. Chem., Int. Ed.* **2014,** *53,* 5210–5213. doi:10.1002/anie.201400627
https://onlinelibrary.wiley.com/doi/abs/10.1002/anie.201400627

23. Wiebe, A.; Schollmeyer, D.; Dyballa, K. M.; Franke, R.; Waldvogel, S. R. *Angew. Chem., Int. Ed.* **2016,** *55,* 11801–11805. doi:10.1002/anie.201604321

24. Lips, S.; Wiebe, A.; Elsler, B.; Schollmeyer, D.; Dyballa, K. M.; Franke, R.; Waldvogel, S. R. *Angew. Chem., Int. Ed.* **2016,** *55,* 10872–10876. doi:10.1002/anie.201605865

25. Schulz, L.; Enders, M.; Elsler, B.; Schollmeyer, D.; Dyballa, K. M.; Franke, R.; Waldvogel, S. R. *Angew. Chem., Int. Ed.* **2017,** *56,* 4877–4881. doi:10.1002/anie.201612613

26. Waldvogel, S. R.; Elsler, B. *Electrochim. Acta* **2012,** *82,* 434–443. doi:10.1016/j.electacta.2012.03.173

27. Ivandini, T. A.; Einaga, Y. *Chem. Commun.* **2017,** *53,* 1338–1347. doi:10.1039/C6CC08681K

28. Wesenberg, L. J.; Herold, S.; Shimizu, A.; Yoshida, J.-i.; Waldvogel, S. R. *Chem. – Eur. J.* **2017,** *23,* 12096–12099. doi:10.1002/chem.201701979

29. Möhle, S.; Herold, S.; Richter, F.; Nefzger, H.; Waldvogel, S. R. *ChemElectroChem* **2017,** *4,* 2196–2210. doi:10.1002/celc.201700476

30. Herold, S.; Möhle, S.; Zirbes, M.; Richter, F.; Nefzger, H.; Waldvogel, S. R. *Eur. J. Org. Chem.* **2016,** 1274–1278. doi:10.1002/ejoc.201600048

31. Arnold, D.; Plank, C.; Erickson, E.; Pike, F. *Chem. Eng. Data Ser.* **1958,** *3,* 253–256. doi:10.1021/i460004a016

32. Verdecchia, M.; Feroci, M.; Palombi, L.; Rossi, L. *J. Org. Chem.* **2002,** *67,* 8287–8289. doi:10.1021/jo0259461

33. Kim, W. B.; Lee, J. S. *Catal. Lett.* **1999,** *59,* 83–88. doi:10.1023/A:1019087530460

License and Terms

Synergistic electrodeposition of bilayer films and analysis by Raman spectroscopy

Saadeldin E. T. Elmasly[1,2], Luca Guerrini[1,3], Joseph Cameron[4], Alexander L. Kanibolotsky[4,5], Neil J. Findlay[4], Karen Faulds[1] and Peter J. Skabara[*4]

Abstract

A novel methodology towards fabrication of multilayer organic devices, employing electrochemical polymer growth to form PEDOT and PEDTT layers, is successfully demonstrated. Moreover, careful control of the electrochemical conditions allows the degree of doping to be effectively altered for one of the polymer layers. Raman spectroscopy confirmed the formation and doped states of the PEDOT/PEDTT bilayer. The electrochemical deposition of a bilayer containing a de-doped PEDTT layer on top of doped PEDOT is analogous to a solution-processed organic semiconductor layer deposited on top of a PEDOT:PSS layer without the acidic PSS polymer. However, the poor solubility of electrochemically deposited PEDTT (or other electropolymerised potential candidates) raises the possibility of depositing a subsequent layer via solution-processing.

Findings

Fabrication of multilayer organic electronic devices has been extensively researched in the past 20 years, resulting in numerous processes and techniques [1]. Recent advances include inkjet printing [2] and direct stamping of the active layer to the substrate [3]. However, such processes involve the use of solvents, which can lead to blending of layers through dissolution of the initial layer [4]. While the use of water or fluorinated solvents can avoid these issues [5,6], materials suitable for use in

such solvents are specifically designed, meaning such processes are less suitable for general use [4]. In this work, we present an alternative process for the fabrication of multilayer organic electronic devices. By electrochemically polymerising two different monomers in a step-wise fashion, a PEDOT/ PEDTT bilayer was fabricated. Crucially, this approach provides an insoluble, conductive PEDOT layer, allowing the second PEDTT layer to be deposited on top (and subsequently de-doped), without compromising the initial deposition. Alemán and co-workers demonstrated this technique through the manufacture of multilayer films [7,8], alternating PEDOT and poly(*N*-methylpyrrole) to develop symmetric supercapacitors [9]. However, in their work there was no attempt to de-dope the second layer, which is necessary for the electrochemical preparation of a hole injection-semiconductor bilayer for solution processing of subsequent layers.

The monomers used in this work, 3,4-ethylenedioxythiophene (EDOT) and 3,4-ethylenedithiothiophene (EDTT), were either purchased commercially or prepared according to literature procedures [10]. Both were chosen due to their ease of electropolymerisation, excellent film-forming properties and because of their likely compatibility with each other [11]. First, PEDOT was deposited on an ITO glass slide by electropolymerisation of EDOT, using a Pt gauze counter electrode and a Ag wire quasi-reference electrode, with cycling between 0 V and +1.4 V over 150 cycles sufficient to achieve good polymer growth. Under similar conditions, the PEDOT/PEDTT bilayer was achieved using EDTT and cycling over the range +0.3 V to +1.78 V over 150 cycles (see Figure S1 in Supporting Information File 1 for the electropolymerisation of the PEDOT and PEDTT layers on a glassy carbon electrode). UV–vis absorption studies for the p-doped bilayer, carried out using ITO glass as the substrate, indicated that the main π–π* peak in the region of 450 nm was diminished, as expected for doped PEDOT and PEDTT (Figure S4a, Supporting Information File 1) [11]. The newly formed bilayer was de-doped by cycling between −0.5 V and −0.3 V over 300 segments in CH$_3$CN (see Figures S2 and S3 in Supporting Information File 1 for the oxidation and reduction waves after dedoping). The UV–vis absorption spectrum of the de-doped bilayer clearly shows the signature of oxidised PEDOT with a broad absorption band in the region of 650–1000 nm (Figure S4b, Supporting Information File 1), similar to that previously reported [11]. Additionally, the λ$_{max}$ of the de-doped bilayer corresponds to that of de-doped PEDTT [11] whilst there is no obvious peak at 580 nm, which would be expected if there was a significant amount of de-doped PEDOT present [11]. The absorption profile of the bilayer therefore clearly shows the selective de-doping of PEDTT. It is evident from Figure 1 that the two polymers show electroactivity in distinctly different potential windows. This has two consequences: (i) during the

polymerisation of PEDTT, PEDOT remains doped and therefore conductive, allowing the polymerisation of EDTT to proceed; (ii) PEDTT can be de-doped within the electroactive window of PEDOT, meaning that the all-sulfur polymer can be successfully de-doped whilst the PEDOT layer remains predominantly doped.
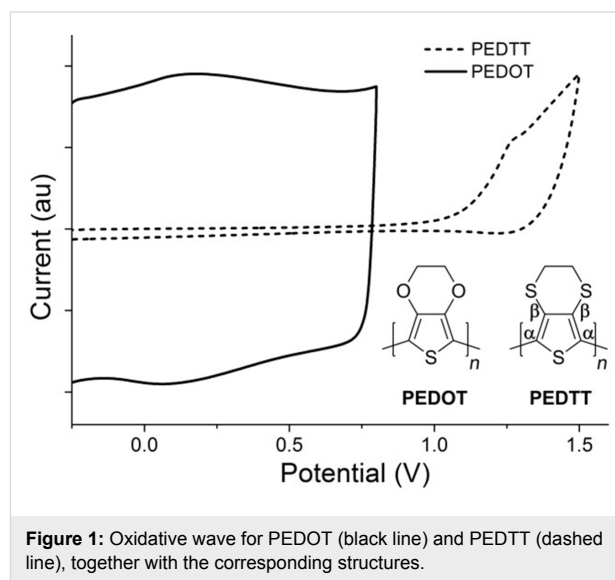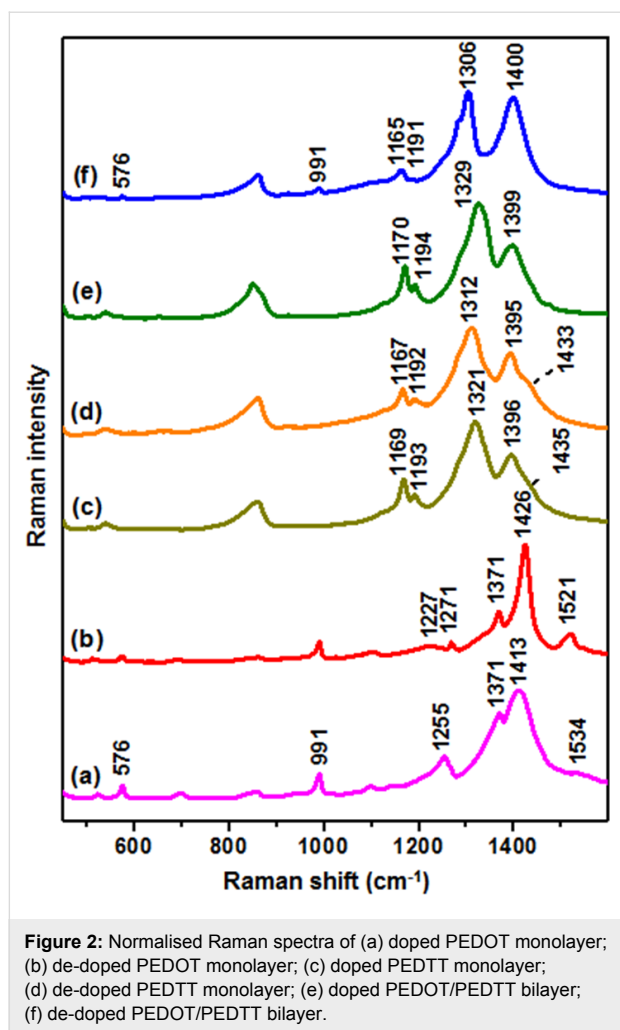

Figure 1: Oxidative wave for PEDOT (black line) and PEDTT (dashed line), together with the corresponding structures.

In order to support the formation of a PEDOT/PEDTT bilayer using this technique and to clarify the nature of doping in the two layers, freshly fabricated bilayers (using 10^{-4} M monomer solution) were grown on ITO and analysed by Raman spectroscopy, alongside doped and de-doped mono-layers of PEDOT and PEDTT for comparison. Figure 2 shows the Raman spectra of pure PEDOT and PEDTT polymers, both in the doped and neutral states (Figure 2a and b, Figure 2c and d, respectively). There are two main spectral regions of interest in the Raman spectra of these polymers. Below approximately 1150 cm^{-1}, the Raman spectra are dominated by medium to weak bands which can be predominantly assigned to out-of-plane deformations [12], which are only weakly sensitive to changes in the electronic properties of the polymers [13]. In comparing PEDOT and PEDTT, contributions relating to the dioxyethylene ring of PEDOT, such as the bands at 576 cm^{-1} and 991 cm^{-1}, assigned to dioxyethylene ring deformations, and at 1099 cm^{-1}, assigned to C–O–C deformation, are absent in PEDTT (Figure 2c and d) [14].

On the contrary, the Raman features appearing above 1150 cm^{-1} are strongly dependent on the π-electron delocalisation within the polymer and, therefore, produce dramatic changes both in frequency and intensity due to the different electronic structure of each polymer. In particular, in the p-doped PEDOT spectrum (Figure 2a), Raman features corre-

Figure 2: Normalised Raman spectra of (a) doped PEDOT monolayer; (b) de-doped PEDOT monolayer; (c) doped PEDTT monolayer; (d) de-doped PEDTT monolayer; (e) doped PEDOT/PEDTT bilayer; (f) de-doped PEDOT/PEDTT bilayer.

sponding to the thiophene ring at 1534 cm^{-1} (C=C asymmetric stretching vibration), 1413 cm^{-1} (symmetric $C_\alpha=C_\beta$ stretching mode), 1371 cm^{-1} ($C_\beta=C_\beta$ stretching vibration), and 1255 cm^{-1} (inter-ring $C_\alpha=C_{\alpha'}$ stretching) are present [12]. When PEDOT is subjected to a de-doping process (Figure 2b) yielding the neutral polymer, the weak band at 1534 cm^{-1} shifts to 1521 cm^{-1} and increases in relative intensity, while the v_{sym}(C=C) band shifts from 1413 cm^{-1} to 1426 cm^{-1}. Additionally, the broad band at 1255 cm^{-1} resolves into two distinct features (at 1227 and 1271 cm^{-1}) [15] and a strong enhancement and sharpening of the Raman bands at 1371 and 1413 cm^{-1} is observed. Similar changes were ascribed by Garreau et al. [12] to the resonant effect of the Raman scattering. The marked intensity increase of the PEDOT Raman spectrum upon the de-doping process further supports this hypothesis (Figure S5, Supporting Information File 1).

By analogy with the band assignment for PEDOT, the Raman features in the PEDTT spectrum (Figure 2c) at 1396 cm^{-1} and 1321 cm^{-1}, can be ascribed to v_s($C_\alpha=C_\beta$) and v_s($C_\beta=C_\beta$) vibra-

tions, respectively. However, the out-of-plane bands appearing in the region below 1150 cm^{-1} are less sensitive to the de-doping process, but the C=C bands show important changes, such as the marked downshift of the $C_\beta=C_\beta$ band from 1321 cm^{-1} to 1312 cm^{-1}, and the relative intensity increase of the $C_\alpha=C_\beta$ band at ≈1396 cm^{-1}. In particular, Kocharova et al. [16] associated the intensity increase of the $C_\alpha=C_\beta$ band in polythiophene structures to the higher localised charge at the $C_\alpha=C_\beta$ linkage as a consequence of the positively charged doping of the material.

Figure 2e and 2f illustrate the Raman spectra of the polymer bilayer in the doped state and after de-doping of the PEDTT layer, respectively. The doped bilayer clearly shows the characteristic Raman profile of doped PEDTT, proving the effective and successful coating of the underlying PEDOT layer (Figure 2e). Once the bilayer is subjected to the de-doping process (Figure 2f), the Raman spectrum retains the spectral features of the PEDTT neutral polymer (Figure 2d). Very weak bands attributed to the PEDOT system, such as bands at 576 and 991 cm^{-1}, can be recognised in the bilayer spectrum. The appearance of signals arising from the underlying PEDOT layer, although distant from the focal point of the laser, is likely the result of a partial de-doping of the underlying PEDOT layer. Thus, the much higher Raman scattering efficiency of PEDOT in the neutral state, as compared to PEDTT (Figure S5, Supporting Information File 1), enables the spectral emergence of these features [17]. Whilst it is not possible to identify the absorption of PEDTT in the broad absorption spectrum of the doped bilayer (Figure S4a, Supporting Information File 1), it has been shown that Raman spectroscopy is an effective technique to confirm the coating of PEDTT onto the doped PEDOT layer. Additionally, the presence of features that are characteristic of neutral PEDTT in the Raman spectrum of the de-doped bilayer confirms de-doping of PEDTT, complementing UV–vis absorption results (Figure S4b, Supporting Information File 1).

Conclusion

In summary, we have shown a novel processing methodology for the fabrication of multilayer organic electronic devices that utilises electrochemical polymerisation to form the first two layers. Successful PEDOT/PEDTT bilayer formation has been confirmed by Raman spectroscopy. Electrodeposition of the bilayer has advantages over traditional processing methods including avoiding the acidity of PSS which is detrimental to the lifetime of devices containing PEDOT:PSS [18] and the ability to use polymers without insulating alkyl chains. It is important to note that the PEDTT layer can be substituted by any electropolymerised material that has a complementary electroactive potential window. Moreover, the insolubility of neutral PEDTT (or any other suitable polymer chosen) allows the bilayer to be

subjected to solution-processing. It is therefore possible to deposit any layer onto the neutral insoluble polymer (e.g., an acceptor material for organic photovoltaics or an electron transport material for OLEDs) illustrating the potential for electrochemically deposited bilayers to be used for the fabrication of complex, multilayer organic electronic devices.

Supporting Information

Supporting Information File 1
General experimental and additional spectra.
[https://www.beilstein-journals.org/bjoc/content/
supplementary/1860-5397-14-191-S1.pdf]

Acknowledgements

ORCID® iDs

Luca Guerrini - https://orcid.org/0000-0002-2925-1562
Joseph Cameron - https://orcid.org/0000-0001-8622-8353
Neil J. Findlay - https://orcid.org/0000-0001-6855-0998
Peter J. Skabara - https://orcid.org/0000-0001-7319-0464

References

1. Menard, E.; Meitl, M. A.; Sun, Y.; Park, J.-U.; Shir, D. J.-L.; Nam, Y.-S.; Jeon, S.; Rogers, J. A. *Chem. Rev.* **2007,** *107,* 1117–1160. doi:10.1021/cr050139y
2. Teichler, A.; Perelaer, J.; Schubert, U. S. *J. Mater. Chem. C* **2013,** *1,* 1910–1925. doi:10.1039/c2tc00255h
3. Huang, J.-H.; Ho, Z.-Y.; Kuo, T.-H.; Kekuda, D.; Chu, C.-W.; Ho, K.-C. *J. Mater. Chem.* **2009,** *19,* 4077–4080. doi:10.1039/b903765a
4. Duan, L.; Hou, L.; Lee, T.-W.; Qiao, J.; Zhang, D.; Dong, G.; Wang, L.; Qiu, Y. *J. Mater. Chem.* **2010,** *20,* 6392–6407. doi:10.1039/b926348a
5. Lee, J.-K.; Chatzichristidi, M.; Zakhidov, A. A.; Taylor, P. G.; DeFranco, J. A.; Hwang, H. S.; Fong, H. H.; Holmes, A. B.; Malliaras, G. G.; Ober, C. K. *J. Am. Chem. Soc.* **2008,** *130,* 11564–11565. doi:10.1021/ja803493m
6. Zakhidov, A. A.; Lee, J.-K.; Fong, H. H.; DeFranco, J. A.; Chatzichristidi, M.; Taylor, P. G.; Ober, C. K.; Malliaras, G. G. *Adv. Mater.* **2008,** *20,* 3481–3484. doi:10.1002/adma.200800557
7. Estrany, F.; Aradilla, D.; Oliver, R.; Alemán, C. *Eur. Polym. J.* **2007,** *43,* 1876–1882. doi:10.1016/j.eurpolymj.2007.01.033
8. Estrany, F.; Aradilla, D.; Oliver, R.; Armelin, E.; Alemán, C. *Eur. Polym. J.* **2008,** *44,* 1323–1330. doi:10.1016/j.eurpolymj.2008.01.046
9. Aradilla, D.; Estrany, F.; Alemán, C. *J. Phys. Chem. C* **2011,** *115,* 8430–8438. doi:10.1021/jp201108c
10. Goldoni, F.; Langeveld-Voss, B. M. W.; Meijer, E. W. *Synth. Commun.* **1998,** *28,* 2237–2244. doi:10.1080/00397919808007039
11. Spencer, H. J.; Skabara, P. J.; Giles, M.; McCulloch, I.; Coles, S. J.; Hursthouse, M. B. *J. Mater. Chem.* **2005,** *15,* 4783–4792. doi:10.1039/b511075k
12. Garreau, S.; Louarn, G.; Buisson, J. P.; Froyer, G.; Lefrant, S. *Macromolecules* **1999,** *32,* 6807–6812. doi:10.1021/ma9905674
13. Tran-Van, F.; Garreau, S.; Louarn, G.; Froyer, G.; Chevrot, C. *J. Mater. Chem.* **2001,** *11,* 1378–1382. doi:10.1039/b100033k
14. Garreau, S.; Louarn, G.; Froyer, G.; Lapkowski, M.; Chauvet, O. *Electrochim. Acta* **2001,** *46,* 1207–1214. doi:10.1016/S0013-4686(00)00693-9
15. Kalbáč, M.; Kavan, L.; Dunsch, L. *Synth. Met.* **2009,** *159,* 2245–2248. doi:10.1016/j.synthmet.2009.07.059
16. Kocharova, N.; Lukkari, J.; Viinikanoja, A.; Ääritalo, T.; Kankare, J. *J. Phys. Chem. B* **2002,** *106,* 10973–10981. doi:10.1021/jp026259g
17. Everall, N. J. *Analyst* **2010,** *135,* 2512–2522. doi:10.1039/C0AN00371A
18. de Jong, M. P.; van IJzendoorn, L. J.; de Voigt, M. J. A. *Appl. Phys. Lett.* **2000,** *77,* 2255–2257. doi:10.1063/1.1315344

License and Terms